Nitric Oxide Signalling in the Inferior Colliculus

Bastiaan Meendert Jan Olthof-Bakker MSc.

Submitted for the degree of Doctor of Philosophy

Institute of Neuroscience, Newcastle University

December 2016

ABSTRACT

This thesis investigates the distribution and function of neuronal nitric oxide synthase (nNOS) in the inferior colliculus (IC) the principal midbrain nucleus in the auditory pathway.

Firstly, experiments using immunocytochemistry and fluorescent microscopy in the rat IC showed two, previously unreported, different subcellular distributions of nNOS in the IC. Secondly, the presence of nNOS positive post-synaptic puncta in the central nucleus suggests that nNOS, contrary to previous reports, is not limited to the IC cortices. Expression of nNOS was observed in both glutamatergic and GABAergic cells. Cells expressing nNOS were shown to often contain calbindin or parvalbumin but rarely calretinin.

In vivo electrophysiological experiments were conducted in the anaesthetised guinea pig. Recording of multiunit neuronal activity was combined with local reverse microdialysis of drugs in the IC.

Dialysis of NMDA increased both spontaneous and sound driven activity in the IC in a dose dependent manner. These effects were blocked when NMDA was paired with L-MeArg, a NOS inhibitor, or ODQ, a soluble guanylate cyclase (sGC) inhibitor. These results suggest that NMDA receptor-mediated effects in the IC involve NO and its action on sGC.

Systemic administration of sodium salicylate, a drug known to induce tinnitus, resulted in a doubling of spontaneous activity in the IC. In contrast, local delivery of salicylate in the IC reduced spontaneous activity in a time/concentration-dependent manner. Both locally and systemically administered salicylate influenced sound driven activity, suggesting these effects are, in part, mediated directly within the IC. No effect of L-MeArg was observed on the salicylate mediated effects, but this could be due to methodological issues.

These results demonstrate that NO play plays a role in sound processing in the IC and further work is required to establish its functional significance.

ACKNOWLEDGEMENTS

I was fortunate enough to have two excellent PhD supervisors, Prof. Adrian Rees and Dr. Sasha Gartside. The wealth of different but complementary experience and knowledge between them and their active involvement in every part of the project made the PhD process to be an enriching experience.

I cannot thank you both enough for granting me the opportunity to study and work with you. I truly appreciate all the efforts you both made to make me feel welcome and at home in your lab and country. Over the last three years, both of you became more than just supervisors to me and I could not have achieved this without your continued support and friendship.

Also, the people who have populated the office in which I have spent so much of my life over the last three years, you all have been great and made this experience so much better. Two people, I have to mention by name are Dr. Llwyd Orton and Reem. Llwyd thank you for sharing the lab and investing time in teaching me the more practical aspects of the in vivo electrophysiology experiments, your experience and friendship were invaluable. Reem, we shared the office from day one and shared this experience together, thank you for all the understanding, wise words and of course all the coffees you bought me.

My dear parents, Jan and Antje, you taught me to always believe in myself and never quit before trying. You have no idea how much I value your unconditional support and encouragement throughout my life and especially in these last few months. Marc, my gratitude and love towards you cannot be expressed in words. Not only did you let me go and take this opportunity but you supported me every step of the way. Thank you for allowing me to pursue my dreams, supporting me in spite of me making your life harder than it needed to be, and above all thank you for your continued love.

I would like to thank Newcastle University for providing the funding for my project.

To all of those listed above and all the others I have met in the last three years, you all have shaped me into the person and scientist I am to today and for that, I thank you all.

LIST OF ABBREVIATIONS

- 2-DG 2-deoxyglucose
- AC Auditory cortex
- aCSF Artificial cerebrospinal fluid
- AMPA α-amino-3-hydroxy-5-methyl-4-isoxazolepropionic acid
- AMPA-R AMPA receptor
- AN Auditory nerve
- ANOVA Analysis of variance
- Arg Arginine binding domain on NOS
- AVCN Anterior ventral cochlear nucleus
- BF Best frequency
- BFE Best frequency electrode
- Ca^{2+} Calcium ion
- CaM Calmodulin
- CBC Comparative Biology Centre
- CF Characteristic frequency
- cGMP Cyclic guanosine monophosphate
- CNC Cochlear nuclear complex
- CNIC Central nucleus of the inferior colliculus
- CNS Central nervous system
- DAS Dorsal acoustic striae
- DAPI 4',6-diamidino-2-phenylindole
- dB Decibel
- DCIC Dorsal cortex of the inferior colliculus
- DCN Dorsal cochlear nucleus
- D-M D-stellate cells
- DMSO Dimethyl sulfoxide

- DNA — Deoxyribonucleic acid
- E^- — Electron
- EF-hand — Electro focus hand
- FAD — Flavin adenine dinucleotide
- FRA — Frequency response area
- FMN — Flavin mononucleotide
- GAD — Glutamic acid decarboxylase
- GABA — Gamma-Aminobutyric acid
- Gi — Giant cells
- GluN — Glutamate receptor ionotropic NMDA
- GBC — Globular bushy cells
- IAS — Intermediate acoustic striae
- IC — Inferior colliculus
- IHC — Inner hair cells
- IP — Intraperitoneal
- kDa — Kilodalton
- kHz — Kilohertz
- K^+ — Potassium ion
- LCIC — Lateral cortex of the inferior colliculus
- L-Arg — L-Arginine
- L-MeArg — N^G-Methyl-L-arginine acetate
- LnTB — Lateral nucleus of the trapezoid body
- LSO — Lateral superior olive
- MGB — Medial geniculate body
- Mg^{2+} — Magnesium ion
- mRNA — Messenger ribonucleic acid
- MnTB — Medial nucleus of the trapezoid body

- MSO — Medial superior olive
- Na^+ — Sodium ion
- NADPH — Nicotinamide adenine dinucleotide phosphate (reduced form)
- nLL — Nucleus of the lateral lemniscus
- NMDA — N-methyl-D-aspartate
- NMDA-R — NMDA receptor
- NO — Nitric oxide
- NOS — Nitric oxide synthase
  - eNOS — Endothelial nitric oxide synthase
  - iNOS — Inducible nitric oxide synthase
  - nNOS — Neuronal nitric oxide synthase
- O — Octopus cells
- O_2 — Oxygen
- ODQ — 1H-[1,2,4]oxadiazolo[4,3-a]quinoxalin-1-one
- PBS — Phosphate-Buffered Saline
- PDZ — post synaptic density protein, Drosophila disc large tumor suppressor, zonula occludens-1 protein
- PFA — Paraformaldehyde
- PKG — Protein kinase G
- PSTH — Peristimulus time histogram
- PSD95 — Postsynaptic density protein 95
- PY — Pyramidal cells
- PVCN — Posterior ventral cochlear nucleus
- SBC — Spherical bushy cells
- sGC — Soluble guanylyl cyclase
- SPL — Sound pressure level
- SPN — Superior paraolivary nucleus

- SPSS Statistical Package for the Social Sciences
- T-M T-stellate cells
- VAS Ventral acoustic striae
- VGLUT1 Vesicular glutamate transporter 1
- VGLUT2 Vesicular glutamate transporter 2

Contents

Chapter 1. Introduction

1.1 Opening statement

This thesis will address the role of nitric oxide (NO) signalling in auditory processing in the inferior colliculus (IC), the principal midbrain nucleus of the auditory pathway.

NO, a gaseous diatomic molecule, highly reactive, non-respiratory and lethal in high quantities, seems an odd choice for nature to use as a ubiquitous signalling molecule. NO is believed to be one of the earliest signalling molecules employed by organisms since the origins of life (Garthwaite, 2008). Today NO signalling is observed both in eukaryotes and prokaryotes and given the fact that it has been part of life right from the outset, it is perhaps less surprising to find that NO is so widely produced in the human body. NO relaxes vascular smooth muscle leading to vasodilation in the cardiovascular system but has also been shown to function as a neurotransmitter in the central nervous system. In the mammalian brain, NO is catalysed by neuronal nitric oxide synthase (nNOS) a protein that catalyses the conversion of L-Arginine to L-Citrulline and NO. nNOS is abundant throughout the brain, but expression is especially pronounced in the brainstem nuclei and cerebellum. Of all brainstem nuclei the inferior colliculus (IC) expresses the most nNOS, in fact, it expresses more nNOS than all other nuclei combined (Coote, 2008). Although nNOS has been identified in the IC, the functional properties of NO signalling in the IC are unknown. In this thesis, I will discuss the results of experiments that have started to address this question as well as investigate whether there is a link between NO and tinnitus.

1.2 Organisation of the Thesis

In order to get a better understanding about the cells that express nNOS in the IC. I will start this thesis with a broad introduction into the relevant topics that are required for the experiments that follow. Key topics that will be addressed are the IC, and its position within the auditory pathway, glutamate signalling, NMDA receptors, nNOS, NO, sGC, and tinnitus. Throughout the Introduction I will highlight the unknowns and identify gaps in our current knowledge and understanding, these gaps will be summarised at the end of the introduction and form the aims and hypothesis tested. Before presenting the experimental data, the methods used throughout this project are discussed in Chapter 2.

In Chapter 3, the first data chapter, I will discuss studies investigating the distribution of NOS through the different subdivisions of the IC, and the neurotransmitter phenotypes of, and glutamatergic inputs to the neurons expressing NOS. Findings from the structural studies in Chapter 3 will feed forward into Chapter 4 in which I will present

electrophysiological recordings from experiments that aim to learn more about the functional role NO has on auditory processing in the IC. NOS activity has traditionally always been described as being closely associated with the NMDA receptors for reasons I will discuss below, therefore the studies presented in the second results chapter (Chapter 4) first investigate the functional role of the NMDA receptor in the responses to auditory stimuli and then the interaction of NMDA receptor signalling with NO. Animal models of tinnitus have shown upregulation of NOS expressing neurons in auditory brainstem nuclei, suggesting that NO signalling might be related to tinnitus, and in Chapter 5 I present electrophysiological data recorded in a salicylate based animal model of tinnitus. The literature discussion from the Introduction and the data discussed in the Chapters 3, 4 and 5 will be summarised and synthesized in Chapter 6 in a final discussion.

The three data chapters aim to further our understanding of NOS and NO signalling in the IC, but before this data is discussed, I will first introduce a number of topics which at first may seem unrelated but are all of vital importance to understanding the full picture.

I will start this Introduction with a discussion of the IC and its place in the auditory brainstem pathway, with a particular focus on the structures and connections that are important to understanding the role of the IC in auditory processing. I will discuss the main cell types and neurotransmission occurring in the IC along with some markers of specific neurotransmitter phenotypes. The neurotransmitter phenotypes will bring me to focus on glutamatergic neurotransmission and in particular on the NMDA receptor. NMDA receptor activity has been linked to the production of NO and is therefore of special interest. Once this link is clear I will explain the NOS protein followed by a discussion of the NO signalling cascade. Because there is a potential link between NO, NMDA and tinnitus I will give a short background on tinnitus and highlight some key elements from the tinnitus research, I will focus on the studies using salicylate to induce tinnitus because in Chapter 5 data extending previous work on salicylate models of tinnitus will be presented. Therefore in the Introduction some discussion of how salicylate affects the brain and the auditory pathway is required.

1.3 The IC and the Auditory Brainstem Pathway

The auditory system is capable of transducing and perceiving an astonishingly large spectrum of frequencies and levels, which in the form of complex sounds, such as conspecific vocalisations and in human speech and music, can be perceived and localised in space and time with remarkable accuracy. Unlike vision where objects imaged on the retina are spatially organised, the location of a sound source is not extracted at the sense

organ (cochlea), it requires the auditory brainstem pathway to compare the inputs from the two ears. Furthermore, because sounds are rapidly changing waveforms the encoding of precise timing is critical in auditory processing. Highly specialised mechanisms are required to extract these features. Neurons in the auditory pathway display some of fastest spike rates observed in the central nervous system (Altschuler and Shore, 2010). Therefore, the organisation of the auditory brainstem pathway leading to the cortex is more complex compared to the visual, olfactory and gustatory systems which have shorter, more direct pathways to the cortex. All features extracted in the auditory brainstem pathway are projected to the IC, the principal midbrain nucleus in the auditory pathway that processes virtually all ascending information before projecting it to the medial geniculate body (MGB) the auditory thalamus.

1.3.1 The IC Structure

The inferior colliculus (IC), meaning lower (posterior) hill in Latin, is located in the posterior half of the midbrain, one colliculus in each hemisphere, connected to one another through the commissure. The IC colliculi lay caudal to the superior colliculus together with which it forms the tectum. The IC is traditionally described as comprised of three principal subdivisions, the central nucleus, the dorsal cortex, and the lateral or external cortex as depicted in Figure 1-1. Although within these subdivisions distinct nuclei that differ in neuronal structure (Morest and Oliver, 1984; Malmierca *et al.*, 2005) and cytoarchitectual makeup (Chernock *et al.*, 2004) have been recognised.

The central nucleus is easily recognised in Golgi labelled preparations by the laminated neuropil showing disc shaped dendritic fields (Figure 1-1 Left), whereas the cortices show a more loosely defined neuropil labelling, with layers running orthogonal to those in the central nucleus (Jhaveri and Morest, 1982). The subdivisions based on Golgi labelling were suggested to have strict boundaries, however, although labelling protocols employing NADPH diaphorase and immunohistochemistry targeting NOS and other markers (e.g. calcium binding proteins) largely follow that architecture, the boundaries appear to be more gradual than previously believed (Druga and Syka, 1993; Coote and Rees, 2008) (Oliver, 2005a).

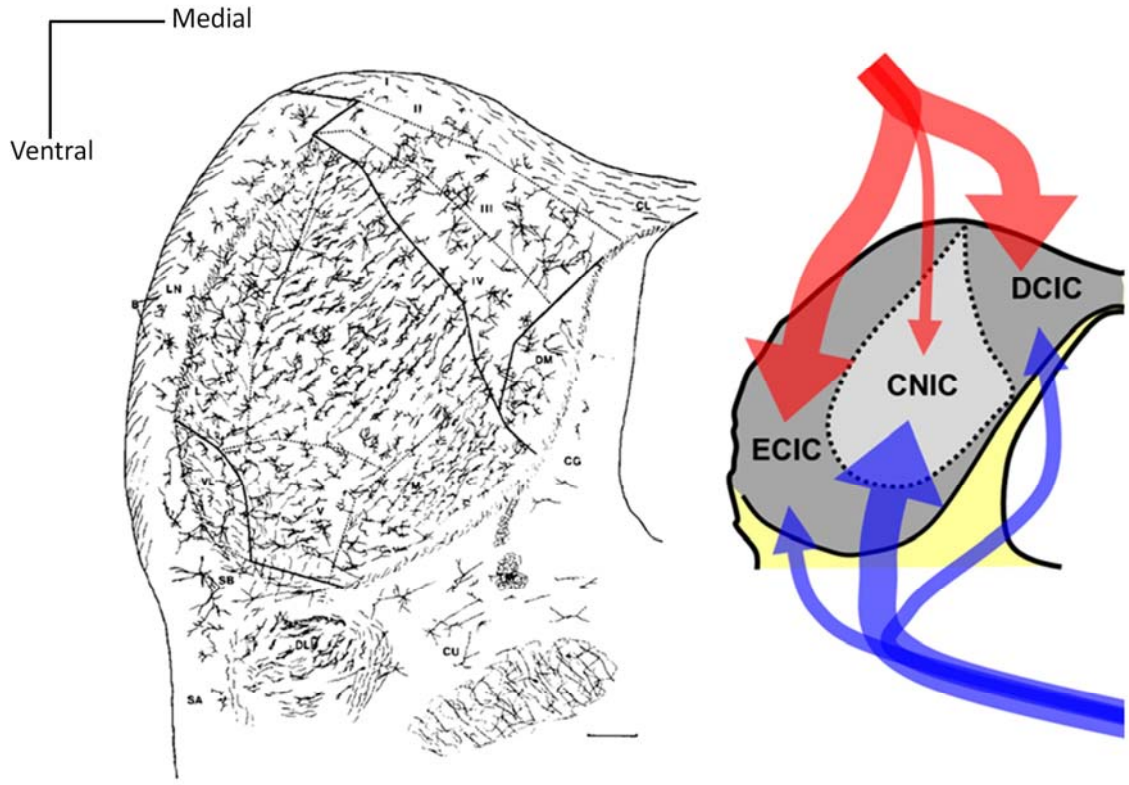

Figure 1-1 Left: a Golgi-impregnated IC coronal section in cat showing the neuronal organisation in the three regions of the IC; the dorsal cortex, the lateral cortex and the central nucleus. Adapted from Morest and Oliver 1984. Right: a schematic drawing of the IC, the arrows indicate its main sources of input. Blue indicates ascending stream of information, while red represent the corticofugal innervation.

The lateral and dorsal cortex receive relatively little ascending auditory input from lower level brain stem nuclei and are believed to get their auditory information from intracollicular connections arising from the central nucleus (Malmierca *et al.*, 1995) and corticofugal connections from the cortex (Winer *et al.*, 1998). The nuclei in the lateral cortex have been described as being multisensory and receive input from and send projections to both auditory and non-auditory structures. Somatosensory information has been shown to influence auditory processing in the inferior colliculus (Aitkin *et al.*, 1978; Aitkin *et al.*, 1981; Szczepaniak and Møller, 1993). Although the auditory cortex has been shown to project most intensely to the dorsal and lateral cortex, a gradient of corticofugal projections that extends well into the central nucleus has been demonstrated (Feliciano and Potashner, 1995), indicating that the auditory cortex directly influences auditory processing in the IC.

The central nucleus is exclusively involved in auditory processing and is an absolute requirement for normal auditory processing (Tokunaga *et al.*, 1984; Jenkins and Masterton, 1982; Kelly and Kavanagh, 1994). The central nucleus is a highly laminated structure which receives the bulk of its information from ascending glutamatergic projections (Winer and Schreiner, 2005b; Ito *et al.*, 2009). Like many other auditory structures, the central nucleus

has a tonotopic organisation that preserves the tonotopic map from the basilar membrane. (Rose *et al.*, 1966; Merzenich and Reid, 1974). The innervating fibres tuned to low frequencies terminating in the dorsal areas of the central nucleus whereas the fibres tuned to high frequencies terminate in ventral areas of the central nucleus.

1.3.2 Input to the IC

The IC is strategically placed at the top of the brain stem and is a central hub for auditory information. The IC receives and processes virtually all ascending auditory information from the lower level auditory brainstem nuclei before projecting it onwards to the auditory thalamus (MGB). In addition to these ascending projections, the IC receives direct projections from its contralateral counterpart as well as corticofugal projections from the auditory cortex (Malmierca, 2004). The most important projections the IC receives are summarised in Figure 1-2.

Auditory brainstem pathway

The changes in air pressure which constitute sound waves are mechanically transmitted through the outer and middle ear to be transduced by the hair cells on the basilar membrane in the organ of Corti in the cochlea. The sound pressure fluctuations in the acoustic environment are conducted by the middle ear to evoke pressure waves in the cochlear fluid. The one row of inner hair cells forming part of the organ of Corti sitting on the basilar membrane detect these pressure waves and transduces them into action potentials which leave the cochlea via the auditory nerve (AN) (Dallos, 1992; Fettiplace and Hackney, 2006). The mammalian cochlea also contains three rows of outer hair cells, which are involved in amplifying the travelling wave on the basilar membrane evoked by the incoming stimuli (Dallos, 1992). The transduced signals from the cochlea enter the brainstem via the auditory nerve (AN), which is the first site in the auditory pathway where action potentials relaying auditory information are observed.

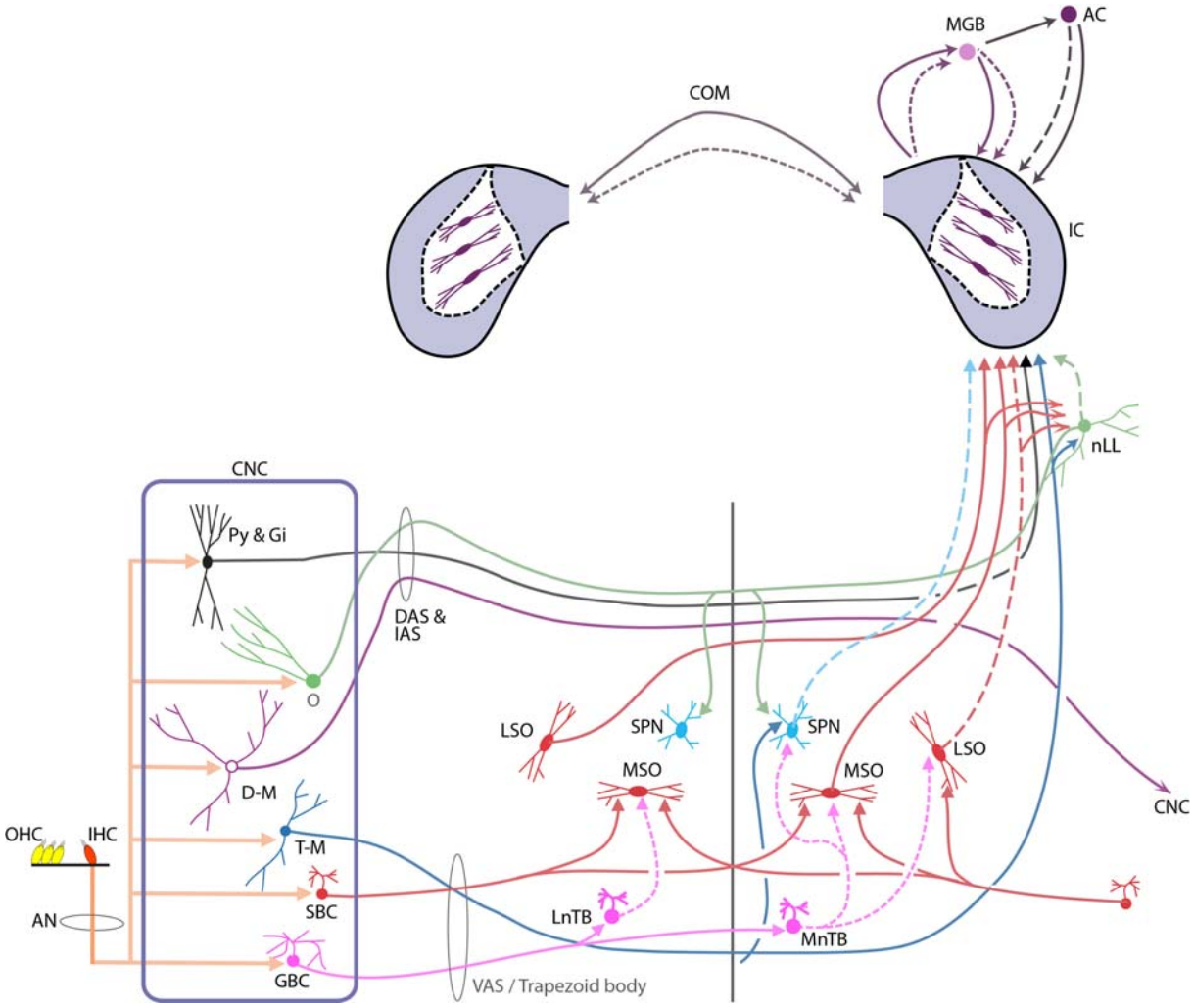

Figure 1-2 Auditory pathway highlighting the projections to the IC. Solid lines: Glutamatergic projections, Dashed lines: GABAergic projections. Terminals are indicated by triangles. The major pathways (DAS, IAS and VAS/Trapezoid body arising from distinct cell types in the CNC (blue rectangle). Abbreviations: OHC(outer hair cells), IHC(inner hair cells), AN (Auditory nerve),CNC (cochlear nuclear complex) GBC (globular bushy cells), SBC (spherical bushy cells), T-M (T-stellate cells), D-M (D-stellate cells), O (octopus cells), PY (pyramidal cells), Gi (giant cells), DAS, IAS and VAS (dorsal, intermediate and ventral acoustic striae), LnTB (lateral nucleus of the trapezoid body), MnTB (medial nucleus of the trapezoid body), MSO (medial superior olive), LSO (lateral superior olive), SPN (superior paraolivary nucleus), nLL (nucleus of the lateral lemniscus), IC (inferior colliculus),COM (commissure of the IC), AC (auditory cortex), MGB (medial geniculate body).Figure adapted with permission from (original by) Prof. E.D. Young.

The auditory nerve bifurcates in the cochlear nuclear complex (CNC) with one branch innervating the anterior ventral cochlear nucleus (AVCN) and the other innervating both the dorsal cochlear nucleus (DCN) and the posterior ventral cochlear nucleus (PVCN) which in turn also innervates the DCN. The tonotopic organisation from the basilar membrane is preserved in all three sub nuclei (Ryugo and Parks, 2003). The AN fibres terminate on distinct highly specialised cell types that in turn give rise to three principal parallel auditory processing pathways the dorsal, intermediate and ventral acoustic striae (DAS, IAS and VAS/trapezoid body). The specialised cells in the CNC and the pathways they give rise to are illustrated in Figure 1-2. The five major cell types have distinct morphologies and

electrophysiological profiles and are associated with specific auditory information and unique projections to other auditory structures.

Pyramidal and giant cells project directly from the DCN through the DAS to the contralateral IC. Octopus cells project via the IAS to the contralateral superior paraolivary nucleus (SPN) and to the ventral nuclei of the lateral lemniscus (VnLL), which in turn projects to the IC (Cant and Benson, 2003). Octopus cells are the only cells in the CNC that do not receive any form of inhibitory input (Osen *et al.*, 1991) and are believed to signal pitch. The multipolar cells are signalling for the spectral properties of the sound. The D-stellate cells project from the CNC directly to the contralateral CNC (Doucet and Ryugo, 1997) and have been shown to be the only glycinergic projections to arise from the CNC (Kolston *et al.*, 1992). The T-stellate cells project through the VAS to both the central nucleus of the IC and to the (nLL) which in turn also projects to the central nucleus of the IC (Adams, 1979; Malmierca *et al.*, 2005). The spherical bushy cells in the VCN project to the medial superior olive (MSO) and the lateral superior olive (LSO). The projections to the MSO are bilateral with symmetrical connections on both sides (Cant and Benson, 2003). The globular bushy cells form large synapses on the contralateral medial nucleus of the trapezoid body (MnTB) which in turn projects an inhibitory glycinergic input to the MSO and LSO (Cant and Hyson, 1992). The globular bushy cells also synapse on the lateral nucleus of the trapezoid body (LnTB) which sends glycinergic projections to the MSO and back to the CNC (not shown in Figure 1-2). The MSO and LSO receive their excitatory input from the spherical bushy cells and their inhibitory, largely glycinergic input indirectly from the globular bushy cells via the MnTB (Cant and Hyson, 1992). Owing to the fact that both the LSO and the MSO receive symmetrical input from both ears allows these centres to perform calculations necessary for sound localisation in the horizontal plane (Shepherd, 2003). The projections of the CNC via the MSO to the nLL and the IC are largely concerned with processing of interaural time difference, and those from the CNC via the LSO and nLL to the IC are principally concerned with interaural level differences. The direct connections from the DCN to the IC carry pinna cues that allow for the location of sounds in the vertical plane.

On top of this large number of ascending neuronal connections, the IC receives a vast number of corticofugal projections from the AC and MGB, which constitute top down inputs. Although, the AC and MGB also project to some of the lower level auditory brainstem nuclei independent from the IC (Schofield, 2010).

1.3.3 Outputs of the IC

The main target of axonal efferent IC projections is the MGB of the thalamus, the connections are bilateral (Andersen *et al.*, 1980) and the projections from the central nucleus of the IC to the ventral MGB retain their tonotopic organisation but are unusual in the sense that these projections are both glutamatergic and GABAergic (Winer *et al.*, 1996; Gelfand, 2016). The IC also has extensive intrinsic connections and forms dense commissural connections with its counterpart in the other hemisphere (Malmierca *et al.*, 1995).

Retrograde and anterograde tracer studies showed that the central nucleus of the IC has direct descending projections to the dorsal nLL, the SPN, MSO, lateral regions of the LSO, the ventral nucleus of the trapezoid body and the CNC (Malmierca and Rees, 1996; Oliver *et al.*, 1999). The external cortex of the IC has been shown to send projections to nucleus sagulum, the rostral periolivary nucleus, the ventral nucleus of the trapezoid body and again the CNC (Caicedo and Herbert, 1993).

The IC also projects to the amygdala via the MGB, and these connection are likely to mediate aversive responses (LeDoux *et al.*, 1984). Although the central nucleus is generally described as being auditory some studies have shown that manipulating neuronal activity in the ventral central nucleus of the IC can impact motor behaviour (De Araújo Moreira *et al.*, 2003) suggesting that the central nucleus does project to non-auditory brain regions. The IC also receives some projections from and sends some projections to non-auditory structures (e.g. the tegmentum, the substantia nigra, the superior colliculus as well as the spinal trigeminal and posterior column nuclei) (Tokunaga *et al.*, 1984) suggesting direct involvement in multisensory integration as well as direct links to orienting behaviour (Casseday *et al.*, 2002; Malmierca, 2004).

Thus the main target of the IC is the MGB, but the IC also projects to many of the auditory structures it receives input from and also has direct inputs to the striatum and sensorimotor areas which are presumed to be related to orienting behaviours necessary for survival (De Araújo Moreira *et al.*, 2003).

1.3.4 Conclusion IC and Auditory Pathway

Thus, four general principles govern the auditory pathway. Firstly, the separation of information is already initiated at the first relay station, the cochlear nuclei. Secondly, the information is processed in highly segregated and parallel pathways dedicated to specific features (frequency, level and timing) of the auditory stimuli. Thirdly, there are many bilateral and commissural projections, such that unilateral lesions within the auditory pathway rarely give rise to hearing deficits in one ear (Hudspeth 2000). Finally, the auditory system has many descending projections from the auditory cortex to almost all brainstem nuclei, suggesting a bidirectional flow of information (Malmierca and Hackett 2010, Schofield 2010, Bajo and King 2012, Nakamoto, Mellott et al. 2013).

1.4 Neuronal Organisation of the IC

The five distinct cell populations in the CNC that give rise to these parallel pathways dedicated to the processing of frequency, level and timing have each their unique morphological characteristics and electrophysiological response profiles, that makes them readily identifiable. Virtually all activity that originates from these five populations that travel through the DAS, IAS and VAS is eventually projected to the IC. However, in the IC the unique and direct mapping of cell morphology to electrophysiological response profile no longer exists. The IC expresses an astonishing number of different cell types and response patterns depending on the subdivision in question and even within these regions a wide variety of cell types and responses have been reported. In spite of this complexity, some broad classes of neurons have been described in the IC.

1.4.1 Cell Types in the IC

The laminar organisation of the central nucleus that provides the structural basis for the tonotopic organisation is observed in all species (Schreiner and Langner, 1997). In Golgi preparations of the rat IC, two broad classes of cells are recognised in the IC, the so called flat cells and less flat cells (Malmierca *et al.*, 1993). The flat and less flat cells broadly correspond to the previously described disc-shaped and stellate cells described in the cat IC (Morest and Oliver, 1984). The flat cells have dense dendritic sprouting which is approximately 50 µm wide, they are oriented parallel to the incoming ascending nerve fibres and form one cell thick laminae (Faye-Lund and Osen, 1985). The laminae comprised of the flat cells are separated by interlaminar layers which are populated by the less flat cells which have less dense dendritic sprouting, but cover a wider area, approximately 100 µm

(Malmierca *et al.*, 1993). The interlaminar compartments are less distinct in the dorsal layers of the central nucleus and it is likely distinct subtypes exist within these two broad subclasses of neurons. Thus far no direct correlation between morphology and electrophysiological response profile has been observed (Sivaramakrishnan and Oliver, 2001; Wallace *et al.*, 2012).

Other methods of classifying cells investigate the protein content of the cells. Markers to be discussed here are NADPH diaphorase, calcium binding proteins and the vesicular transporters VGLUT1 and VGLUT2.

NADPH Diaphorase

NADPH diaphorase was shown to label exclusively nitric oxide synthase in glutaraldehyde fixed preparations (Bredt *et al.*, 1991; Dawson *et al.*, 1991; Hope *et al.*, 1991). NADPH diaphorase preparations show dense neuropil labelling in the dorsal and lateral cortex leaves the central nucleus virtually unlabelled, suggesting that little to no NOS is expressed in the central nucleus (Druga and Syka, 1993). NADPH diaphorase has been shown to exclusively label these three NOS proteins (Bredt *et al.*, 1991; Dawson *et al.*, 1991; Hope *et al.*, 1991) and has enabled identification of tissues and brain-regions expressing these genes.

Calcium binding proteins

The three calcium binding proteins, calbindin D-28k, calretinin and parvalbumin are three of the best known members of a large superfamily of EF-hand calcium binding proteins. These three proteins are the most abundant fast acting cytoplasmic calcium buffers in the central nervous system and are often implicated in neurological disorders and age related decline. They have also been used extensively as cell type markers in studies of the central nervous system. In the cerebral cortex, the EF-hand calcium binding protein parvalbumin has been shown to mark a distinct group of GABAergic interneurons (Cowan *et al.*, 1990; Demeulemeester *et al.*, 1991; Schwaller *et al.*, 2002).

Calcium binding proteins are involved in calcium signalling and maintaining calcium homeostasis and can be broadly subdivided into two different classes, the calcium buffering class and a calcium sensor class (Schwaller, 2009). Although the boundaries between these classes have begun to blur, the distinction is still relevant. Calcium sensors depend on specific calcium levels to undergo a conformational change which acts as an on-off switch (Ikura, 1996). One of the most studied calcium sensors is calmodulin and this still serves as a prototypical calcium binding protein (Kretsinger and Wasserman, 1980).

Calmodulin is essential for the functioning of NOS. Whilst calcium sensor proteins undergo a conformational change and can alter downstream signalling, calcium buffering proteins show no sign of this but seem purely to regulate intracellular calcium levels (Augustine *et al.*, 2003). Calbindin and calretinin have been shown to have calcium sensor functions whereas parvalbumin is believed to be a true calcium buffer due to the absence of a conformational change by binding calcium (Baldellon *et al.*, 1998).

In humans over 240 different EF-hand proteins have been identified thus far. Within this family, two calbindin proteins are known, calbindin D-9k and calbindin D-28k, where the D signifies their dependence on vitamin D and the numbers refer to their molecular weight in kDa (Schwaller, 2009). In spite of their similar names, there is little similarity between these two proteins. In this thesis wherever calbindin is mentioned this will refer to calbindin D-28k, which is closely related to calretinin.

In the IC the calcium binding proteins calbindin, calretinin and parvalbumin have been shown to delineate the three subdivisions remarkably well. Parvalbumin has been shown to be densely expressed in the central nucleus while calbindin and calretinin are exclusively expressed in the dorsal and lateral cortex (Oliver, 2005a) although the specific roles of the cells expressing them are largely unknown.

Vesicular transporters

The vesicular transporters VGLUT1, VGLUT2 and VGLUT3 have been used extensively as markers for glutamatergic neurotransmission. Because glutamate is present in all cells, it has been difficult to identify glutamatergic cells. The VGLUTs are transporters responsible for packaging glutamate into vesicles, and as such are present only in cells which use glutamate as a neurotransmitter (Altschuler *et al.*, 2008; Altschuler and Shore, 2010). There is no evidence for the presence of VGLUT3 positive terminals in the IC (Ito *et al.*, 2009) and they will not be discussed further. Both VGLUT1 and VGLUT2 positive terminals have been observed in abundance in the IC (Altschuler *et al.*, 2008; Ito *et al.*, 2009; Altschuler and Shore, 2010).

Thus far no evidence has been found suggesting that VGLUT1 is synthesized in the IC indicating that these terminals are projections from elsewhere, but predominantly from the cortex (Ito *et al.*, 2011; Fujimoto *et al.*, 2016). In situ hybridization studies have shown that only VGLUT2 is actively synthesized in the IC (Ito and Oliver, 2010; Ito *et al.*, 2011; Fujimoto *et al.*, 2016) as well as in other auditory brainstem structures. Cells receiving only VGLUT2 terminals are therefore necessarily connections from lower level auditory structures to the

IC or internal connections. Cells receiving mixed terminals containing both VGLUT1 and VGLUT2 have been shown to originate largely from the VCN with minor contributions from the SOC and the nLL (Ito and Oliver, 2010). Altschuler et al. (2008) reported that large cells in the IC were surrounded densely by VGLUT2 positive terminals, which were later shown to be large GABAergic neurons in the central nucleus of the IC (Ito *et al.*, 2009). Smaller GABAergic cells did not receive this dense input onto their cell bodies.

Conclusion Cell Types in the IC

Cell morphology and protein content can tell us about the functions cells perform, but neurons transmit information to the cells with which they connect, and their phenotypical neurotransmitter profile can tell us whether cells are excitatory or inhibitory in nature. Because this phenotypical neurotransmitter profile is important for this thesis this topic has its own section but forms a natural extension of the types of cells expressed in the IC. Whether a neurotransmitter exerts an excitatory or inhibitory effect on the recipient cell is governed by the receptor, not the signalling molecule itself. However, glutamate is recognised as an excitatory neurotransmitter in the adult mammalian nervous system whereas gamma-aminobutyric acid (GABA) and glycine mediate inhibitory signalling in the adult mammalian nervous system.

1.5 Transmitter Phenotype in the IC

It comes as no surprise that a structure that receives a diverse set of the inputs from a large number of distinct brain regions shows immunoreactivity for a wide variety of neurotransmitters, among which but not limited to glutamate, glycine, GABA, dopamine, serotonin and acetylcholine (Wynne *et al.*, 1995; Winer and Schreiner, 2005a). However, the only two neurotransmitters synthesized in the IC are glutamate and GABA. About 20-25% of the neurons in the IC are believed to be GABAergic (Riquelme *et al.*, 2001; Merchán *et al.*, 2005), and because there are no glycinergic cell bodies in the IC, the remaining neurons are believed to be glutamatergic and hence involved in excitatory neurotransmission. Since only GABA and glutamate are synthesized in the IC, I will focus the discussion on those two neurotransmitters.

1.5.1 GABA

GABA is the main inhibitory neurotransmitter in the adult nervous system of vertebrates. Exogenous GABA cannot penetrate the blood brain barrier and has to be produced within the brain. The production of GABA is governed by glutamate decarboxylase (GAD). GAD catalyses the decarboxylation of glutamate to GABA and carbon dioxide. In mammals two isoforms, GAD65 and GAD67, with distinct subcellular location are known, the numbers refer to their respective molecular weight in kDa. GAD67 is cytosolic and can be found anywhere in the cell whereas GAD65 is only found in the terminals (Esclapez et al., 1994). Cells expressing either or both GAD proteins are able to catalyse the reaction from glutamate to GABA are considered to be GABAergic.

The IC receives ascending GABAergic and glycinergic projections from the lower brainstem nuclei as well as descending GABAergic projections from the auditory cortex. In addition, the IC contains GABAergic cell bodies that project internally and via commissural connections to the contralateral IC. The IC sends GABAergic ascending projections to the MGB and descending projections to the lower level auditory brainstem nuclei (Schofield, 2010; Malmierca, 2010).

GABA has been shown to play a crucial role in temporal processing and sound localisation in the IC (Caspary *et al.*, 2008). GABA and glycinergic synapses in the central nucleus of the IC are actively involved in generating frequency-responses areas (LeBeau *et al.*, 2001), as well as strongly influencing the temporal response patterns (Le Beau *et al.*, 1996). Thus indicating that the IC plays an active role in shaping the auditory precepts it projects to the MGB.

Also GABA projections from the IC to pedunculopontine tegmental nucleus, the laterodorsal tegmental nucleus and substantia nigra pars reticulata have been related to pre-pulse inhibition of the startle reflex (Fendt *et al.*, 2001) and reduced GABAergic activity in the IC has been shown to be involved in the generation of audiogenic seizures (Faingold, 2002).

1.5.2 Glutamate

Due to the transitory nature of sound, any system trying to capture, analyse and extract information from the auditory environment has only a short time window in which to do so. The brain goes to extraordinary lengths to capture and analyse as much information from the auditory environment as it can. Excitatory neurotransmission is of essential importance for the relay of the sound signals, transduced in the cochlea, to the auditory cortex. The

main neurotransmitter employed in excitatory neurotransmission anywhere in the vertebrate brain, accounting for around 90% of the total synaptic connections in the brain, is the amino acid glutamate (Meldrum, 2000). Glutamate has been shown to be the main excitatory neurotransmitter in the IC (Faingold *et al.*, 1989; Kelly and Caspary, 2005) and the release of glutamate is detected and transduced by a set of glutamate receptors with distinct properties.

1.5.3 Glutamate Receptors

Glutamate receptors come in two families, both of which are present in the IC, the ionotropic and the metabotropic receptors; both comprise a substantial number of family members with different properties (Meldrum, 2000). The ionotropic, ligand-gated ion channel receptors are fast acting, whereas the metabotropic G-coupled receptor proteins produce slower, longer lasting signals. Within the ionotropic family, we recognise three different types of ionotropic glutamate receptors which derive their name from the pharmacological agonists that selectively bind to these receptors (Patneau and Mayer, 1990; Dingledine *et al.*, 1999; Platt, 2007). The α-amino-3-hydroxy-5-methyl-4-isoxazolepropionic acid (AMPA) and N-methyl-D-aspartate (NMDA) receptors are the most abundant in the auditory pathway (Parks, 2000), therefore I will focus on those two and not discuss the third class of ionotropic glutamate receptors, the kainate receptor.

The permeability of the AMPA and NMDA receptors to the cations calcium (Ca^{2+}), sodium (Na^{+}) and potassium (K^{+}) is determined by the subunit composition (Dingledine *et al.*, 1999; Platt, 2007). The subunit configuration of AMPA and NMDA receptors varies between brain areas, cells and even between individual synapses of the same cell (Martin *et al.*, 1993; Law *et al.*, 2003; Altschuler and Shore, 2010). AMPA receptors and NMDA receptors are usually expressed in the same cells and fulfil complimentary roles (Ma *et al.*, 2002).

1.5.4 AMPA Receptors

In the auditory brainstem pathway, a specific AMPA receptor subunit composition dubbed ‘auditory specific’ is described in all brainstem nuclei (Trussell, 1997). This specific AMPA subunit composition results in rapid deactivation and desensitisation and leads to a relatively high permeability to Ca^{2+} (Hollmann and Heinemann, 1994). This ‘auditory specific’ composition is observed in virtually all auditory brainstem nuclei but is absent in the IC (Schmid *et al.*, 2001), where the AMPA subunit composition in the IC confers a low Ca^{2+} permeability.

Although exceptional circumstances exist as discussed below, glutamate exerts its initial and almost instantaneous effect by binding to the AMPA receptors. Binding of glutamate to the AMPA receptor opens the ion channel almost instantaneously (Tzschentke, 2002) but AMPA receptors undergo rapid deactivation and desensitisation, the ion channels governed by the receptor can close within one millisecond of activation (Platt, 2007), allowing neurons expressing this receptor to display incredibly fast firing rates. These firing rates allow the auditory system the fast temporal coding required to keep up with the acoustic environment.

1.5.5 NMDA Receptors

In resting state conditions the NMDA receptors are blocked in a voltage dependent manner by extracellular magnesium (Mg^{2+}) preventing the opening of the ion channel (Kelly and Zhang, 2002). The activation of the AMPA receptor causes a depolarisation of the cell membrane and repels the Mg^{2+} from the NMDA receptor allowing the glutamate, or any other NMDA receptor agonist, to bind to the NMDA receptor and open the ion channels allowing the cations calcium (Ca^{2+}), sodium (Na^{+}) and potassium (K^{+}) to flow through the channel in a voltage dependent manner.

NMDA receptor coupled ion channels open about 10 ms after the release of glutamate in the synaptic cleft and can remain open for hundreds of milliseconds, only closing when glutamate detaches from the receptor (Dzubay and Jahr, 1996). NMDA receptors are built from a variety of subunits with a mandatory GluN1 subunit and a variable mix of GluN2A, B, C or D and GluN3A or B subunits: although a functional receptor requires at least one GluN2 subunit. The NMDA receptor possesses two agonist binding sites and requires glycine as co-agonist to glutamate (Kleckner and Dingledine, 1988) (Johnson and Ascher, 1987). Receptors with a blocked or unoccupied glycine binding site will not be able to respond to the binding of glutamate (Qian and Johnson, 2002). It is generally believed that glycine binds to GluN1 and glutamate to the GluN2 subunits explaining the need to have both a GluN1 and GluN2 subunit in a functional NMDA receptor complex (Cull-Candy *et al.*, 2001). NMDA receptor subunit composition in the auditory brainstem structures has been shown to change during maturation and aging. Young and developing auditory structures show high expression of GluN2A subunits which are characterised by fast but relatively short lived opening times of the associated ion channels, lasting tens of milliseconds. Mature auditory structures show less GluN2A in favour of GluN2B resulting in long opening times in the hundred plus millisecond range (Faingold *et al.*, 1989; Knipper *et al.*, 1997; Knipper *et al.*, 2013; Van De Heyning *et al.*, 2014). Gene expression studies investigating the different subunits show that the mRNA of the GluN1A receptor is by far the most

expressed in the IC making up over 93% of the mRNA related to NMDA receptors expressed (Goebel and Poosch, 1999). The remaining 7% is reasonably equally divided among the other subunits with a slight preference for GluN2D and GluN3A of which the latter makes the receptor less permeable to calcium (Goebel and Poosch, 1999; Cull-Candy *et al.*, 2001). However, these findings do not necessarily relate to the protein content of the cells because, due to post translational processes, mRNA expression levels do not translate one to one to protein content. Currently, the NMDA subunit composition at the protein level among the subdivisions of the IC is unknown.

NMDA receptor activity in the cochlea and auditory brainstem pathway has been linked to several pathological states. Blocking NMDA functioning with an NMDA antagonist post noise trauma delayed the reformation of synapses and restoration of cochlear functioning (D'Aldin *et al.*, 1997). Although NMDA receptor activity was shown to have neuroprotective effects in age related hearing loss in spiral ganglion cells (Peng *et al.*, 2013), hyperactivity of this receptor has been linked to long lasting and/or permanent neuronal damage. This is believed to be related to prolonged influx of calcium in the cells, due to the NMDA receptor activity, triggering several signalling cascades and ultimately resulting in cell death (Sahley *et al.*, 2013). Reducing NMDA receptor activity following noise-induced trauma has been shown to reduce chronic damage to the cochlea (Puel *et al.*, 1998) and prevents salicylate-induced tinnitus (Puel, 2007).

1.5.6 Glutamate Signalling in the IC

The speed with which the AMPA currents are generated throughout the auditory brainstem pathway is important for the maintenance of high fidelity signalling and underlies the pathway's fast and precise temporal coding (Trussell, 1998; Sanchez *et al.*, 2015). AMPA receptors are mainly involved in the short latency responses (<20 ms), of a cell to the presence of glutamate, whereas the NMDA receptors are more heavily involved in maintaining and modulating the later, longer lasting (>100 ms) cellular response to the release of glutamate (Ma *et al.*, 2002).

Although dominated by AMPA receptor-related mechanisms, the fast spiking process in the IC is not completely independent of NMDA receptors and, a subset of NMDA receptors has been shown to be involved in fast spiking activity. Blocking these NMDA receptors, abolished the neurotransmission completely, including the early components of the cellular response, indicating that both AMPA and NMDA receptors are required for successful neurotransmission in the IC (Sanchez *et al.*, 2007). The effects of the NMDA receptor on

the early component of the cellular response are most likely governed by subunit GluN2D which has a lower affinity for magnesium in resting state conditions (Kirson and Yaari, 1996) and in in-vitro studies has been shown to trigger action potentials without the need for depolarization caused by AMPA receptors (Wenzel *et al.*, 1996) (Sivaramakrishnan and Oliver, 2006). In vitro studies show that NMDA receptor activity can actively regulate surface AMPA receptors (Noel *et al.*, 1999; Beattie *et al.*, 2000). In vivo studies have shown that by blocking NMDA mediated activity, the number of AMPA receptors are decreased (Chen *et al.*, 2007).

Even though both NMDA and AMPA receptors can be involved in the generation of immediate fast spiking activity, for the majority of IC neurons, it is the AMPA receptor that facilitates the immediate response to the release of glutamate while the NMDA receptor modulates this response (Bengzon *et al.*, 1999; Altschuler and Shore, 2010). NMDA receptors in the IC have been shown to be an required for long term potentiation (LTP) to take place (Zhang and Wu, 2000). A recent study suggests that NMDA receptors in the IC appear to be involved in LTP and long term depression (LTD) type processes in young animals, although, it remains uncertain whether this is true in mature animals (Sanchez *et al.*, 2015).

The influx of calcium through the NMDA receptor is thought to underlie the involvement of the NMDA receptor in processes that underlie neural plasticity and subsequently facilitates learning and memory (Maren and Baudry, 1995; Feldman and Knudsen, 1998; Lee *et al.*, 2009; Li and Tsien, 2009) (Sanchez *et al.*, 2015). Non-NMDA glutamate receptors in the IC have been shown to have little permeability to calcium (Dingledine *et al.*, 1999; Meldrum, 2000; Platt, 2007) (Pellegrini-Giampietro *et al.*, 1997). Thus most calcium enters the cell through the NMDA receptor channel, triggering several secondary signalling cascades.

The NMDA receptor is anchored in the post synaptic density via its interaction with PSD95, a post synaptic density scaffolding protein. PSD95, as will be discussed in Section 1.7, also associates nNOS and underlies the close coupling in activity observed between the NMDA receptor activity and nNOS activity.

1.6 Nitric Oxide Synthase and Nitric Oxide

1.6.1 The Nitric Oxide Synthase Protein Family

The catalysis of NO in all mammals is governed by the nitric oxide synthase (NOS) family. This family of proteins catalyse the enzymatic conversion of L-arginine to L-citrulline and NO (Alderton *et al.*, 2001; Steinert *et al.*, 2010). In mammals three NOS genes are recognised two of which derive their name from the tissues in which they were first identified- namely neuronal (nNOS) and endothelial (eNOS), the third NOS gene is only expressed under pathological circumstances and is called inducible (iNOS) (Brenman *et al.*, 1996; Steinert *et al.*, 2010; Doucet *et al.*, 2012). Although the names eNOS and nNOS suggest tissue-specific expression some overlap does occur but this can be ignored for our current discussion.

The three NOS genes, which have been conserved through evolution to a high degree, show similarity in their genomic structure suggesting a common ancestral source (Alderton *et al.*, 2001). Each gene codes for a different protein with distinct properties, as illustrated in Figure 1-3, which depicts the three NOS isoforms and their domain structures, eNOS and iNOS are truncated versions of the nNOS protein. nNOS represents the complete protein and includes a PDZ binding motif which both eNOS and iNOS lack. The other domain structures of these proteins have been highly conserved, although iNOS has a different calmodulin domain (CaM). All three NOS isoforms contain a CaM domain but the two constitutive isoforms eNOS and nNOS require free calcium (Ca^{2+}) to bind to this CaM domain in order to be activated (Garthwaite, 1991). Both constitutive NOS complexes are inactive at normal resting state cytosolic free Ca^{2+} levels (approximately 50nM) and maximally activated between 0.4 – 1.0 μM Ca^{2+} (Garthwaite, 1991). The iNOS isoform, on the other hand, has no need for calcium signals as calcium is permanently bound to its CaM domain keeping it in a perpetually active state. Because little eNOS is expressed in the brain, and iNOS is only expressed in pathological states, I will not discuss those two isoforms any further, but instead, focus on nNOS which is the main enzyme for NO production in the brain.

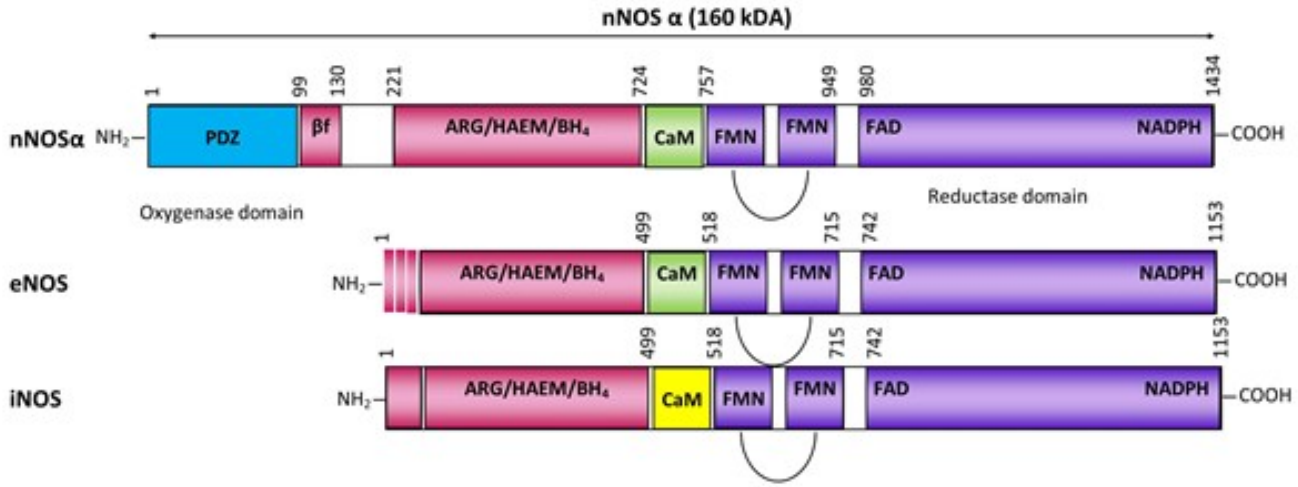

Figure 1-3 Domain structures of nNOSα, eNOS and iNOS. The PDZ binding motif is shown in blue. The oxygenase domain shown in pink contains binding sites for L-Arginine (ARG), haem and tetrahydrobiopterin (BH4). The calmodulin domain that activates NOS in the presence of calcium is depicted in green for nNOS and eNOS but yellow to highlight its difference for iNOS. The reductase domain contains binding sites for NADPH which donates an electron to facilitate the reaction of L-Arginine to L-Citrulline and further binding sites for flavin adenine dinucleotide (FAD) and flavin mononucleotide (FMN). The reductase domain is shown in in purple. The auto inhibitory loop between the FMN regions is also displayed. The amino residue numbers at the start and end of each domain are shown for the human sequence.

1.6.2 Neuronal NOS Splice Variants

The nNOS protein in its complete form is a 1434 amino acid protein, encoded by a gene located on chromosome 12 (Alderton *et al.*, 2001; Doucet *et al.*, 2012). nNOS is abundantly expressed throughout the developing and mature central nervous system but is also observed in the skin, bronchial epithelium, skeletal muscles, kidney and liver cells (Alderton *et al.*, 2001; Guix *et al.*, 2005). nNOS comes in five distinct splice variants, three of which have been shown to be physiologically active, but only two are important for our current discussion. The three physiological active splice variants are depicted in Figure 1-4, but nNOSϒ shows little (<3%) catalytic activity under physiological conditions compared to nNOSα (Corso-Díaz and Krukoff, 2010) and will not be further discussed. That leaves us with nNOSα which is the complete original protein containing the PDZ binding motif on the N-terminal, and nNOSβ which is an exact copy of nNOSα except lacking a PDZ

binding motif (Cho *et al.*, 1992; Brenman *et al.*, 1996; Doucet *et al.*, 2012) (Figure 1-4). Because nNOSβ has no PDZ binding motif it cannot associate itself with PSD95 and is therefore coupled to NMDA receptor activity to a lesser extent. Both nNOSα and nNOSβ are expressed throughout the brain, but under normal circumstances nNOSα accounts for 90% of all nNOS expression in the brain (Langnaese *et al.*, 2007), although higher levels of nNOSβ are observed in the brainstem and cerebellum.

The first nNOS knock-out study reported that nNOS knockout mice were viable without any obvious abnormalities in their central nervous system (Huang *et al.*, 1993). However, by knocking out exon 2 of the nNOS gene, only nNOSα was affected- at the time the splice variants were unknown. The seemingly normal phenotype led to the discovery of nNOSβ which is upregulated and rescues the phenotype when nNOSα is lost (Langnaese *et al.*, 2007). Knock out studies with nNOSα knockouts showed how this affected NMDA receptor GluN1 expression. Although the mRNA expression of GluN1 was unchanged, the actual presence of this subunit in functional proteins was greatly diminished in the absence of nNOSα (Putzke *et al.*, 2000). A full nNOS knockout, however, is also viable although it shows developmental problems, lower bodyweight, infertility and increased aggression (Gyurko *et al.*, 2002).

These data suggest that even though NOSβ is not associated with the NMDA receptor under normal circumstances, in an upregulated state it is capable of performing, at least partly, the necessary functions nNOSα performs. Very little data regarding the expression of nNOSα and nNOSβ is available. In most cells which express nNOS both variants are present, although in the striatum cells expressing only nNOSβ have been observed (Eliasson *et al.*, 1997). nNOSβ has been shown in virtually all brain areas including the IC but remains under researched and there is little information about its functions under normal circumstances. It is currently unknown whether the isoforms nNOSα and nNOSβ perform different functions under normal circumstances. We know little about the expression of either splice variant in the IC. The one mRNA study performed thus far indicated that both are expressed (Eliasson *et al.*, 1997), but took the IC as a whole, and no efforts thus far have been made to study the expression of either splice variant in the different subdivisions of the IC. The in situ hybridization studies also tell us little about the protein content of the cells, since owing to post translational processing, the mRNA content of a cell does not directly translate to protein content.

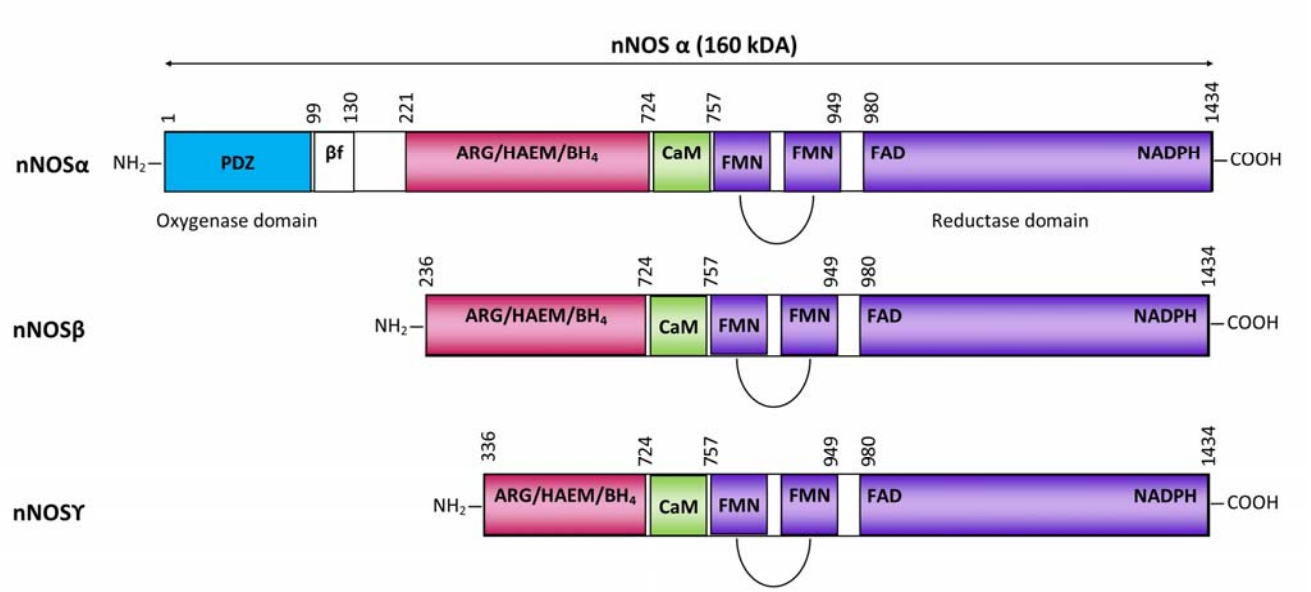

Figure 1-4 nNOS physiological active splice variants, nNOSα is the only splice variant containing a PDZ binding motif (blue). The oxygenase domain shown in pink contains binding sites for L-Arginine (ARG), haem and tetrahydrobiopterin (BH4). The calmodulin domain that activates NOS in the presence of calcium is depicted in green. The reductase domain contains binding sites for NADPH which donates an electron to facilitate the reaction of L-Arginine to L-Citrulline and further binding sites for flavin adenine dinucleotide (FAD) and flavin mononucleotide (FMN). The reductase domain is shown in in purple. The auto inhibitory loop between the FMN regions is also displayed. The amino residue numbers at the start and end of each domain are shown for the human sequence.

1.6.3 NO Formation

NOS proteins catalyse the synthesis of NO and citrulline from L-Arginine (L-Arg), NADPH and O_2 by the following reaction (Feng, 2012):

L-arginine + 3 NADPH + 3 H^+ + 4 O_2 → 3 $NADP^+$ + L-citrulline + NO + 3 H_2O

The L-arginine, H^+ and O_2 bind to the oxygenase domain, whereas the NADPH binds on the reductase domain of the protein. The NADPH functions as the electron donor that allows the conversion of L-arginine to N-hydroxy-L-arginine and subsequently to L-citrulline, NO and H_2O. Quite remarkable is the fact that the NOS proteins produce such high levels of NO while the reaction could just as easily lead to the production of other potentially damaging reactive oxygen species; how the NOS proteins accomplish this level of specificity is currently unknown (Santolini, 2011).

NOS proteins are inactive in their monomeric state (Zhou and Zhu, 2009) because a NOS monomer is unable to transfer the electron obtained from NADPH at the reductase domain through its calmodulin (CaM) domain to the oxygenase domain (Santolini *et al.*, 2001; Santolini, 2011). However, the CaM domain undergoes a conformational change upon the binding of Ca^{2+} and this allows the NOS protein to fold and bind another NOS molecule thus forming a stable and active homodimeric structure (Marletta, 1993; Zhou and Zhu, 2009).

Figure 1-5 shows the nNOSα dimeric structure formation and the electron transfer this arrangement allows (Figure 1-5C). This explains the calcium dependency of nNOS activity. Currently, it is unknown whether heterodimers of nNOSα/nNOSβ are functional or even occur in vivo, but both splice variants are expressed in the IC and this could potentially be an interesting line of research.

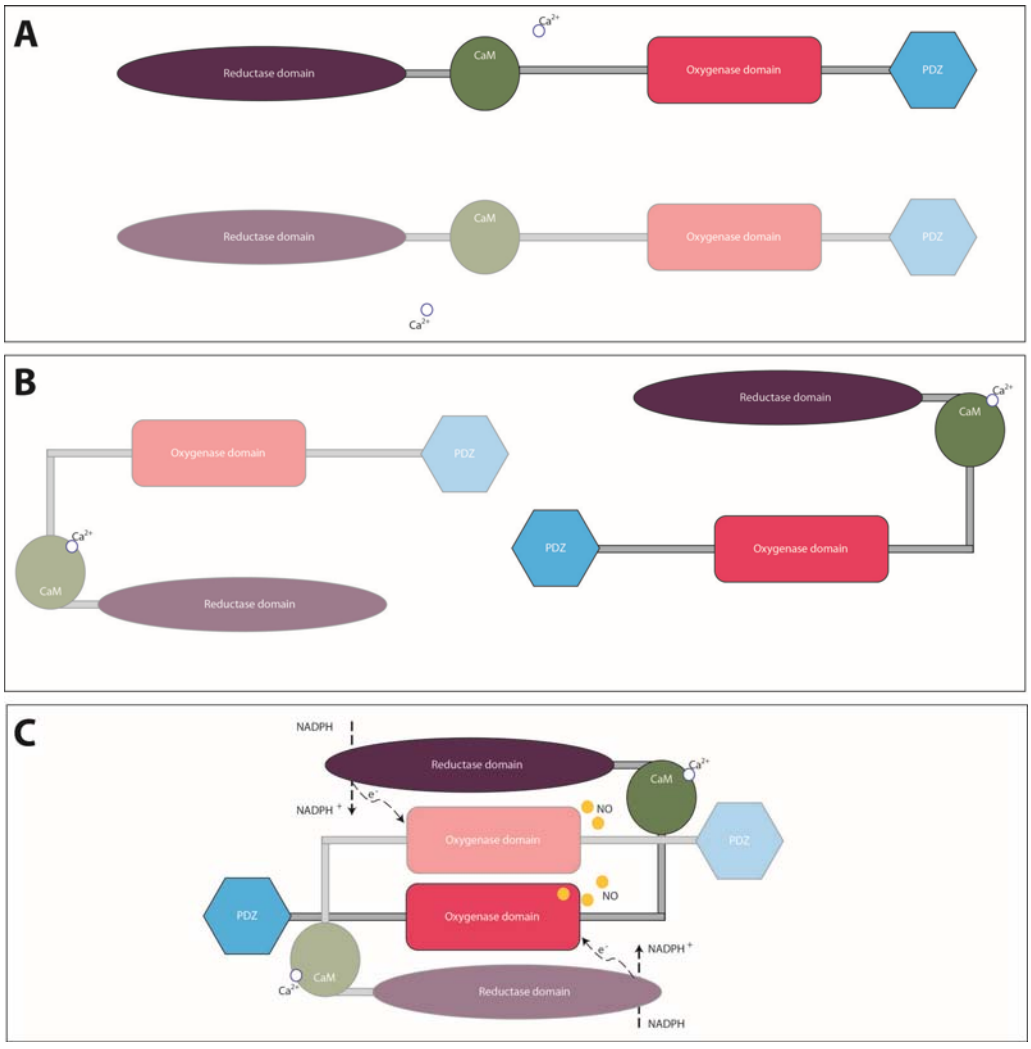

Figure 1-5 sequence depicting the formation of the nNOS homodimeric complex. A. Two inactive nNOSα proteins requiring Ca^{2+} to be activated. B. upon the binding of Ca^{2+} both nNOSα proteins undergo a conformational change, allowing them to bind to each other as displayed in panel C. C. nNOSα homodimer structure where the electrons obtained from the NADPH are transferred to the oxygenase domain of the other nNOS monomer. The conformational change due to calcium binding to the CaM domain is essential for this step to take place. NOS proteins are unable to pass electrons onto their own oxygenase domains. PDZ domains in blue, the reductase domains with the NADPH electron transfer, in purple, the CaM modules in green and the oxygenase domains in pink, Ca^{2+} in white and NO in yellow.

1.6.4 Targets of Nitric Oxide

Because NO is a reactive diatomic gas with a half-life of a few seconds (Cary *et al.*, 2006) it is not constrained by the synaptic or intracellular environment. Due it its gaseous nature NO has the capacity to freely diffuse through cell membranes potentially reaching targets far from the production site. It does not follow the 'normal' rules that apply to neurotransmitters and messenger molecules, thus far NO is always considered a co-transmitter, a messenger molecule operating alongside the main neurotransmitter operating in that cell (e.g. glutamate or GABA). NO has often been described as a possible volume transmitter, and models predicted diffusion over considerable distances from its site of production. However, more recent studies and predictions suggest that the production of NO is strictly regulated and only produced in picomolar concentrations (Hall and Garthwaite, 2009; Wood *et al.*, 2011; Garthwaite, 2016). NO cannot be stored in vesicles and has to be generated when required, the solubility of NO in water is limited to 1mM but due to its gaseous nature it diffuses readily through cell membranes and thus has the potential to exert its effect over an extended area (Garthwaite, 1991).

Figure 1-6 shows the many targets that NO has been shown to regulate. It is unlikely that NO is performing all these functions in all cells and it seems more plausible to assume that different cell types utilise NO for different functions.

NOS is the first target of NO

The first target of NO is the NOS protein itself. At physiological temperatures, the NO produced binds to the Fe^{+} haem domain of NOS that normally binds O_2. While NO is bound to the haem, oxygen cannot bind, and the reaction that produces NO is temporarily blocked (Salerno, 2008). This results in NO being produced in pulses which suggests that information transmission is taking place (Salerno, 2008; Salerno and Ghosh, 2009).

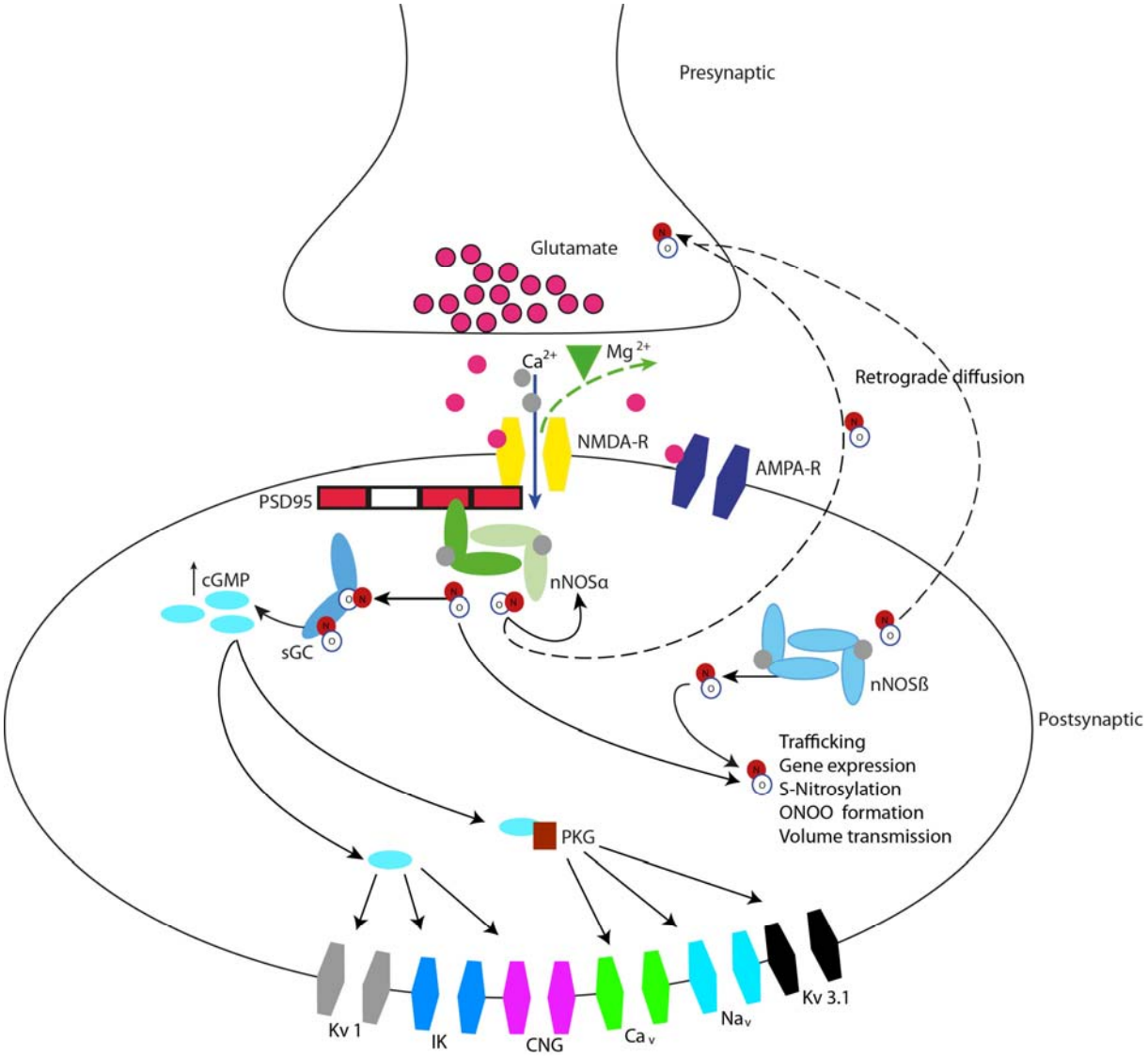

Figure 1-6 Schematic overview of NO and the potential targets it has. NO acts on many ion channels, the most important ones are drawn, via its action on sGC but can perform functions independent of sGC action which are listed in the bottom right. Adapted from Steinert et al (2010). Abbreviations: AMPA-R (AMPA receptor), NMDA-R (NMDA receptor), NO (Nitric Oxide), sGC (soluble Guanylate Cyclase), PKG (protein Kinase G), Kv3.1 (voltage gated potassium channel), Na_v (voltage gated sodium channel), Ca_v (voltage gated calcium channel), CNG (cyclic nucleotide gated ion channels), IK (Adenosine Triphosphate (ATP) sensitive potassium channel), Kv1 (voltage gated potassium channel).

Soluble guanylate cyclase is the main target of nitric oxide

Soluble guanylyl cyclase (sGC) has been shown to be the main target of NO in most brain regions, although some regions show NOS positive labelling but no sGC positive labelling suggesting that NO does not always regulate sGC (Schmidt *et al.*, 1992) and presumably acts via a different intracellular mechanism. sGC is composed of two subunits that both come in a variety of splice variants, interestingly though the splice variant most expressed in the brain is the α2β1 which also has a PDZ domain and is known to associate with PSD95 PDZ domain 3 (Russwurm *et al.*, 2001), thus strongly suggesting that sGC is part of a NOS-PSD95-NMDA receptor signalling complex. The binding of NO to sGC switches on the

conversion of GTP to cGMP (Ahern *et al.*, 2002; Garthwaite, 2005). cGMP acts as a second messenger and its main function is the activation of the protein kinases which then, in turn, phosphorylate other proteins (e.g. Kv 3.1, Ca_v), as depicted in Figure 1-6.

Remarkable is the high specificity with which sGC is able to detect NO over O_2 and CO since sGC employs the same haem domain for binding NO as haemoglobin uses for binding O_2. Yet sGC manages to detect nanomolar concentrations of NO in the constant presence of millimolar concentrations of O_2 (Cary *et al.*, 2006). This is accomplished by sGC undergoing a conformational change upon binding of NO to its haem but not by binding CO or O_2. Any diatomic gas containing oxygen in the form of XO where X can be either N, C or another O can bind to the haem in either a bend or linear configuration. The configuration of choice is dependent on the electrons in the π^* orbitals of the XO molecule. CO has empty π^* orbits and the electrons from the Fe in the haem flow to empty π^*CO and this molecule is most stably bound in a linear configuration which is thus its 'preferred' binding pattern. Oxygen has 2 electrons and NO 1 in the π^* orbitals and hence they bind more stably to sGC in a bend configuration. Because NO has only one electron combined with its 'preferred' bend binding to the haem will alter the stability of the tertiary structure of the sGC protein which than undergoes its conformational change. So O_2 and CO bind with equal affinity to sGC as NO, but only NO binds in the right configuration, destabilising and hence folding the protein to its active state (Poulos, 2006).

In vivo studies have suggested that sGC/cGMP pathway exists in two different states: a tonic and an acute state (Kurtz and Wagner, 1998; Cals-Grierson and Ormerod, 2004). During normal resting state conditions, steady state levels of NO are produced and occupy the haem domain of sGC (Cary *et al.*, 2006). In vitro experiments show that 80% haem occupation by NO produces only 10% catalytic activity in sGC (Russwurm and Koesling, 2004). Dissociation of NO from the haem has been shown to be slow and NO level dependent. When bursts of NO occur the excess NO binds to an as yet unidentified part of sGC producing a hundred fold times more cGMP(Cary *et al.*, 2006) (Zhao and Marletta, 1997; Zhao *et al.*, 1999). Taken together this means that sGC is kept in a low though activated state during resting state conditions, but is capable of detecting increasing pulses of NO. Thus normal steady state activity generated in the auditory pathway may only cause small amounts of NO to be produced, while over excitation may result in the high levels of NO that result in an acute adjustment of the synaptic strength.

Other potential targets of nitric oxide

Another route via which NO is believed to influence cellular activity is S-nitrosylation. However, this requires high amounts of NO to be present and although iNOS is able to produce the required amount of NO, this mechanism probably does not operate in vivo under non-pathological conditions. Evidence suggests that nNOS only produces picomolar concentrations of NO (Hall and Garthwaite, 2009; Wood *et al.*, 2011) while S-nitrosylation requires orders of magnitude higher concentrations of NO (Steinert *et al.*, 2010).

NO production in the brain is believed to be involved with LTP and LTD and through these mechanisms, to be important for memory and learning (Boxall and Garthwaite, 1996; Garthwaite, 2008; Steinert *et al.*, 2010; Hardingham *et al.*, 2013). Different hypothesis about the role NO performs in these processes exist. Most prominent is the hypothesis that NO acts as a retrograde messenger from the post synaptic domain to the presynaptic domain (Steinert *et al.*, 2010). In the cerebellum, a presynaptic role has been established (Jacoby *et al.*, 2001). NO diffusion back to the presynaptic environment has been shown to affect presynaptic calcium-dependent potassium channels (Ahern *et al.*, 1999) resulting in modulation of presynaptic glutamate and GABA release. In order for this to work, the NO produced must be able to target the presynaptic domain with great precision and speed, the nNOS protein must, therefore, be tightly coupled to the receptors transducing the glutamate signals, the only nNOS protein known to associate itself directly with the glutamate receptor NMDA is nNOSα. However, alternative hypotheses have been proposed that suggest the main function of NO in LTP is targeted at postsynaptic sites and not presynaptic (Malenka and Bear, 2004). These hypotheses suggest that synaptic plasticity is achieved by altering the post synaptic currents, for example by modulating voltage gated ion channels (Ahern *et al.*, 2002). NO has been shown to be able to induce phosphorylation of a range of ion channels, as depicted in Figure 1-6, as well as affecting the trafficking of AMPA and NMDA receptors through the cell to the active synaptic zone, thereby further regulating the synaptic strength.

Recent evidence shows that NO targets post synaptic potassium channels (e.g. Kv1 and Kv3) in the medial nucleus of the trapezoid body (Steinert *et al.*, 2008). Increased expression of cGMP by increased NO levels was followed by a reduction in functional Kv3 potassium channels. This resulted in prolonged action potential duration, an effect that was blocked by NMDA receptor antagonists, nNOS and sGC inhibitors, and was absent in nNOS knockout mice (Steinert *et al.*, 2008). Although the largest effects were observed in the potassium channels, modulation of sodium channels, AMPA and NMDA receptors was also

observed. It has been suggested that this mechanism could act as a gain control reducing action potential transmission during periods of high activity. Thus, although NO has the potential to function as a retrograde messenger, that is almost certainly not its only function.

Conclusion nitric oxide

Most studies have been focused on nNOSα which is coupled to the NMDA receptor activity and is believed to be expressed in greater abundance compared to nNOSβ. However, the expression levels of nNOSβ mRNA are higher in the brainstem and midbrain compared to the cortical and hippocampal regions where most functional nNOS studies have been performed (Eliasson *et al.*, 1997). Thus currently little is known about the function of nNOSβ in the brain and we know even less about its potential function in the IC. We know it is expressed in the IC, but not in which subdivisions and whether there is a contrast to be made with nNOSα.

To summarise we can conclude that NO has several potential targets but mainly exerts its effects by binding to sGC. Most targets of NO lead directly or indirectly to changes in synaptic strength. NO binds both to sGC in the pre and post synaptic domain, but due to sGC having a PDZ binding motif like nNOS, most of the NO will most likely bind to sGC postsynaptically. NO temporarily inhibits nNOS leading to pulses of NO. Large bursts of NO bind to a non-haem domain of sGC, increasing cGMP production a hundred fold. nNOSα does not produce enough NO to function as a volume transmitter. However, nNOSβ although less directly influenced by the NMDA receptor activity, could possibly function as volume transmitter.

1.7 Scaffolding Protein PSD95 Essential in Effective NMDA receptor Activity

The postsynaptic density (PSD) is, as the name suggests, located in the postsynaptic part of the synapse. This membrane associating mega-organelle is located in the head of the dendritic spines and is required for postsynaptic signal transduction (Doucet *et al.*, 2012). The PSD ensures that receptor proteins in the active zone of the post-synaptic domain are aligned with the presynaptic active zone. In addition, it provides a framework to connect the receptor proteins and their second messenger proteins to one another (Hering and Sheng, 2001). There are four PSD family members that derive their name from their molecular weight, I will focus on PSD95 due to its involvement with the NMDA receptor and nNOSα. PSD95 is functional as a monomer but can form multimers with other PSD95 proteins and interacts both with ionotropic and metabotropic glutamate receptors and regulates their

coupling to downstream second messengers (Scannevin and Huganir, 2000). An example of such an arrangement is depicted in Figure 1-6, where the interaction between PSD95, the NMDA receptor and the nitric oxide synthase protein (nNOSα) is depicted. In order for calcium influx into the cell to function as a signal carrier, intracellular calcium receptors need to be within 50 nm of the ion channel (Augustine *et al.*, 2003), PSD95 enables downstream targets of the calcium influx to be closely linked to the ion channels. PSD95 associates with receptor proteins via PDZ binding domains. PSD95 has three of these domains and these domains allow proteins that contain a PDZ binding motif to associate themselves with it (Dev, 2004; Feng and Zhang, 2009). Because PSD95 has the ability to associate with many proteins, including other PSD95 molecules it is often referred to as a scaffolding protein, providing a structure on which other proteins can attach (Scannevin and Huganir, 2000). The PDZ domain 1 and 2 of PSD95 are in close proximity to one another and form a rigid structure (Feng and Zhang, 2009; Doucet *et al.*, 2012). NMDA receptors bind preferentially and most stably to PDZ domain 1 and rarely to domain 2 (Kornau *et al.*, 1995; Niethammer *et al.*, 1996) while nNOSα preferably binds to PDZ domain 2 (Brenman *et al.*, 1996). These preferential binding patterns bring the NMDA receptor and the nNOSα protein in close proximity to one another. There is the strong suggestion that at least one subunit composition of sGC can interact with PDZ domain3 of PSD95 (Russwurm *et al.*, 2001), and thus form a multi-protein signalling complex, effectively forming a NO receptor producing cGMP in direct response to the NMDA receptor activity.

1.8 Tinnitus and NOS

NOS expression in the auditory brainstem pathway has been linked to tinnitus. Animal models of tinnitus showed increased expression of NOS in the VCN (Zheng *et al.*, 2006) (Coomber *et al.*, 2015). Also, acamprosate, an NMDA receptor antagonist has been shown to have some efficacy as a treatment for tinnitus (Elgoyhen and Langguth, 2010; Langguth and Elgoyhen, 2011). Since NMDA receptor activity influences the activation of NOS, this suggests that NOS might be involved in the development of tinnitus.

1.8.1 Tinnitus

The word tinnitus meaning the conscious perception of a phantom sound in the absence of a corresponding acoustic stimulus (Schaette, 2014), is derived from the Latin *tinnire* which translates as ‘to ring’ (Berger and Coomber, 2015). Most of us have experienced transient tinnitus after exposure to loud sounds, for example after visiting nightclubs or attending concerts. Though annoying, transient tinnitus rarely has a major impact on the sufferer.

Chronic tinnitus is a widespread disorder, with estimates suggesting that 10 to 15% of the world's population is suffering from a chronic (>6 months) form of tinnitus and for 3-4% of the population this impacts on quality of life (Schaette, 2014). Although tinnitus comes in a wide variety of sounds like ringing, buzzing, cricket like hissing, whistling and humming, the high pitched tone is most often reported (Lockwood *et al.*, 2002). Tinnitus is necessarily a subjective phenomenon. In more than 90% of the cases, no physical cause for the tinnitus percept can be found, this most prevalent form is often called either subjective or idiopathic tinnitus.

About 30% of people suffering from hearing loss develop tinnitus (Lockwood *et al.*, 2002; Eggermont and Roberts, 2015), and tinnitus patients often match the pitch of their tinnitus percept to the frequencies at which their hearing is impaired (Kaltenbach, 2011; Schaette, 2014; Vogler *et al.*, 2014). Other common causes of tinnitus are acoustic trauma, ototoxic drugs (e.g. salicylate), head and neck injuries (Elgoyhen and Langguth, 2010) and drugs that lower serotonin levels (Belli *et al.*, 2012).

Treatment of the hearing loss, if possible, does often reduce the experienced tinnitus (Schaette, 2014). However hearing loss, based on audiometric thresholds, is not a requirement for the persistence of tinnitus, about 15% of the people experiencing chronic tinnitus display normal audiograms (Eggermont and Roberts, 2015). Strong evidence that loss of sensory input (i.e. hearing loss) can cause tinnitus comes from studies that had participants wear a silicon earplug for a week. Eleven out of 18 participants experienced tinnitus in the plugged ear, the perception of tinnitus gradually disappeared after removal of the plug (Schaette *et al.*, 2012). Further evidence for the link between tinnitus and hearing loss comes from patients with otosclerosis in which corrective surgery has been shown to improve or even abolish the perception of tinnitus in almost all patients (Schaette, 2014). It appears that the auditory system increases the gain to compensate for the reduction of input, which in turn may give rise to tinnitus (Eggermont and Roberts, 2004; Sun *et al.*, 2009). Recent fMRI data in human patients showed increased activity in resting state networks in tinnitus patients implicating increased activity in the IC and Heschl's gyrus (Leaver *et al.*, 2016).

Many studies have shown tinnitus to be comorbid with depression, anxiety and insomnia (Lockwood *et al.*, 2002; Hébert *et al.*, 2012a; Hébert *et al.*, 2012b). Currently, no cure is available to treat tinnitus, although the depression and anxiety often accompanying tinnitus can be treated with high success rates.

Diagnosing and measuring subjective tinnitus in an objective manner in humans is currently impossible. Attempts in defining a measurable, reliable and repeatable outcome measure for tinnitus are so far unsuccessful (Dobie, 1999) (Basile *et al.*, 2013). It is hard to objectively compare the tinnitus percept of one person to that of another; it is also impossible to objectively track the progress, either worsening or improving, of the disorder over time. The subjectivity of 'measuring' the tinnitus experienced by the patient has hampered drug testing in clinical trials. Tinnitus treatment suffers from placebo effects often masking any possible drug effect (Dobie, 1999). Usually, the treatment goals target the relief of symptoms and management of associated distress (Elgoyhen and Langguth, 2010).

1.8.2 Mechanisms of Tinnitus

Early research towards the neural underpinnings of tinnitus in the late 1970s and early 1980s focused heavily on the peripheral auditory sense organs as the origin of tinnitus (Kaltenbach, 2011). A major shift in the paradigm came when House and Brackmann showed in 1981 that the tinnitus percept continues in around half of patients after sectioning of the eighth nerve (House and Brackmann, 1981). Suggesting that plastic changes beyond the cochlea are important mediators of tinnitus. It has since become increasingly clear that, although the initial onset of tinnitus may be caused by damage to the cochlea or inner ear, tinnitus itself is caused by aberrant processing in the brain and not by (persistent) defects of the ear (Roberts *et al.*, 2010; Knipper *et al.*, 2013). Injection of lidocaine intravenously results in a temporary relief of the tinnitus percept in 70% of patients (Duckert and Rees, 1983), this indicates that tinnitus is a neuronal activity driven disorder (Elgoyhen and Langguth, 2010; Langguth and Elgoyhen, 2011).

Changes in auditory brainstem responses (ABR) indicate that multiple centres in the auditory brainstem pathway are affected (Schaette, 2014). There is growing evidence that tinnitus percepts are caused or at the very least associated with hyperactivity in neural activity within the DCN, the IC and the AC (Dehmel *et al.*, 2012; Robertson *et al.*, 2013; Vogler *et al.*, 2014) (Manabe *et al.*, 1997; Bauer *et al.*, 2000; Bauer *et al.*, 2008). This hyperactivity is often linked to a shift in the excitatory/inhibitory balance within the auditory pathway (Bauer *et al.*, 2000; Elgoyhen and Langguth, 2010). An fMRI study investigating the entire auditory pathway showed increased activity in tinnitus patients in the IC, AC and MGB (Smits *et al.*, 2007) thus suggesting that the tinnitus originates in these 'higher' auditory structures. Whether the IC is generating the tinnitus, or merely passing on the aberrant neuronal activity generated elsewhere in the auditory pathway, is currently an open question. Although, given its strategic position in the auditory pathway, and its

involvement in processing virtually all ascending information, the IC might be a particularly important structure for the generation of tinnitus.

Animal models have been used to study the hyperactivity phenomena in more detail. The increased activity is usually observed in frequency specific regions close to frequencies in which the hearing loss occurs. This hyperactivity develops over time, with no change in the spontaneous firing rate observed immediately after the noise trauma but developing in the days and weeks after the trauma (Dong *et al.*, 2010a; Dong *et al.*, 2010b) and possibly leaving a window of opportunity for treatment. As is the case with any other disorders, some individuals may be more predisposed than others. Ahlf et al. (2012), showed that gerbils that developed tinnitus after noise trauma had lower auditory brainstem and cortical responses before the noise induction compared to animals that did not develop tinnitus (Ahlf *et al.*, 2012).

Unilateral noise-induced trauma results in bilateral changes in the IC. Increased spontaneous activity can last up to weeks after the event. Interestingly the gene expression of NMDA subunit 1 (GluN1) is decreased immediately after the noise trauma but returns back to normal levels after four weeks (Dong *et al.*, 2010b). This suggests that NMDA mediated activity might be involved in observed increases in spontaneous activity and therefore could be involved in the development of chronic tinnitus.

The subjective nature of tinnitus makes proving the presence of tinnitus in animals difficult. In recent years methods to verify the presence of tinnitus in animals have been developed. One of the first animal models to investigate tinnitus was developed by Jastreboff et al., (Jastreboff and Sasaki, 1986; Jastreboff *et al.*, 1988) and used salicylate to induce tinnitus. Later tests to verify the presence of tinnitus in animals were always validated using salicylate, because of its reliability in inducing tinnitus (Berger *et al.*, 2013; Kaltenbach, 2011; Turner *et al.*, 2006).

Although the pharmacologically induced tinnitus possibly has a different mechanism via which it induces tinnitus compared to acoustic trauma, both result in an indistinguishable perception of tinnitus. The fact that salicylate is possibly acting directly on the brain in generating the tinnitus makes this a powerful method, because it allows us to directly target specific structures in the auditory pathway.

1.8.3 Salicylate

Subjective tinnitus is notoriously difficult to investigate in humans but even harder to asses in animals. Salicylate, chemically related to aspirin (acetylsalicylic acid), one of the world's oldest, and still one of the most widely used analgesics, has been long known to be ototoxic in high doses reliably causing transient / reversible tinnitus in humans (Sée, 1877; Day *et al.*, 1989). Systemic administration of sodium salicylate in animal models has been used to induce temporary tinnitus (Evans *et al.*, 1981; Jastreboff and Sasaki, 1986; Jastreboff *et al.*, 1988) and validate behavioural models of tinnitus (Kizawa *et al.*, 2010; Berger *et al.*, 2013). The mechanism via which salicylate induces tinnitus has yet to be fully clarified. Studies have shown that systemic administration of salicylate may impact directly onto the peripheral and central auditory structures.

Salicylate application most commonly causes an increase of the spontaneous neuronal discharge in the absence of any auditory stimulation, throughout the auditory pathway (Guitton *et al.*, 2003; Ma *et al.*, 2006; Hwang *et al.*, 2011). Besides the increase in spontaneous discharge in the central auditory structures, at the periphery of the auditory pathway reductions in cochlear blood flow (Didier *et al.*, 1993), a reduction in outer hair cell mobility (Shehata *et al.*, 1991), via blocking of the motor protein prestin, and direct activation of NMDA receptors in the cochlea (Guitton *et al.*, 2003) have been reported. Because systemic administration of salicylate affects the entire animal, modes of action can be difficult to disentangle. Application of salicylate directly onto the round window of the cochlea results in a decreased output from the cochlea to the auditory nerve (Sun *et al.*, 2009), which is the opposite effect when applied systemically. These findings have been interpreted as ruling out the cochlea out as a source of the increased spontaneous discharge that propagates throughout the central auditory system after systemic salicylate application.

Direct application of salicylate in vitro and in vivo has demonstrated that salicylate can have a direct effect on neuronal firing in the IC (Basta and Ernst, 2004; Patel and Zhang, 2014) . Three hours after salicylate injection a reduction in energy consumption, as measured by 2-DG uptake (Wallhäusser-Franke *et al.*, 1996) and an increase in c-fos (Wallhäusser-Franke, 1997) as well as a decrease in GABA receptors in the IC but not in other non-auditory brain structures have been reported (Butt *et al.*, 2016). Further evidence for salicylate acting directly on brain tissue comes from iontophoretic studies, in which salicylate is directly applied to the cell recorded. A recent study showed that salicylate can induce hyperactivity by iontophoretic application to neurons in the IC (Patel and Zhang,

2014). So in summary, salicylate appears to reduce the spontaneous firing rate in most auditory structures (Ochi and Eggermont, 1996; Yang *et al.*, 2007; Wei *et al.*, 2010; Zhang *et al.*, 2011) except for the auditory nerve, the secondary auditory cortex and the IC, in these three structures spontaneous firing rates are increased (Stypulkowski, 1990; Manabe *et al.*, 1997; Eggermont and Kenmochi, 1998; Patel and Zhang, 2014; Eggermont and Roberts, 2015). Interestingly, chronic dosing of salicylate leads to metabolic changes in IC. These changes are reversible by stopping the salicylate treatment (Yi *et al.*, 2016).

Both noise induced, as well as salicylate-induced, tinnitus have a close relationship to NMDA mediated activity (Peng *et al.*, 2003; Ruel *et al.*, 2008). Ruel showed that spontaneous firing, as well as sound driven responses in, in vivo recordings in auditory nerve fibres in adult guinea pigs, were increased when perfused with salicylate; applying an irreversible NMDA antagonist, MK-801, abolished the observed effects. The obvious connection between the NMDA receptor and NOS makes NO signalling a viable candidate to be involved in the generation of tinnitus.

1.9 Aims and Hypotheses

As identified in the Introduction, many gaps exist in our knowledge about nNOS and nitric oxide in the IC and their role in auditory processing. The following aims and hypotheses will be addressed in this thesis:

1. nNOS has been shown to be present in IC, but we have a limited understanding of its distribution, co-expression with other proteins and neurotransmitter phenotype. I am to answer the following questions:
    - Does nNOS co-localise with other markers that enable us to identify nNOS neurons?
    - Is nNOS limited to neurons of a particular neurotransmitter phenotype?
    - Is there evidence in the IC for the occurrence of the two splice variants of nNOS reported elsewhere in the brain?
2. Our current knowledge about the physiology of the NMDA receptor in the IC is sparse and even less is known about the role it plays in auditory processing in-vivo. Evidence suggests that nNOS activity is often closely associated with NMDA receptor activity. Thus I aim to :
    - Determine if selective activation of NMDA receptors influences spontaneous activity and acoustically driven neural responses in the IC.

- Test the hypothesis that NO signalling participates in spontaneous activity and acoustic driven neural responses in the IC.
- Test the hypothesis that effects of NMDA receptor activity in the IC are mediated by the NO signalling cascade.

3. Salicylate has often been used in inducing and studying tinnitus but the mechanisms by which this drug induces tinnitus are poorly understood. Previous studies have not looked at salicylate effects over a longer time scale recorded from the same unit, nor have they been able to untangle direct and indirect effects of salicylate on the IC. Also, the link between salicylate and the NMDA receptor activity in other auditory structures raised the question about whether direct effects of salicylate on the IC might be mediated by the NO signalling pathway. Thus the aims for this topic are:
   - Determine the time course of the effects of systemically administered salicylate on neural activity recorded in the IC over the course of several hours
   - Compare and contrast the effects of systemic and local administration of salicylate on spontaneous activity and acoustically driven neural responses in the IC.
   - Test the hypothesis that salicylate induced effects on neuronal activity in the IC are influenced by NO signalling

Chapter 2. Methods

This chapter describes the general methods applicable to all immunohistochemistry and in vivo electrophysiological experiments. Some more specific details are described in the methods section of the relevant chapters.

2.1 Animals and Ethics

All experiments reported here were performed in accordance with the terms and conditions as they apply to all licences issued by the UK Home Office under the Animals (Scientific Procedures) Act 1986 under Project Licence PPL 70/7831 issued to Adrian Rees. All experiments were performed in laboratory environments approved by the Comparative Biology Centre (CBC) at Newcastle University and the Home Office.

2.2 Immunohistochemistry

2.2.1 Animals

Lister-hooded rats, males only (200-300g) were either obtained from Charles River, ordered specifically for this study, or were left over after non-invasive behavioural experiments. Animals were housed in groups of 2-4 living under standard conditions, with a twelve-hour light-dark cycle, a constant temperature (22 °C ± 2 °C) and cage enrichment. Food and water were given ad libitum. Animals that had been delivered from Charles River were given 2-3 days to acclimatise before being used in experiments. Efforts were made to reduce animal numbers and prevent all forms of animal suffering.

2.2.2 Perfusion, Sectioning and Storage

Animals used for immunohistochemistry received a lethal intraperitoneal (IP) injection of sodium pentobarbital (3.75 ml/kg). Under this terminal anaesthesia, animals were perfused through the left ventricle initially with 0.9% saline buffer with heparin (4 I.U. per ml) followed by a 4% paraformaldehyde (PFA) solution in 0.1 M PBS (137mM NaCl, 2.7mM KCl, 10mM Na_2HPO_4, 2mM KH_2PO_4). The brains were removed from the skull and post-fixed overnight at room temperature in the 4% PFA solution. After post-fixation, to cryoprotect the tissue the brains were transferred to 30% sucrose in 0.1M PBS solution and stored at 4 °C until they sank. Coronal 40 µm sections were cut on a freezing microtome or cryostat starting at the caudal end of the IC. Sections were collected into 0.1 M PBS in 24 well plates. If sections were to be stored, the PBS was replaced by an antifreeze solution (30%

Sucrose w/v, 30% ethylene glycol w/v and 0.01 % polyvinyl-pyrrolidone (PVP-40) in 0.1M PBS) and the sections were stored at -20 °C.

2.2.3 Immunolabelling protocol

All procedures were performed at room temperature unless otherwise stated. The required sections were transferred from the antifreeze solution to a new 24 well plate, the sections were washed 3x 10 minutes in 0.1M PBS. To reduce the autofluorescence caused by tissue-bound free aldehyde groups and reveal the epitopes, an antigen retrieval step was performed. Sections were incubated in a 1% sodium borohydride solution in 0.1 M PBS for 20 minutes on a shaker plate and then washed 3 x 10 minutes in 0.1M PBS. To further reduce autofluorescence, sections were incubated in a 50 mM glycine solution in 0.1M PBS for 20 minutes (the glycine binds to free aldehyde groups thereby preventing unspecific binding of the antibody to these 'sticky' ends). After the glycine incubation, sections were washed 3 x 10 minutes in 0.1M PBS before being placed in a block buffer of 0.1M PBS containing 0.1% gelatin and 5% serum of the host species in which the secondary antibodies are raised. For some primary antibodies, 0.3% of Triton-X was added to this buffer, see Table 2-1 for a complete overview. Triton is a detergent which punctures the membranes and so allows access of antibodies to the interior of the cell, however, it can destroy the epitope of membrane-bound proteins. Thus, for some of the primary antibodies, better results were obtained by leaving Triton out of the buffer, while others performed better with the addition of Triton. Particular the antibodies targeting the NOS protein performed better in the absence of Triton. In double labelling experiments occasionally Triton and No Triton antibodies would be paired, here the Triton was left out, or reduced to 0.003%. Sections were incubated in this block buffer for at least two hours at room temperature. Antibody dilutions were made in the same block buffer. Sections were incubated in the antibody solution either overnight at 4 °C or 48 hours at 4 °C see Table 2-1 for the specific details for each antibody. In double labelling experiments, both antibodies were added at the same time, and the longer of the two incubation periods was used. A negative control using the same protocol, excluding the primary antibody was included in all experiments. All incubations and wash steps were performed on plate shakers to constantly agitate the contents of the wells.

2.2.4 Primary antibodies

Table 2-1 Primary antibodies used in the experiments. For each individual antibody, information is given about the clone, the host, the manufacturer, dilution range, the optimised incubation times and whether triton was added to the block buffer. The following abbreviations have been used: SYSY (Synaptic Systems), 48H (48 hours), O.N. (Overnight).

Target	Host	Dilution	Supplier	Clone	Incubation	Block buffer
nNOS	Mouse	1:250	Sigma	N2280	48h - 4 °C	No Triton
nNOS	Rabbit	1:250	Santa Cruz	SC-648	48h - 4 °C	No Triton
Vglut1	Rabbit	1:2000	SYSY	135 303	o.n. - 4 °C	Triton
Vglut2	Rabbit	1:2000	SYSY	135 403	o.n. - 4 °C	Triton
Parvalbumin	Mouse	1:2000	Sigma	Parv-19	o.n. - 4 °C	Triton
Calbindin-D28K	Mouse	1:1000	Sigma	CB-955	o.n. - 4 °C	Triton
Calretinin	Mouse	1:1000	Millipore	MAB1568	o.n. - 4 °C	Triton
GABA	Rabbit	1:1000	Sigma	A2052	48h - 4 °C	Triton
GAD65/67	Goat	1:1000	Santa Cruz	SC7513	o.n. - 4 °C	No Triton
PSD95	Mouse	1:500	Thermo Scientific	MA1-046	o.n. - 4 °C	Triton

Once the primary antibody incubation was completed, the sections were washed 3 x for 10 minutes in 0.1M PBS. Sections retrieved from the 4 °C environment were allowed to warm up to room temperature before being washed.

Secondary antibody solutions were prepared in the previously described block buffer. Different secondary antibodies have been used to allow for different combinations of primary antibodies see Table 2-2. Where possible, in double fluorescent protocols both secondary antibodies were raised in the same host species. The secondary antibodies either had a fluorescent label or a biotin label attached to them. Sections were incubated in secondary antibodies for two hours at room temperature before being washed 3 x 10 minutes in 0.1M PBS. When biotinylated antibodies were used a third, one-hour incubation step was needed in which a fluorescent avidin was added. The fluorescent avidin binds to the biotin tail of the biotinylated secondary antibody.

Negative controls were used in which the primary antibody was omitted to control for non-specific binding of the secondary antibody. For the biotinylated protocol another control omitting the secondary antibody was used as well to control for unspecific binding of fluorescent avidin. To label the nuclei the sections were incubated for 10 minutes in a

solution containing 4',6-diamidino-2-phenylindole (DAPI), a DNA labelling dye binding to A-T rich regions. Sections were incubated for 10 minutes in 0.1 M PBS containing 1 in 10.000 parts of DAPI and washed 3x 10 minutes in 0.1M PBS. Sections were then mounted on glass slides and air dried for approximately an hour before being coverslipped using Vectashield mounting medium hard set.

Table 2-2 Secondary antibodies used

Host	Target	Dilution	Supplier	Label
Goat	Mouse	1:500	Life Technologies	Alexa 488
Goat	Rabbit	1:500	Life Technologies	Alexa 568
Donkey	Goat	1:500	Santa Cruz	Rhodamine
Goat	Rabbit	1:500	Vector	Biotinylated
Goat	Mouse	1:500	Vector	Biotinylated
Mouse	Goat	1:500	Vector	Biotinylated
	Biotin	1:500	Vector	Rhodamine Avidin D
	Biotin	1:500	Vector	Fluorescein Avidin D

In double immunofluorescent experiments, ideally, it is best to use primary antibodies that have been raised in different host species. To allow for multiple combinations, two different NOS antibodies were used one raised in mouse produced by Sigma and another raised in rabbit produced by Santa Cruz. To verify that both antibodies have the same affinity for NOS using the same protocol, I directly compared both antibodies in the same tissue. Figure 2-1 shows the result of this immunohistochemistry experiment and both antibodies clearly label the same cells and subcellular compartments.

2.2.5 Microscopy

Sections were imaged on a Zeiss AxioImager with an automated stage or a Nikon NiE upright fluorescence. Both are wide field microscopes with a wide range of filter settings allowing multi-channel acquisition and automated stages allowing for Z-stack image acquisition. The Zeiss Axiometer also allowed for the acquisition of mosaic imaging. All sections to be analysed were first imaged at 10x magnification using the Zeiss Axiometer and the IC was reconstructed from sections using the mosaic function. Areas of interest in the dorsal cortex, lateral cortex and central nucleus were located within these mosaic images and imaged at 40x, 63x or 100x magnification.

Whenever required, z-stacks of these regions or individual cells could be acquired at high power, thus allowing 3D rendering.

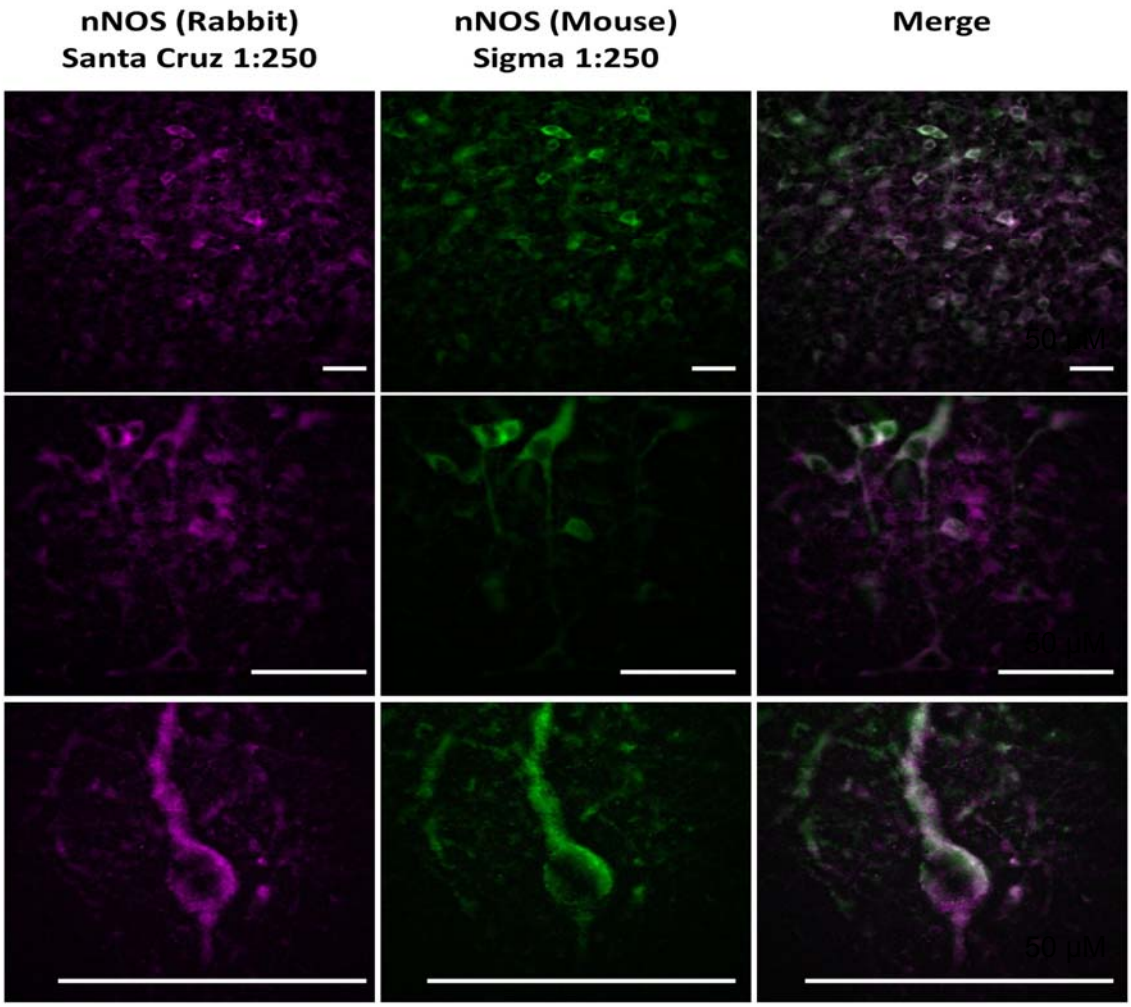

Figure 2-1 Double labelling with two different nNOS antibodies showing identical cell labelling. The left column shows images resulting from the nNOS antibody raised in rabbit obtained from Santa Cruz. In the second column shows labelling with the antibody against nNOS raised in mouse obtained from Sigma. In the third column, the previous two images are merged. The three rows show increased magnification levels, the scale bar indicates 50 µm. Images were obtained from the dorsal cortex in rostral IC.

All images were subjected to offline processing using Fiji (Schindelin *et al.*, 2012) which is the complete version of ImageJ (Schindelin *et al.*, 2015) with all plugins installed. Image files were loaded, the colour channels were split in red, green and blue and a background subtraction with a rolling ball radius of 100 pixels was performed on each channel. Channels were stored separately before being put together to study colocalisation. For 3D rendering and multi-dimensional image analysis the functions Z-project (for the maximum intensity projection), orthogonal views and the 3D viewer provided by Fiji were used.

2.3 In Vivo Electrophysiology & Microdialysis

The in vivo electrophysiology experiments all involved the combination of multi-electrode electrophysiological recording and reverse microdialysis. This section describes the surgery, the electrophysiology and the microdialysis parts separately followed by the experimental protocol.

2.3.1 Animals

All experiments reported here were performed on adult pigmented guinea pigs, bred at the CBC, Newcastle University. In total 42 guinea pigs were used (11 male, 31 female) aged between 2 and 6 months, weighing between 372-912g. Animals were housed in groups of 2-6 living under standard conditions, with a twelve-hour light-dark cycle, a constant temperature (20 °C ± 2 °C) and cage enrichment. Food and water were given ad libitum. The standard diet of food pellets was supplemented daily servings of fresh fruit.

2.3.2 Anaesthesia Induction and Maintenance

Two different anaesthetic protocols were used, due to one anaesthetic, Hypnorm (0.315 mg Fentanyl citrate and 10 mg Fluanisone per ml), being off the market for a considerable time. A summary of the anaesthetics used is supplied in Table 2-3.

All animals were anaesthetised using an IP injection of urethane (1mg/kg in a 20 % solution, dissolved in 0.1M PBS). In the first eight experiments, this initial anaesthetic was followed by an intramuscular injection in the gluteus maximus of 0.2 ml of Hypnorm containing, Fentanyl citrate and Fluanisone (®Veta Pharma). The depth of anaesthesia was checked at regular intervals during the experiment by testing the pedal reflex. When necessary supplementary doses of 0.15 ml Hypnorm were administered. In the latter 34 experiments, the urethane was supplemented by an IP injection of fentanyl (0.3 mg/kg) and an intramuscular injection in the hind leg of midazolam (5mg/kg). When necessary an extra full dose of fentanyl was administered IP. In this anaesthetic protocol, the animals were actively pumped with 100% oxygen, due to the respiratory depressant effects of fentanyl. All guinea pigs were given a subcutaneous injection of atropine sulphate (0.05 mg/kg) to suppress bronchial secretion.

Table 2-3 Anaesthetics used

Anaesthetic	Initial dose	Top up dose	Concentration	No. Experiments
Urethane	1 g/kg		1g/5ml (20%)	51
Hypnorm	.2 ml	0.15 ml		17
Fentanyl	0.3 mg/kg	0.3 mg/kg	0.05mg/ml	34
Midazolam	5mg/kg		5mg/ml	34

2.3.3 Surgery

The animal's head and neck were shaved in preparation for surgery. The animal was allowed to breathe freely at this point but was supplied with oxygen enriched air. A tracheotomy was performed and a polyethylene cannula was inserted into the animal's trachea to allow for active ventilation with oxygen. The tragus of the outer ear was surgically removed from both ears to facilitate the fitting of the ear bars. The animal was then brought into a sound insulated room and placed on a heating pad controlled by the output of a rectal thermometer (Harvard Apparatus). The animal's core temperature was maintained between 37 °C and 38 °C. The animal was fitted in a stereotaxic frame using ear bars with perspex specula into which removable headphones could be inserted. Care was taken to ensure that the specula were inserted in the auditory canal with a clear view of the tympanic membrane. Once the animal was fixed in the frame, in animals that were ventilated the tracheal tube was attached to a ventilator and the animal ventilated with 100% oxygen.

A single scalp incision was made from rostral to the caudal over the midline of the skull the skin was retracted and the muscles overlying the cranium scraped away. All further procedures took place using an operating microscope to ensure minimal damage to the brain surface and blood vessels. Using a hand drill and a rongeur, a craniotomy was performed over predefined coordinates overlying the IC. The dura was then removed using a bent needle and a steel dental instrument. A glass Pasteur pipette, which had been heat-treated to blunt it, was used to aspirate the cortex overlying the IC. All cortex above the IC was removed to enable a clear sight of the dorsal surface of the IC. The microdialysis probe (described in 2.3.5 below), was inserted mid IC on the rostral-caudal axis 0.5 mm lateral from the midline with a 10 ° angle, angled away from the midline Figure 2-2. The electrode (described in 2.3.4 below) was placed rostral to the microdialysis probe, but as close as physically possible without coming in contact with it. The electrode was inserted vertically.

The angled microdialysis probe and straight electrode configuration allowed both devices to be placed in close proximity to one another, without compromising each other's functionality.

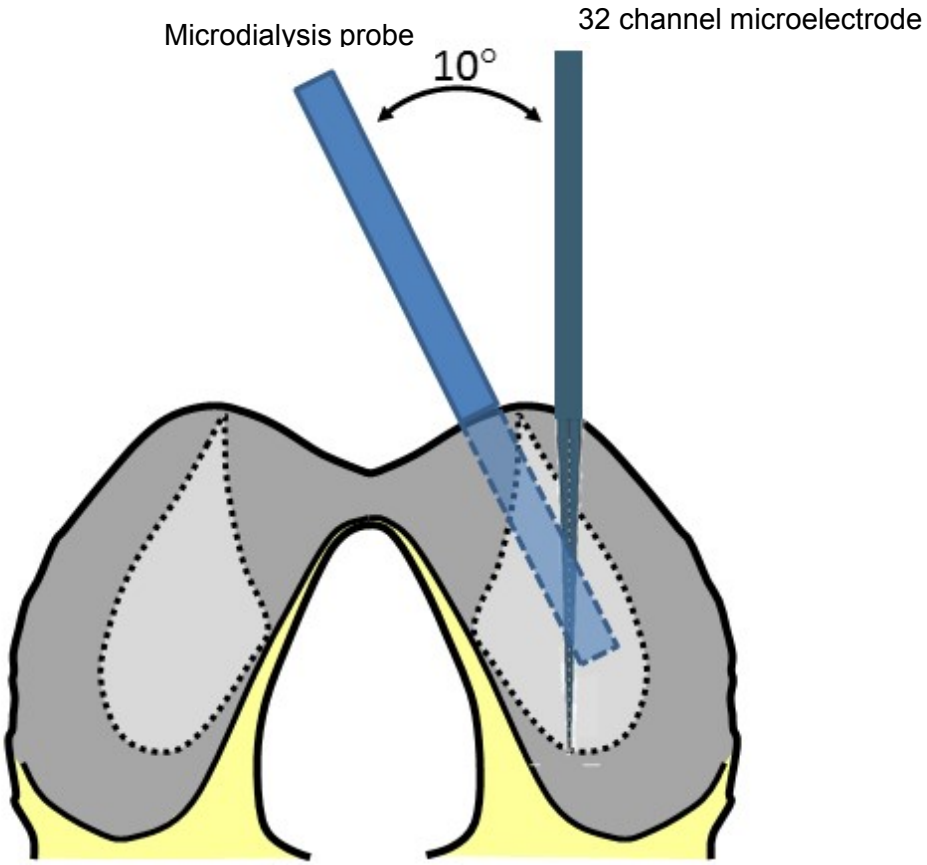

Figure 2-2 Schematic drawing of the microdialysis probe and multi-electrode recording probe in the IC. The dialysis probe was inserted at a 10° angle, away from the midline, placed caudal from the electrode.

2.3.4 Electrode

To record the multiunit neurophysiological signals, probes with multichannel microelectrode arrays (NeuroNexus) were used. In all experiments, a single shank electrode fitted with a 32 channel linear microelectrode array was employed (A1x32-10mm-100-177-A32 50). The electrode sites on this particular probe configuration were spaced 100 µm apart, giving the probe a functional recording depth of 3.2 mm. This particular configuration was chosen because it allowed recordings to be obtained through the several frequency laminae of the CNIC simultaneously. The electrode was placed in a NN32AC headstage (Tucker Davis Technologies (TDT), Alachua, Florida) connected to a PZ2-32 channel Preamplifier (TDT) which fed the signals to a RZ2 BioAmp Processor (TDT) which was connected and controlled by a PC running custom made Matlab scripts on which the data was stored for later offline analysis. The sampling rate was set at 24.414 kHz

2.3.5 Microdialysis

The microdialysis probes were hand made and used once. The microdialysis probes were manufactured by glueing three pieces of hollow steel with a diameter of 0.5 mm (Goodfellow stainless steel (AISI 304 (Fe/Cr18/Ni10) diameter 0.5mm, wall thickness 0.06mm) together in a Y-shaped body as depicted in Figure 2-3. A silica fused fibre (110µm/170 µm, SGE analytical Science, Australia) was threaded through the short ends of the probe. One of the fibres, the inlet, extended out of the bottom of the probe's body, while the outlet fibre stayed inside the body of the probe. The probe was completed by a semipermeable membrane (Hospal AN-69), allowing diffusion of molecules up to 10 kDa.

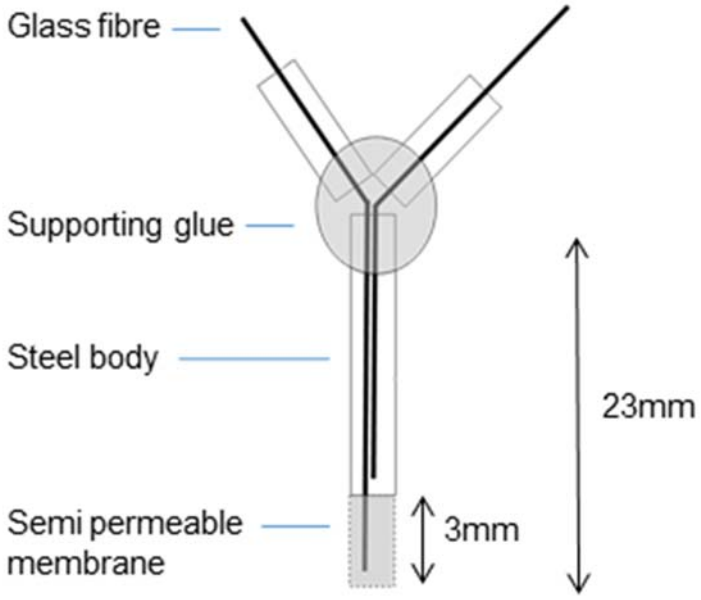

Figure 2-3 Schematic drawing of the microdialysis probe

The semipermeable membrane lets molecules diffuse down their concentration gradient, allowing the microdialysis probes to be used in reversed dialysis. The probes were used to deliver drugs locally into the areas of interest. The drugs used, all manipulated different stages in NOS signalling pathway. Every experiment started with baseline recording lasting at least an hour in which only normal artificial cerebrospinal fluid (aCSF) (140 mM NaCl, 3 mM KCl, 707 µM Na_2HPO_4, 272 µM NaHPO4 and 1mM $MgCl_2$, 10 mM D-glucose ($C_6H_{12}O_6$), 240 µM $CaCl_2$) was perfused through the probe at a constant rate of 2 µl /min. After this baseline condition one or multiple types of bioactive molecules could be pumped through the probe; every drug condition was always followed by an aCSF washout condition in which only aCSF was pumped through the probe. The aCSF and the drug dilutions used in a particular experiment were all freshly made on the day of the experiment. Once the

microdialysis probe was inserted care was taken to ensure a constant flow rate through the probe. Syringe pumps (Harvard apparatus) with four slots for 2.5 ml disposable syringes were used. Syringes were loaded with aCSF and aCSF containing drugs at the start of the experiment. Non-sterile Portex tubing, inner diameter 0.5 mm, were attached to the syringes. Care was taken to fill the lines and avoid any air bubbles. Syringes were placed on the syringe pump and ran throughout the experiment to allow for smooth transition between drug conditions. A connecting piece of tubing permanently attached to the dialysis probe was used as an inlet to the probe. Lines from the syringes were manually coupled and uncoupled when switching between drug conditions, the connecting tube ensured that the dialysis probe was undisturbed. All drugs used are listed in Table 2-4, specific concentrations are discussed in the relevant chapters.

Table 2-4 Drugs used in the microdialysis probe.

Drug name	Function	Company	Product code	FW
NMDA	NMDA receptor agonist	Sigma	M3262	147.13
L-MeArg	Blocking endogenous NO production	Cambridge Bioscience	CAY10005031	248.3
ODQ	Blocking sGC	Santa Cruz	SC-200325A	187.15
Sodium salicylate	Tinnitus inducing agent	Sigma	S3007-500G	160.10

2.3.6 Sound Stimuli

The stimuli were presented using Sony MDR 464 earphones, each housed in an alloy enclosure which fitted in the Perspex speculum inserted into the animal's ear canal (Rees et al., 1997). The output of the system was calibrated using a 1⁄8 inch Bruel and Kjaer 4138 microphone, a Type 2639 preamplifier, and Type 2610 measuring amplifier. The microphone was seated in a small coupler made from silicon tubing that sealed the narrow end of the speculum. The maximum output of the system was approximately flat from 0.1 to 9 kHz (100 ± 8 dB SPL) and then fell with a slope of ~20 dB/octave to give a maximum output at 16 kHz of ~80 dB SPL from both the left and right earphones (Figure 2-4).

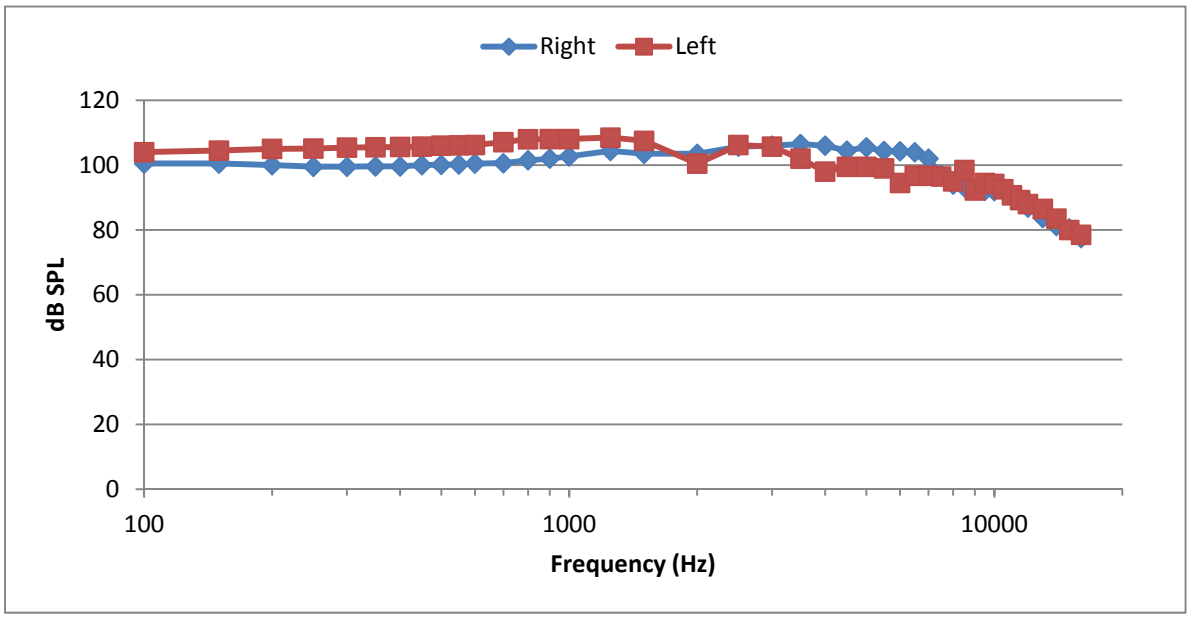

Figure 2-4 Maximum output of earphones Measured in small tubing coupler with Bruel & Kjaer Type 4138 1/8 inch microphone, Type 2639 Preamplifier and Type 2610 Measuring Amplifier.

Pure tone stimuli were generated by a Tucker-Davis Technologies System Z6 at a sampling rate of 97.656 kHz controlled by a custom made Matlab code (kindly made available by Dr Nicholas Lesica, UCL). This software allowed the user to set frequency and sound level parameters within fixed ranges which could then be presented in a random fashion. All stimuli had a duration of 75 ms while the response was recorded over a period of 150 ms starting with the onset of the stimulus at time 0, repetition rate 6.6 Hz. Data were recorded by a TDT System comprising a PZ2-32 Channel preamplifier and a Z2 Z6 at a sampling rate of 24.414 kHz. All data recorded per stimulus set was stored in a separate data files for offline analysis.

The activity recorded in these experiments is multi-unit activity comprised of the summed activity of all cells in the proximity of the electrode. The measures taken from the electrode sites are therefore a combination of multiple sources.

Frequency response area

A way of capturing the frequency response at a recording site is obtaining the frequency response area (FRA). Many possible combinations of frequency and sound level within a given range are presented to the animal in a pseudo-random fashion. The frequency range for the FRA‘s in all experiments ranged from 128 Hz to 16384 Hz with a stepwise fixed increase of 7% between frequencies. The sounds levels (represented as attenuations from the maximum level of the stimulus ranged from 5- 85 dB separated in steps of 5 dB. Each

of the 1296 possible combinations of frequency and attenuation represents one pixel in the overall FRA matrix. In these experiments, every combination of frequency and attenuation level was presented once. Though prone to noise, the FRA provides us with an excellent overview of a multiunit cluster's sensitivity over a wide range of frequencies and levels. In order to capture and describe the possible changes over time over a wide range of frequencies, FRAs were captured at regular intervals during each experiment. The CF calculated does not represent the CF of one single cell but should be thought of as CF of the activity at the recording site.

PSTH

PSTH analysis gives detailed information about the firing pattern of multi-units over the duration of the stimulus. PSTH traces in these experiments were collected by summing the response over 150 repeats of the same frequency and attenuation level. To allow for comparisons between animals and study possible adaptations in auditory processing over a wide range of frequencies, in each experiment five fixed frequencies were presented at two different attenuation levels. The frequencies chosen were 256 Hz, 512 Hz, 1024 Hz, 2048 Hz and 4096 Hz all of which were presented at two different attenuation levels around 30 and 60 dB. All PSTH frequencies and attenuation levels were set and then presented in a pseudo-random order to avoid adaptation. 120 dB attenuation trials or silent trials recording spontaneous activity were interspersed in this sequences.

2.3.7 General Experimental Protocol

Once the microdialysis probe and electrode were inserted, the headphones were slotted into the hollow ear bars to allow for auditory stimuli to be presented to the animal. To ensure recordings were made from the central nucleus, a set of FRA recordings was made. The tonotopic sequence was inspected to ensure that a wide frequency range was captured. If necessary the electrode would be moved up or down, to capture as many unique frequencies as possible. Once the electrode was in the best position a set of baseline recordings with the dialysis probe perfused with aCSF was obtained. These baseline recordings lasted for at least an hour after the last electrode movement and consisted of repeated measures of PSTHs and FRA's. The raw digitised neurophysiological responses were stored in individual datafiles. After baseline recordings the drugs were perfused through the probe in sequence and the responses to the same auditory stimuli as presented in the baseline recording were recorded during the application of each drug. The protocols for the different drugs are described in the relevant chapters.

2.3.8 Termination of Experiment

When the full protocol of baseline, drug and washout recordings had been performed the animal was killed by an IP injection of sodium pentobarbitone (2ml/kg).

2.4 Data Analysis

To process the data collected the basic processing steps were automated using custom written Matlab scripts, developed by me. I will give short descriptions of the different scripts and their functions and workings where deemed necessary.

Every set of stimuli presented whether it was FRA or a PSTH were stored in individual blocks, containing the multi-unit data recorded from all 32 electrodes. The custom made Matlab scripts were used to extract the data from the tanks into Matlab (.mat) files containing the raw multi-unit data traces of, stimulus parameter information and time stamps. A threshold was applied to the raw time series to extract the spiking activity. One FRA from the baseline period was selected and the standard deviation was calculated of the activity in the 120dB attenuation row of the FRA matrix. The threshold was set at 2.5x the standard deviation of this spontaneous activity. The threshold level was calculated for every individual electrode and applied to the raw multi-unit data collected from that channel in the experiment. All spikes passing the threshold were stored together with their stimulus information and timestamps in .mat files. The FRA and PSTH give complementary information but take different forms and require different post-processing steps.

PSTH data analysis

Raw multi-unit data sampled at 24 bins/ms were aggregated into 1 ms bins in a linear array. Each PSTH trace is a summation of 150 trial repeats. The PSTH trace can be divided in a number of different segments. The PSTH stimulus lasted 75 ms while the PSTH trace was recorded over a period of 150 ms starting with the onset of the stimulus at time 0. Due to latency within the auditory pathway, activity evoked by the stimulus begins in the IC around ~12-18 ms. This first block, marked in the figure with number 1, is spontaneous, non-stimulus driven, activity and will be referred to as pre-stimulus activity. The biggest peak in activity in the multi-unit PSTH marks the stimulus onset, marked in Figure 2-5 by the red arrow. This onset peak is quantified by capturing all spikes occurring in a 10 ms time window, starting from the beginning of the onset peak. To detect the onset peak a standard Matlab peak detection function was used, which was set to detect the first peak occurring between 10 and 20 ms.

In blocks where no onset peak was detected, which is the case for spontaneous activity and or for stimuli which evoked no driven response, the onset time was set at 15 ms.

Sound driven spikes are the spikes fired during the duration of the stimulus. The sound driven activity is obtained by summing all the spikes between the onset peak plus 80 ms (marked in Figure 2-5 by the line labelled 2). The additional 5 ms over the length of the stimulus duration was to ensure the whole of the driven response was captured. The latter part of the multi-unit PSTH trace, marked in the graph by the number 3 is post-stimulus activity.

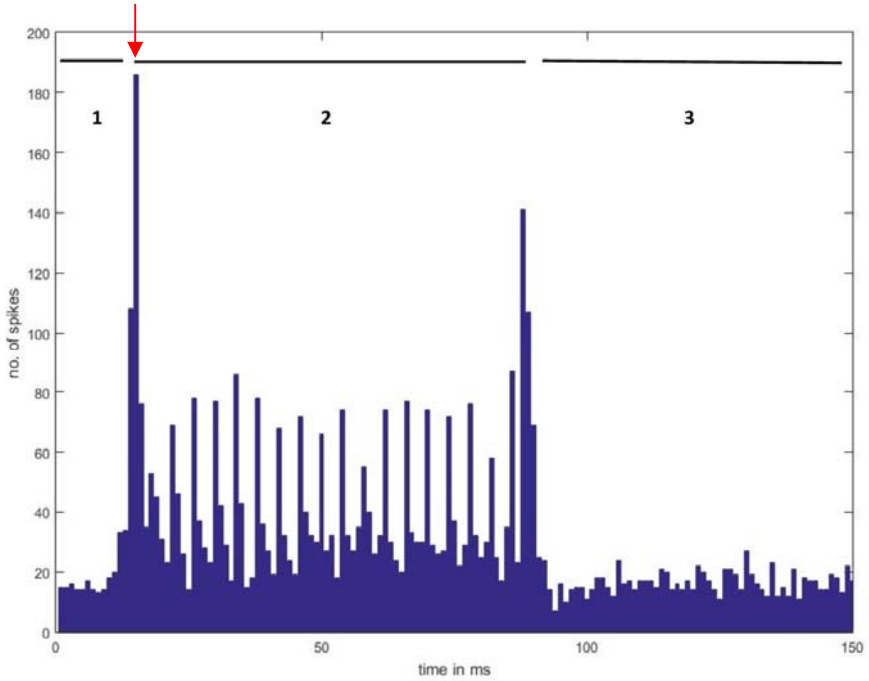

Figure 2-5 Example PSTH trace where 1 denotes the baseline / spontaneous activity, 2 is the stimulus driven part of the PSTH response, area 3 represents the offset activity. The red arrow indicates the onset peak.

All spike counts collected for the different bins, pre-stimulus, onset, sound driven and post stimulus were translated to ratios from the original baseline.

To study auditory processing over a wide range of frequencies and to permit comparison between animals, the electrodes best representing five fixed PSTH frequencies, 256 Hz, 512 Hz, 1024 Hz, 2048 Hz and 4096 Hz were analysed. These electrodes will be called ‘best frequency electrodes’. An electrode was selected as the best electrode for a given frequency if it recorded the highest number of sound driven spikes in response to this frequency. The frequency represented by this multi-unit activity will be referred to as the best frequency (BF). A Matlab script was employed to loop through all PSTH blocks, channels and PSTH stimuli presentations to find the electrode that responded best to a frequency.

FRA analysis

FRAs were captured at regular intervals during the experiment. FRAs obtained in each experiment consisted of a single repeat and randomly occurring noise can therefore have quite a big impact on the value of a single pixel in the FRA matrix. To create a more robust baseline two baseline FRAs were averaged post-hoc to create a new baseline.

FRAs can be characterised in a number of ways but most commonly used are the active area and the characteristic frequency (CF). The CF in this thesis is the CF of the multi-unit activity and represents the frequency at which the multi-unit is still responding to the lowest attenuation or smallest sound intensity, in Figure 2-6 a FRA is displayed and the CF marked.

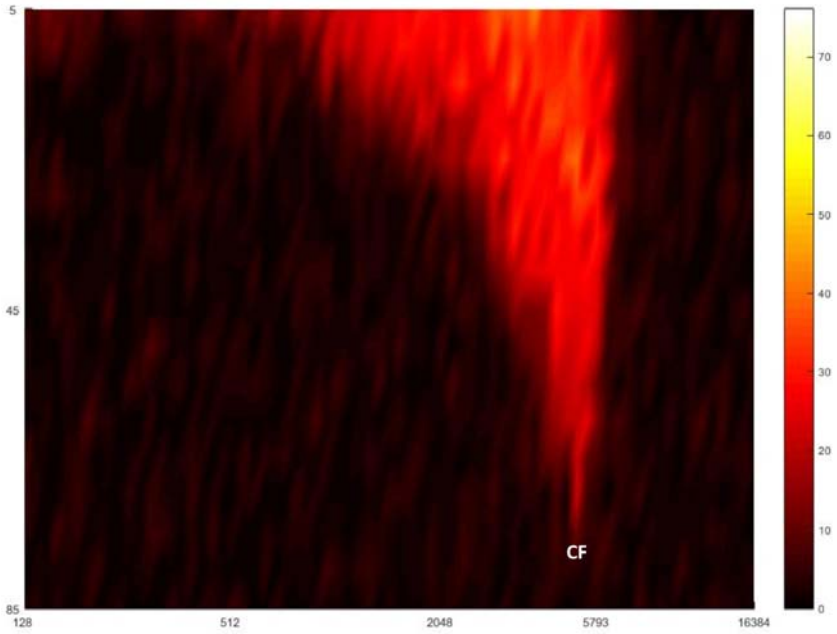

Figure 2-6 Example FRA, the colour scale represents the number of spikes.

A Matlab script was used to determine the CF of every FRA captured in the experiment. This script calculated the mean and standard deviation from the highest attenuation level of the FRA. A threshold of the mean plus three times the standard deviation was applied to the entire FRA to determine those pixels representing sound driven activity, this step creates a binary image of pixels representing spontaneous or sound driven responses. In calculating the excitatory area any area smaller than 25 pixels was ignored. To calculate the size of the excitatory region of the FRA all cells that survived these thresholding and segmentation steps were summed to obtain the excitatory area. The same binary matrix was used to find the CF and its corresponding attenuation. The CF defined as the lowest pixel on the Y-axis (attenuation levels) to be included in the binary FRA.

Differences in the patterns of activity observed between FRAs provide clues about changes in responsivity in the auditory system and contrasting systemic and local applications of drugs in the IC allow us to disentangle where in the pathway this drug exerts its effects.

Figure 2-7 shows an example FRA. In the top row, three raw FRAs from different time points in the experiment are depicted. Changes in the FRA are evident but are sometimes difficult to identify. To highlight the changes and permit their quantification the FRAs were analysed as follows: the baseline FRA was subtracted from every other FRA in the experiment, resulting in the subtracted FRAs displayed in the 2nd row. Blue always represents a reduction in activity, whereas red represents increased activity. Note that reductions are often smaller than the increases. In order to capture the changes in area and be able to describe them in a systematic way, the subtracted FRAs were subjected to a thresholding step. For each pixel in the subtracted FRA, when the change in spiking in either direction was larger than the average spontaneous firing rate (calculated as above from the baseline) the pixel was set to 1 if the firing rate for the pixel did not exceed the threshold it was set to 0. This process produced a binary version of the subtracted FRA. To avoid random single pixels in the binary image from contributing to the area calculations a segmentation step was included. Areas consisting of six or more connected pixels were included in the area calculations. The total areas for decreased and increased activity were calculated by adding up the number of pixels remaining. These two binary FRA's were superimposed, as displayed in the third row. The firing rates associated with each pixel in the binary FRA were then used to calculate the magnitude of the change in either direction in each pixel. An average magnitude change over the entire area was then calculated. The size of the increased and decreased areas, as well as the individual pixel magnitude values and average magnitude in each area, were stored in separate Matlab files for later analysis.

A way of depicting what the magnitude measure extracts from the FRA is best illustrated in Figure 2-8. The traditional 2D view of the FRA is a top view of a 3D image, in which the colours indicate the magnitude of change. By tilting the figure by 90° as depicted in panel B, the 3D aspect of the figure becomes apparent. The magnitude measures, established the average change in either direction as indicated in the flattened FRA in panel C.

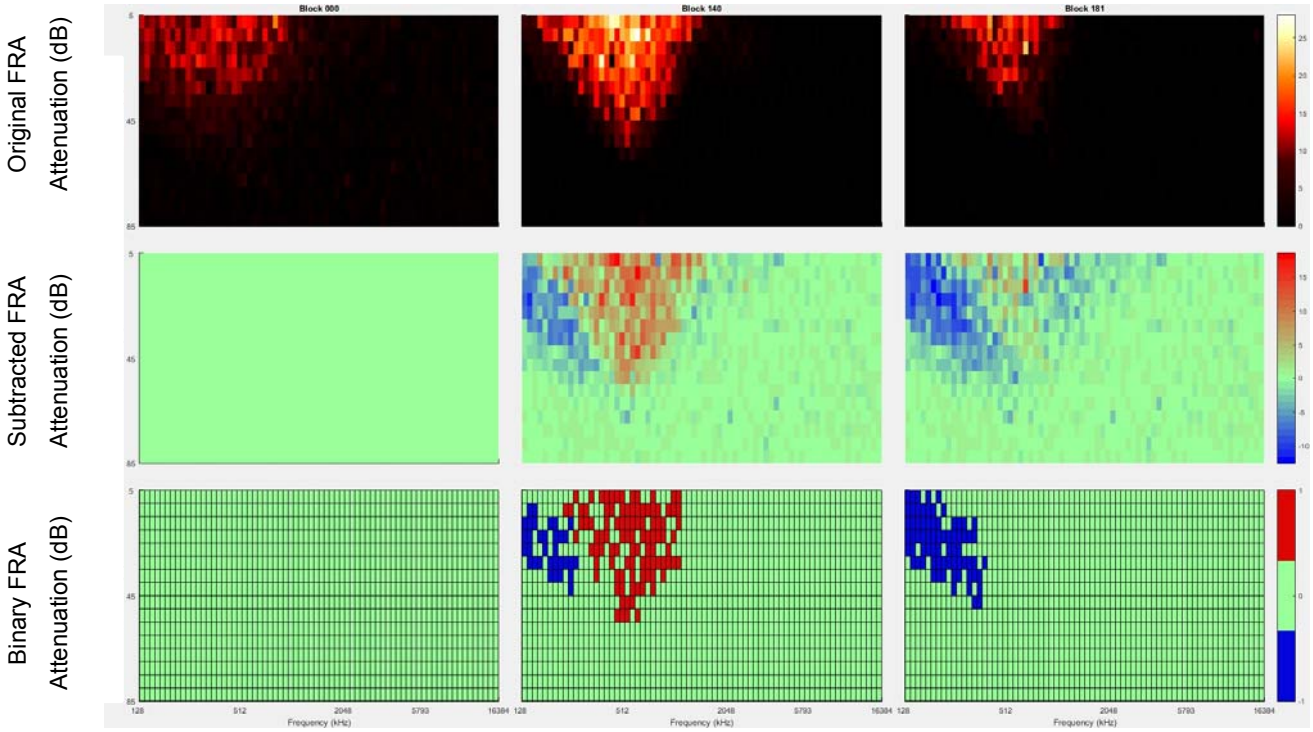

Figure 2-7 Example of FRA analysis. Top row: raw FRAs. Middle row: subtracted FRA following subtraction of the spontaneous rate from the raw FRA. Bottom row: a binary FRAs clearly showing areas where firing rate has increased or decreased.

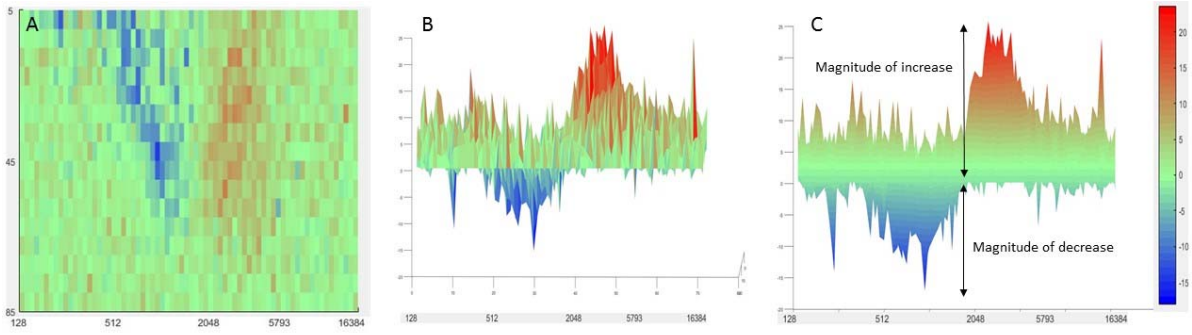

Figure 2-8 Illustration of the information extracted from the subtracted FRA. P A shows a subtracted FRA Figure. B this plot has been tilted through 90° to reveal the 3D aspect of the figure. C the magnitude of the increase and decrease in firing rate n is indicated by the arrows.

Chapter 3. Cytoarchitecture and Phenotypic Features of nNOS Expressing Cells

3.1 Introduction

The presence of nNOS in the IC is established, but we have a limited understanding about what function these cells perform let alone how nNOS is involved. Currently, we don't know whether NO functions as a trans-synaptic neurotransmitter or whether it functions as a second messenger within the cells that produce it. Given the long evolutionary history and different splice variants of nNOS which occur it might perform both functions. One way of gaining insight into the functional properties of the nNOS positive cells of the IC is by studying their distribution, and their features. The aims of the studies presented in this chapter were listed in Chapter 1 but can be summarised as the aim to characterise nNOS positive neurons in the IC in terms of their distribution in the subdivisions of the IC and their expression along the rostral-caudal axis, their neurotransmitter phenotype, the presence of calcium binding proteins within them, and the types and origins of the inputs that innervate them.

Neurons can be characterised by many different properties but an important determinant of their function is the neurotransmitter utilised by the neuron. In the IC both excitatory (glutamatergic) and inhibitory (GABAergic) neurons are observed. Virtually all neurons present in the IC fall within either one of those two categories. Although some studies have reported around 10% of the cells to be uncategorised by either of those two labels (Wu *et al.*, 2008; Fujimoto *et al.*, 2016), it is currently unclear what these cells represent. Although other projections (e.g. serotonin, dopamine, acetylcholine and glycine) originating from different brain areas terminate in the IC, as discussed in the Introduction (Chapter 1), none of these have cell bodies in the IC.

As described in Chapter 1 in more detail, nNOS is dependent on calcium binding to calmodulin in order for it to become active and catalyse the synthesis of NO. The calcium binding proteins calbindin and calretinin have been described in IC as having a similar gross regional distribution to nNOS (i.e. high expression in cortices and low expression in the central nucleus), whereas parvalbumin shows an 'inverse' distribution. It is unclear which, if any, of the calcium binding proteins are expressed in nNOS containing neurons. Given the need for tight calcium regulation in nNOS expressing neurons, it was hypothesized that such cells also employ one or more calcium binding proteins to regulate the amount of free calcium in the intracellular environment. Because little is known about the cells expressing

calcium binding proteins they were subjected to a similar investigation as the nNOS expressing cells, with the aim of learning more about these cells investigating their phenotypical make up and expression along rostral-caudal axis of the IC.

Knowing whether nNOS expressing cells in a region are predominantly GABAergic or glutamatergic is of interest because the IC is an integrating structure where several streams of excitation and inhibition converge. Therefore understanding where the projections that the nNOS positive neurons receive originate from would be of value and mark a step forward in our understanding of the functioning of these cells. The vesicular transport proteins have been used as markers for glutamate transmission, but they only label in terminals, not cell bodies. Both VGLUT1 and VGLUT2 terminals have been observed in the IC but only VGLUT2 mRNA expression has been observed in the IC (Altschuler *et al.*, 2008). Although there is an abundance of VGLUT1 positive terminals in the IC, these do not originate from cells with cell bodies in the IC (Ito *et al.*, 2011; Fujimoto *et al.*, 2016). These two markers give clues about the sources of input and can potentially help to distinguish different subtypes of nNOS expressing cells.

Expression of these proteins has been described in all major subdivisions of the IC showing an overlap in areas of distribution (Paxinos *et al.*, 1980). Thus far the presence of nNOS and calcium binding protein expressing neurons have been shown in overlapping subdivisions of the IC, but no extensive study of whether these proteins show co-expression in the same cells has been conducted.

To sum up, the questions addressed in this chapter:

1. In what subdivisions of the IC are nNOS labelled cells observed and is there a change along the rostral-caudal axis?
2. Are the cells expressing nNOS predominantly glutamatergic or GABAergic and are there gross differences to be observed between the different subdivisions?
3. Do nNOS positive cells co-express the calcium binding proteins calbindin, calretinin or parvalbumin, and are there differences between subdivisions?
4. What type of glutamatergic inputs do the cells expressing nNOS receive, can distinct subpopulations be discriminated by their VGLUT1 and VGLUT2 inputs?

Owing to the number of neuronal markers used, the data reported in this chapter is largely descriptive in nature.

3.2 Methods

The immunohistochemical protocol, including the specific antibodies used in these studies have been described in detail in Chapter 2. All studies in this chapter were performed in adult, Lister-hooded rats, males only (200-300g). In these experiments, the IC was cut in 40 µm coronal sections caudal to rostral. Every fourth section was taken for a specific set of immuno-labelling experiments. This enabled the expression of the proteins to be characterised along the rostral-caudal axis through the IC at an interval of 160 µm. Thus the IC from one animal gave rise to four different sets of double immunofluorescent experiments. Labelled sections were mounted on slides and stored at 4°C in the dark to preserve the fluorescent labels. Imaging of the sections was performed at different magnifications with the appropriate filter sets as described in Chapter 2. Automated image acquisition protocols ensured minimal bleed through between the channels, but negative controls were included as an extra safeguard.

To measure a large number of cell diameters from calbindin, calretinin, parvalbumin and nNOS positive cells, mosaic image files containing the appropriate labels were loaded in Fiji (Schindelin *et al.*, 2012) a complete version of ImageJ with all plugins (Schindelin *et al.*, 2015). The colour channels were split into red, green and blue. The appropriate channel was selected depending on the label of interest and the other channels were stored for later analysis.

The background was subtracted from the image with a rolling ball radius of 100 pixels, a manually adjusted threshold was applied to the mosaic images, and inspected to ensure that individual cells were visible. These thresholded images were stored as binary images. The binary image was subjected to the automated cell measuring protocol in Fiji ('Analyze' – 'Analyze particles'). The size was set to a range between 5-120 µm and the full range of circularity was allowed (0.00-1.00). Fiji was instructed to return the number of cells and their Feret's diameter as well as a map of the outlines of the counted cells. The outlines were superimposed with the original images and erroneously included counts, mainly in edge areas, were removed from the data table. All cell counts and diameter measurements were stored in SPSS. To validate the automated cell counts three sections for each label one taken from the caudal, middle and rostral IC were analysed manually. The manual measurements were compared to the automated measures to check the two methods were consistent.

The statistics of the cell diameters were analysed using a two way ANOVA with cell type and area along the rostral caudal axis as factors. Owing to the large number of cells

measured, the smallest difference in diameter will appear significant, therefore for both the main effect and the interaction effect, only effect sizes larger than 1 μm will be reported. Significant main effects were followed up by post-hoc Tukey tests. For the interaction effect, the data file was split into the different immunohistochemical labels and one way ANOVAs performed with the position of the labelled cell along the rostral caudal axis as a factor. Again significant ANOVA results were followed up with post hoc Tukey tests.

Some of the immunohistochemistry experiments, nNOS and calcium binding proteins and parvalbumin and VGLUT1 and VGLUT2 reported here were conducted as part of undergraduate student projects I helped to supervise.

3.3 Results

3.3.1 nNOS Expression in the Inferior Colliculus

nNOS expression in the dorsal and lateral cortex

Neurons showing nNOS labelling throughout the cell (diffuse labelling), including dendrites and proximal axons, were observed along the rostral-caudal axis of the IC in both the dorsal and lateral cortex. In the lateral and dorsal cortex neurons showing punctate nNOS expression were also observed, although impossible to distinguish in diffuse labelled cells. The density of nNOS positive cells was highest in the dorsal cortex near the commissure as seen in Figure 3-1. Cells in the dorsal cortex tended to be simpler in morphology, in the sense that they show little or no dendritic branching, compared to cells in the lateral cortex and border area of lateral cortex and central nucleus. The cells in the lateral cortex, as shown in the inserts in Figure 3-1 and Figure 3-2, showed a more complex morphology with intricate dendritic branching. An ANOVA showed that nNOS positive cells in the lateral and dorsal cortex varied in size by region($F(2, 6068) = 373.35$, $p < 0.0001$). Post hoc Tukey tests showed that nNOS cells in rostral regions were larger compared to both those in the middle regions Figure 3-41.

nNOS expression in the central nucleus

As illustrated in Figure 3-1, at lower magnifications few NOS positive cells were observed in the central nucleus and, those present were faintly labelled. However, at higher magnification punctate nNOS labelling could be seen in all subdivisions of the IC; this was particularly noticeable in the central nucleus due to the absence of cells with nNOS labelling in all cellular compartments. These nNOS ‘puncta’ appeared as bright, small but clearly delineated dots found in apparent association with the neuronal cell body, as indicated by

the presence of DAPI labelling. Figure 3-2 illustrates the nNOS positive punctate labelling observed in the central nucleus. This punctate labelling is in contrast to the cells showing nNOS labelling throughout all cellular compartments as observed in the lateral cortex. For illustrative purposes in Figure 3-3 a cartoon version of this phenomenon is shown.

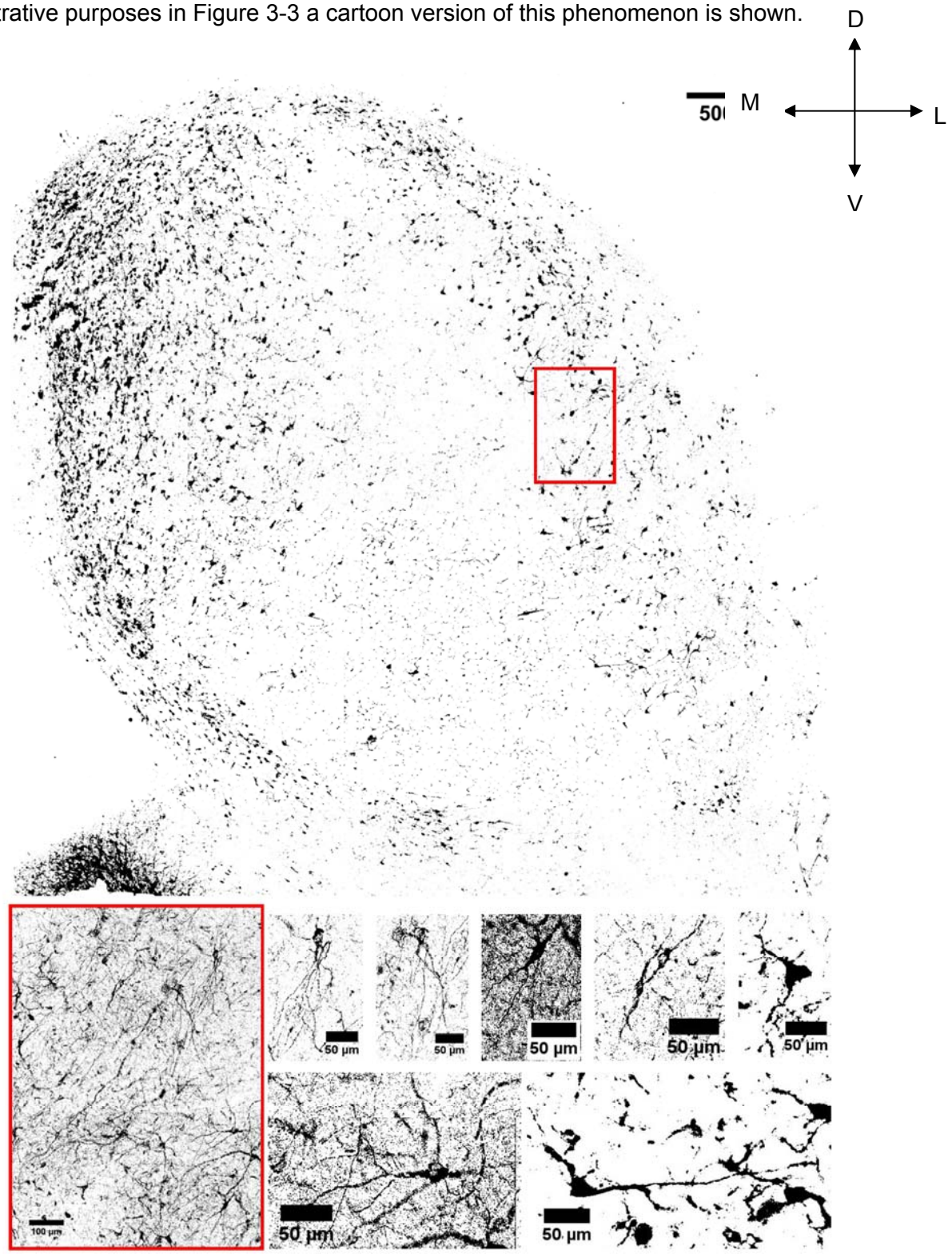

Figure 3-1 above a thresholded mosaic image of nNOS positive labelled cells in a whole coronal IC section midway along the rostro-caudal length of the IC. The area outlined by the red rectangle is enlarged at the bottom left of the figure and individual neurons from within this area are shown enlarged to its right.

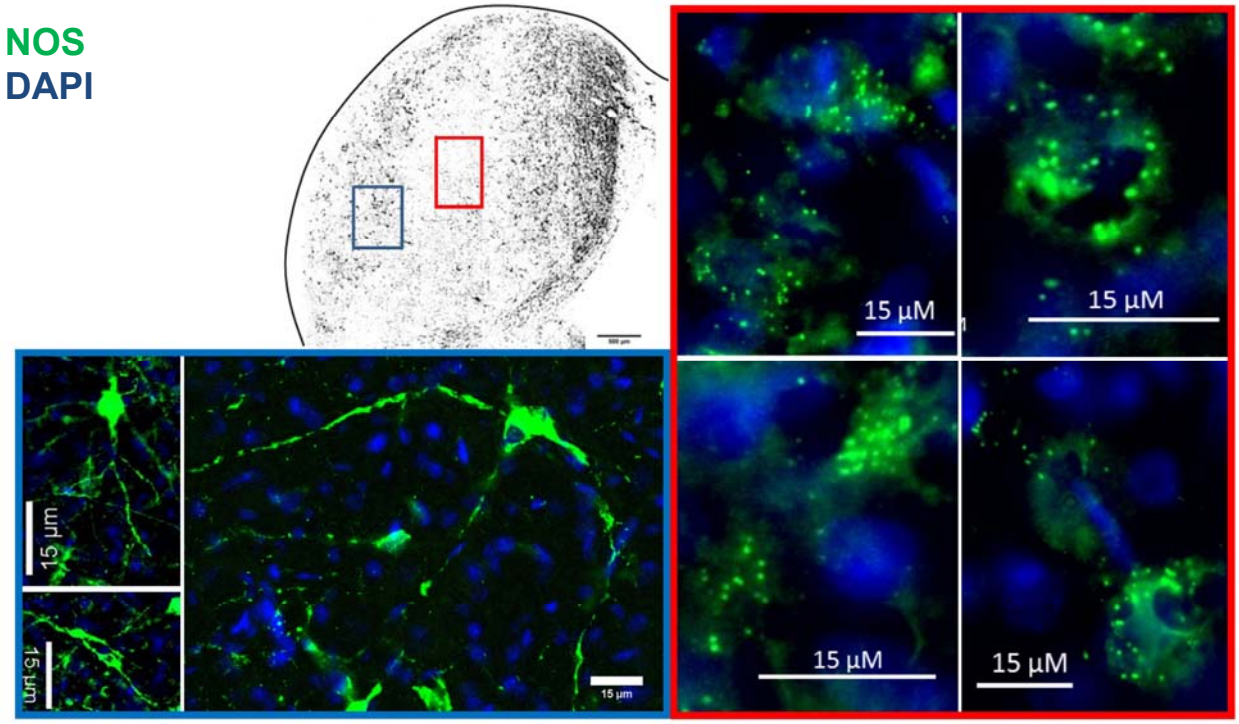

Figure 3-2 in the top left the nNOS distribution in the IC is shown, the scale bar indicates 500 µm. The blue and red boxes indicate areas in the lateral cortex and central nucleus respectively where the high magnification examples of nNOS positive cells were obtained. Note the complex dendritic branching and nNOS labelling throughout the cell in the cells observed in the lateral cortex (blue rectangle), some elements of the image are saturated in order to bring out the finer dendritic branching. Neurons in the central nucleus (red rectangle) exhibit nNOS puncta mainly on the soma, however, dendritic presence is not unlikely but more difficult to observe.

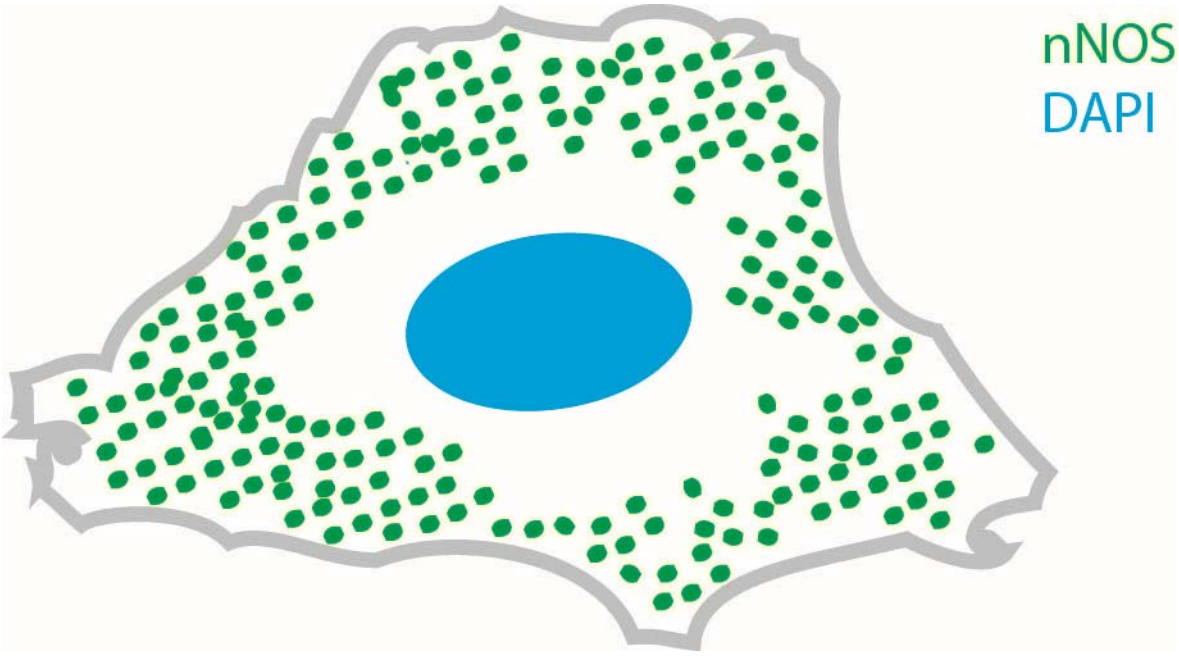

Figure 3-3 Cartoon of nNOS punctate labelling. The nNOS positive punctate labelling is recognised by dense clusters of bright dots of nNOS labelling surrounding the soma, indicated by the nuclear label DAPI.

3.3.2 nNOS is Associated with PSD95

The co-labelling of PSD95 with the nNOS Puncta demonstrating a post synaptic location.

To test the hypothesis that the nNOS positive puncta observed in the central nucleus of the IC were localised in the post synaptic density and form part of the nNOS-NMDA receptor-PSD95 complex, immuno labelling experiments were performed with antibodies against nNOS and PSD95. PSD95 labelling in the central nucleus of the IC appeared as puncta distributed throughout the subdivisions of the IC usually outlining cell bodies, as indicated by DAPI. The nNOS labelled puncta were closely associated with PSD95 (Figure 3-4). Many PSD95 labelled puncta with no associated nNOS labelling were also observed. However punctate labelling is, by definition, small and extremely bright, and punctate labelling deeper in the tissue and out of focus in the current image is visible as diffuse labelling. In order to make qualified decisions whether punctate labelling was solely PSD95 positive, solely nNOS positive or co-labelled for both, 3D rendering and layer by layer analysis was used (Figure 3-5). Flattening the 3D rendering as a maximum intensity projection as displayed in Figure 3-6 shows that virtually all the nNOS labelling is also PSD95 positive. Although in this view some nNOS positive only labelling still appears to occur, careful Z-stack layer by layer analysis illustrated in Figure 3-7 demonstrates that the nNOS positive puncta observed in the central nucleus are consistently co-labelled by PSD95.

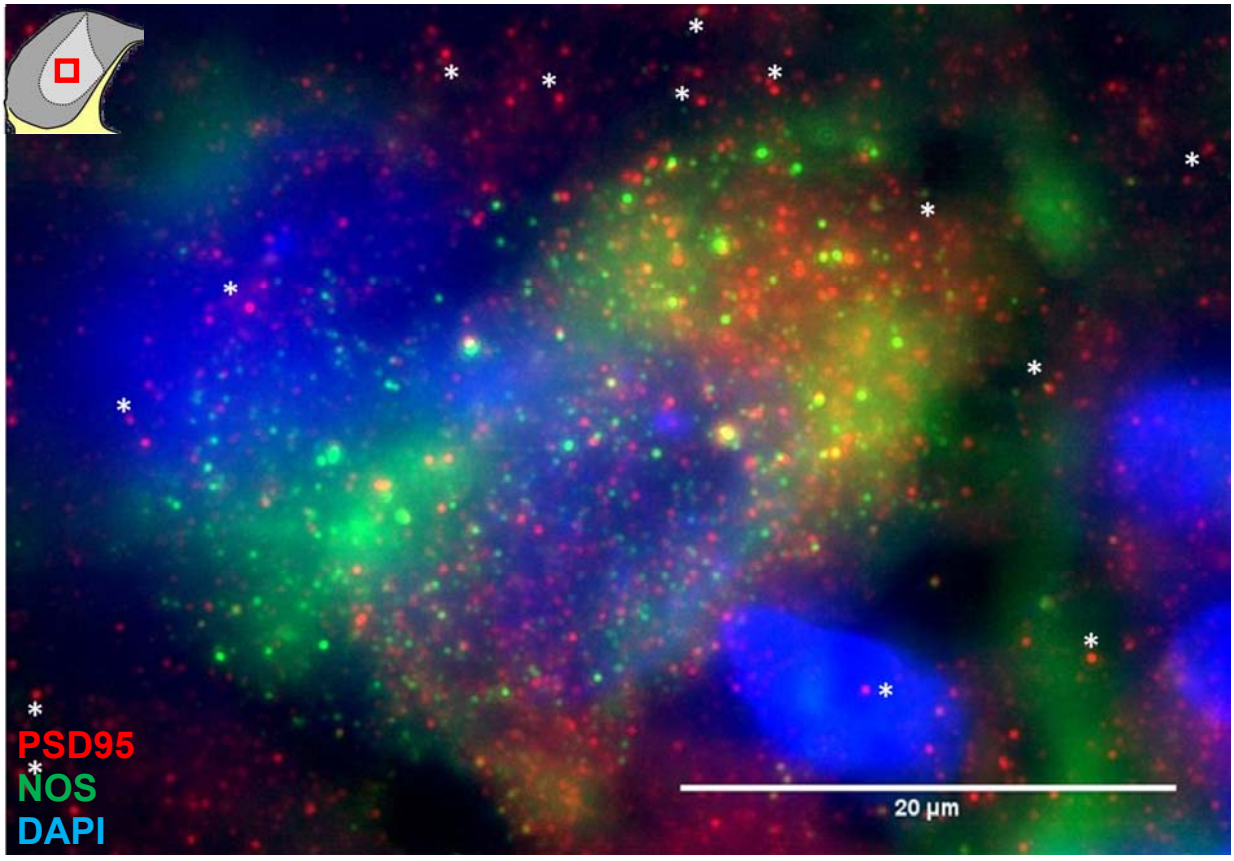

Figure 3-4 one slice from a Z-stack series depicting PSD95 and nNOS punctate labelling in central nucleus of the IC. PSD95 without nNOS labelling are indicated by *.

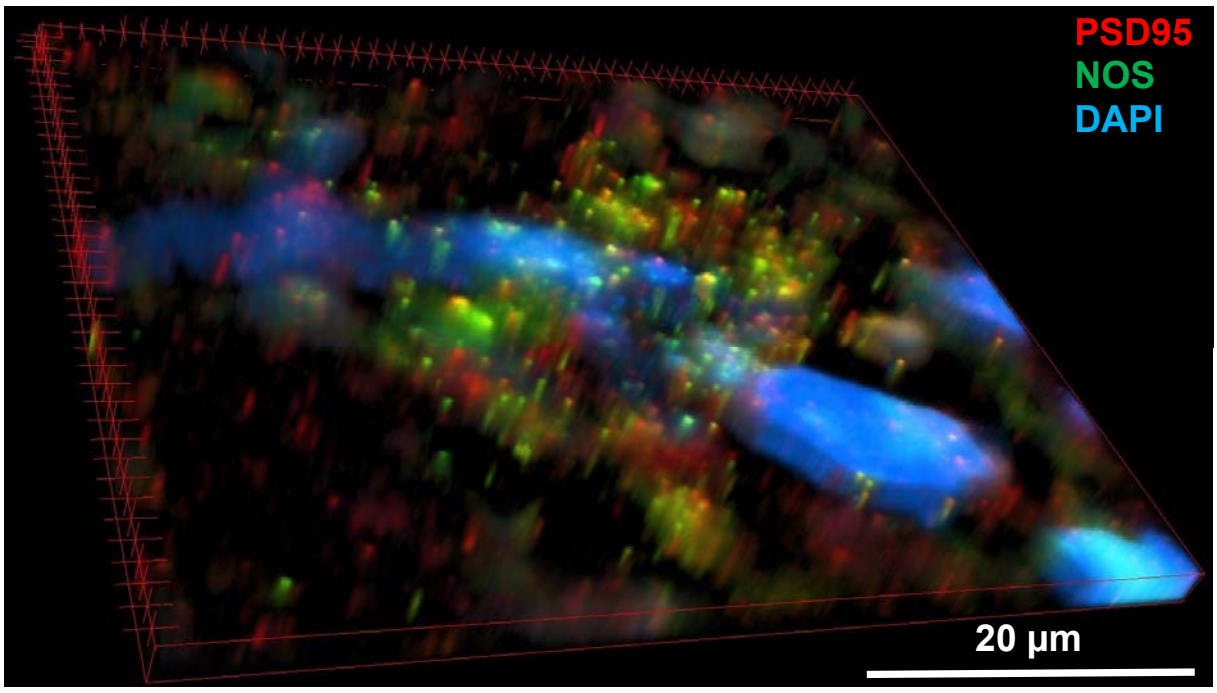

Figure 3-5 zoomed out view of 3D rendered cell in Figure 3-4 showing nNOS (green) and PSD95 (red) punctate labelling in the central nucleus of the IC. This 3D model allows rotation and every dot can be inspected in a 3D environment to observe whether it is co-labelled.

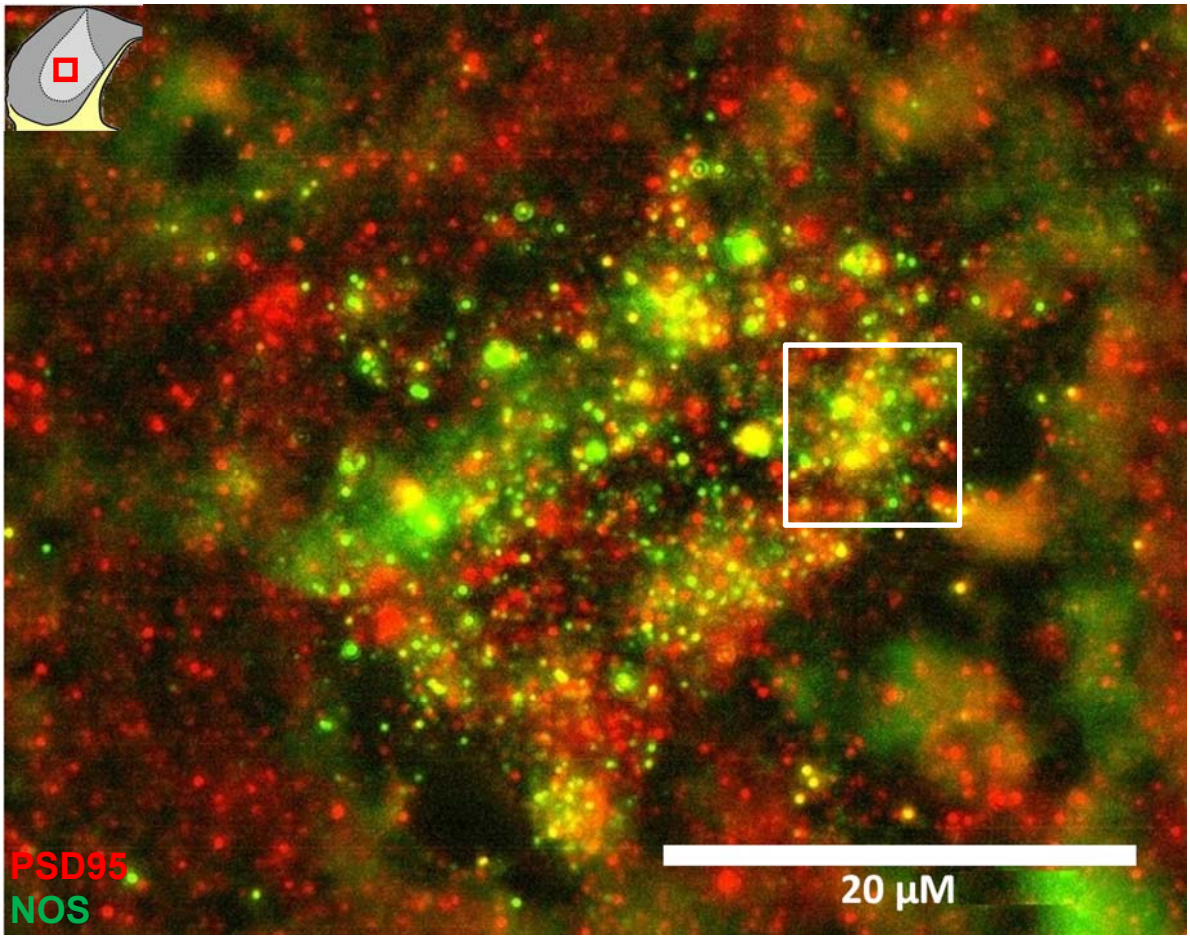

Figure 3-6 a maximum intensity projection from nNOS and PSD95 labelling in the central nucleus of the IC. nNOS positive puncta are closely associated with PSD95. The square indicates the area on which Figure 3-7 is based. Yellow indicates strong co-labelling of nNOS and PSD95. The red punctate labelling indicates PSD95 only labelling.

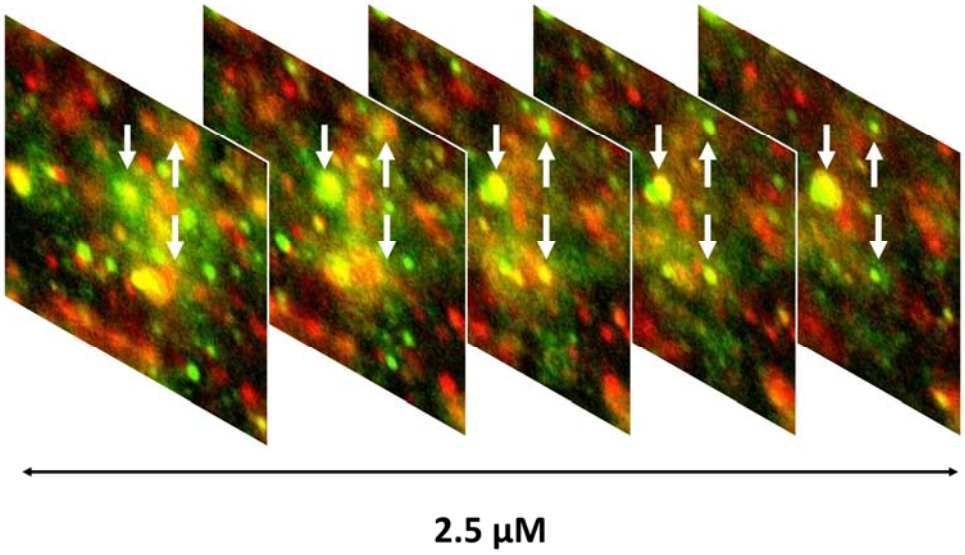

Figure 3-7 five consecutive 0.5 um optical slices from the central nucleus of the IC labelled for PSD95 and nNOS. This image illustrates that co-labelling of PSD95 and nNOS requires layer by layer analysis because co-labelling of both proteins can be observed in some, but not in all layers (indicated by arrows). Images collected from the square in Figure 3-6.

3.3.3 Different GABA Expression in Subdivisions of the IC

GABA labelling was observed throughout the IC (Figure 3-8) but the large GABAergic cells with a diameter >15 µm were observed exclusively in the central nucleus and border regions of the lateral cortex. Smaller GABAergic cells with diameters between 5 and 15 µm were observed throughout the dorsal and lateral cortex as well as in the central nucleus but were particularly abundant in the dorsal cortex near the commissure. Although GABA neuropil labelling was observed in the cortices the labelling thinned out considerably towards the outer edges.

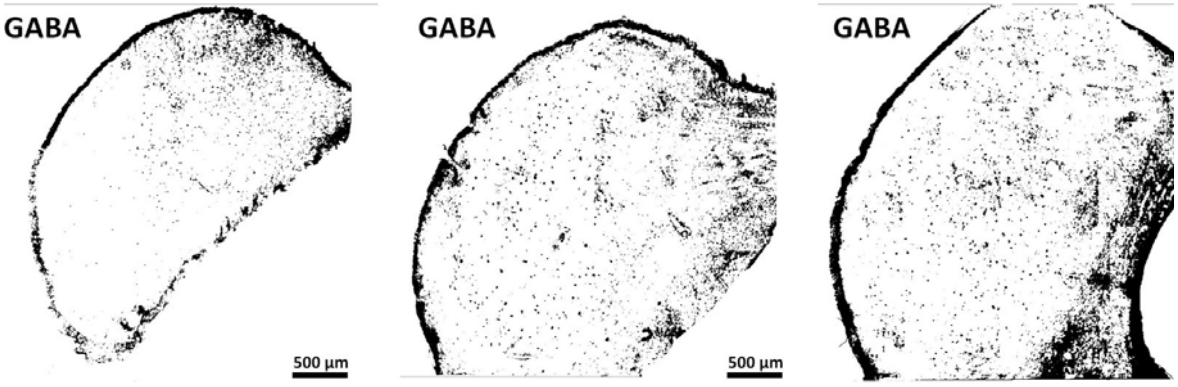

Figure 3-8 mosaic images showing GABA expression along the rostral-caudal axis, a manual threshold was applied to these images to enhance the contrast. Caudal, mid and rostral sections of the IC are depicted from left to right. The scale bar indicates 500 µm. Note how the section is outlined by labelling, this appeared to be an artefact.

3.3.4 nNOS and GAD are Rarely Co-expressed

GAD65/67 labelling was observed throughout all subdivisions of the IC both as cellular and neuropil labelling with a similar distribution to GABA. GAD65/67 positive neuropil was observed in the lateral and dorsal cortex, as indicated in Figure 3-9. However, even though these regions also contain the cells showing distributed nNOS labelling, the GAD and nNOS markers rarely labelled the same cell. GAD positive cell body labelling was mainly observed in the central nucleus. Few of those GAD labelled cell bodies in the central nucleus showed nNOS positive puncta. Thus, the majority of the nNOS positive cells did not appear to express GAD, suggesting that they were glutamatergic.

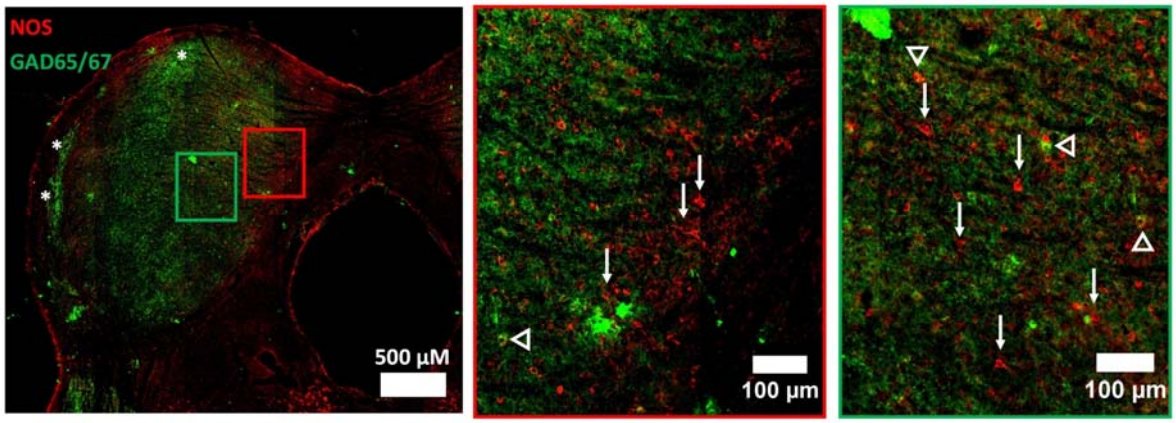

Figure 3-9 a coronal section midway along the rostro-caudal length of the IC labelled for NOS and GAD65/67. Open arrowheads indicate cells that are both nNOS and GAD positive. Arrows indicate examples of nNOS positive cells that show no immunoreactivity to GAD. GAD positive neuropil labelling is indicated by *.

3.3.5 Patterns of Calcium Binding Protein Expression in the IC and Colocalisation with nNOS

Calbindin is expressed exclusively in the dorsal and lateral cortex

Expression of calbindin was exclusively observed in the dorsal and lateral cortices of the IC in discreet and distinct patches. Figure 3-10 shows the calbindin expression in two coronal IC sections. In the inserts, higher magnifications of areas containing calbindin labelling are displayed. Calbindin labelling appears to be restricted to the cell nucleus. Calbindin labelling is restricted to the dorsal and lateral cortex and consisted of small cells with an average diameter of 19.50 µm with a SEM = 0.16 µm. Calbindin labelling was densest in the dorsal cortex especially in the region adjacent to the commissure of the IC. Calbindin expression was observed along the rostro-caudal axis of the IC as illustrated in Figure 3-11. Calbindin positive cell counts, summarised in Figure 3-40, indicated that the number of cells labelling positive for calbindin was highest in caudal areas of the IC and declined gradually towards the mid and rostral areas of the IC.

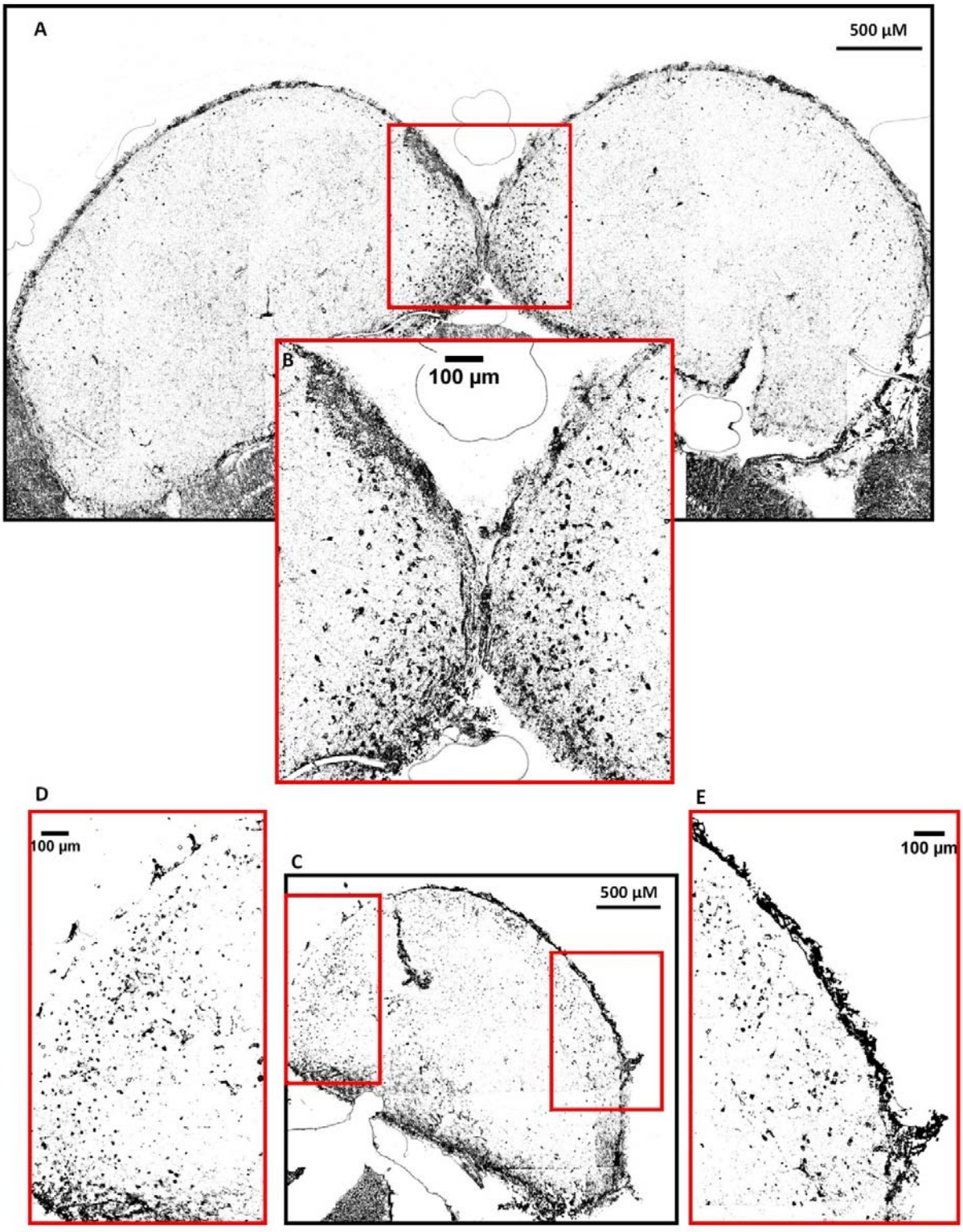

Figure 3-10 calbindin labelling in the caudal IC, a manual threshold was applied to these images to enhance the contrast. Images in the black box A and C show the entire IC while the images in the red boxes show higher magnifications of these areas.

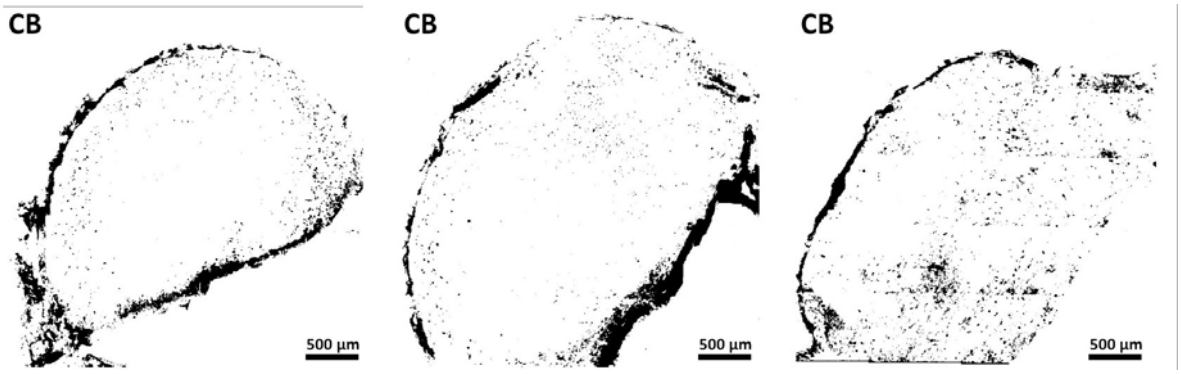

Figure 3-11 Mosaic images showing calbindin expression along rostral-caudal axis, a manual threshold was applied to these images to enhance the contrast. From left to right are depicted caudal, mid and rostral sections of the IC. The scale bar indicates 500 µm.

Most Calbindin positive cells expressed nNOS

Calbindin positive cells and cells with distributed nNOS labelling were both abundant in the dorsal and lateral cortex. Figure 3-12 shows nNOS and calbindin positive cells in the dorsal cortex mid-way along the rostral caudal axis of the IC. Cells were defined by having clear nuclear DAPI labelling. Although in some cases nNOS was faint, careful inspection showed that virtually all calbindin labelled cells also showed immunoreactivity for nNOS (Figure 3-12 by closed arrowheads). However not all nNOS positive cells showed immunoreactivity for calbindin (Figure 3-12 open arrowheads).The same pattern of virtually all calbindin positive cells also being nNOS positive was observed in the lateral cortex as illustrated in Figure 3-14 by open arrowheads. Again nNOS cells not showing any hint of calbindin were also present, as pointed out in Figure 3-14 by the arrows. The nNOS labelling forms circles around cell bodies (indicated by the DAPI labelled nuclei) both for calbindin positive and calbindin negative cells, both of which are illustrated at a higher magnification in Figure 3-13. Calbindin was often only observed in the nucleus of the cell. Calbindin and nNOS labelling were co expressed in the same subdivisions of the IC and in the same cells but showed different subcellular localisations, making co-localisation sometimes hard to judge.

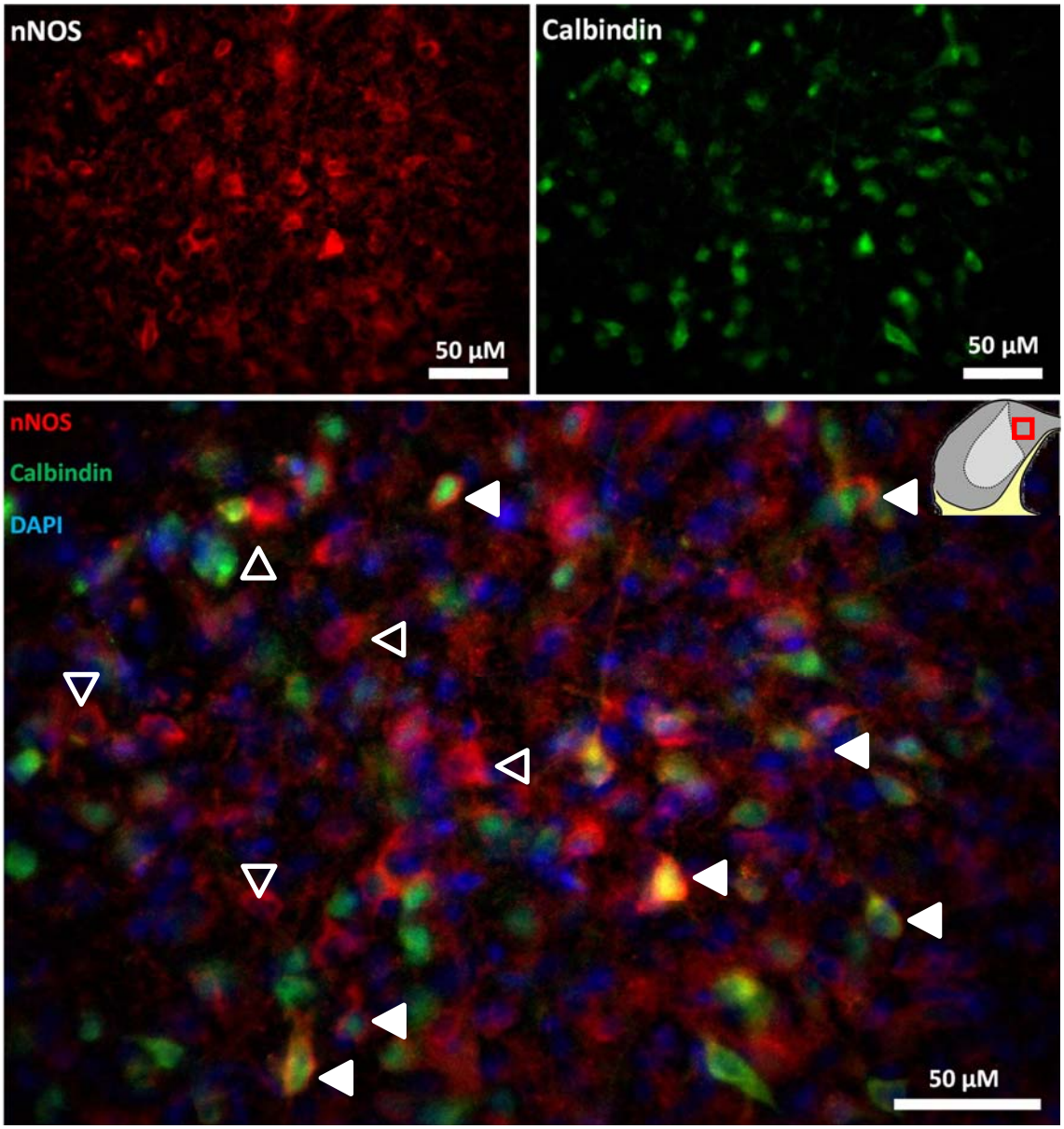

Figure 3-12 nNOS and calbindin expression in the dorsal cortex of IC. Closed arrowheads indicate nNOS positive cells that are also calbindin positive. Open arrowheads indicate nNOS positive cells that show no immunoreactivity for calbindin.

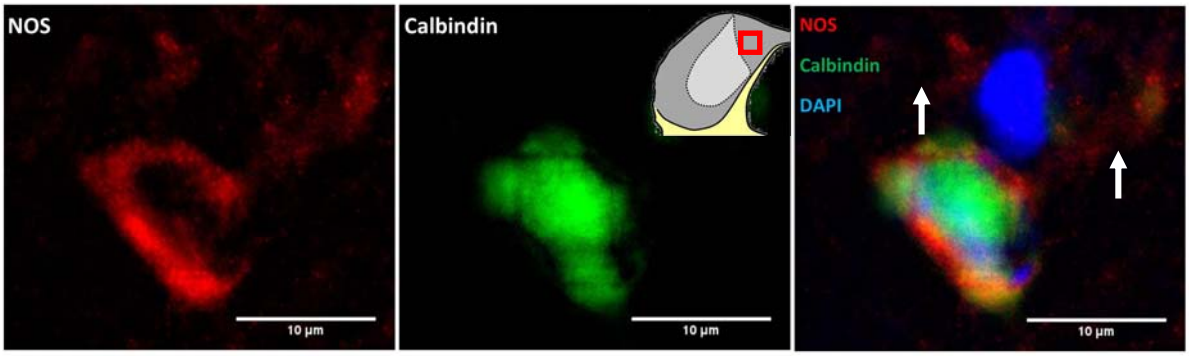

Figure 3-13 higher magnification of nNOS and calbindin labelling in the dorsal cortex. In the centre is a calbindin and nNOS positive cell. The arrows indicate two nNOS only positive cells that show no immunoreactivity for calbindin.

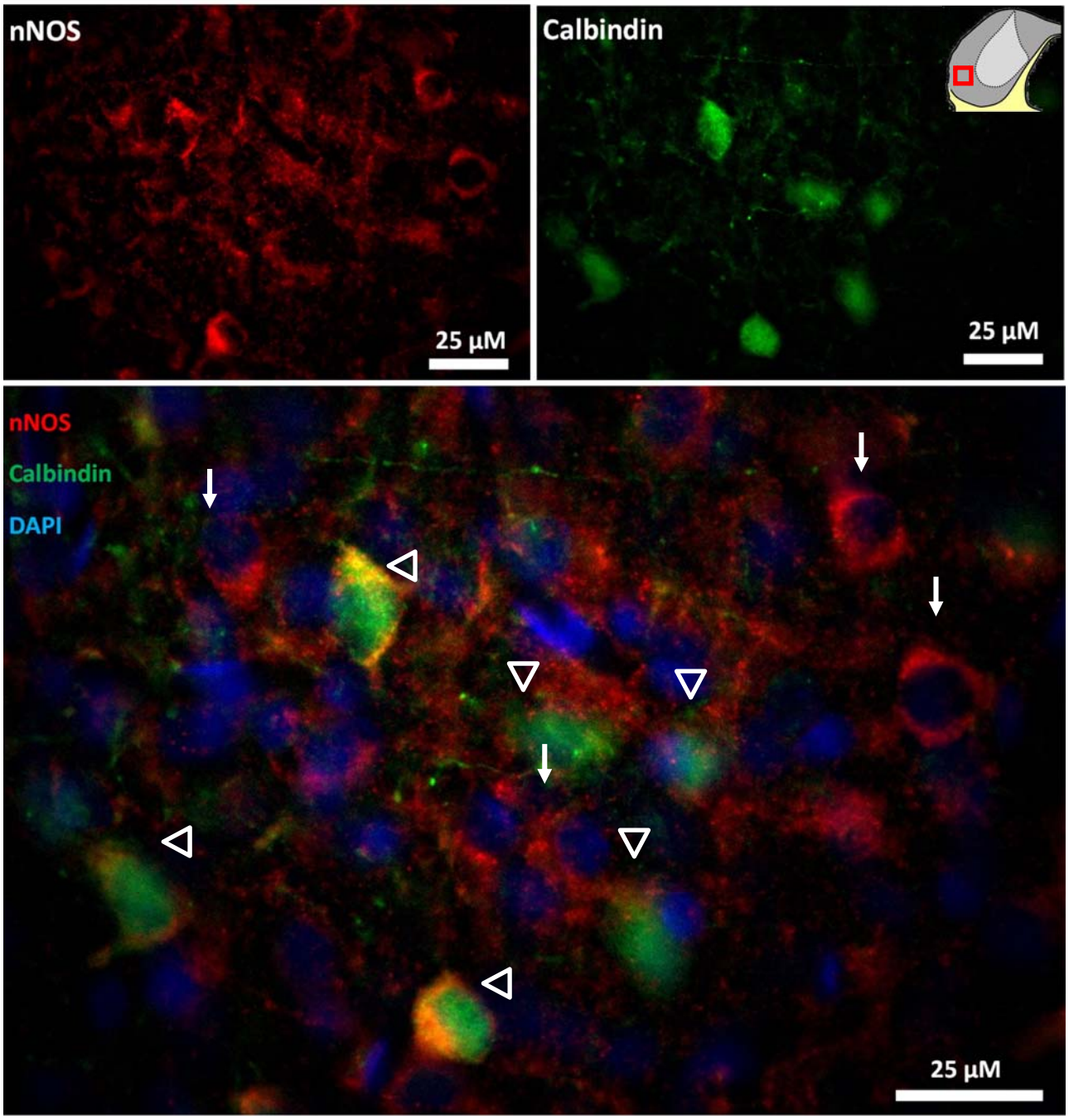

Figure 3-14 nNOS and calbindin expression in lateral cortex. Open arrowheads show cells labelling nNOS and calbindin positive. Arrows point out nNOS positive cells that show no labelling for calbindin.

Calbindin and GABA can be co-expressed

As described earlier, calbindin and GABA positive cells were both observed in the dorsal and lateral cortex of the IC. About half of the calbindin positive cells, in both cortices, also showed immunoreactivity for GABA (Figure 3-15).

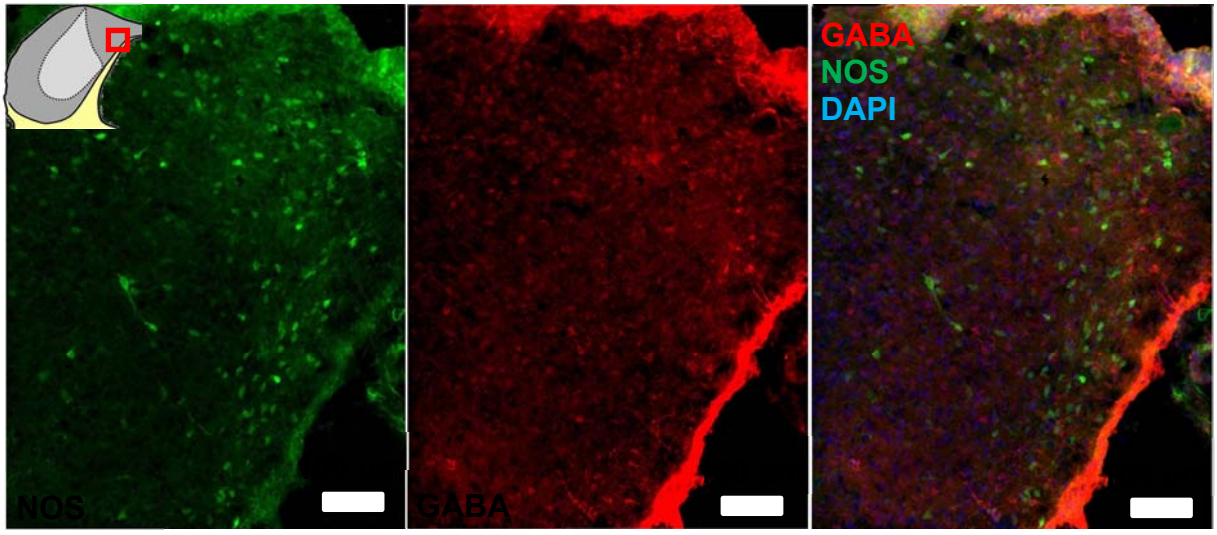

Figure 3-15 calbindin and GABA labelling in the dorsal cortex. Note the absence of co-labelled neurons. The scale bar indicates 100 µm.

Calretinin is expressed exclusively in the dorsal and lateral cortex

Calretinin positive cells were exclusively observed in the lateral and dorsal cortices. Figure 3-16 shows the distribution of calretinin in the subdivisions of the IC. In the dorsal cortex dense calretinin labelling fanning out from the commissure is observed (Figure 3-16A and B). Calretinin positive cells were small cells with an incredibly similar size to calbindin cells with an average diameter of 19.25 µm and a SEM of 0.14µm. No differences were detected in the number of calretinin positive cells along the rostral-caudal axis (Figure 3-17). Compared to calbindin, expression of calretinin appeared less dense in the lateral cortex, but in the dorsal cortex similar numbers of cells labelled for calretinin and calbindin (Figure 3-41).

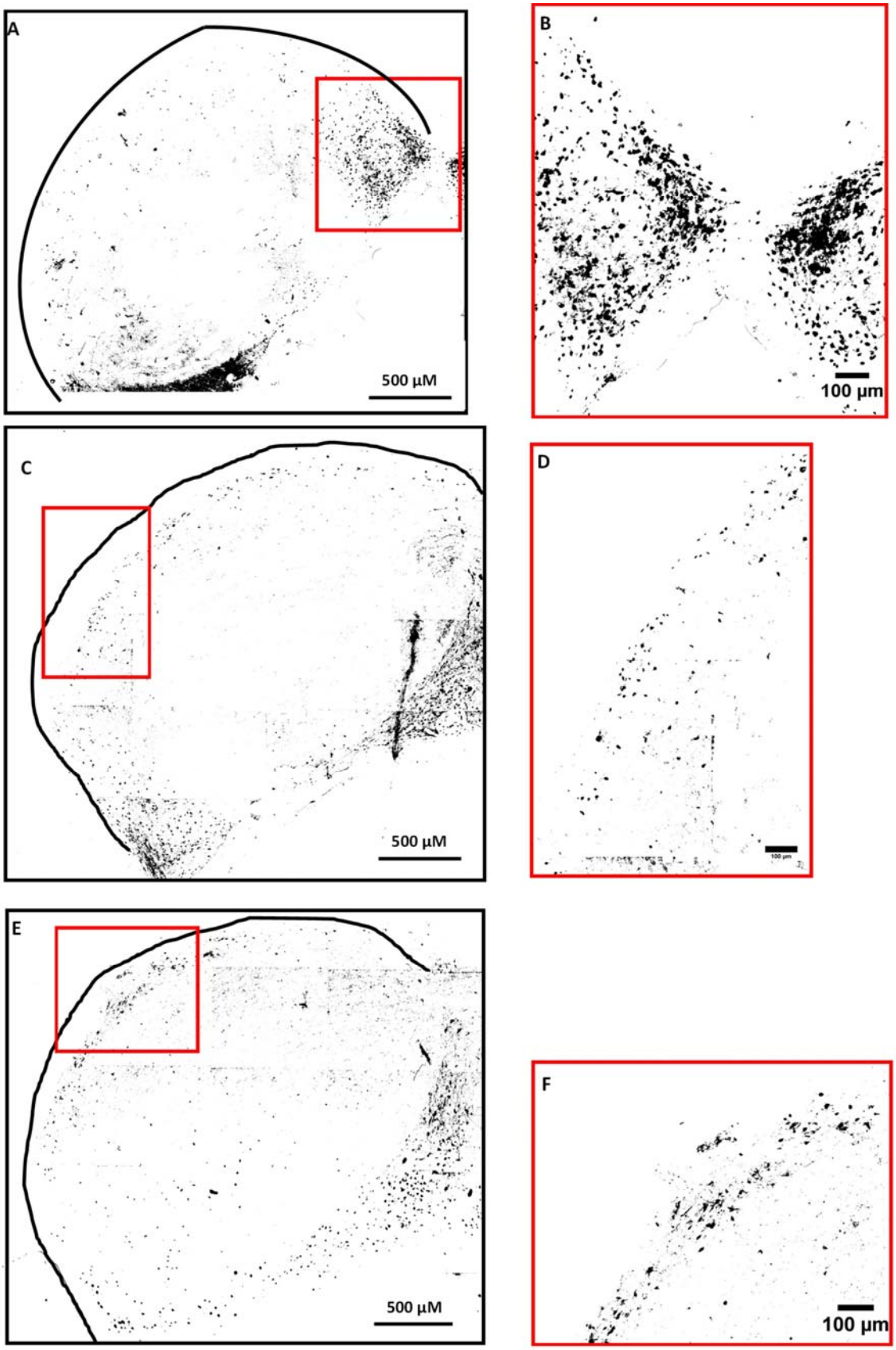

Figure 3-16 Calretinin labelling in the caudal IC. In this region the entire IC is comprised of cortex. A manual threshold was applied to the images to enhance the contrast. Images in the black box A and C show the entire IC while the images in the red boxes show magnifications of regions of interest. Examples A and C are obtained from two different animals. Note that the black stripe on section C is an artefact.

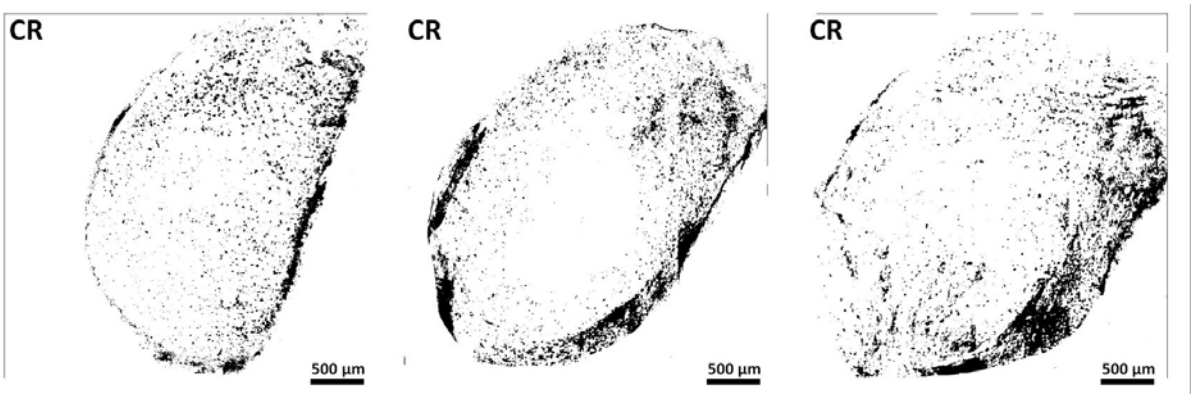

Figure 3-17 Mosaic images showing calretinin expression along the rostral-caudal axis, a manual threshold was applied to these images to enhance the contrast. From left to right are depicted caudal, mid and rostral sections of the IC. Note that in the caudal section where the IC is entirely comprised of cortex, calretinin can be observed throughout the section.

Most calretinin positive cells do not express nNOS

Although calretinin and nNOS labelled cells were both present in the same subdivisions of the IC, in stark contrast to calbindin, few calretinin positive cells showed co-labelling with nNOS. Figure 3-18 shows an area of the dorsal cortex in which both nNOS (red) and calretinin (green) positive cells were abundant but rarely was co-labelling within the same cell observed. However, as illustrated in Figure 3-19 (dorsal cortex) and Figure 3-20 (lateral cortex) a few cells co-express calretinin and nNOS as indicated by the open triangles in both figures. In the central nucleus, no calretinin cell bodies were observed.

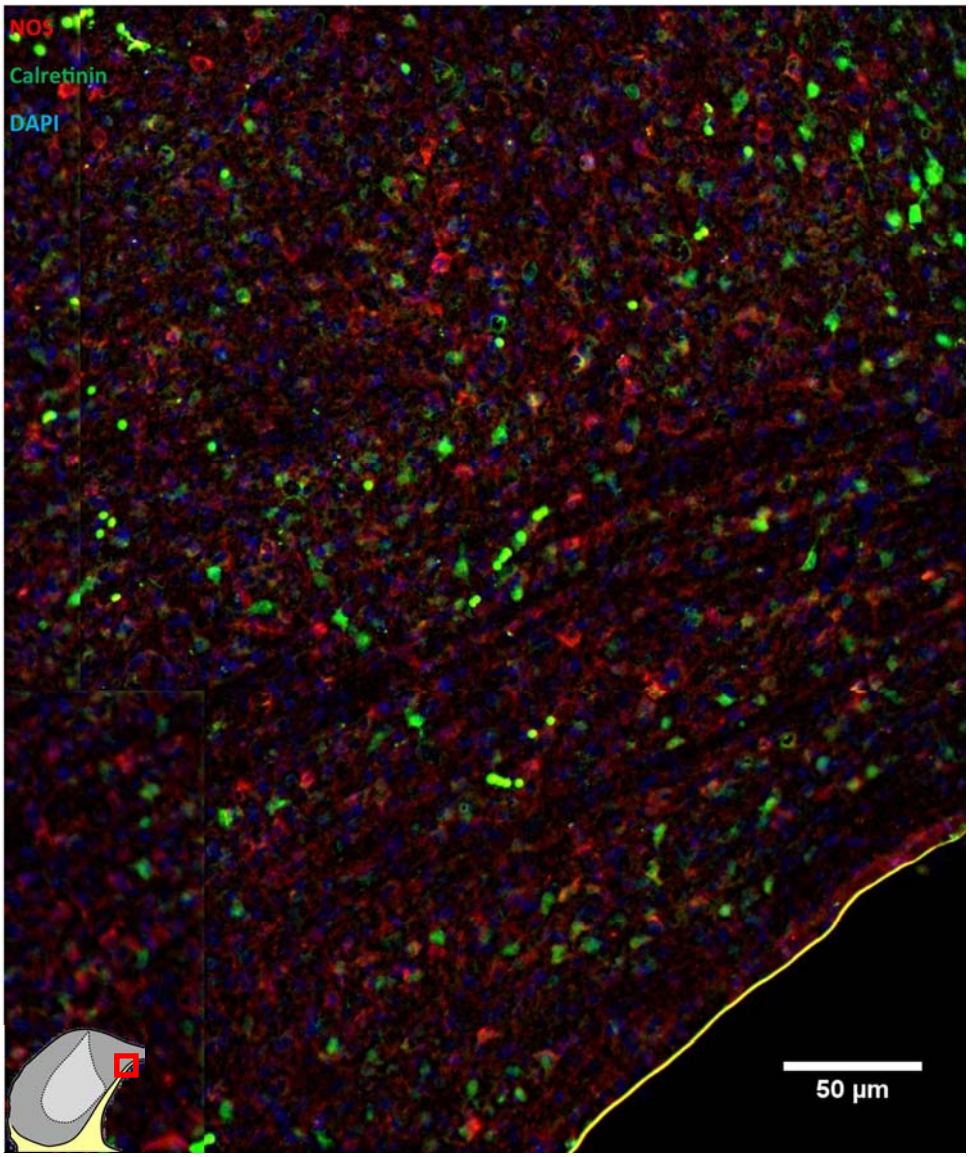

Figure 3-18 nNOS and calretinin positive cells in the dorsal cortex. Note the vast majority of calretinin labelled cells do not express nNOS.

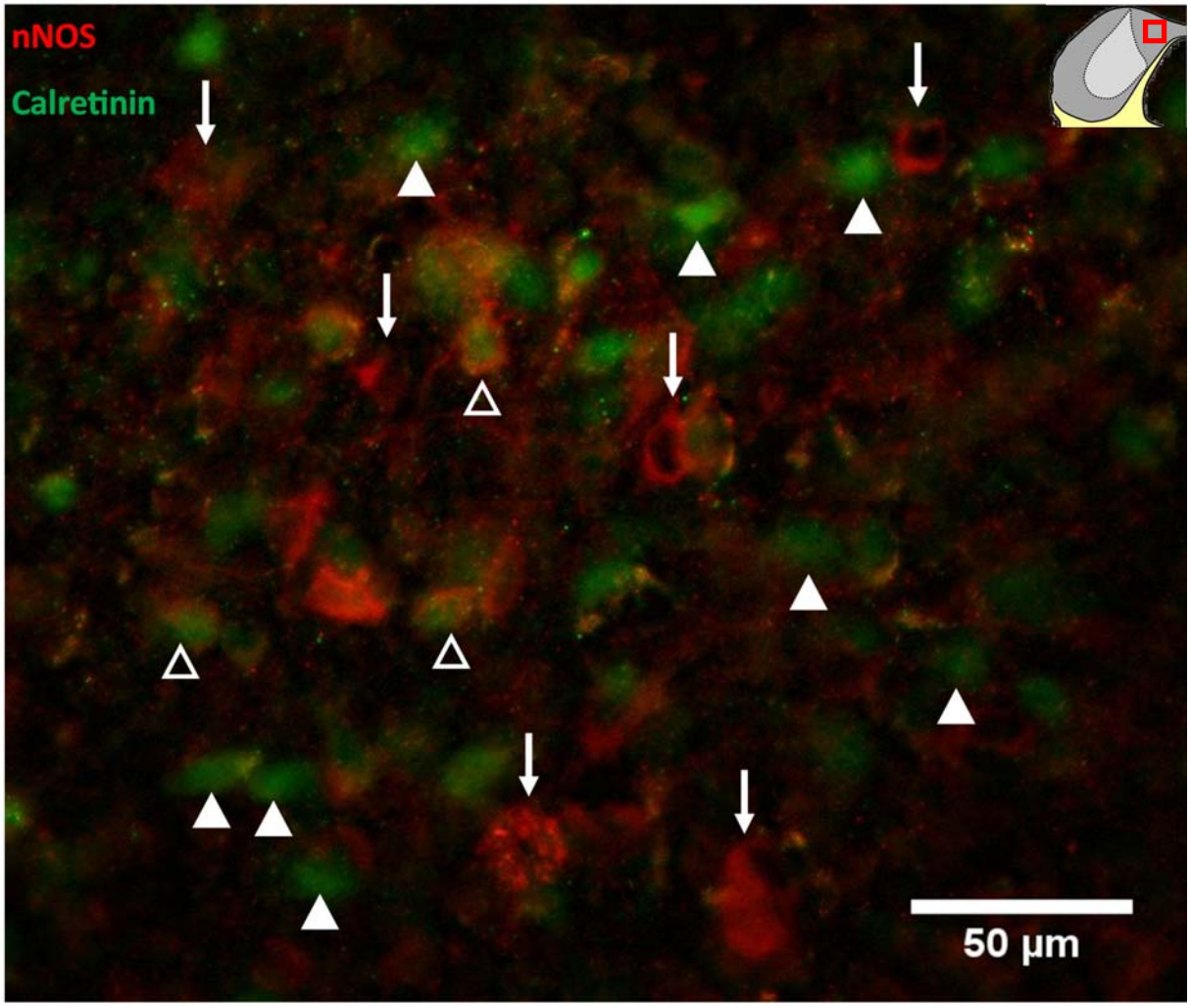

Figure 3-19 calretinin and nNOS positive cells in the dorsal cortex. The arrows indicate nNOS positive cells, the filled arrowheads indicate calretinin only cells and the open arrowheads indicate cells labelling positive for both nNOS and calretinin.

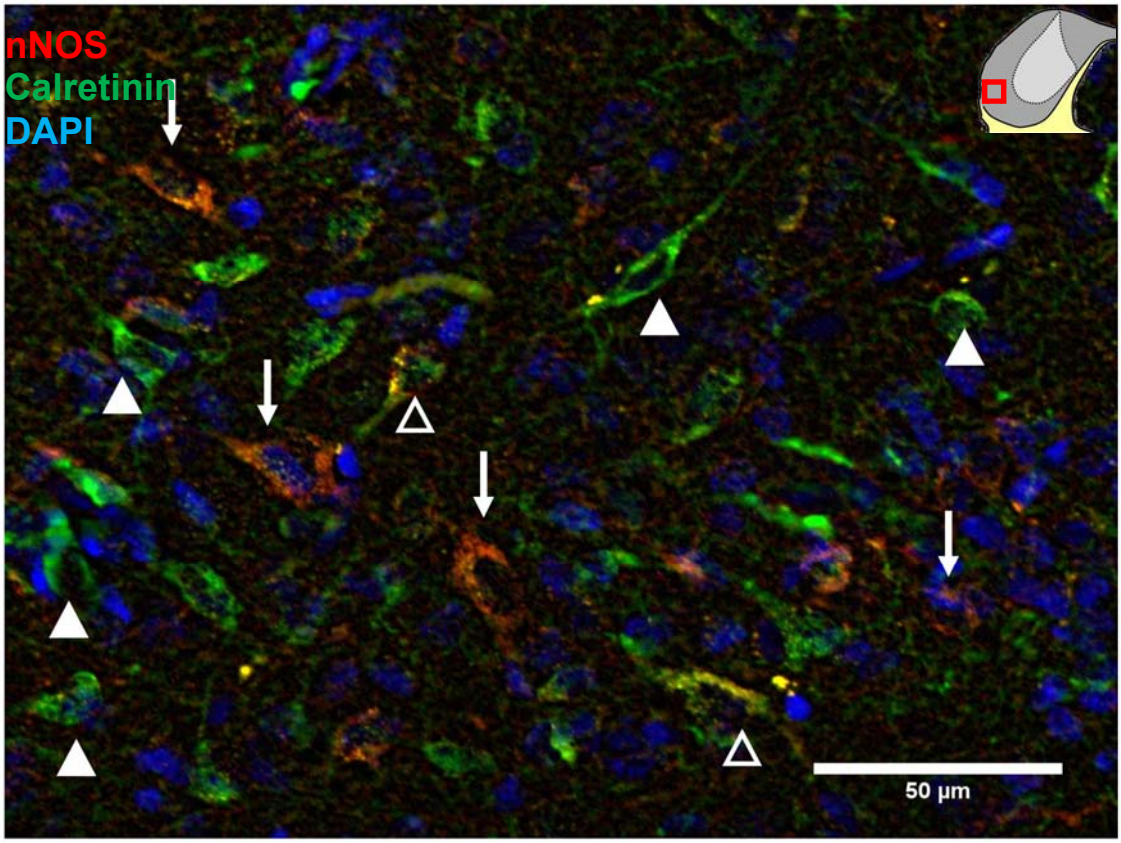

Figure 3-20 calretinin and nNOS positive cells in the lateral cortex. The arrows indicate nNOS positive cells, filled arrowheads indicate calretinin only cells, and open arrowheads indicate cells labelling positive for both nNOS and calretinin.

Calretinin and GABA can be co-expressed

As with calbindin cells, although a substantial number of calretinin positive cells did show immunoreactivity for GABA not all calretinin positive cells were also GABA positive. The majority of GABA positive cells were observed in the central nucleus where no calretinin labelled cells were observed. However, GABA positive cells were observed both in the dorsal (Figure 3-21) and lateral (Figure 3-22) cortex where calretinin positive cells are abundant. Some cells showed immunoreactivity for both labels. In the lateral cortex some dense calretinin positive neuropil clusters were observed (Figure 3-22). These dense calretinin rich clusters also showed high levels of GABA labelling, however, even in these regions of heightened expression both labels appear in different elements and were only rarely observed in the same cell.

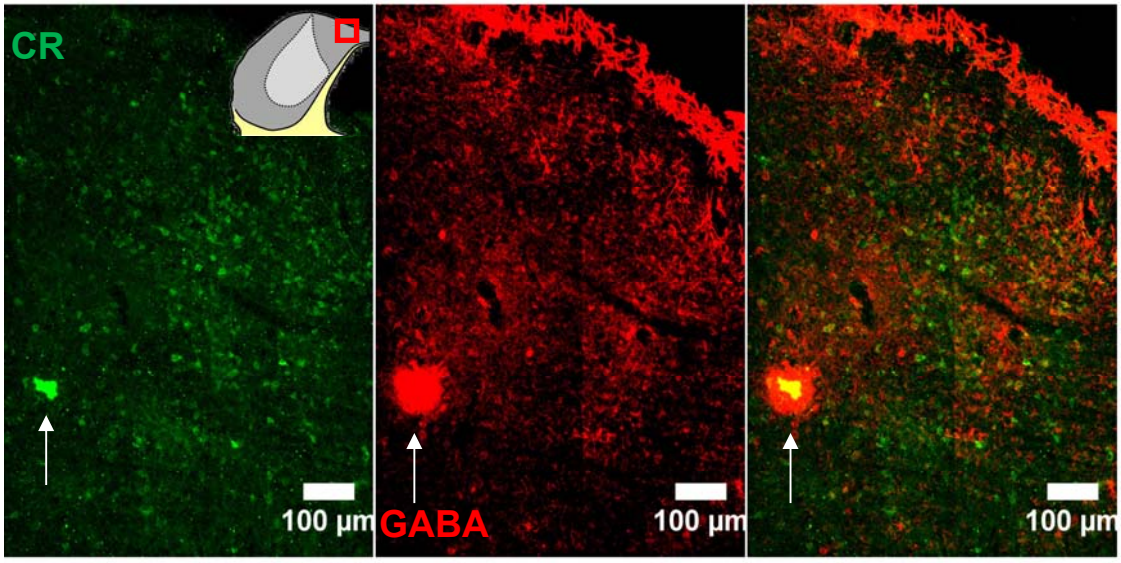

Figure 3-21 calretinin and GABA labelling in the dorsal cortex. The bright dot visible in both channels and indicated by the arrow is an artefact.

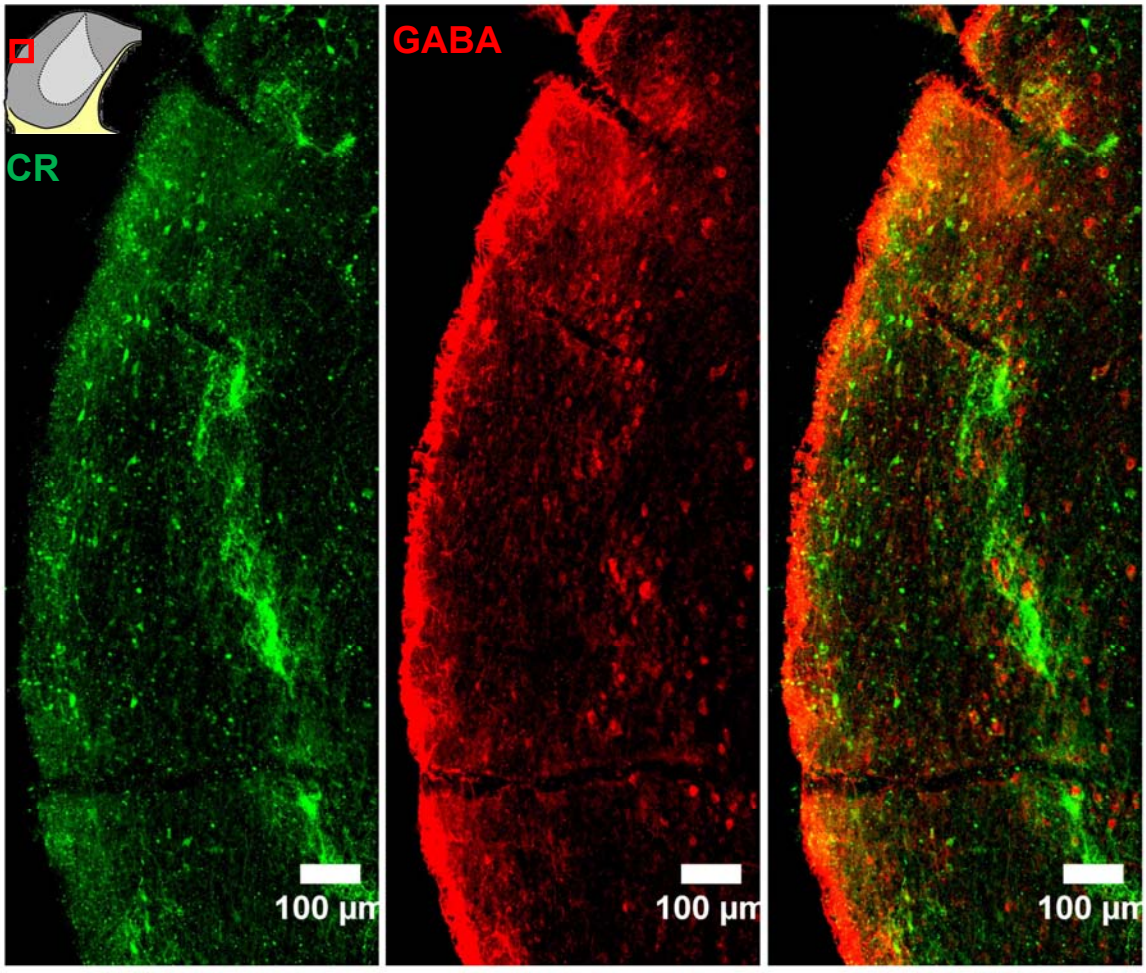

Figure 3-22 calretinin and GABA labelling in the lateral cortex. Note the regions containing dense clusters of calretinin positive neuropil also containing GABA positive cell bodies.

Parvalbumin is abundant in the central nucleus

Parvalbumin positive cells were abundant throughout the IC, but labelling was particularly pronounced in the central nucleus (Figure 3-23). A wide range of morphologies were observed in parvalbumin labelled cells. Parvalbumin positive cells showed cytoplasmic labelling with some showing somatic only labelling and other cells had clear labelling of the axons and dendrites (Figure 3-38 and Figure 3-39). No obvious difference in the number of parvalbumin positive cells was observed along the rostro-caudal axis (Figure 3-24). Parvalbumin labelled cells were bigger compared to calbindin and calretinin labelled cells, with an average cell diameter of 21.34 µm, SEM = 0.11 µm. Parvalbumin cell body diameter did not differ along the rostral caudal axis, although the ANOVA as discussed in section 3.3.8 returned a significant P value, the effect size was below 0.5 µm suggesting that the significance was driven by the large number of cells present in the sample.

Parvalbumin is coexpressed with nNOS in the ventral CNIC

Parvalbumin and distributed nNOS positive cells were mainly observed in different subdivisions and their distribution patterns showed little overlap. Very few distributed nNOS positive cells were observed in the central nucleus, the region where most parvalbumin was expressed, however in the ventral IC on the border of the central nucleus and the lateral cortex, co-labelling of nNOS and parvalbumin was observed in some cells. Figure 3-25 shows a high magnification image from this ventral IC region. In this image both punctate and diffuse nNOS expression are observed. nNOS positive punctate labelling (squares) outlines both parvalbumin positive (closed arrow head) and parvalbumin negative cells (arrows with squares). The cells with distributed nNOS labelling (stars) are mainly parvalbumin negative (arrow with stars) but co-labelling does occur (open arrow head). nNOS positive puncta within the parvalbumin positive cells are easier to see in Figure 3-26 (open arrowheads), however even in this image examples of cells only expressing nNOS can be observed (arrows). As was the case with the VGLUT2, discussed below, the nNOS punctate labelling was seen to be arranged in circles around presumed cell bodies (indicated by the presence of DAPI) which are not parvalbumin positive (arrows).

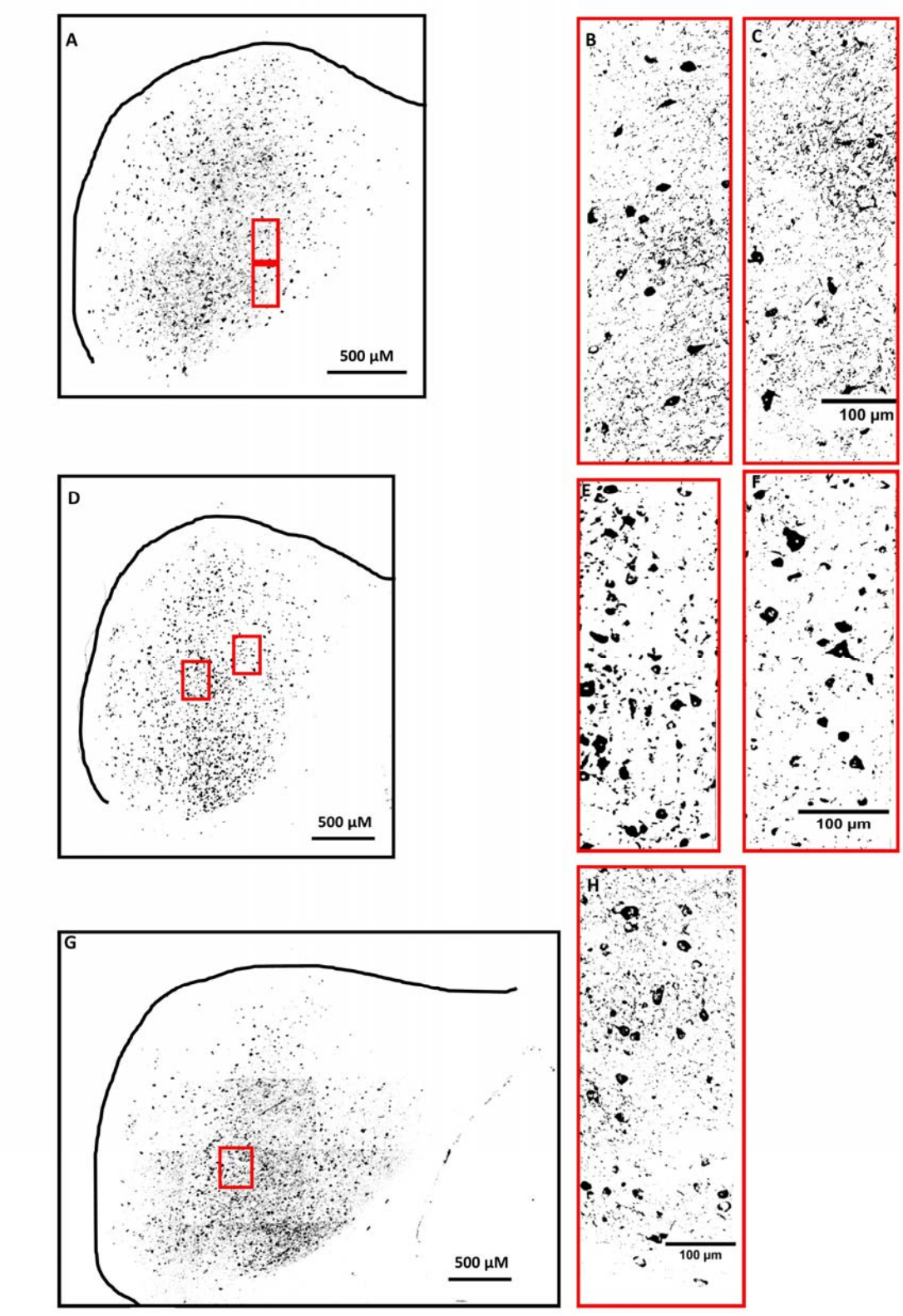

Figure 3-23 parvalbumin labelling in caudal (A), mid (D) and rostral (G) IC. A manually adjusted threshold was applied to the images to enhance the contrast. Images in the black box A and C show the entire IC while the images in the red boxes show magnifications of regions of interest. The examples from A, D and G obtained from three different animals.

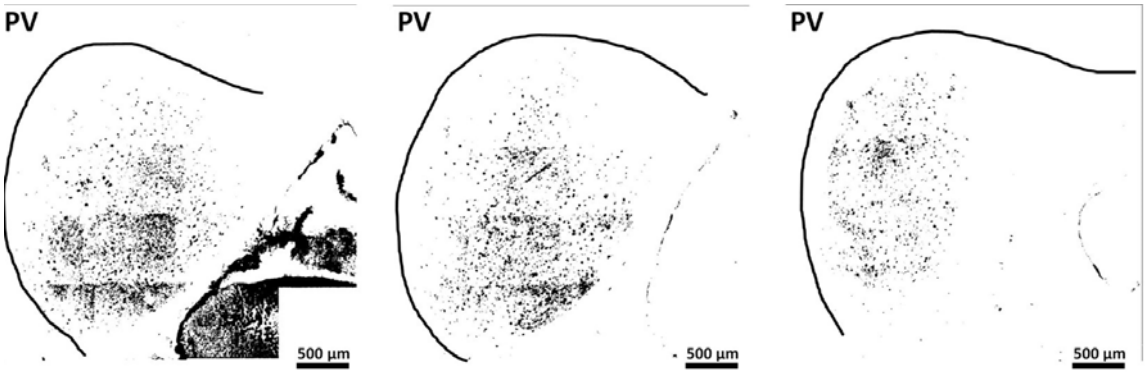

Figure 3-24 Mosaic images showing parvalbumin expression along the rostral-caudal axis, a manual threshold was applied to these images to enhance the contrast. From left to right are depicted caudal, mid and rostral sections of the IC. The scale bar indicates 500 µm. Note how the expression is pronounced in the central nucleus and thins out towards the cortices. Outline drawn by hand.

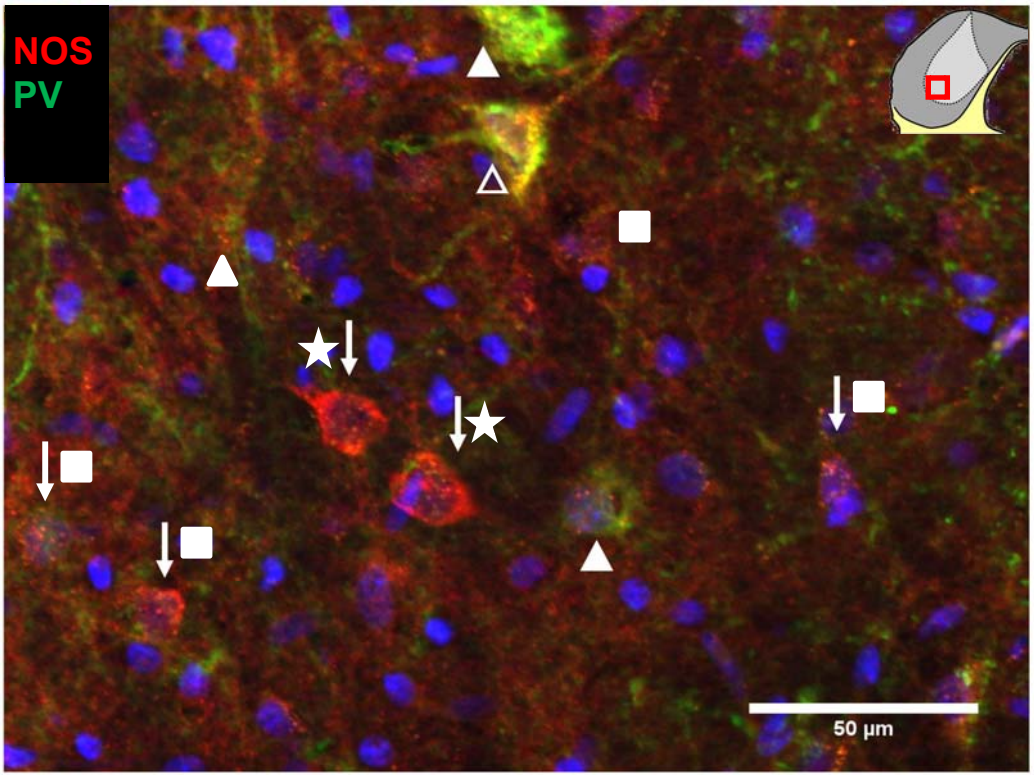

Figure 3-25 parvalbumin and nNOS labelled cells in ventral IC. A cell in which co-expression occurs is indicated by the open arrow head. The closed arrowheads shows NOS positive puncta on parvalbumin cells. nNOS only cells are shown by the arrows. Note that both punctate (white square) and diffuse (marked by *) nNOS expression, are present in this section.

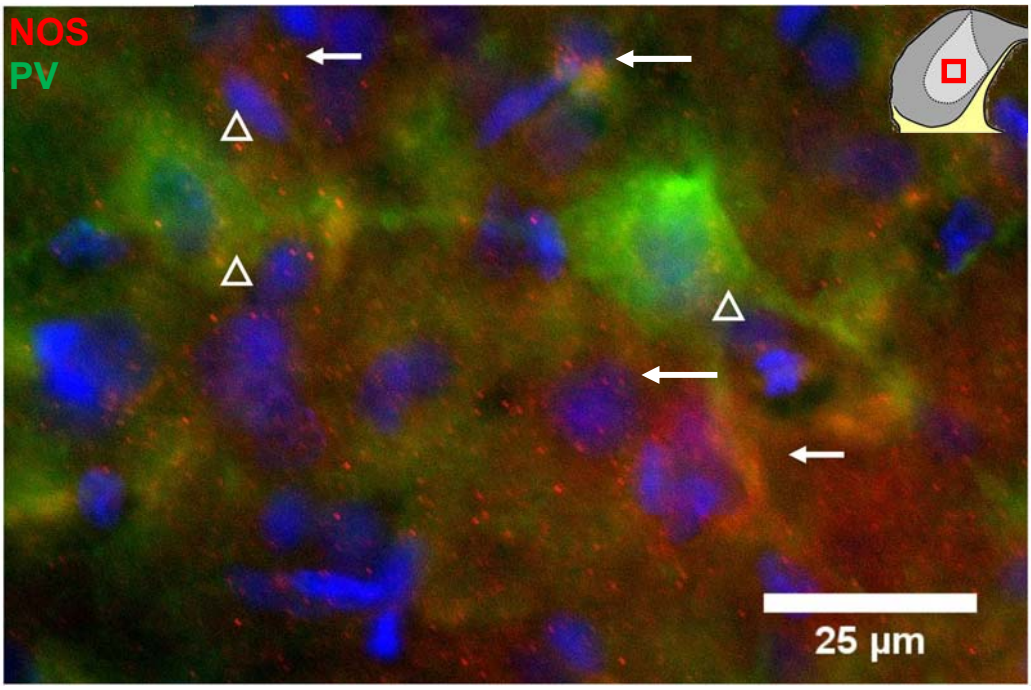

Figure 3-26 parvalbumin and nNOS labelling in the central nucleus. Open arrowheads show nNOS puncta in parvalbumin positive cells. Arrows point to cells labelled with nNOS only.

Most, but not all, Parvalbumin cells are GABAergic

GABA positive cells were present in all subdivisions of the IC with large GABA positive cells located in the central nucleus (Figure 3-27). Parvalbumin labelling was mainly observed in the central nucleus, although some smaller cells were observed in the dorsal cortex (Figure 3-23). The vast majority of parvalbumin positive cells also showed immunoreactivity for GABA or GAD65/67, although about 30% of the parvalbumin labelled cells did not show immunoreactivity for GABA or GAD65/67 and are presumably glutamatergic.

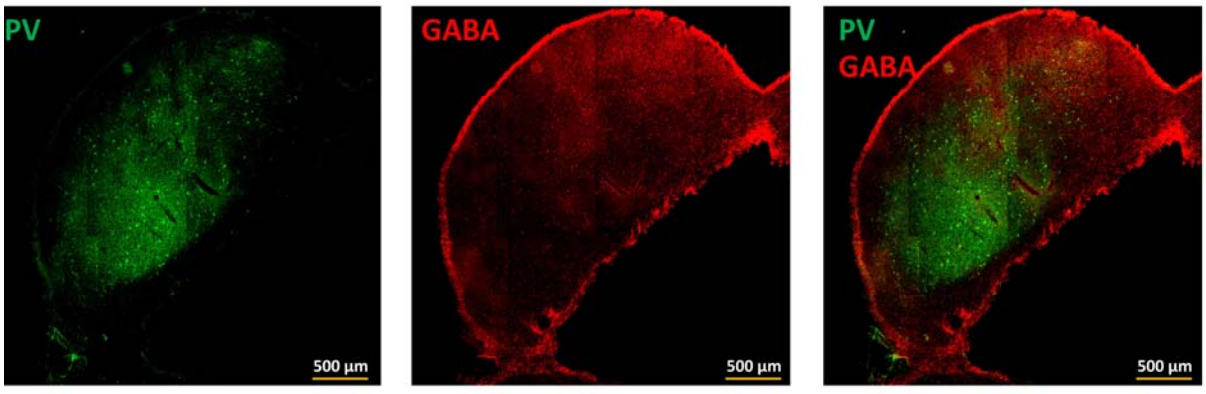

Figure 3-27 Mosaic low power images showing from left to right parvalbumin labelling, GABA labelling and the merge of the two. The scale bar indicates 500 µm.

Some parvalbumin cells are innervated by GAD labelled puncta

An example of a parvalbumin positive neuron that shows no immunoreactivity for GAD65/67 is depicted in Figure 3-28. The maximum intensity insert on the left in this image shows that GAD65/67 is abundant in the central nucleus but not in this parvalbumin positive cell. This point is further substantiated by the orthogonal views insert on the right which show the virtual cuts through the section along the yellow lines and this clearly demonstrates that no GAD65/67 is present in this parvalbumin labelled cell. Note however, that parvalbumin positive cells do receive GABAergic inputs on their proximal dendrites (Figure 3-29).

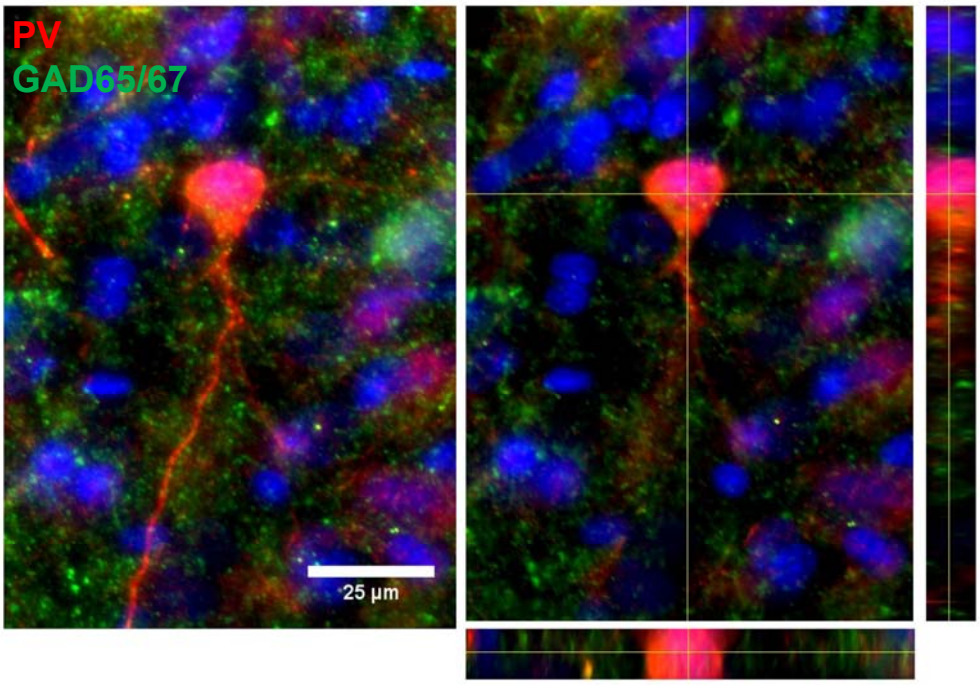

Figure 3-28 parvalbumin and GAD65/67 labelling in the central nucleus. On the left a maximum intensity projection revealing the presence of GAD65/67 in the section but not in the parvalbumin cell. On the right orthogonal views again showing thatGAD65/67 labelling is absent from the parvalbumin positive cell.

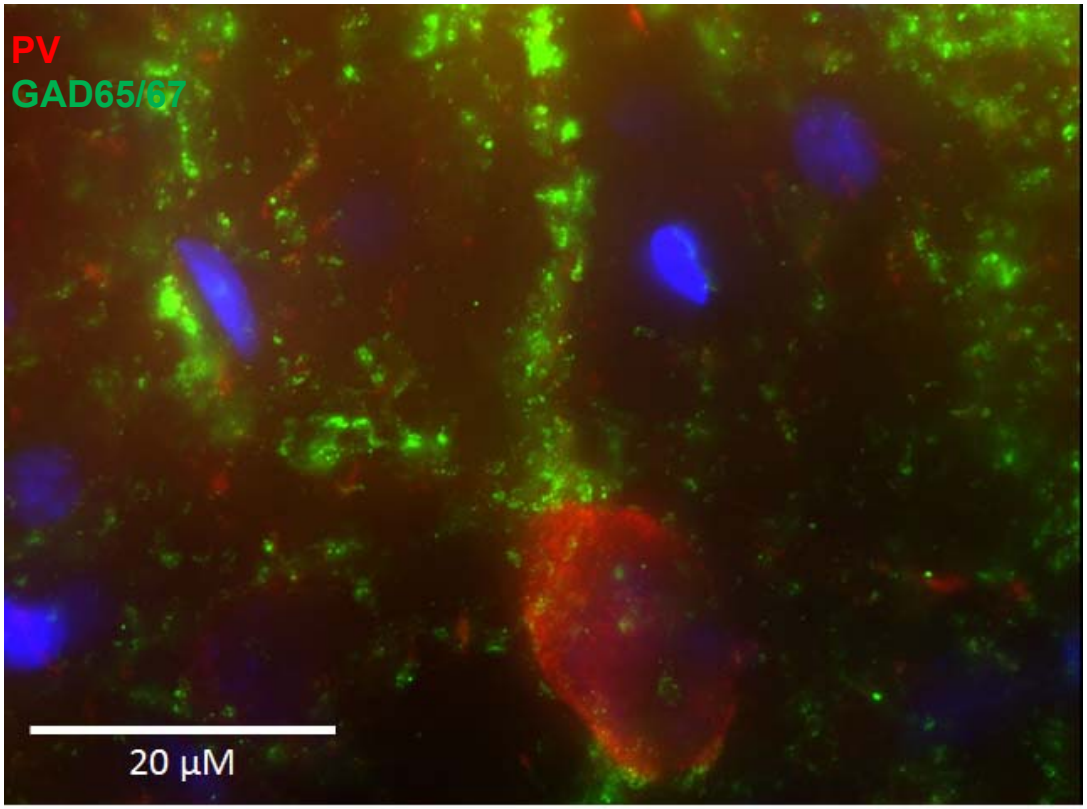

Figure 3-29 high power image of a parvalbumin positive neuron in the IC that receives GAD positive puncta on its dendrite.

3.3.6 Distribution of Glutamatergic Terminals in Subdivisions of the IC

To understand how glutamatergic projections are distributed throughout the IC I will first discuss the expression patterns of the vesicular transport proteins for glutamate VGLUT1 and VGLUT2. Vesicular transporters are indicative of the glutamatergic inputs a cell receives, it is likely that the cell bodies of many cells giving rise to the VGLUT positive terminals are not in the IC. In the case of the VGLUT1 this is necessarily the case because VGLUT1 is not synthesised in the IC. This general expression pattern will be followed by inspection of VGLUT positive terminals innervating cells labelling positive for nNOS or calcium binding proteins. Data will be presented along the rostral-caudal axis and the main subdivisions of the IC. Given that no positive label for glutamate can be used, a cell is deemed glutamatergic due to the absence of GAD or GABA.

VGLUT1 and VGLUT2 labelled excitatory terminals were observed throughout all subdivisions of the IC. In Figure 3-30 and Figure 3-31 examples of VGLUT1 and VGLUT2 labelling along the rostral caudal axis in the same animal are shown. Labelling of VGLUT1 and VGLUT2 was assessed by eye and appeared at low magnification to vary along the rostral caudal axis with denser labelling observed in the middle and caudal areas of the IC.

Within the caudal and middle sections, VGLUT1 shows a relatively even labelling through subdivisions of the IC although clusters of denser labelling were observed, marked by * in Figure 3-30. At higher magnification VGLUT1 appeared to associate with cell bodies as indicated by a VGLUT1 positive puncta forming circles around the nucleus indicated by DAPI labelling (Figure 3-38). No obvious consistent differences were observed between the subdivisions, although three out of five animals showed denser labelling in the lateral cortex. VGLUT2 was also abundant in all subdivisions of the IC, but showed differences between the subdivisions with denser labelling observed in the dorsal and lateral cortices and considerably less labelling in the central nucleus, as outlined in Figure 3-31. At higher magnification, VGLUT2 appeared to densely innervate cell bodies and processes as the VGLUT2 labelling was frequently arranged in circles and long chains (Figure 3-39).

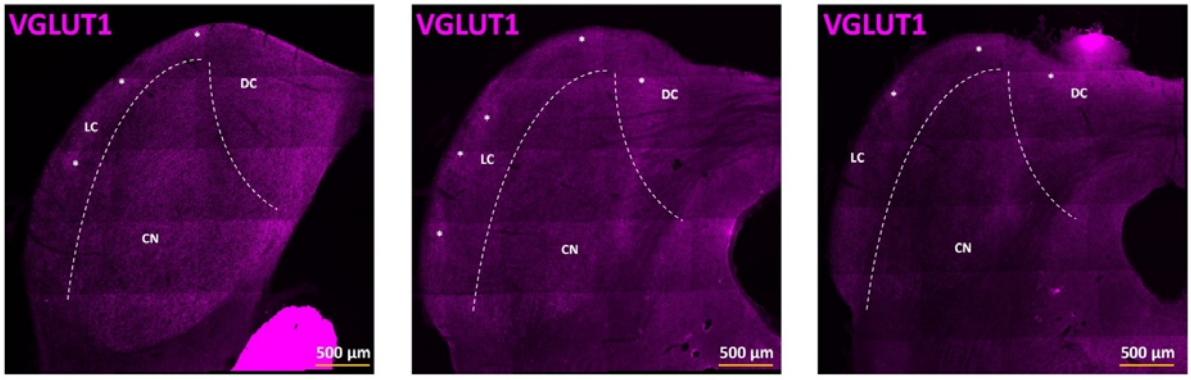

Figure 3-30 Mosaic images showing VGLUT1 labelled excitatory terminals along the rostral –caudal axis of the IC. From left to right are depicted caudal, mid and rostral sections of the IC. The scale bar indicates 500 µm. Areas indicated by * show cluster of denser VGLUT1 labelling.

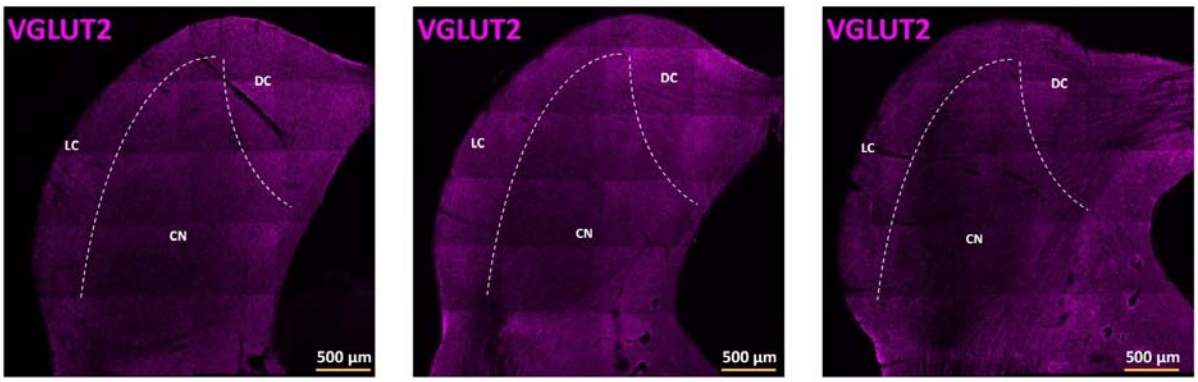

Figure 3-31 Mosaic images showingVGLUT2 labelled excitatory terminals along the rostral –caudal axis of the IC. From left to right are depicted caudal, mid and rostral sections of the IC. The scale bar indicates 500 µm.

3.3.7 nNOS and Glutamatergic Input

nNOS and VGLUT1

In Figure 3-32 nNOS and VGLUT1 in the central nucleus appeared to label different populations. The nNOS positive puncta in the central nucleus were not associated with VGLUT1 positive puncta. In the dorsal and lateral cortex the picture was more complex, in these subdivisions both cells with punctate and distributed nNOS labelling were observed. As was the case in the central nucleus, cells with solely nNOS punctate labelling did not appear to be innervated by VGLUT1 puncta (Figure 3-33). However, cells filled with nNOS labelling did show VGLUT1 labelled innervations. The VGLUT1 positive contacts were observed on both the soma and the dendritic branching (Figure 3-34).

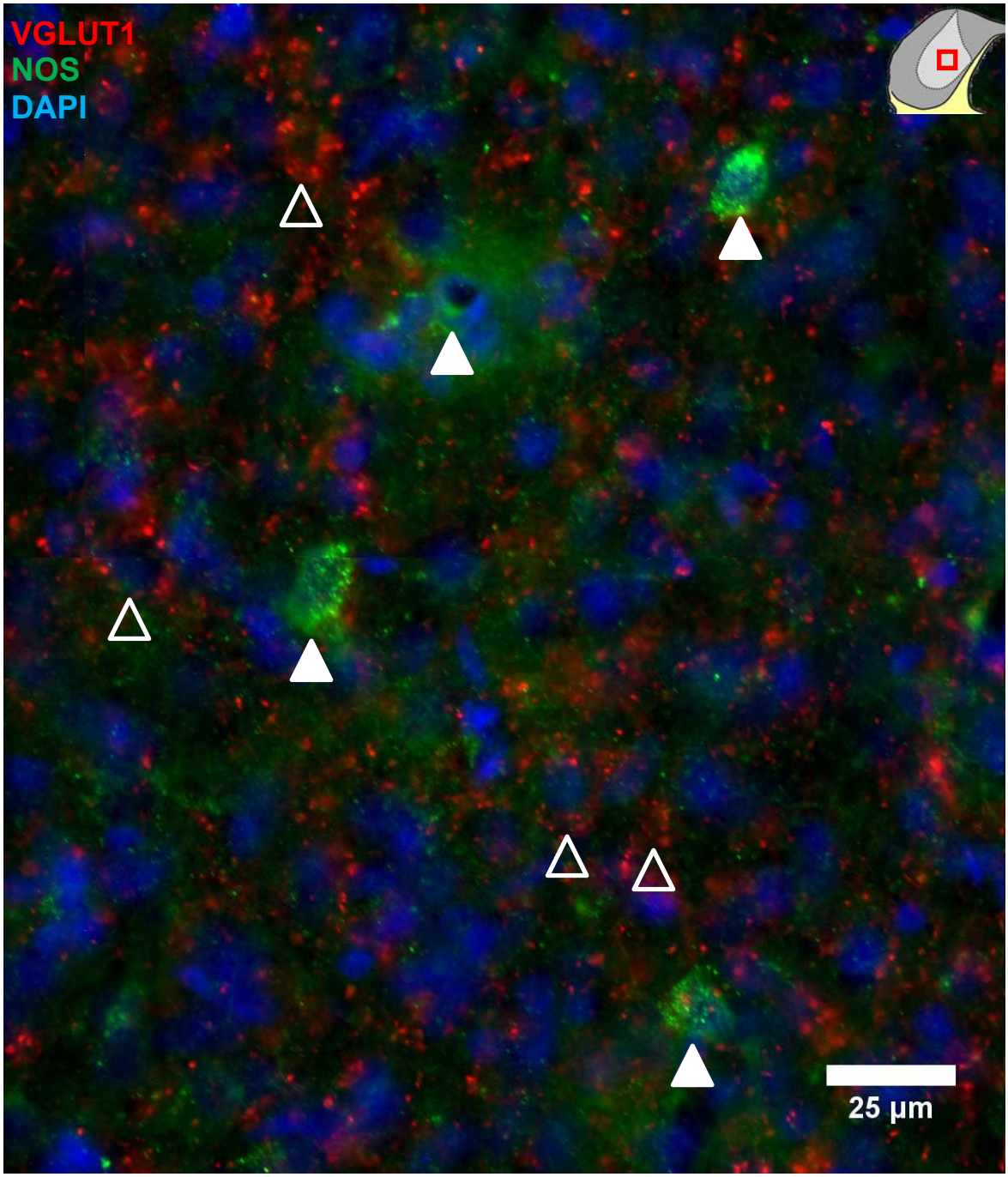

Figure 3-32 nNOS and VGLUT1 labelling in the central nucleus of the IC. The solid arrowheads indicate cells with nNOS labelling which are not associated with VGLUT1 positive puncta, none of the nNOS labelled cells appeared to be associated with VGLUT1. Open arrowheads indicate examples of cells receiving VGLUT1 puncta in which no nNOS labelling was observed.

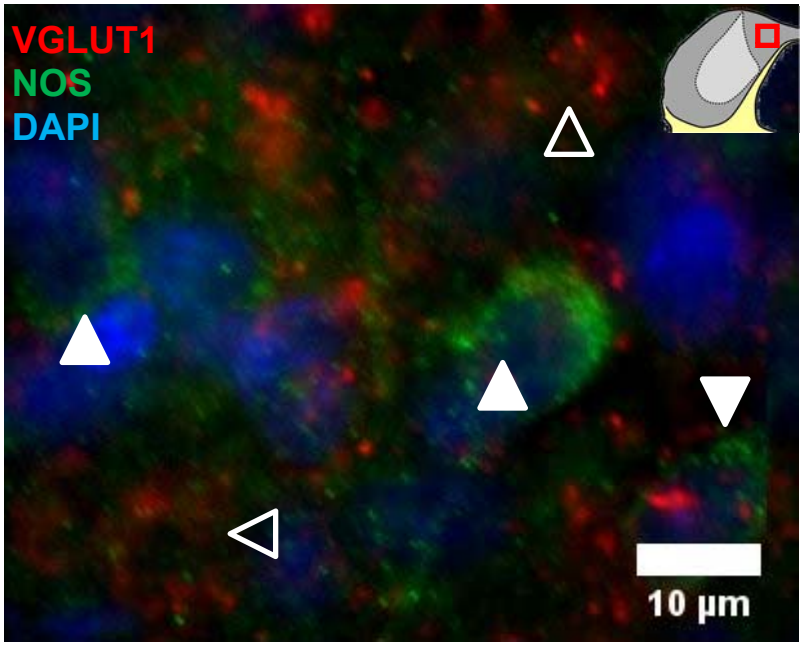

Figure 3-33 nNOS and VGLUT1 labelling in the dorsal cortex. Open arrowheads indicate cells receiving VGLUT1 innervation but showing no nNOS labelling. The solid arrowheads point out cells with nNOS labelling but no VGLUT1 positive innervation.

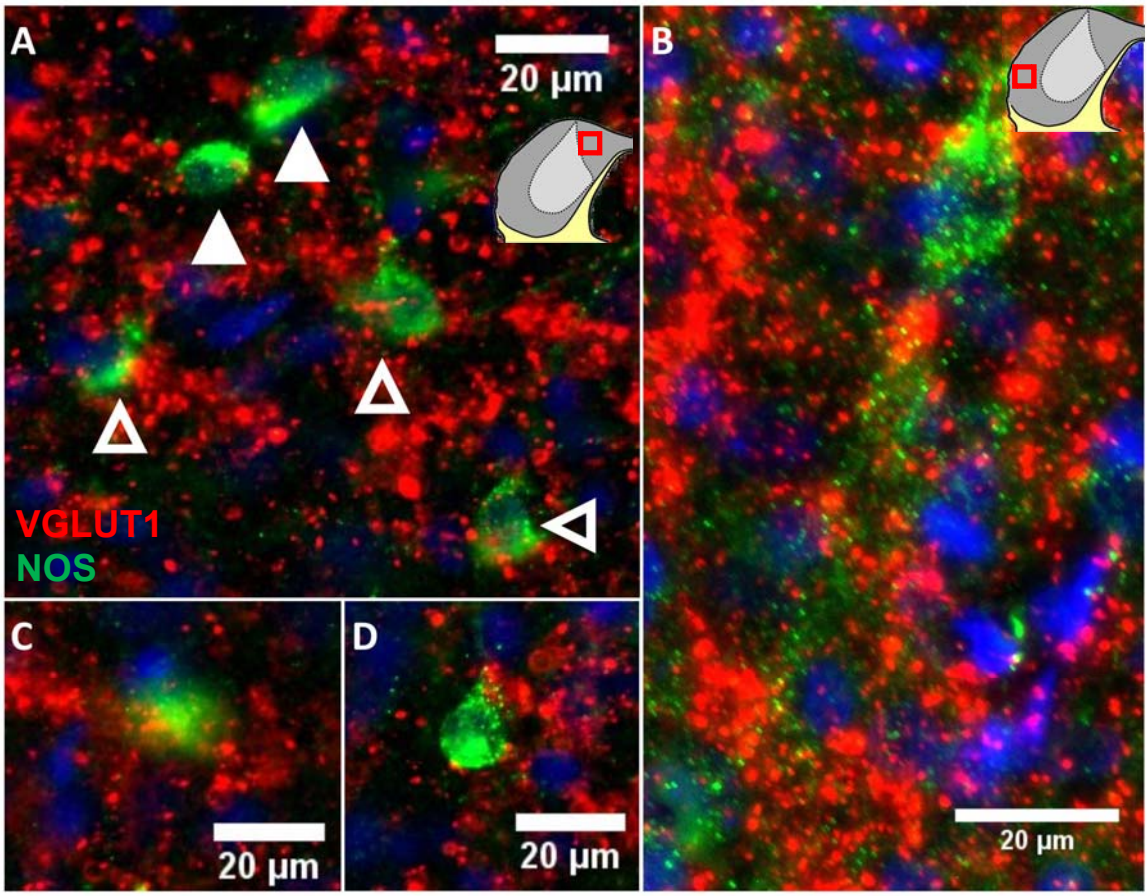

Figure 3-34 A, C and D show cells with nNOS labelling throughout the cell in the dorsal cortex. Open arrowheads indicate VGLUT1 innervated nNOS cells. Closed arrowheads indicate cells that show nNOS cells that receive no VGLUT1 positive innervation. Figure B shows a maximum intensity projection of a Z-stack series showing a NOS positive cell in the lateral cortex that is densely innervated by VGLUT1 positive terminals both on the soma and the dendrite, outlined by nNOS positive puncta. Note that maximum intensity projections do contain saturated pixels.

nNOS and VGLUT 2

Both cells with nNOS punctate labelling and cells with distributed nNOS labelling in all sub-divisions of the IC showed VGLUT2-labelled innervation on their somata and dendrites, though the latter was harder to discern. Both cells with nNOS punctate labelling and cells with distributed nNOS labelling were innervated by VGLUT2 positive puncta in the dorsal cortex (Figure 3-35). VGLUT2 labelling formed dense rings around nNOS positive cells in the dorsal cortex. In the lateral cortex most nNOS labelled cells, of both types, were encapsulated by VGLUT2 puncta, however, in this subdivision, some nNOS positive cells were observed not receiving any apparent VGLUT2 innervation (Figure 3-36). In the central nucleus, where virtually all nNOS labelling was of the punctate type most nNOS labelled cells received innervation from VGLUT2 positive puncta (Figure 3-37). In contrast to the cortices few nNOS positive cells in the central nucleus were entirely encapsulated by VGLUT2 terminals.

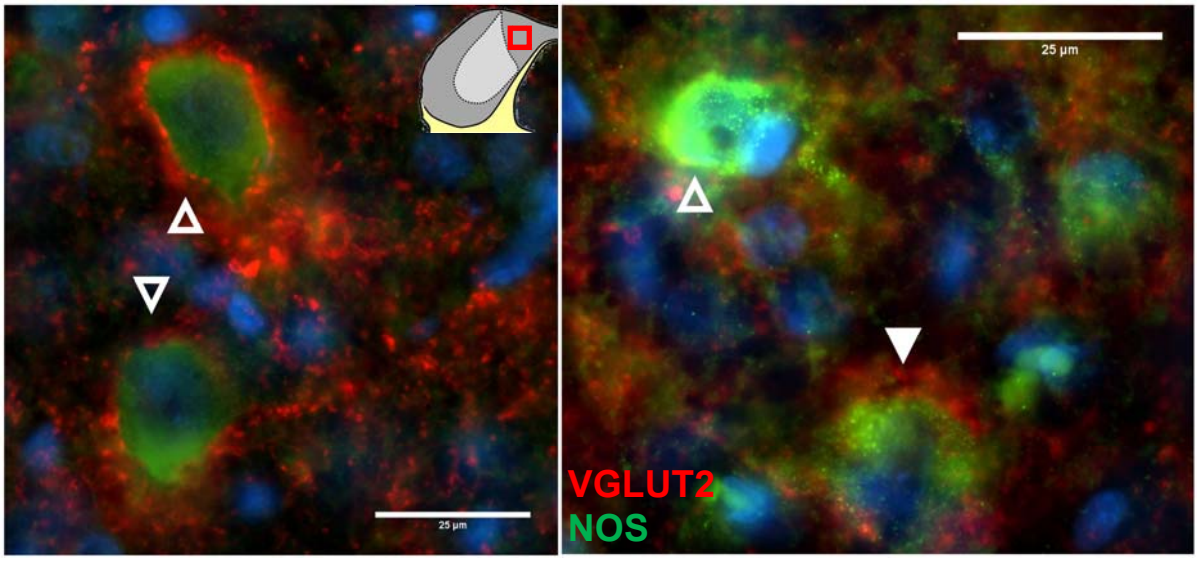

Figure 3-35 nNOS and VGLUT2 in the dorsal cortex. Open arrowheads show cells with distributed nNOS labelling. Closed arrow head shows cell with nNOS positive puncta that is surrounded by GLUT2 positive terminals.

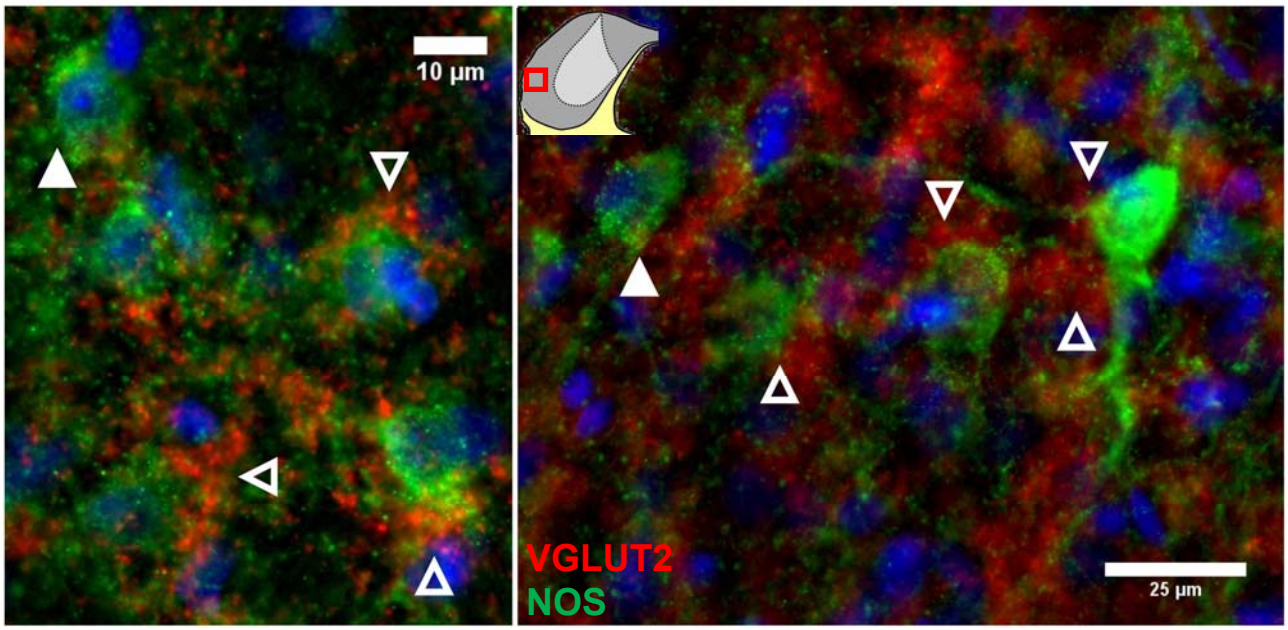

Figure 3-36 nNOS and VGLUT2 .in the lateral cortex. Open arrowheads show nNOS cells contacted by VGLUT2 terminals. Closed arrowheads show nNOS positive cells that lack apparent VGLUT2.

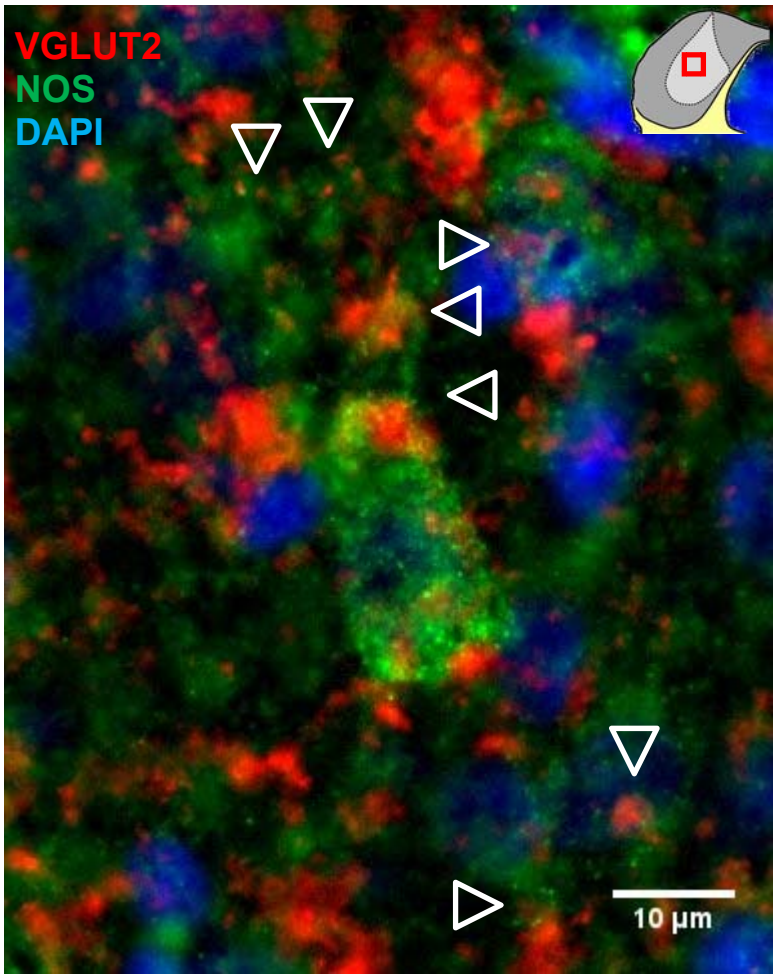

Figure 3-37 nNOS and VGLUT2 .in the central nucleus. The arrowheads show cells with nNOS positive puncta innervated by VGLUT2.

Parvalbumin cells in the central nucleus receive VGLUT2 but no VGLUT1 input.

Although abundant in the central nucleus VGLUT1 labelled puncta rarely made contact with cells expressing parvalbumin (Figure 3-38). However, VGLUT1 labelled terminals were observed that appeared to encircle parvalbumin negative cell bodies (Figure 3-38).

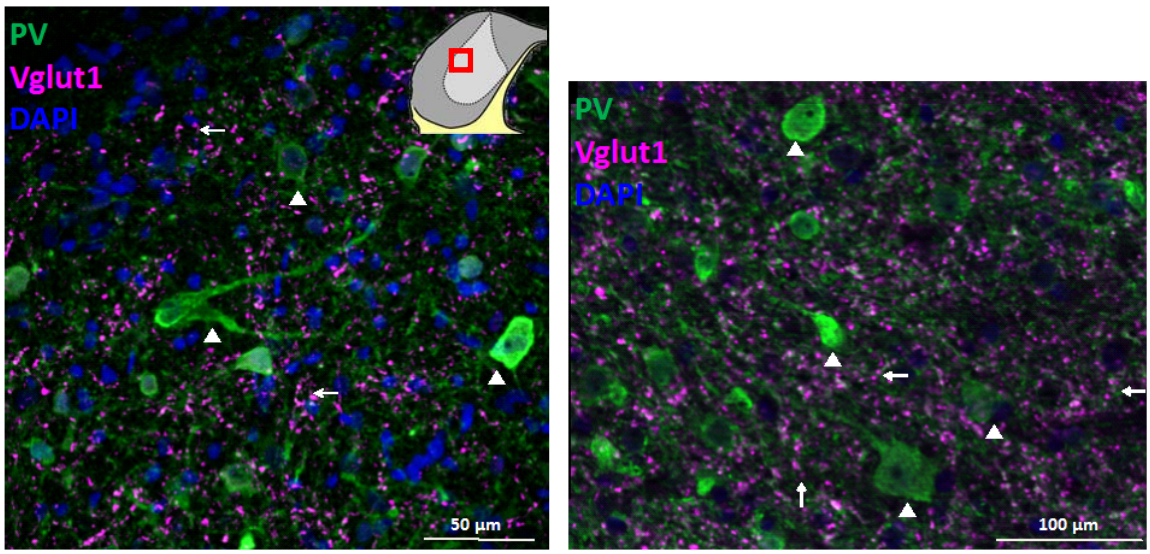

Figure 3-38 Parvalbumin positive cells and VGLUT1 positive puncta in the central nucleus. Arrowheads indicate parvalbumin positive cells, which did not appear to receive VGLUT1 innervation. Arrows point to parvalbumin negative cells that did receive VGLUT1 positive innervation.

Parvalbumin positive cells did receive dense VGLUT2 positive innervation (Figure 3-39). The VGLUT2 labelled terminals formed dense clusters around the soma, dendrites and axons of parvalbumin positive cells in the central nucleus. Large parvalbumin positive cells (diameter >25 µm) appeared to be more densely innervated by VGLUT2 puncta (white arrows) compared to the smaller parvalbumin positive cells (closed arrowheads). Non-parvalbumin cells outlined by dense clusters of VGLUT2 puncta (open arrowheads) were also seen.

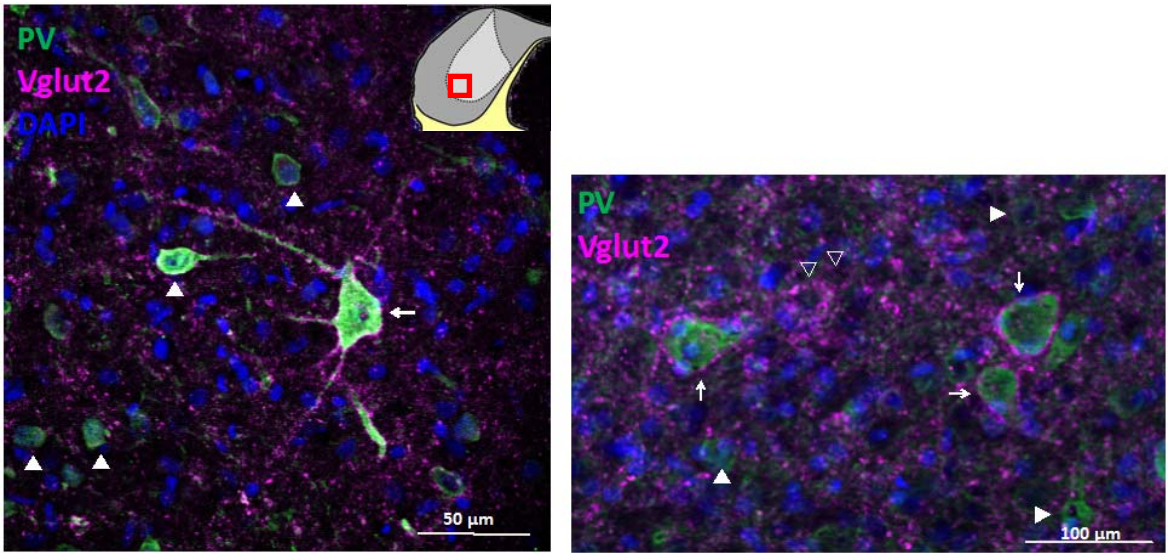

Figure 3-39 parvalbumin positive cells and VGLUT2 positive puncta in the central nucleus. Arrows indicate large parvalbumin cells with dense VGLUT2 innervations. Closed arrowheads indicate small PV cells and open arrowheads non-parvalbumin cells that receive dense VGLUT2 innervations.

3.3.8 Parvalbumin, Calbindin, Calretinin & nNOS cell size

In Figure 3-40 the total cell counts within each section along the rostrocaudal axis are displayed for the cells expressing calbindin, calretinin, parvalbumin or nNOS.

The total cell counts showed the relative proportions of the four cell types within each area along the rostro-caudal axis. In the caudal areas of the IC, which consist of only cortex there appeared to be equal numbers of all four cell types. However, in the middle and rostral areas, in which large parts of the section were central nucleus, the numbers of parvalbumin and nNOS cells were considerably higher than the numbers of calbindin and calretinin positive cells. Although in these areas few nNOS positive cells were observed in the central nucleus. A higher number of nNOS positive cells was observed in the dorsal and lateral cortex mid-way along the rostro-caudal axis of the IC. The highest number of cells expressing parvalbumin were observed in both mid and rostral areas of the IC. Calretinin and calbindin positive cells are most abundant in the caudal areas of the IC and their expression levels are lower in the mid and rostral areas of the IC.

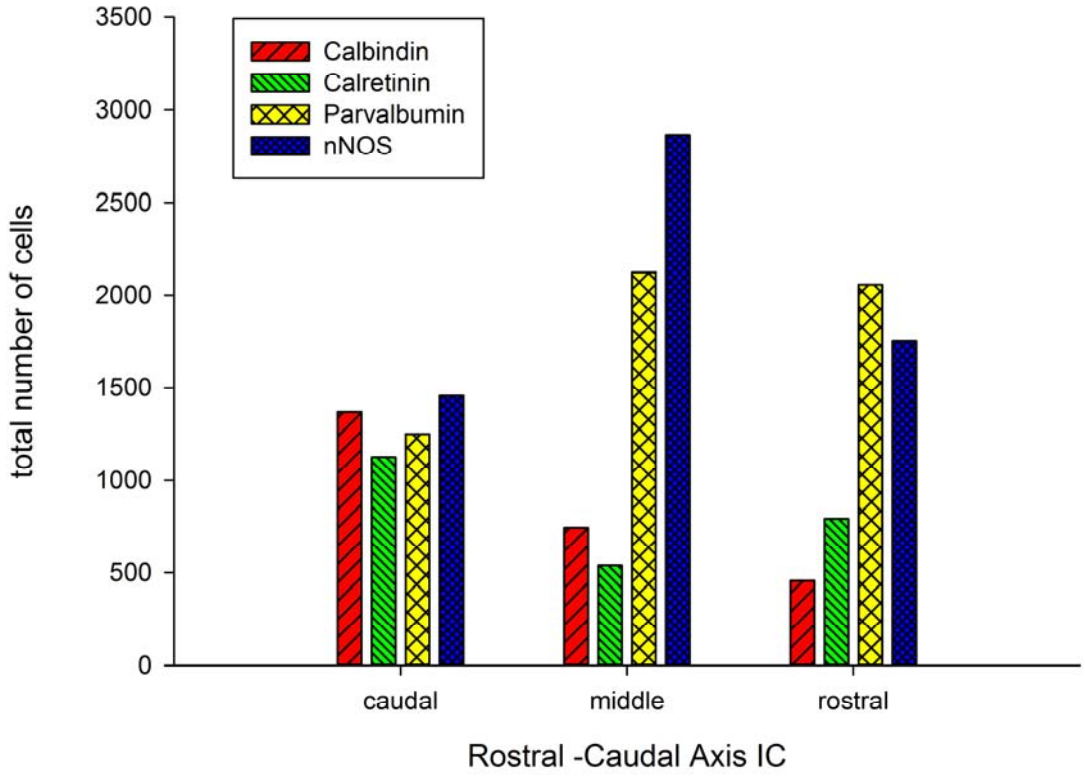

Figure 3-40 cell counts for calbindin, calretinin, parvalbumin and nNOS cells along rostral caudal axis of the IC

There were no differences in the distribution of cell diameter between the three calcium binding protein expressing cells (Figure 3-41). All cell types show a skewed distribution peaking around ~20 µm diameter but with a relatively large number of bigger cells. The nNOS cells show a different distribution along the rostral caudal axis with larger cells appearing in the middle and rostral parts of the IC.

A two way ANOVA testing the cell diameters, revealed a main effect for area along the rostral caudal axis ($F(2,16517) = 100.64$, $p < 0.0001$) and a main effect for cell markers ($F(3,16517) = 100.31$, $p < 0.0001$) as well as an interaction effect between the two ($F(6,16517) = 68.56$, $p < 0.0001$).

Post hoc Tukey tests revealed that parvalbumin positive cells were bigger (21.34 µm ± 0.11 µm) on average than the other three markers, parvalbumin vs. calbindin (1.81 µm ± 0.18 µm), parvalbumin vs. calretinin (2.10 µm ± 0.18 µm) and parvalbumin vs. nNOS (2.49 µm ± 0.14 µm). The differences among the other cell markers although significant had small effect sizes and will not be reported here. Post hoc Tukey tests for area showed that cells in rostral areas were larger compared to cells in the middle IC (2.00 µm ± 0.14 µm) and cells in caudal areas (2.81 µm ± 0.15 µm).

For the interaction effect calretinin, positive cells showed an increase in cell sizes along the rostral caudal axis with the cells in the rostral areas being larger compared to the middle areas (1.45 µm ± 0.38 µm) and caudal areas (2.73 µm ± 0.32 µm). nNOS positive cells showed even larger differences in average cell size along the rostral caudal axis with cells in the rostral areas again being larger compared to the middle areas (4.41 µm ± 0.21 µm) and the caudal areas (6.49 µm ± 0.25 µm), and cells in areas mid-way through the IC were bigger than the ones observed in the caudal areas (2.09 µm ± 0.22 µm).

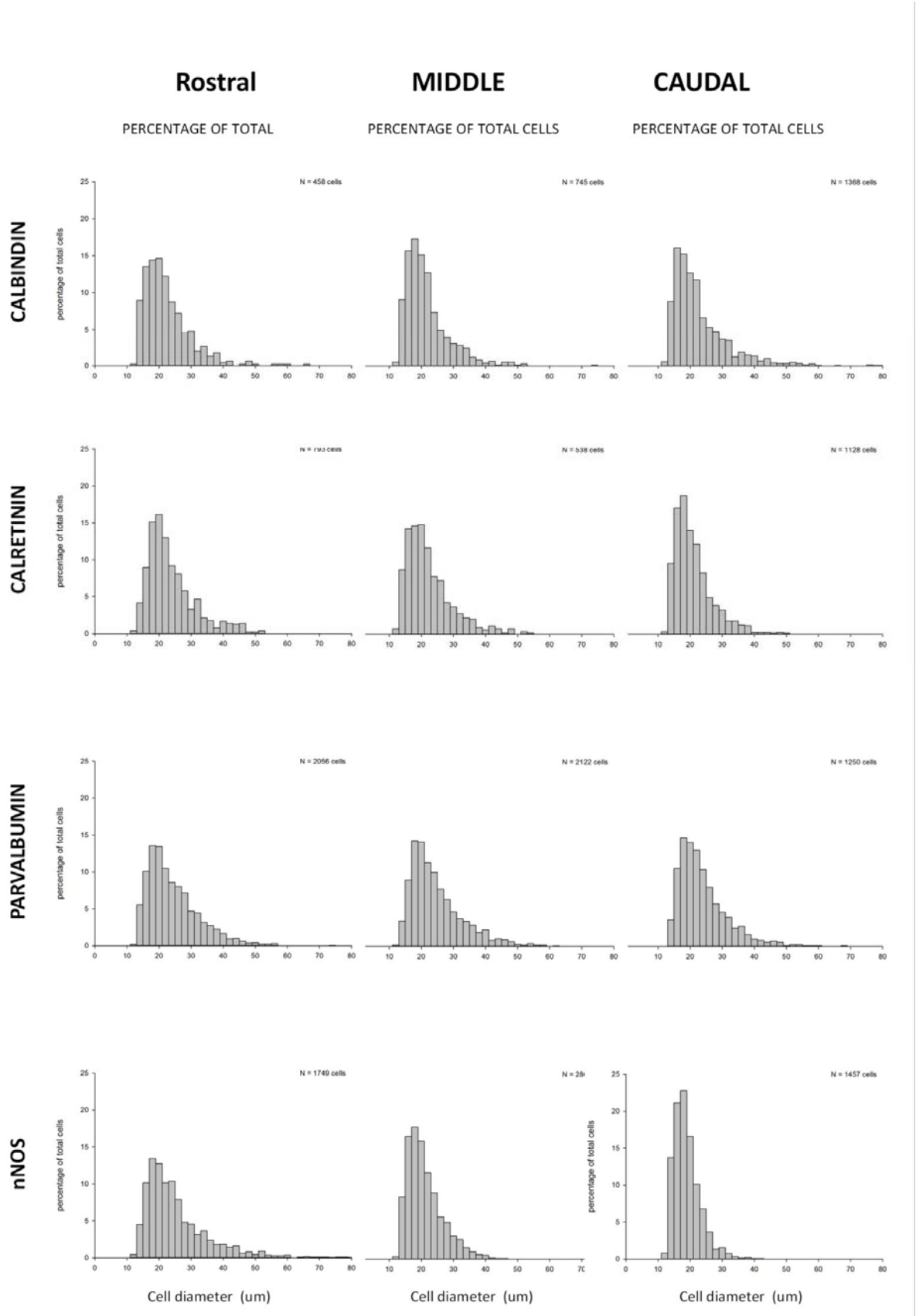

Figure 3-41 relative distributions of calbindin, calretinin, parvalbumin and nNOS cells along the rostral caudal axis of the IC

3.4 Discussion

In this Chapter, I presented immunohistochemical observations made throughout the IC. The following questions regarding the distribution of nNOS cells, their neurotransmitter phenotype, their co-expression of calcium binding proteins and the nature of afferent glutamatergic inputs to them were addressed:

1. In what subdivisions of the IC are nNOS expressing cells found and what is the subcellular distribution of nNOS?
2. What is the neurotransmitter phenotype of the nNOS expressing cells?
3. In what subdivisions of the IC are cells expressing the calcium binding protein calbindin, calretinin and parvalbumin found and are these cells GABAergic?
4. Do nNOS expressing cells selectively express calbindin, calretinin or parvalbumin?
5. Do the cells expressing nNOS or calcium binding proteins receive glutamatergic inputs and if so, what is the nature of these inputs?

nNOS labelling was observed in cells in the lateral and dorsal cortex as previous reports have described. Here the nNOS labelling was distributed evenly through the soma and dendrites of the cells. One of the major findings reported in this chapter, in contrast to previous reports, is that nNOS was also found to be expressed in the central nucleus. In the central nucleus, nNOS labelling was observed in discrete puncta. This punctate labelling was also seen in the cortices in cells which also had distributed nNOS labelling. The nNOS expressed in these puncta was associated with the postsynaptic density protein PSD95.

Although some nNOS positive neurons in the IC were found to express the GABAergic marker GAD65/67, the vast majority did not and are presumed to be glutamatergic. The regional expression of nNOS and the expression of both calbindin and calretinin overlap in the dorsal and lateral cortex, but, within cells, nNOS was rarely co-localised with calretinin. Calbindin expression, on the other hand, was virtually always an indicator for nNOS expression in that cell, although many calbindin negative nNOS cells were also observed. Cells with puncta and/or diffuse nNOS expression also expressed parvalbumin, but many parvalbumin positive cells were nNOS negative.

The calcium binding proteins calbindin and calretinin were observed in the cortices along the rostral caudal axis of the IC. Calbindin cells show no difference in size along this axis whereas calretinin cells are larger in the rostral areas compared to the caudal areas of the IC. Parvalbumin positive cells were the largest cells observed throughout. Neurons showing

positive labelling for parvalbumin, calbindin or calretinin in the IC were not always positive for GABA or GAD suggesting that neurons expressing calcium binding proteins in the IC can be glutamatergic. A finding that fits with evidence that 20% of the parvalbumin cells in the visual cortex are not GABAergic (Demeulemeester *et al.*, 1991).

Both VGLUT1 and VGLUT2 labelled terminals were found associated with the soma and dendrites of the nNOS filled cells in the cortices. But the punctate nNOS cells in the central nucleus showed a different pattern of VGLUT innervation.

In summary, nNOS expression is observed in all divisions of the IC but with distinct subcellular expression patterns. Cells expressing nNOS are largely glutamatergic, but co-labelling with GABAergic markers does occur. Cells expressing nNOS can contain either calbindin or parvalbumin but rarely calretinin. Cells exhibiting either the punctate or diffuse nNOS expression showed distinct patterns of glutamatergic innervation.

The range of questions was chosen because currently little is known about these neurons. Using this wide range of markers allowed me to identify a wide range of potential markers for future studies. Due to the number of markers used, most of the studies reported here are descriptive in nature laying the groundwork for future more rigorous quantification. The current results have brought about exciting novel findings and provide a framework for future research. The phenomena to be quantified have been identified and that is a major step forward.

3.4.1 Distinct Patterns of nNOS Labelling

The presence of NADPH diaphorase (which is now known to be nNOS (Bredt *et al.*, 1991; Dawson *et al.*, 1991; Hope *et al.*, 1991; Coote and Rees, 2008)) has been recognised in the auditory pathway and most prominently in the IC for a long time (Herbert *et al.*, 1991; Druga and Syka, 1993). In the IC, NADPH-diaphorase activity/nNOS labelling can be seen in cell bodies and extensive dendritic processes in some cells. Previously nNOS has been shown to be differentially expressed in the three subdivisions of the IC, the dorsal cortex, the lateral cortex and the central nucleus with little to no expression reported in the central nucleus (Coote and Rees, 2008). The current findings are consistent with the previous reports of nNOS positive cytoplasmic labelling in somata, dendrites and axons of neurons in the dorsal and lateral cortex (Coote and Rees, 2008). The density of nNOS positive cells decreases progressively in areas where the cortices blend into the central nucleus.

A major finding here is the nNOS positive punctate labelling that is not only present in the cortices on or in the cells with distributed cytoplasmic labelling but is also abundant in the central nucleus where it appears in or on the somata of cells which otherwise have no discernible cytoplasmic nNOS labelling. This finding has the potential to change our views of nNOS in the IC. The two different expression patterns strongly suggest different potential roles NO can play in modulating neuronal activity. The puncta were observed with both the nNOS antibodies used, which were raised in different species, obtained from different companies and raised against different epitopes, making it unlikely that the puncta are not related to nNOS expression. The question remains whether the nNOS puncta can be observed in NADPH diaphorase labelled sections, one report suggested observing punctate NADPH diaphorase labelling in the lateral cortex (Wu *et al.*, 2008), but failed to provide any evidence for this. The NADPH diaphorase method often results in dark neuropil labelling making detection of small puncta difficult, possibly this method is not refined enough to discern small structures like puncta with great precision. Also, the product is soluble and may not stay in association with the site in which it is formed- in contrast to the antibody labelling where the fluorophore is in physical association with the antigen.

3.4.2 Subcellular Localisation of nNOS

The vast majority of these nNOS positive puncta co-localise with PSD95. PSD95 is a protein located in the post synaptic density and the association between the two proteins strongly suggests that the nNOS puncta are associated with the synapse. Wide field microscopy does not allow for the definitive determination of whether the nNOS puncta are pre or postsynaptically localized. However, given that we know that the nNOSα protein contains a PDZ binding domain via which it associates itself with PSD95, it is justified to assume that I) nNOS puncta are associated with PSD95, 2) that this nNOS is nNOSα, 3) since PSD95 also anchors the NMDA receptor this co-labelling likely represents the nNOS-PSD95-NMDA complex. Previous reports have suggested that nNOS might occur presynaptically on rare occasions (Atkinson *et al.*, 2003; Fernández-Alvarez *et al.*, 2011) and some of the nNOS puncta here could, therefore, be presynaptic. However given the current evidence that seems unlikely and I will assume that these nNOS puncta contain nNOSα.

3.4.3 nNOSα and nNOSβ Expression in the IC

If nNOSα is associated with PSD95 and appears as puncta then this raises the question of which isoform of nNOS is present in the cells in the cortices which show distributed labelling for nNOS. The cells showing distributed nNOS labelling could, of course, be filled with

nNOSα, representing nNOSα that has yet to be transported to the postsynaptic densities or is currently unattached to PSD95. However, this seems an unlikely scenario because the cells only expressing nNOS punctate labelling show no nNOS labelling anywhere in their cell contents. A theoretical possibility that we cannot discard currently is the possibility that nNOSα and nNOSβ proteins may form functional heterodimers. The existence of these has never been shown in vivo and we don't know whether this configuration could be functional, but the diffuse distribution of nNOS in the cells in the cortex could in theory present such a heterodimer complex. That, however, would still not explain why the cells in the central nucleus show punctate labelling only. In situ hybridization studies showed that most areas in the brain express mRNAs for both nNOSα and nNOSβ, although in normal physiology mRNA for nNOSα is detected in higher quantities compared to nNOSβ (Langnaese *et al.*, 2007). mRNA quantification does not, however, directly translate to protein quantities, due to post-translational processing, and knock-out studies suggest that nNOSβ can rescue the phenotype when nNOSα is lost (Langnaese *et al.*, 2007). Some efforts have been made to investigate the expression of the two splice variants and they appear to occur largely in the same areas as well as in the cells making it harder to disentangle their roles (Eliasson *et al.*, 1997; Brenman *et al.*, 1997). Nevertheless, some cells throughout the mammalian body have been reported to express either nNOSα or nNOSβ (Percival *et al.*; Giove *et al.*, 2009; Jang *et al.*, 2015; Rothe *et al.*, 2002; Saur *et al.*, 2002). In skeletal muscle, nNOSβ was shown to be associated with the Golgi-complex that controlled its expression (Percival *et al.,* 2010). Even though this finding is not in neuronal tissue, it does suggest that nNOSβ does have its own regulators. The two expression patterns observed in the IC may be related to these two different splice variants and if we hope to understand the role NO plays in auditory processing in the IC it is important that we are able to distinguish between them.

Currently, no commercial antibodies targeting specifically nNOSα or nNOSβ proteins exist making it impossible to investigate whether different cells in the subregions of the IC express different nNOS splice variants at the protein level. However, custom made antibodies targeting nNOSα and nNOSβ have been made and successfully used in a previous study (Langnaese *et al.*, 2007), demonstrating that a study of nNOSα and nNOSβ is feasible. In situ hybridization studies reporting nNOSα and nNOSβ mRNA levels in the midbrain and brain stem made no distinction between the subregions of the IC (Eliasson *et al.*, 1997), future studies would benefit greatly by making this distinction. Even though it would not tell us how much protein is present in the cells, it would help to verify whether nNOSβ expression is absent in the central nucleus and strengthen the hypothesis that the

puncta consist of nNOSα. Regardless, even if all nNOS in the IC turns out to be nNOSα, the question remains why some cells are filled while others show discrete punctate labelling.

3.4.4 Some nNOS Cells in the IC are GABAergic

Some nNOS positive cells do express GABA but the vast majority show no immunoreactivity for GABA or GAD. Because the IC has no neurons synthesizing dopamine, serotonin, acetylcholine or glycine hence the absence of GABA suggests that the cells have a glutamatergic neurotransmitter phenotype. Wu *et al.* (2008) combined NADPH diaphorase and immunofluorescent protocols labelling GABA and glutamate and found that 77% of the NOS positive neurons in the cortices were glutamatergic, 11% GABAergic and the remaining 12% of undetermined phenotype. Since glutamate is present in all cells due to its involvement in the Krebs cycle, the glutamatergic phenotype of neurons is usually inferred by their lack of labelling for GABA or other neurotransmitters. Close inspection of the images presented in the Wu et al. (2008) study, highlights the difficulty of labelling for glutamate. Some cells showed immunoreactivity for both GABA and glutamate, which is not unexpected but some cells showed no immunoreactivity for either marker which is cause for concern. Recent in situ hybridization studies (in which the presence of VGLUT2 mRNA was used to define glutamatergic phenotype) have shown that 70-80% of the nNOS cells in the IC have a glutamatergic phenotype (Fujimoto *et al.*, 2016), the authors suggested that the remainder are likely to be GABAergic. Because the presence of nNOS in the central nucleus was unknown, no study has addressed whether nNOS punctate labelled cells are GABAergic. When I performed the GABA studies I was unware of the punctate nNOS labelling in this region and hence no high power images were collected in the central nucleus. The currently existing low power images obtained for my studies do not provide enough detail to allow for accurate observations about whether nNOS positive punctate labelling is co-expressed with GABA markers in the same neurons, but this would be an important question to address in future studies.

3.4.5 nNOS Labelled Cells Express Calcium Binding Proteins

I have shown evidence that calbindin cells in the dorsal and lateral cortex almost always express nNOS while calretinin cells seldom do. Because calbindin positive cells in the IC virtually always express nNOS, labelling for calbindin can be used to identify at least a subset of nNOS cells in the IC.

Although they have been used extensively to delineate specific subpopulations of neurons particularly in the cerebral cortex, relatively little is known about the function of these

calcium binding proteins. However, recent findings suggest they are more than simple calcium buffers, and like calmodulin, undergo a conformational change when binding calcium, triggering further signalling cascades (Schwaller, 2009). Given the possibility that nNOSβ is expressed in the IC and presumably not directly linked to NMDA receptor activity, future research should address the possibility that nNOSβ is always co-expressed with one or more EF-hand calcium binding proteins.

In the current set of experiments no differences between the two nNOS expression patterns were observed regarding the calcium binding protein content of the cells. It is likely that nNOSα expressing neurons also have EF-hand calcium binding protein to keep the intracellular levels of free calcium low. In my experiments I always tested a single calcium binding protein together with nNOS, but there is no reason to limit oneself to one calcium binding protein marker at a time. A valuable experiment would be to label the same section for nNOS and with a combination of at least the three calcium binding proteins described in this chapter to establish whether or not nNOS is always expressed in conjunction with one or other of these proteins.

Parvalbumin positive cells in the neocortex have been shown to represent a unique population of GABAergic interneurons (Cowan *et al.*, 1990; Demeulemeester *et al.*, 1991). However, from a study in the visual cortex we know that 20% of the parvalbumin positive cells in V1 show no immunoreactivity for GABA (Demeulemeester *et al.*, 1991), clearly illustrating that parvalbumin is not a definitive marker for GABAergic neurons in all brain regions.

In this chapter, I reported that although many parvalbumin positive neurons in the IC co-express GABA there are parvalbumin cells in the IC that are GABA negative. This agrees with recent findings showing that 10 % of the parvalbumin positive cells in the IC have a glutamatergic phenotype (Fujimoto *et al.*, 2016). The same study demonstrated that around 5-15% of nNOS cells in the IC express GAD67 and so can be regarded as GABAergic (Fujimoto *et al.*, 2016). But all of these GABAergic nNOS cells showed immunoreactivity for parvalbumin (Fujimoto *et al.*, 2016). So while not all parvalbumin positive cells in the IC are GABAergic, the ones that express nNOS appear to be GABAergic. Again pointing towards an important role for the calcium binding proteins in relation to nNOS related activity.

The number of cells co-expressing parvalbumin and nNOS is low (Fujimoto *et al.*, 2016), which agrees with findings reported in this chapter. The area in which cells with a diffuse

nNOS distribution and parvalbumin positive phenotype occur is restricted to the borders of the cortices and central nucleus. My results show nNOS positive punctate labelling was observed in parvalbumin positive cells in this border region, but these labelling experiments were performed before I was aware of the existence of the nNOS puncta in the central nucleus. New labelling studies specifically targeting this phenomenon could find more nNOS positive parvalbumin cells.

3.4.6 Evidence for Differential Glutamatergic Inputs to nNOS Cells

The glutamatergic inputs received by neurons in the IC can be divided in ascending and descending connections. VGLUT1 and VGLUT2 have been shown to be markers for the terminals of glutamatergic cells (Altschuler *et al.*, 2008). Since VGLUT1 and VGLUT2 are synthesized in different brain areas, the specific labelling can inform us from where in the auditory pathway a cell in the IC receives glutamatergic projections.

VGLUT1 is not synthesized in the IC, inputs that are exclusive VGLUT1 have been shown to originate from the ipsilateral auditory cortex (Ito and Oliver, 2010). Cells that are innervated by fibers ending in terminals containing both VGLUT1 and VGLUT2 have been shown to originate from auditory brainstem areas but mainly from the VCN (Ito and Oliver, 2010). VGLUT2 is not synthesized in the cortex thus these connections necessarily represent ascending or internal connections (Ito and Oliver, 2010). Ito and Oliver (2010) showed that most of the VGLUT1 observed throughout the IC represents cortical innervation. This underscores the central role this auditory structure has in integrating ascending and descending streams of information. In accordance with previous studies, I showed that VGLUT1 and VGLUT2 have different innervation patterns on cells in the IC. Although, in my current studies the VGLUT2 labelling appeared denser in the dorsal and lateral cortex suggesting more ascending or internal connections in these areas. However, previous studies have reported denser VGLUT2 innervation in the central nucleus (Ito and Oliver, 2010).The cells only showing nNOS puncta appear not to receive any VGLUT1 innervation and hence appear not to receive any descending input from the cortex. The lack of VGLUT1 innervation in neurons with nNOS puncta is in stark contrast with the cells expressing diffuse nNOS labelling in the dorsal and lateral cortex which do receive dense VGLUT1 innervation. This distinction suggests that these cell types not only have a different subcellular nNOS distribution but also receive different sources of input. The diffuse nNOS cells in these subdivisions may receive dense corticocollicular connections from the auditory cortex. A key marker that should be considered in future IC studies would be VGAT, which labels both glycinergic and GABAergic inhibitory terminals, in conjunction with

VGLUT1 and VGLUT2 this marker can be used to estimate the balance between excitatory and inhibitory input a cell receives. In the current study data was presented showing GAD labelled innervation on some parvalbumin cells, however, GAD labelling tends to be more diffuse compared to the VGLUT1 and VGLUT2 puncta and it can be difficult to link it to the innervation of a specific cell.

It is important to note that my current results have not been quantified and before further claims can be made about the amount of VGLUT1 and VGLUT2 innervation in the subdivisions of the IC, careful inspection of the sections followed by rigorous quantification is needed. Also, the current image acquisition was optimised on a section by section basis, thus luminescent quantification across sections cannot be done on the current data set. Keeping image parameters the same between labelling protocols will be essential.

3.4.7 Functional Difference Between nNOSα and nNOSβ

Given the possibility that nNOSβ is not directly dependent on NMDA receptor activity a question that needs to be addressed is what could regulate the activity of nNOSβ. NMDA receptor activity has long been linked to nNOS activity but there are many other signalling cascades employing calcium signals. Because free calcium is potentially dangerous to cells, the levels are tightly regulated. The EF-hand calcium binding proteins have been shown to be involved in regulating the intracellular levels of calcium in the brain (Schwaller *et al.*, 2002; Schwaller, 2009). Findings indicate that calbindin and calretinin are more than simple calcium buffers (Schwaller *et al.*, 2002), but are also calcium sensors, which makes them potentially interesting targets that could regulate other secondary messengers like nNOSβ. The finding from non-neuronal cells showing nNOSβ being linked to and regulated by the Golgi complex (Percival *et al.,* 2010) would be a good starting point.

The two nNOS expression patterns observed in the IC likely represent cells in which nNOS performs different functions. The nNOS punctate labelling is observed in all subdivisions of the IC, and I showed differences in the inputs the two types of nNOS cells receive. The activity of NOSα is dependent on NMDA receptor activity due to its close proximity to the NMDA receptor via their mutual interaction with PSD95. However, there is no reason to suspect that nNOSβ proteins are dependent on the activity of this receptor. In fact given the importance and multitude of functions calcium signals perform within the postsynaptic domain, calcium diffusion within the cell is severely limited (Augustine *et al.*, 2003). Dendritic spines generate calcium signals due to the opening of ion channels governed by receptors like the NMDA receptor, but these signals decay within 1 µm (Augustine *et al.*,

2003). Thus it is highly unlikely that the nNOSβ located throughout the cell body is regulated by NMDA receptor mediated calcium signals. The different NMDA subunits have been shown to display a different permeability to calcium. Investigating whether the diffuse nNOS cells always have NMDA receptors and determining the subunit expression of these receptors could tell us more about their dependency on calcium. A related question to learn more about the nNOS puncta would be to investigate whether these puncta are associated with different NMDA receptor subunits compared to the diffuse nNOS expressing cells. Future studies also need to address to what extent nNOS is expressed in the presynaptic terminals which might again perform a different function from nNOS observed in the postsynaptic density and cytoplasm.

Hall and Garthwaite (2009) demonstrate that NO production based on the number of NMDA receptors present in the active zone of a synapse only allows for the production of picomolar concentrations of NO (Hall and Garthwaite, 2009; Wood *et al.*, 2011). They argue that due to the low quantities of NO produced by nNOSα in the active zone at any given time, it seems unlikely that this type of nNOS expression acts as a volume transmitter. The arguments made are persuasive but they hinge on the notion that nNOS is solely activated by the NMDA receptor activity. While this notion may be valid for the nNOSα protein, I would argue that the picture is far from clear or convincing with respect to the nNOSβ protein. The sheer quantity of nNOS present in the cells in the cortices of the IC could give them the ability to produce a large quantity of NO which could potentially diffuse out of the cell and exert its influence over a wider area.

3.4.8 Cell Sizes and Rostral-Caudal Distributions

In the current set of results I tried to gauge whether different cell size distributions exist in the IC subdivision and how that differs along the rostral caudal axis for the cells expressing one or more of the following markers; calbindin, calretinin, parvalbumin or nNOS. The cell number measure showed similar distributions on the whole IC level. These cell counts were done as a preliminary study to investigate whether it would be worthy of further study. In retrospect, it would have been better to further subdivide sections into dorsal cortex, lateral cortex and central nucleus, but no obvious difference was observed. The total number of nNOS and parvalbumin cells was larger compared to the number of cells expressing calbindin or calretinin as expected given the more restricted distribution of such neurons which are mainly limited to the cortices of the IC. Though simpler in shape, the nNOS positive cell bodies in the rostral regions of the IC were larger compared to the nNOS

positive cell bodies in the mid and caudal regions. The significance of this finding is currently unknown.

The cell counting exercise identified that nNOS positive neurons are bigger on average in the rostral regions of the IC compared to the caudal and middle regions. Besides the obvious differences in gross morphology the phenotype and connectivity of these NOS positive neurons was shown to differ tremendously, though no systematic differences were observed along the rostral- caudal axis of the IC.

3.4.9 Conclusion

This chapter set out to discover more about the nNOS positive neurons in the IC. A key message from these experiments is that neurons expressing this protein represent a complex and heterogeneous population. Exciting evidence was presented demonstrating that different cellular expression patterns of nNOS, perhaps reflecting different splice variants, are present in the IC. Most significant is the finding of expression in the central nucleus, a region previously described as having little or no nNOS labelling. This finding together with the different inputs both nNOS cell types receive suggests that NO performs different functions in these cell populations. These findings open up new and intriguing questions regarding the role of NO in neuronal processing. A key issue is whether these different expression patterns are linked to the different nNOS splice variants which could potentially perform different functions within the same cells. The presence of nNOS in the central nucleus in a distinctly different subcellular expression pattern compared to the cortices dramatically alters our view of nNOS activity in the IC.

Chapter 4. NMDA Receptor Mediated Activity in the IC

4.1 Introduction

In the previous chapter, I demonstrated the presence of nNOS in the central nucleus, in this chapter, I will present data that addresses the functional role it plays in auditory processing. In Chapter 3, immunohistochemical evidence was presented that in contrast to previous reports, nNOS is not solely present in the dorsal and lateral cortices but nNOS is abundant in the central nucleus of the IC. In contrast to the cortices where nNOS labelling is observed throughout the cell, the nNOS expression in the central nucleus is restricted to discrete punctate labelling. In the same chapter, evidence was put forward that the nNOS punctate labelling was associated with PSD95, a post synaptic scaffolding protein. Two different nNOS splice variants have been shown to be active in the brain, only one of which, nNOSα, possessing a PDZ binding motif which permits binding to PSD95 (Brenman *et al.*, 1996). Thus it is likely that the punctate labelling in the central nucleus represents nNOSα. PSD95 is known to facilitate the functional coupling of the NMDA receptor and the nNOS protein (Kornau *et al.*, 1995; Niethammer *et al.*, 1996; Brenman *et al.*, 1996). Both proteins come in close proximity to one another due to their mutual PDZ binding motif interactions with the PDZ binding domains 1 and 2 of PSD95. This interaction allows for the formation of the nNOS-PSD95-NMDA receptor complex and directly couples the activity of the NMDA receptor to the production of NO by nNOSα.

As discussed in Chapter 1 the central nucleus of the IC receives an enormous number of glutamatergic inputs from a number of auditory structures. In the previous chapter, I showed evidence of a wide abundance of VGLUT1 and VGLUT2, markers for glutamatergic terminals, in the central nucleus. Glutamate acts on different receptors with AMPA and NMDA receptors being the most abundant glutamate receptors in the auditory pathway (Parks, 2000). While AMPA receptors are coupled to Na^+ selective ligand gated ion channels and have been shown to have low permeability to calcium, NMDA receptors have been shown to be Ca^{2+} permeable (Dingledine *et al.*, 1999; Meldrum, 2000; Platt, 2007) (Pellegrini-Giampietro *et al.*, 1997).

In resting state conditions, the NMDA receptors are blocked in a voltage dependent manner by Mg2+ thus preventing the opening of the ion channel. The activation of AMPA receptors depolarises the cell membrane and repels the Mg2+ from the NMDA receptor allowing the glutamate (or other NMDA receptor agonist) to bind to the NMDA receptor opening the ion channel and allowing Ca2+ into the cell. As discussed in Chapter 1, nNOS is non-active at normal resting state calcium levels and requires an intracellular rise in free calcium levels.

Due to the co-labelling of PSD95 and the punctate nNOS positive labelling (Chapter 3), it seems justified to conclude that the punctate nNOS in the central nucleus forms an integral part of the nNOS-PSD95-NMDA receptor complex and that nNOS activity is directly dependent on calcium entering the cell due to NMDA receptor activity. NO signalling is entirely dependent on its production because there is no storage or release of this gaseous neurotransmitter. An increase in the NMDA receptor activation would, therefore, lead to an increased production of NO.

In order to investigate the relation between NMDA receptors and the NO signalling cascade and their mutual effect on auditory processes in the IC, a series of experiments were designed. The experiments designed relate directly to the aims formulated at the end of Chapter 1.

The aims of this chapter were to:

- Investigate how selective activation of the NMDA receptor influences the spontaneous and acoustic driven response properties of the multi-unit activity.
- Investigate whether and how the NO signalling cascade is participating in the spontaneous and acoustic driven responses of the multi-unit activity.
- Investigate the potential link between the NMDA receptor and the NO signalling cascade.

4.2 Methods

Each experimental group consisted of three female pigmented guinea pigs aged approximately 2-3 months. All animals received the urethane, fentanyl and midazolam anaesthesia protocol as described in Chapter 2 had a multichannel electrode and microdialysis probe surgically implanted in the IC as described.

4.3 Protocols

The first protocol established a concentration response curve for NMDA (Figure 4-1A). In these experiments, increasing concentrations of NMDA (30, 100 and 300 μM) were perfused. FRA and PSTH data were collected (see Chapter 2). Perfusion of NMDA was alternated with aCSF to investigate whether observed effects were reversible. The dose response experiments were used as pilot experiments to find the optimal NMDA concentration that gives a robust response without completely saturating the system.

The second set of data reported here, pools data from the 100 μM NMDA condition from nine animals across all three protocols. The pooling of the data resulted in higher statistical power. The NMDA concentration response data and the 100 μM NMDA data provided me with a description of the neuronal activity in the central nucleus of the IC in response to the selective activation of the NMDA receptor in vivo.

The other two protocols were designed to probe to what extent the observed NMDA effect was mediated by NO signalling.

Protocol 2. Experiments started with a 45 minute perfusion of NMDA (100 μM), followed by a 45 minute aCSF washout. This was followed by a 20 minute perfusion of the nNOS inhibitor L-MeArg (1000μM) immediately followed by a 20 minute perfusion of both L-MeArg (1000 μM) and NMDA (100 μM). Again this was followed by a 45 minute washout.

Protocol 3. Experiments started with a 45 minute perfusion of NMDA (100 μM), followed by a 45 minute aCSF washout. This was followed by a 20 minute perfusion of the sGC inhibitor ODQ (500 μM) immediately followed by a 20 minute perfusion of both ODQ (500 μM) and NMDA (100 μM). Again this was followed by a 45 minute washout.

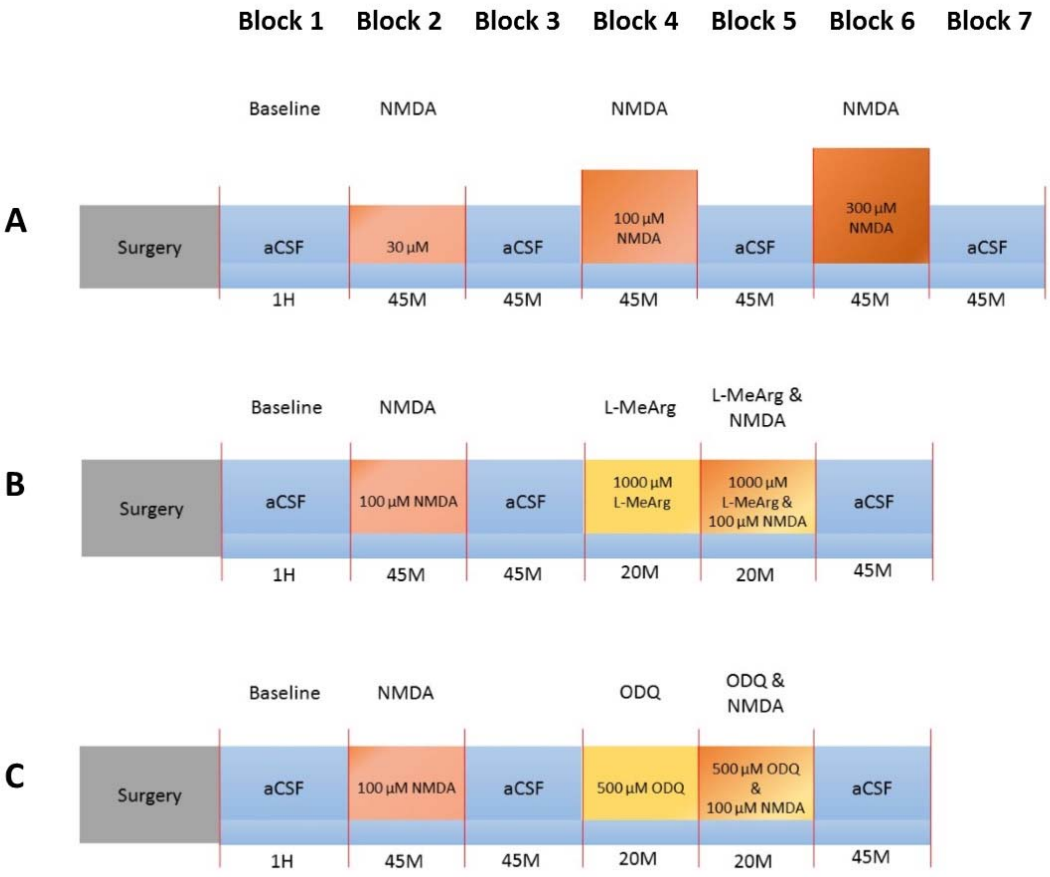

Figure 4-1 Experimental protocols. A. NMDA dose response (N=3). B. NMDA & L-MeArg (N=3). C. NMDA & ODQ (N=3)

4.3.1 Data Analysis and Statistics

Measures

In the earliest experiments the frequency range with which animals were stimulated varied such that not all frequencies were presented to all animals in all conditions. The lowest frequency that was presented to all animals was 1024 Hz. Thus, the multi-unit activity recorded at the electrode best representing this frequency was extracted and analysed. The following measures were calculated;

- Characteristic Frequency (CF)
- Threshold attenuation at CF
- Spontaneous activity
- PSTH onset response
- PSTH sustained response
- PSTH total driven response
- FRA area of increased activity

- FRA magnitude of increased activity
- FRA area of decreased activity
- FRA magnitude of decreased activity

The methods for deriving the above listed measures are described in detail in Chapter 2. The CF was determined objectively by use of a custom written Matlab algorithm, written by me.

Contrasts

All data analysed was expressed as a ratio to baseline.

The first analysis in this chapter focussed on the NMDA concentration response protocol, depicted in Figure 4-1 A. Here a within subjects contrast was used. The NMDA perfusions (block 2, 4 and 6 in Figure 4-1A) were compared to the original aCSF baseline (block 1 in Figure 4-1A). Each NMDA perfusion was also compared to the aCSF perfusion before and after it. The data used in the analysis was obtained 45 minutes into the respective perfusion.

For the 100 µM NMDA experiments, data recorded at 20 minutes into the NMDA perfusion condition were used. This allowed determination of whether NMDA effects saturate over time, also this allowed for future comparisons between the NMDA only and NMDA + L-MeArg or NMDA + ODQ.

The second analysis investigated the effect of L-MeArg on auditory processing in the IC. The experimental protocol is depicted in Figure 4-1B, again employing a within subjects contrast. The L-MeArg perfusion (block 4 Figure 4-1B) was compared to the preceding aCSF perfusion (block 3 Figure 4-1B) and the following aCSF washout (block 6 Figure 4-1B), note that there was NMDA perfusion in between the L-MeArg block and the aCSF washout (block 5 Figure 4-1B).

The third analysis investigated the effect of ODQ on auditory processing in the IC. The experimental protocol is depicted in Figure 4-1C and matches protocol B. The ODQ perfusion (block 4 Figure 4-1C) was compared to the preceding aCSF perfusion (block 3 Figure 4-1C) and the following aCSF washout (block 6 Figure 4-1C). Note that there was NMDA perfusion in between the ODQ block and the aCSF washout (block 5 Figure 4-1C).

In the fourth analysis, a mixed design with a between and a within subjects contrast was used. For the between subjects the 100 µM NMDA perfusion block 4 protocol A was contrasted with the NMDA + L-MeArg perfusion (block 5 protocol B) and NMDA + ODQ

perfusion (block 5 protocol C). The within contrast (baseline, NMDA, washout) included blocks 3, 4 and 5 from protocol A, and blocks 4, 5 and 6 from protocols B and C.

Following this mixed design, for both protocol 2 and 3, a within animal contrast was performed over all conditions.

Statistical analysis

Data in which the effect of one drug was studied were analysed using a one-way repeated measures ANOVA in which the different experimental conditions over time were entered as the within subjects factor. When significant main effects for these experimental conditions were obtained, post hoc t-tests were used with a Bonferroni correction. NMDA perfusions were compared to the original baseline, the aCSF washout preceding the NMDA perfusion and the aCSF washout following the NMDA perfusion. Significant differences between conditions are expressed as a mean difference in ratio between conditions and its standard error.

Data investigating the possible interaction between the NO modulators (L-MeArg or ODQ) and NMDA were analysed with a two-way mixed design ANOVA in which the experimental condition was entered as the within subjects factor and the presence/absence of the NO modulator as the between subjects factor. From this two-way mixed ANOVA, only significant interaction effects are reported, because the main effects in a mixed design can be misleading. A significant interaction was followed up by three one-way ANOVAs on the three experimental conditions comparing the different groups (NMDA + aCSF, NMDA + L-MeArg and NMDA + ODQ). Significant main effects from this one-way ANOVA were followed up by a post hoc Tukey test. Significant differences between groups are expressed as a mean difference (M) between groups and the standard error (SEM).

To enable a within animal comparison for this data, all conditions from the experimental protocols (Figure 4-1B and C) were included in a one way ANOVA. Significant main effects were followed up by post hoc t-tests testing the baseline (block 1) against the NMDA (only) (block 2), the NMDA (only)(block 2) against the aCSF washout (block 3) and the aCSF washout (block 3) against the NMDA + NO modulator (L-MeArg or ODQ) (block 5).

4.4 Results

4.4.1 Local Perfusion of NMDA Increases Neuronal Activity in a Concentration Dependent Manner

FRA measures

NMDA caused a concentration-dependent increase in activity. The effects of local perfusion of NMDA were evident not only at or near the CF of the multiunit activity but were observed across the FRA a wide range of frequencies and attenuations (see Figure 4-2). Data reported in this chapter was obtained from the electrode best responding to 1024 Hz, but similar effects were observed on different electrodes (data not shown). Formal analysis of the effects of NMDA on measures taken from the FRA are reported below.

Characteristic frequency and threshold attenuation

Local perfusion of increasing concentrations of NMDA into the IC did not alter the CF of the multi-unit activity recorded on the electrode (Figure 4-2, Figure 4-4A). The CF was determined objectively using a software algorithm. A one way ANOVA showed no significant effect of condition ($F(6,12) = 0.462$, $p = 0.687$ (Figure 4-4A). The threshold attenuation at CF was also unchanged in response to the increasing concentrations of NMDA (Figure 4-2B) as evidenced by the fact that there was no significant effect of condition ($F(6,12) = 0.712$, $p = 0.647$) (Figure 4-4B).

Spontaneous activity

Local perfusion of NMDA into the IC resulted in an increase in the spontaneous activity (obtained from the lowest attenuation level of the FRA) which was concentration dependent and only partially reversible. Thus the one way ANOVA showed a significant effect of the experimental condition ($F(6,12) = 9.70$, $p = 0.001$) (Figure 4-4C). Post hoc tests revealed that the spontaneous activity during NMDA perfusion was significantly higher compared to that during the perfusion of aCSF at the start of the experiment (original baseline) both after local perfusion of 100 µM NMDA (2.22 ± 0.07 (3)) and local perfusion of 300 µM NMDA (3.03 ± 0.39 (3)). Spontaneous activity was significantly lower after 45 minutes of aCSF washout following the local perfusion of 300 µM NMDA (-0.62 ± 0.20 (3)). The spontaneous activity during the local perfusion of 300 µM NMDA was also significantly higher than during the aCSF washout condition preceding it (1.92 ± 0.39 (3)).

PSTH measures

An example of the PSTH data recorded in the NMDA dose response experiments is shown in Figure 4-3. This figure shows the aCSF baseline recording, subsequent perfusions of 30 µM, 100 µM and 300 µM NMDA interspersed with aCSF washout conditions. Measures derived from the PSTH are detailed below:

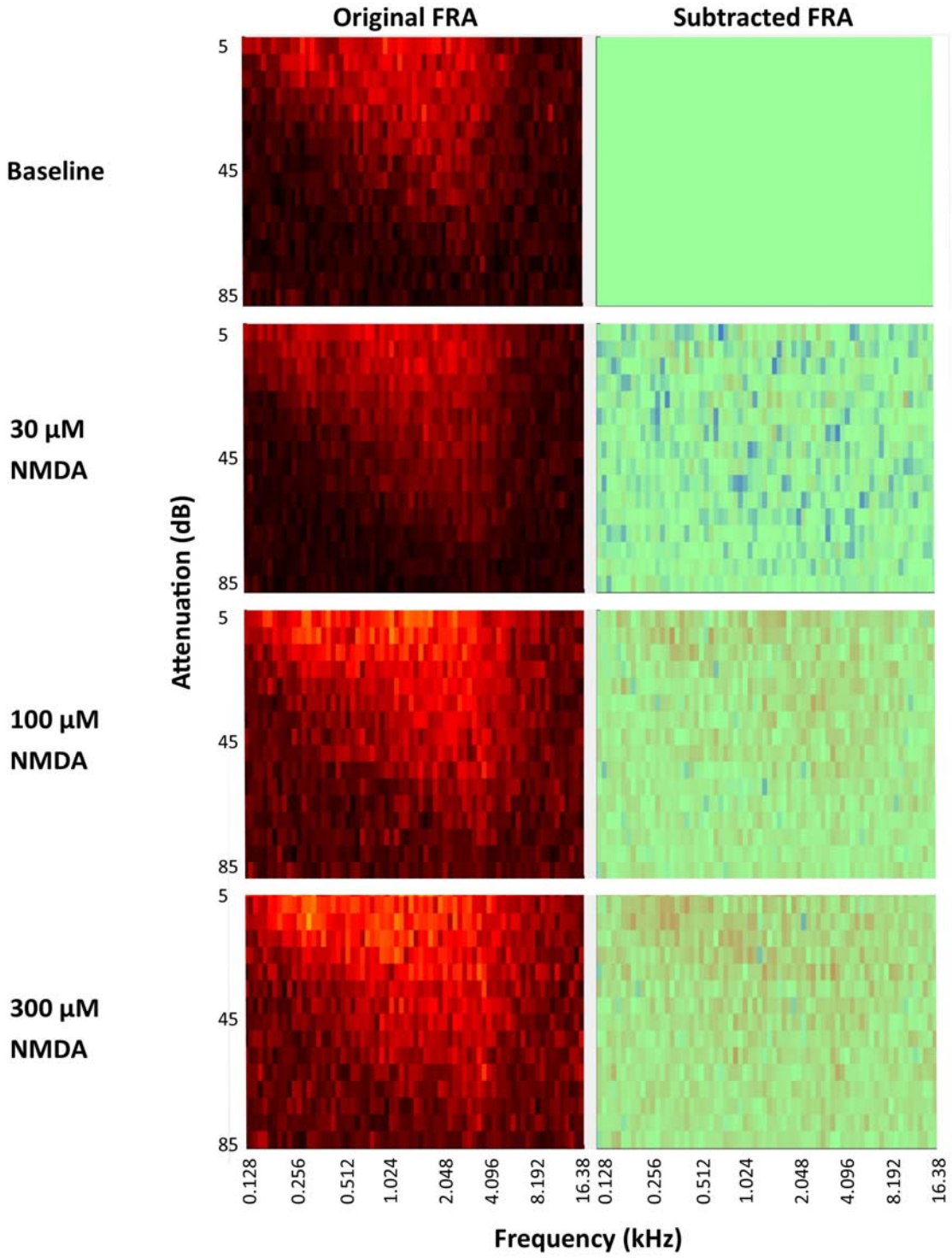

Figure 4-2. Example FRA showing the effect of three different concentrations of NMDA perfused into IC. The original FRA for each block shown in the left column while the right column shows the baseline FRA subtraction from the block in question. Note how following perfusion of higher concentrations of NMDA, increased activity (red pixels) is seen across the whole FRA although it is most concentrated in the sound driven part of the FRA. Note also how the CF and threshold at CF as well as the overall shape of the FRA appear unchanged.

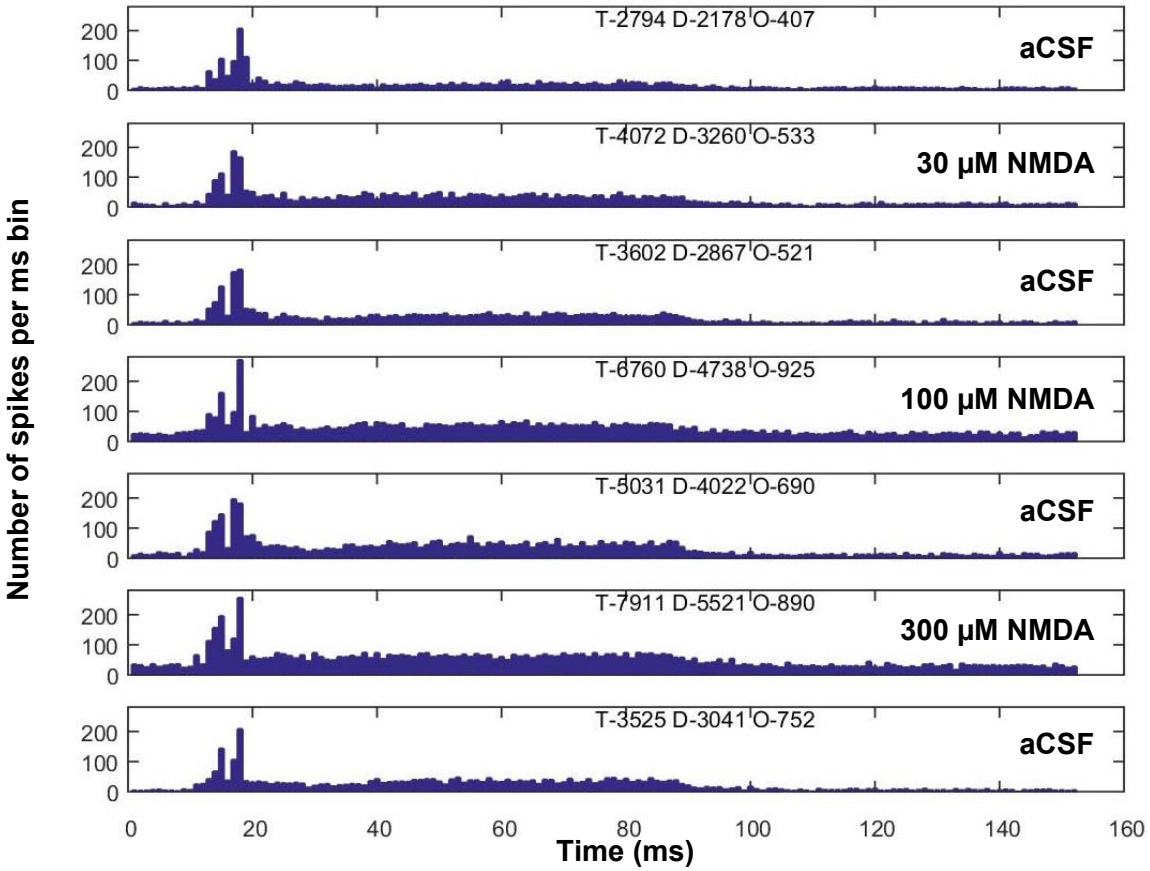

Figure 4-3 example PSTH data for the aCSF baseline, 30, 100 and 300 µM NMDA interspersed with aCSF washout conditions all data recorded at 45 minutes perfusion. T stands for the total number of spikes, D for the driven number of spikes and O for the number of spikes in the onset peak.

PSTH total driven activity

Local perfusion of NMDA significantly increased the total driven activity in a concentration-dependent manner ($F(6,12) = 11.79$, $p < 0.001$) (Figure 4-4D). The post hoc tests showed significant increases in driven activity between the original baseline and both 100 µM NMDA (2.05 ± 0.14 (3)) and 300 µM NMDA (2.64 ± 0.37(3)). Total driven activity was significantly lower after 45 minutes of aCSF washout following the local perfusion of 300 µM NMDA (-0.87 ± 0.18(3)) but not after 100 µM NMDA. The differences between both the NMDA blocks and the aCSF blocks immediately preceding them were not significant after the Bonferroni correction was applied. To examine whether the effect of NMDA was specific to different parts of the PSTH, the activity in the first 10 ms of the onset peak (Onset activity) and a 10 ms block during the sustained response was examined.

PSTH onset activity

Local perfusion of NMDA caused an increase in the onset peak activity ($F(6,12) = 22.25$, $p < 0.001$) (Figure 4-4E). The post hoc tests showed significant differences between the original baseline and both 100 µM NMDA (1.63 ± 0.13 (3)) and 300 µM NMDA (2.63 ± 0.28 (3)). Total onset activity was significantly decreased after the 45 minute aCSF washout following the local perfusion of 300 µM NMDA (-1.10 ± 0.43 (3)) but no significant change was observed following the 100 µM washout. The differences between both the NMDA blocks and the aCSF blocks preceding them were not significant after the Bonferroni correction.

PSTH sustained activity

Local perfusion of NMDA increased the sustained activity ($F(6,12) = 9.36$, $p = 0.001$) (Figure 4-4F). The post hoc tests showed significant differences between the original baseline and both 100 µM NMDA (2.14 ± 0.26(3)) and 300 µM NMDA (2.84 ± 0.17 (3)). Following the local perfusion of 100 µM NMDA, a 45 minute aCSF washout failed to significantly reduce sustained activity. However, following the local perfusion of 300 µM NMDA a 45 minute aCSF washout resulted in a significant reduction in sustained activity (-1.12 ± 0.61 (3)). The total sustained activity increased significantly between the 300 µM NMDA condition and the aCSF block preceding it (2.36 ± 0.10 (3)).

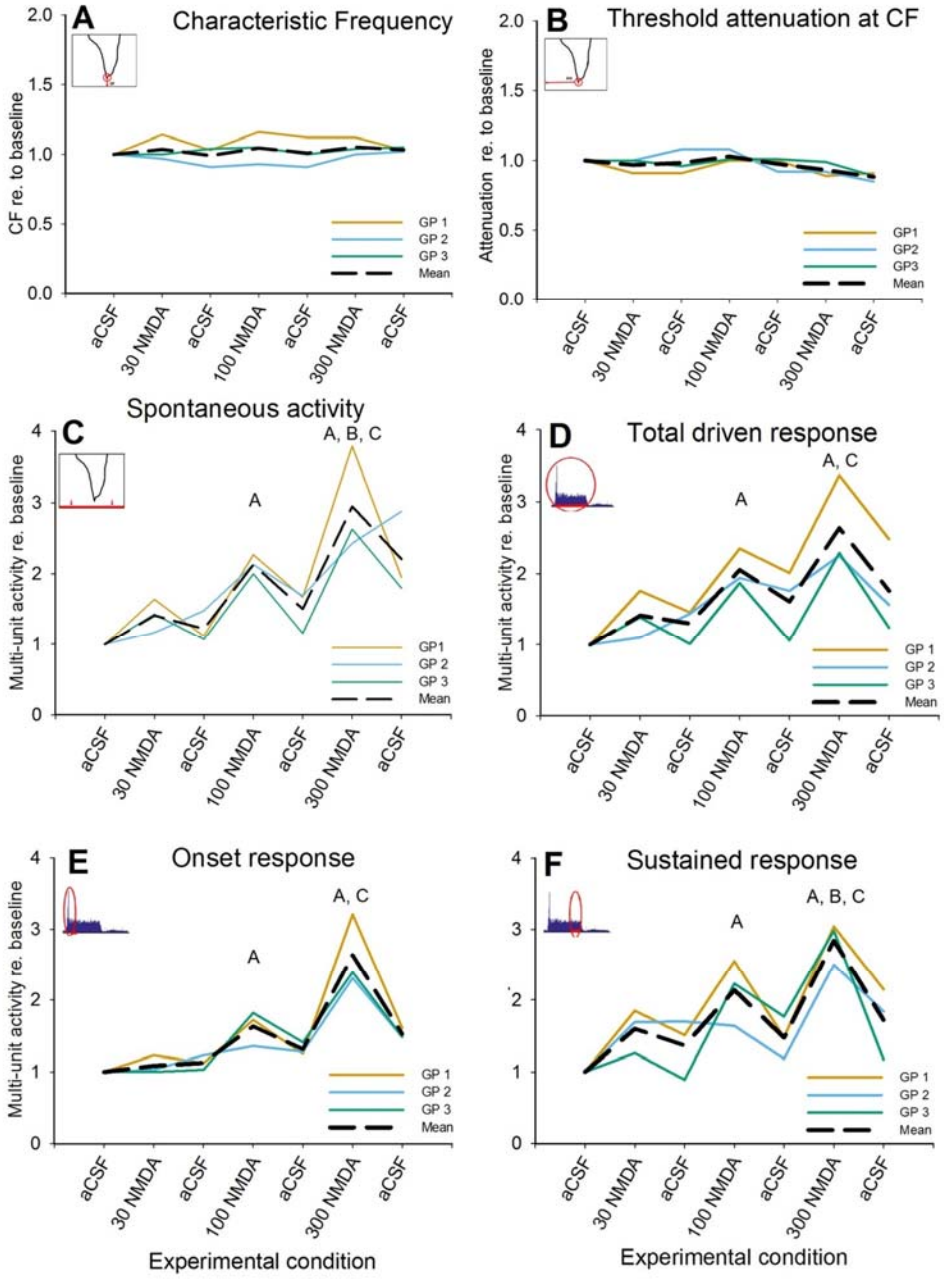

Figure 4-4 NMDA dose response curve for measures of spontaneous and sound-driven neuronal firing in the IC (N=3). The individual data points are given for each animal plus the mean across animals is shown as the dashed black line. A. CF changes. B. Attenuation at the CF. C. Spontaneous activity. D. PSTH onset activity. E. PSTH sustained sound-driven response. F. PSTH total sound-driven activity. Significant post hoc contrasts p<0.05 are indicated by A) vs original baseline, B) vs preceding aCSF block, C) vs following aCSF block

4.4.2 Local Perfusion of 100 µM NMDA Increases Neuronal Activity

The dose response studies (reported in section 4.4.1 above) revealed that the lowest concentration to consistently increase spontaneous and sound-driven neuronal activity in the IC was 100 µM NMDA (45 minutes). This concentration was therefore chosen to assess the effects of NOS modulators on the response to NMDA. To substantiate the findings that NMDA increases spontaneous and sound-driven neuronal firing in the IC but does not alter the CF or threshold attenuation, all NOS modulator experiments began with a 45 minute 100 µM NMDA perfusion (Figure 4-1A Block 4, 1B Block 2 and 1C Block 2). Investigating the data showed that NMDA reached its maximum effect 10-15 minutes after starting the perfusion. To allow comparisons with NOS modulator experiments, in this section the data recorded 20 minutes after the start of the local perfusion of 100 µM NMDA were analysed and are reported. Note that the data from the washout block was recorded 70 minutes later (25 minutes remaining NMDA + 45 minutes aCSF washout).

FRA measures

Characteristic frequency and threshold attenuation

Consistent with the observation from study 1, the local perfusion of 100 µM NMDA (20 minutes) had no effect on CF (Figure 4-6A) or on the threshold attenuation at CF (Figure 4-6B). Thus, the ANOVA showed no significant effect of condition on either CF ($F(2,16) = 0.085$, $p = 0.919$) or threshold ($F(2,16) = 2.08$, $p = 0.162$).

Spontaneous activity

Spontaneous activity (taken from the lowest attenuation in the FRA) increased significantly in response to 100 µM NMDA (20 minutes) (Figure 4-6C). There was a significant main effect for the condition ($F(2,16) = 37.73$, $p < 0.001$) the post hoc tests showed that the spontaneous activity in the 100 µM NMDA condition was significantly higher than in the preceding aCSF condition (2.46 ± 0.21). The recorded activity during the aCSF washout condition varied considerably between animals and was not statistically different from NMDA condition.

PSTH measures

An example of the PSTH data recorded in the NMDA experiments is shown in Figure 4-5. This figure shows the baseline recording, a 20 minute perfusion of 100 µM NMDA, 40 minute perfusion of 100 µM NMDA and the washout condition.

This figure also illustrates that the NMDA evoked increase is present at 20 minutes and does not increase further up to 40 minutes of perfusion.

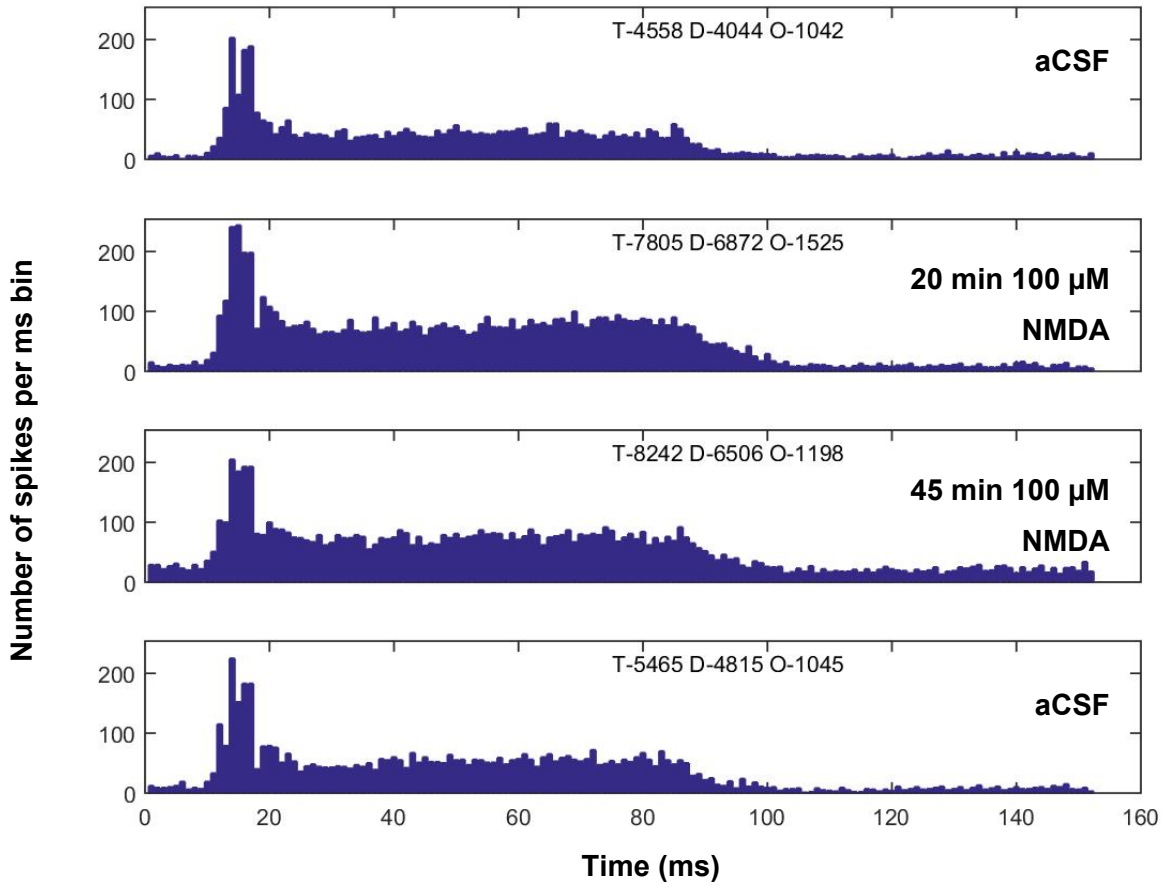

Figure 4-5 PSTH data for the baseline, 100 µM NMDA condition at 20 and 45 minutes and the washout condition. T stands for total number of spikes, D for the driven number of spikes and O for the number of spikes in the onset peak. This figure also illustrates that the NMDA evoked increase is present at 20 min and does not increase further up to 40 minutes of perfusion, also note the partial reversal during the aCSF washout.

Total driven response

NMDA (20 minutes) increased the total sound driven response ($F(2,16) = 8.81$, $p = 0.003$) (Figure 4-6D). The post hoc tests showed that total driven activity was higher during NMDA perfusion compared to the aCSF condition (1.93 ± 0.16 (9)). The sound driven response was significantly reduced after the 45 minute aCSF washout compared to the 20 minute NMDA perfusion (-0.98 ± 0.37 (9)). To examine whether the effect of NMDA was specific to different parts of the PSTH, the activity in the first 10 ms of the onset peak (Onset activity) and a 10 ms block during the sustained response was examined.

Onset activity

NMDA (20 minutes) increased the onset response significantly ($F(2,16) = 54.89$, $p < 0.001$) (Figure 4-6E). Post hoc tests showed that the onset activity in the NMDA condition was significantly higher compared to the preceding aCSF condition (1.76 ± 0.06 (9)). The aCSF washout (45 minutes) caused a decline in the observed onset activity compared to the NMDA condition (-0.83 ± 0.27 (9)).

Sustained activity

Local NMDA (20 minutes) perfusion caused an increase in the sustained response ($F(2,16) = 17.15$, $p < 0.001$) (Figure 4-6F). The post hoc tests showed that the sustained response increased in response to the NMDA perfusion compared to the preceding aCSF baseline (2.19 ± 0.22 (9)). The washout condition varied considerably between animals and was therefore not statistically different from NMDA condition, although the overall trend was a decline in sustained activity during the washout.

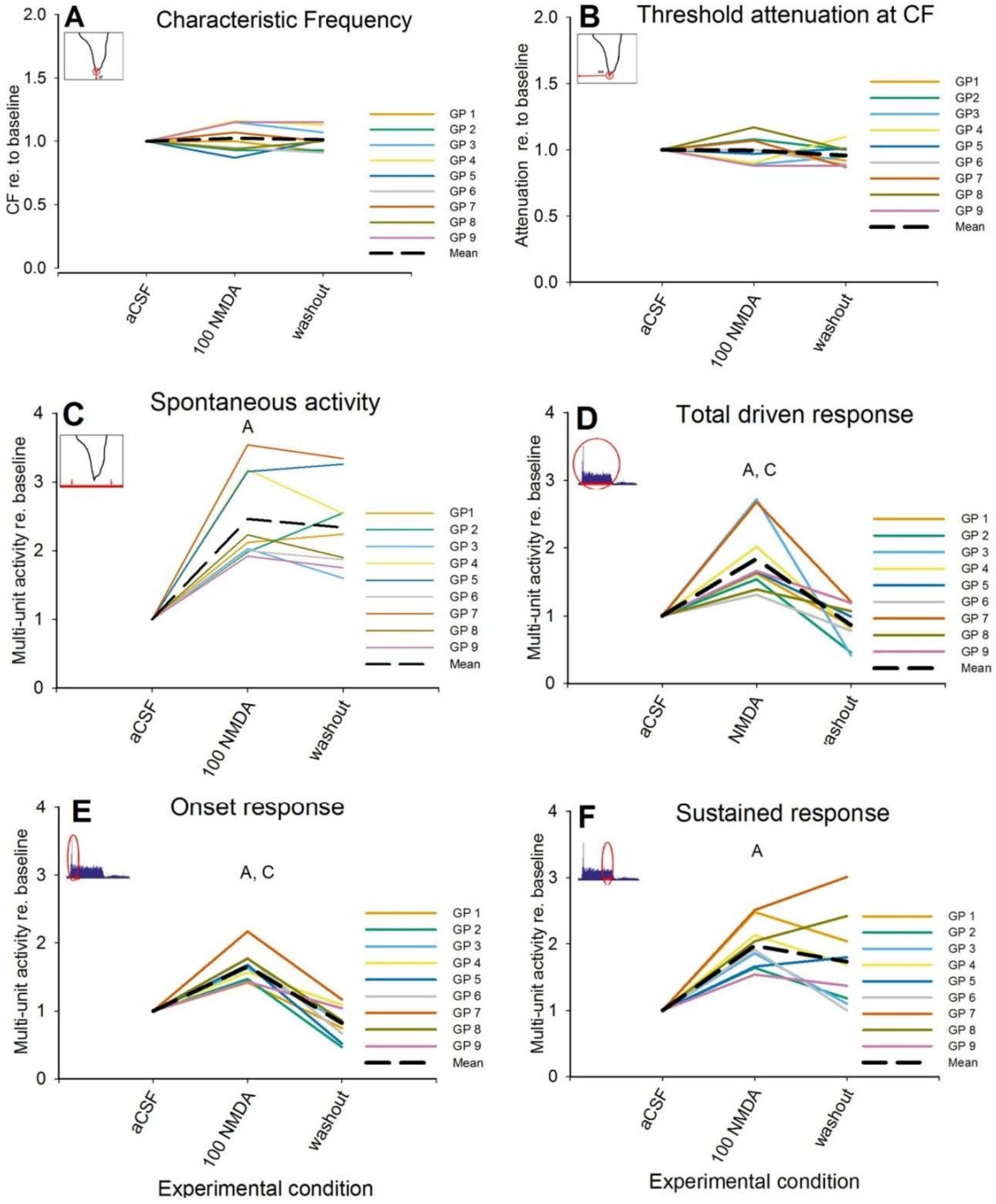

Figure 4-6 Effects of 100 µM NMDA for several pure tone response measures of neuronal firing in the IC. The individual data points are shown per animal, with the mean by the black dashed line. A. CF. B. threshold at CF. C. Spontaneous activity. D. PSTH onset activity. E. PSTH sustained driven response. F. PSTH total sound driven activity. Significant post hoc contrasts p<0.05 are indicated by A) vs original baseline, B) vs preceding aCSF block, C) vs following aCSF block.

4.4.3 Local Perfusion of L-MeArg has No Effect on Neuronal Response

As discussed in Chapter 1, NO signalling may act through two different modes of action, a tonic low concentration state and a short pulsed high concentration state. In order to investigate whether NO signalling has an influence on normal auditory processing in the IC, the NOS inhibitor L-MeArg was perfused in the IC.

PSTH measures

An example of the PSTH data recorded in the L-MeArg experiments is shown in Figure 4-7. This figure shows the baseline recording, a 20 minute perfusion of 1000 µM L-MeArg the washout condition, note that there was an L-MeArg + NMDA condition in between the L-MeArg and the washout condition. There were no significant changes in measures taken from the PSTH: driven response ($F(1,2) = 6.50$, $p = 0.126$) (Figure 4-8D) onset response ($F(1,2) = 0.01$, $p = 0.996$) (Figure 4-8E) and the sustained response ($F(1,2) = 0.01$, $p = 0.992$) (Figure 4-8F).

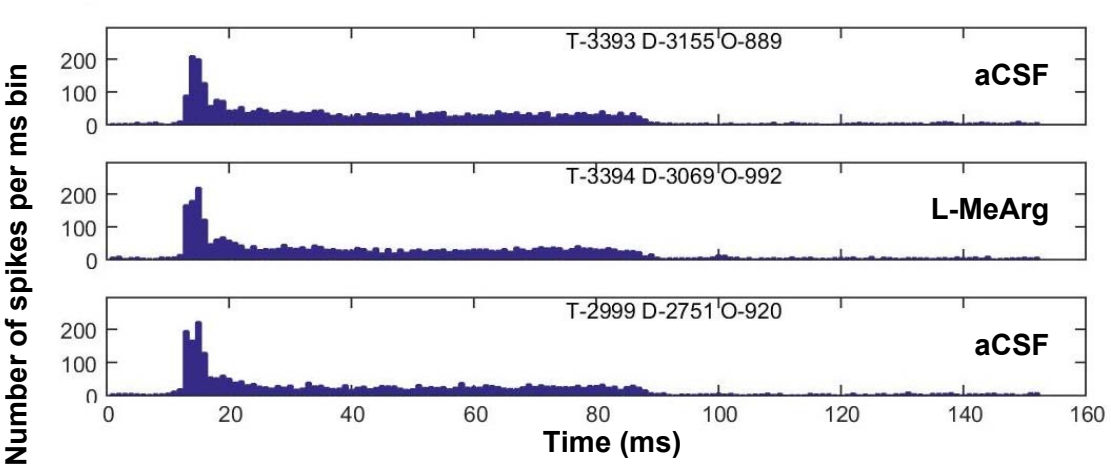

Figure 4-7 PSTH data for the aCSF baseline, 1000 µM L-MeArg and aCSF washout condition. T stands for the total number of spikes, D for the driven number of spikes and O for the number of spikes in the onset peak.

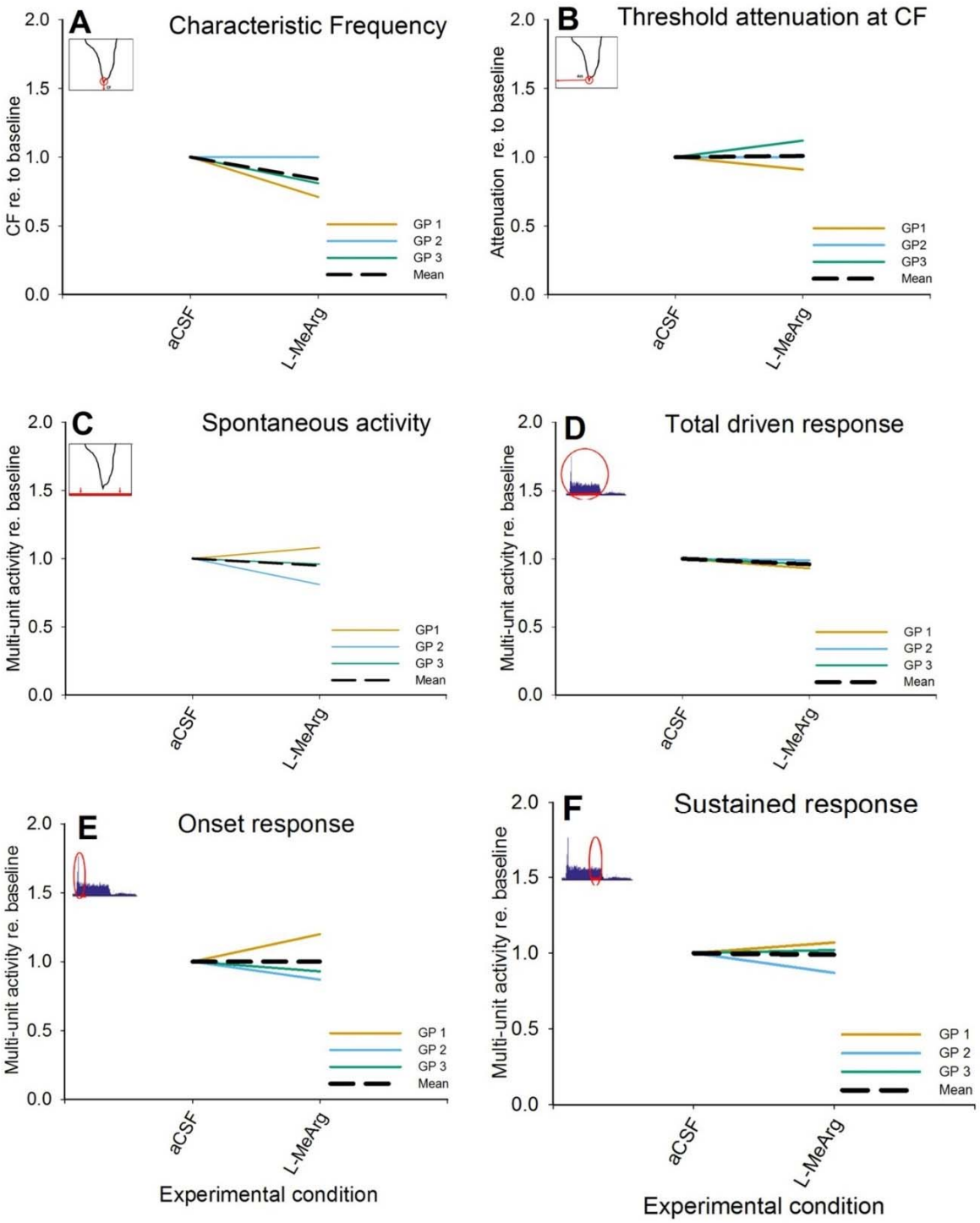

Figure 4-8 Effects of L-MeArg on neuronal firing in the IC, activity recorded on the electrode recording multi-unit clusters responding best to stimulation of 1024 Hz. A. CF B. Attenuation on which the CF was obtained C. Spontaneous activity D. PSTH total activity E. PSTH sound driven activity F. PSTH Onset activity. There were no significant post hoc contrasts.

FRA measures

The PSTH analysis performed at 1024 Hz, reported above, revealed no significant changes in neuronal activity due to the perfusion of L-MeArg in the IC. The FRA permits investigation of a wider range of frequencies and attenuations on the same electrode. In Figure 4-9 the original FRA (left column) and the result of subtracting the baseline FRA (right column) are shown for the aCSF baseline and the L-MeArg condition, examples come from two different animals. Some pixels representing different frequencies did show changes in activity, but no systematic statistically significant consistent patterns were observed during the perfusion of L-MeArg.

The local perfusion of L-MeArg in the central nucleus of the IC had little effect on the measures of neuronal firing recorded (Figure 4-8). The CF did not change significantly ($F(1,2) = 3.47$, $p = 0.203$) (Figure 4-8A) and the threshold attenuation at CF was also unaffected, ($F(1,2) = .031$, $p = 0.877$) (Figure 4-8B). Similarly, the 20 minute perfusion of L-MeArg produced no systematic change in spontaneous activity ($F(1,2) = .351$, $p = 0.614$) (Figure 4-8C).

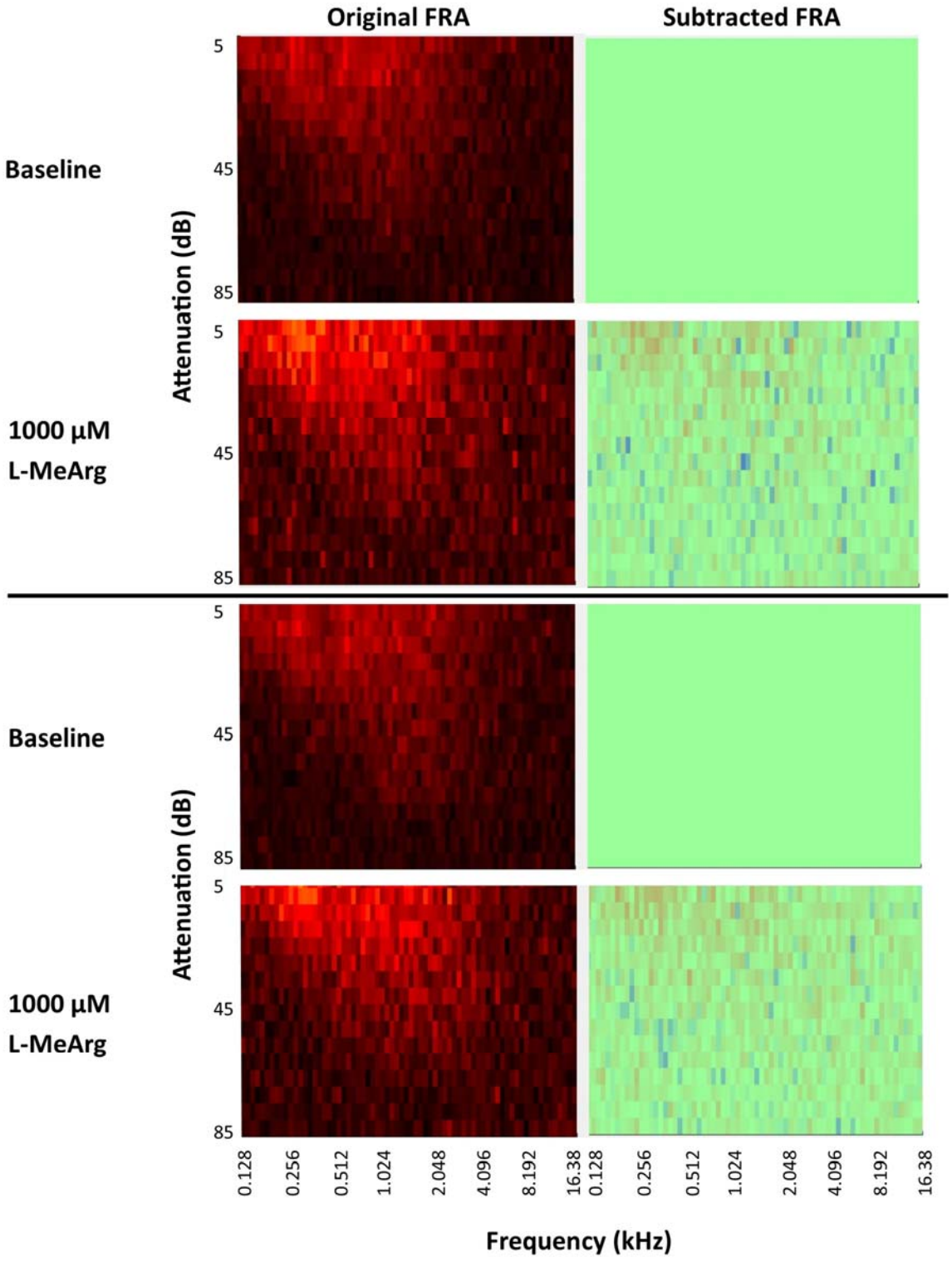

Figure 4-9 FRAs collected at baseline and during the perfusion of 1000 µM L-MeArg. Shown in the left column are the original FRAs, in the right column the baseline FRA is subtracted from the L-MeArg block. The top example originates from GP4, the bottom example from GP6.

4.4.4 Local Perfusion of ODQ has No Effect on Neuronal Response

As discussed in the Introduction, sGC - the main downstream receptor target of NO remains in a stable low active state under normal conditions producing solid but low levels of cGMP due to the tonic levels of NO binding to the haem domain of sGC. The uncoupling of NO from the haem of sGC is slow and the blocking of NO production by L-MeArg may leave the low level activity of sGC in place. To investigate whether this tonic state of sGC might contribute to normal auditory processing in the IC, ODQ, a drug that blocks sGC was perfused in the IC through a microdialysis probe, thereby inhibiting the functioning of sGC.

PSTH Measures

An example of the PSTH data recorded in the ODQ experiments is shown in Figure 4-10. This figure shows the baseline recording, a 20 minute perfusion of 500 µM ODQ and the washout condition, note that there was an ODQ + NMDA condition in between the ODQ and the washout condition. The perfusion of ODQ also failed to induce any systematic changes in neuronal firing in the IC. No changes were observed in any of the three measures obtained from the PSTHs. Thus there was no significant effect of condition for total driven activity ($F(1,2) = 0.399$, $p = 0.592$) (Figure 4-11D), onset ($F(1,2) = 0.144$, $p = 0.741$) (Figure 4-11E) or sustained ($F(1,2) = 0.274$, $p = 0.653$) (Figure 4-11F).

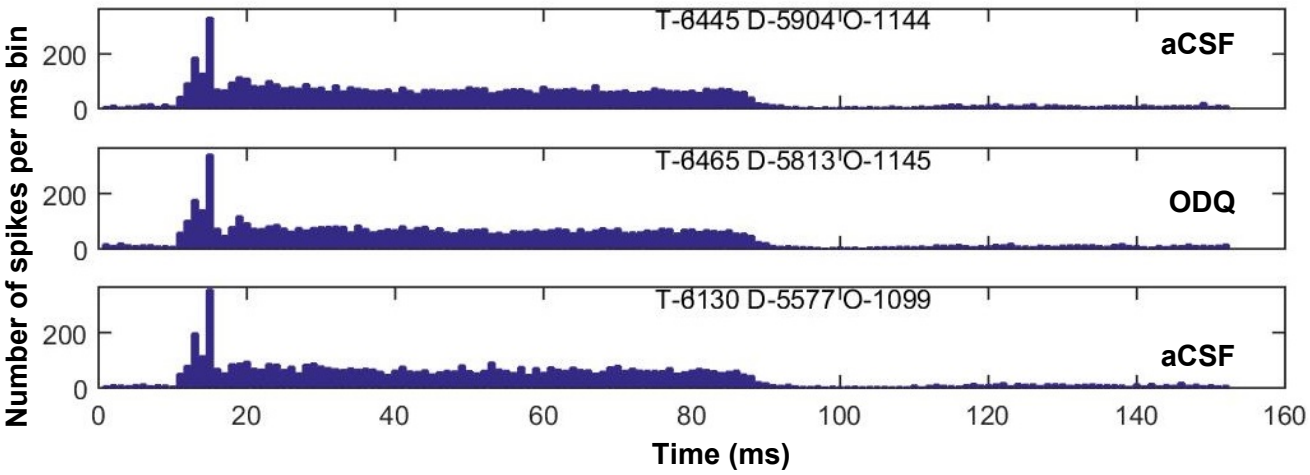

Figure 4-10 PSTH data for the aCSF baseline, 500 µM ODQ and aCSF washout condition. T stands for the total number of spikes, D for the driven number of spikes and O for the number of spikes in the onset peak.

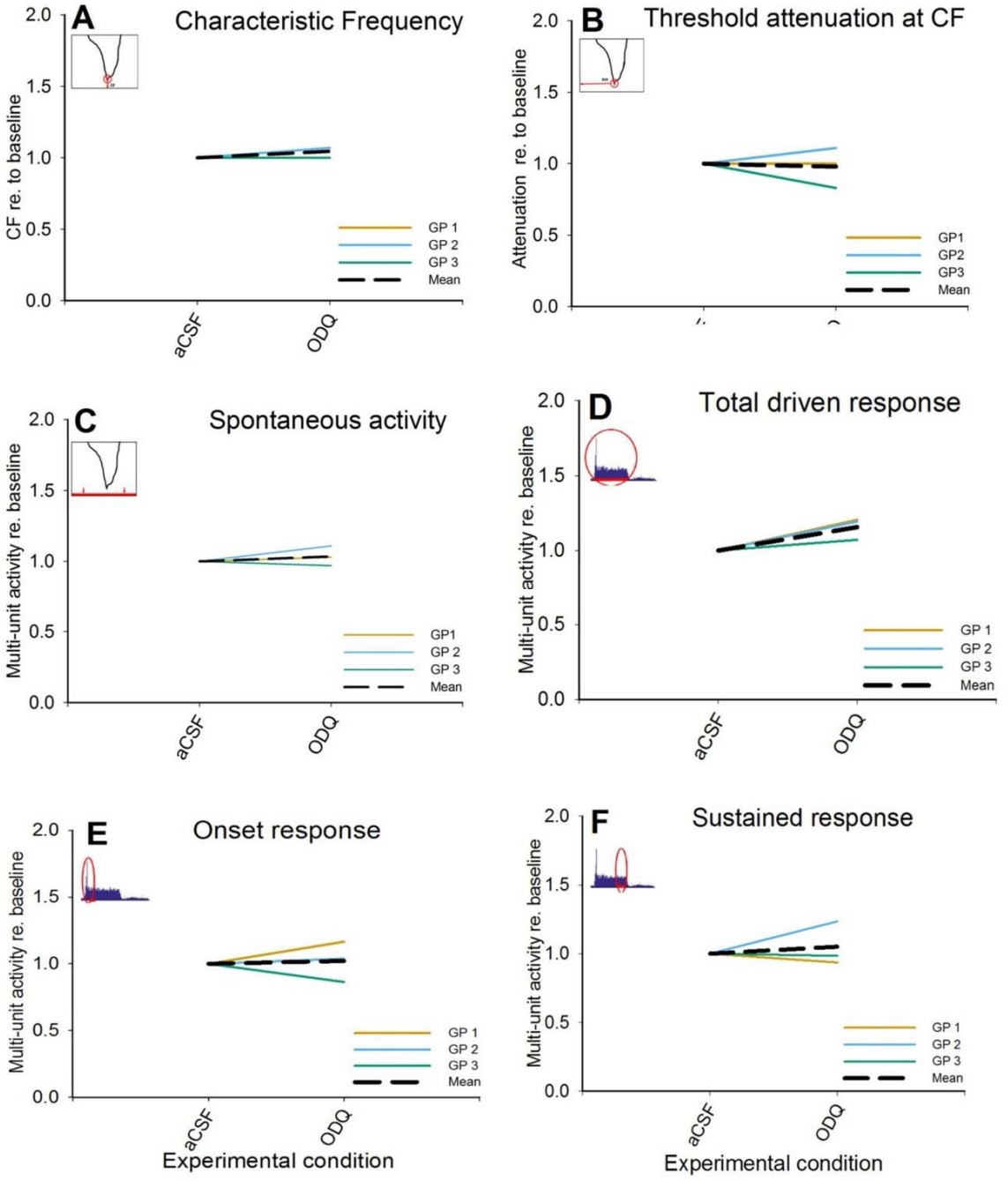

Figure 4-11 Effects of ODQ on neuronal firing in the IC, activity recorded on the electrode recording multi-unit clusters responding best to stimulation of 1024 Hz. A. CF B. Attenuation at which the CF was obtained C. Spontaneous activity D. PSTH onset activity E. PSTH sustained activity F. PSTH total driven activity. There were no significant post hoc contrasts.

FRA measures

The PSTH analysis performed at 1024 Hz, reported above, revealed no significant changes in neuronal activity due to the perfusion of ODQ in the IC. As discussed before, the subtracted FRA allows me to investigate a wider range of frequencies and attenuations on the same electrode. In Figure 4-12 the original FRA (left column) and the result of subtracting the baseline FRA (right column), are shown for the aCSF baseline and the ODQ condition, examples come from two different animals and randomly selected electrodes to illustrate that the lack of effect was observed on different electrodes. A few pixels representing different frequencies did show a change in activity, but no systematic statistically significant patterns were observed during the perfusion of ODQ. Due to the lack of any systematic change, no further analysis was applied to this data.

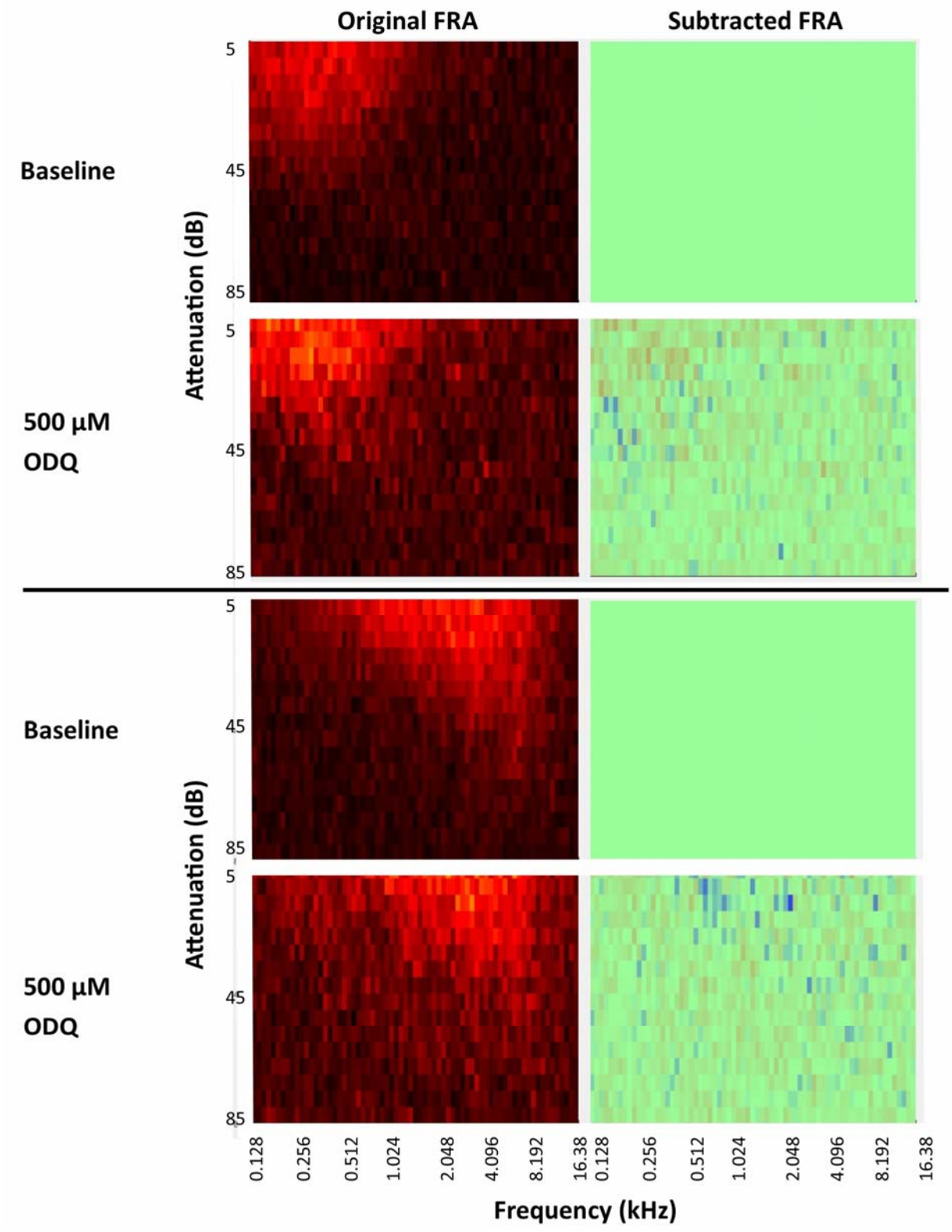

Figure 4-12 FRAs recorded during the perfusion of 500 µM ODQ. In the left column, the original FRAs are displayed, in the right column the baseline FRA is subtracted from the current condition. The top example originates from GP7 the bottom example from GP8.

4.4.5 L-MeArg and ODQ modulate the NMDA Effect

The results presented in sections 4.4.3 and 4.4.4 show that local perfusion in the IC of the NO modulators L-MeArg and ODQ did not have an effect on recorded multi-unit activity and suggest spontaneous and sound-driven activity are not mediated by tonic levels of NO. As discussed in Chapter 1 increasing NMDA receptor mediated activity will lead to an increase in NO which will trigger sGC to increase its cGMP production a hundredfold. Here I tested whether increasing the NMDA mediated activity in response to sound can be attenuated by co-perfusing either L-MeArg or ODQ with the NMDA.

FRA measures

Characteristic Frequency and threshold attenuation

Previously I showed that the perfusion of NMDA, L-MeArg and ODQ individually have no effect on the CF (Figure 4-14A) or threshold attenuation at CF (Figure 4-14B). The combination of either NO modulator with NMDA also failed to significantly alter CF and threshold of the multi-unit activity at CF.

Spontaneous activity

The perfusion of 100 µM NMDA in the IC increased the spontaneous firing rate (see section 4.4.2) this effect was blocked by the co-perfusion of either L-MeArg or ODQ as depicted in Figure 4-14C. The two way ANOVA showed a significant interaction term ($F(4,12) = 4.452$, $p < 0.020$). The one way between groups ANOVAs showed that the groups did not statistically differ from each other during the aCSF baseline or the washout condition, but they did differ significantly in the NMDA (alone or +L-MeArg/ODQ) condition ($F(2,6) = 14.793$, $p < 0.005$). Post hoc tests showed that the NMDA (alone) group had a higher spontaneous firing rate than either the NMDA + L-MeArg group (2.15 ± 0.221) or the NMDA + ODQ group (1.95 ± 0.221). The NMDA+L-MeArg and NMDA+ODQ groups did not differ significantly from each other.

PSTH measures

An example of the PSTH data recorded in the NMDA+L-MeArg protocol is shown in Figure 4-13. This figure shows the baseline recording, a 20 minute perfusion of 100 µM NMDA, 20 minute perfusion of L-MeArg followed by 20 minutes of L-MeArg and NMDA, interspersed with aCSF washout conditions.

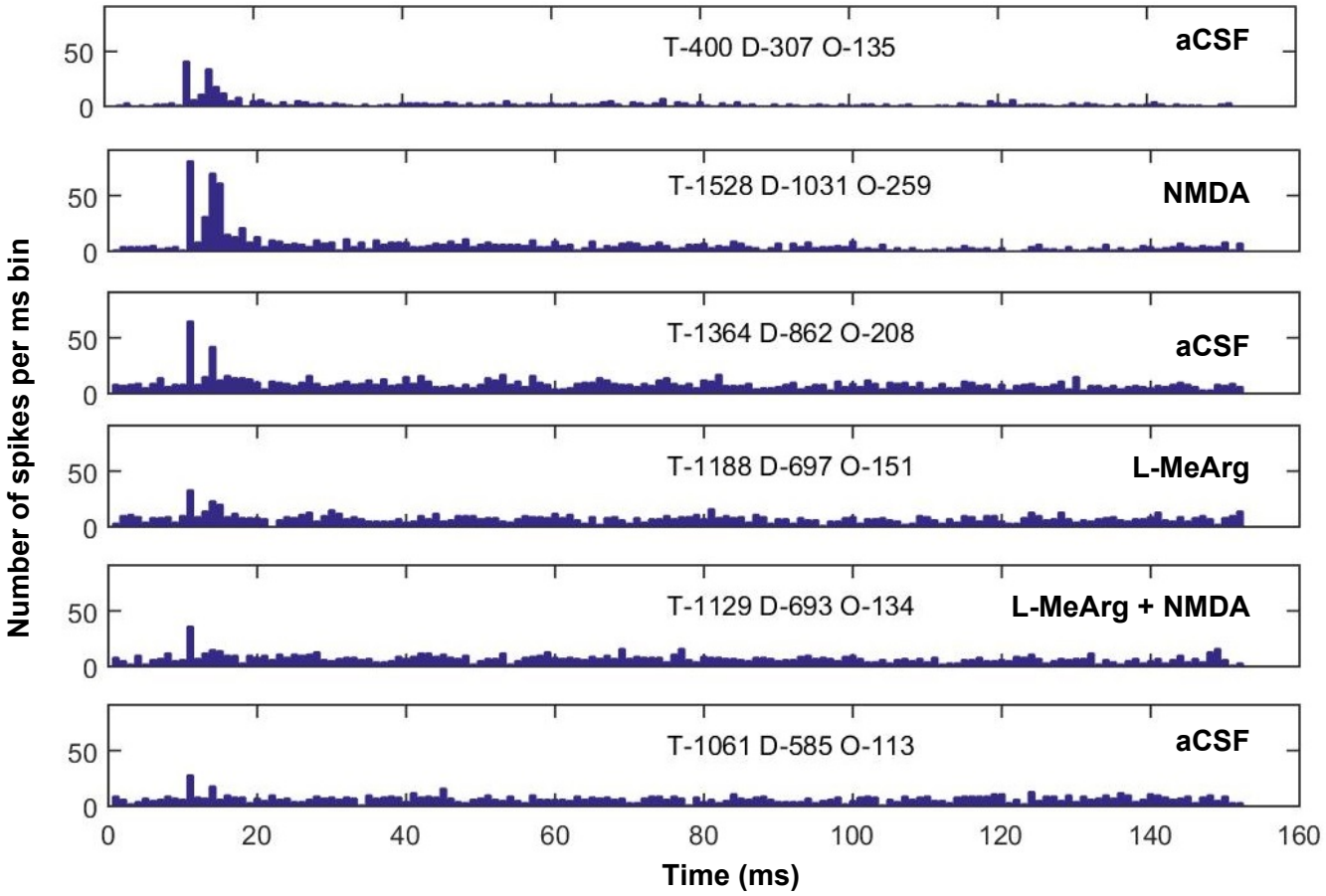

Figure 4-13 PSTH data for the aCSF baseline, 100 µM NMDA, aCSF washout, 500 µM L-MeArg, 500 µM L-MeArg + 100 µM NMDA and the aCSF washout condition. T stands for the total number of spikes, D for the driven number of spikes and O for the number of spikes in the onset peak.

Total driven activity

The perfusion of 100 µM NMDA in the IC increased the total driven activity (see section 4.4.2). This increase in total driven activity was blocked when either L-MeArg or ODQ were co-perfused with the NMDA, as depicted in Figure 4-14D. The two way ANOVA showed a significant interaction term ($F(4,12) = 7.751$, $p < 0.003$). The one way between groups ANOVAs showed that the groups did not differ during the baseline or washout conditions, but during the NMDA (alone or +L-MeArg/ODQ) condition there was a significant difference between the groups ($F(2,6) = 14.126$, $p < 0.005$). Post-hoc tests showed that the NMDA (aCSF) group had a greater total driven response than either the NMDA + L-MeArg group (2.09 ± 0.233) or the NMDA + ODQ group (2.05 ± 0.233). The NMDA+L-MeArg and NMDA+ODQ groups did not differ significantly from each other.

To examine whether the observed effect could be observed in the different parts of the PSTH, the activity in the first 10 ms of the onset peak (Onset activity) and a 10 ms block during the sustained response were examined.

Onset response

Previously the local perfusion of NMDA in the IC increased the onset response. There was no such increase when the NMDA was co-perfused with either L-MeArg or ODQ ($F(4,12) = 5.397$, $p < 0.010$) (Figure 4-14E). The one way between groups ANOVAs showed that groups did not differ during the aCSF baseline and washout condition but the groups proved to be different from each other in the NMDA (alone or +L-MeArg/ODQ) block ($F(2,6) = 9.863$, $p < 0.013$). In this condition, the NMDA (alone) group had a significantly greater onset peak compared to the NMDA+L-MeArg group (2.05 ± 0.27) and the NMDA + ODQ group (2.06 ± 0.25). The NMDA+L-MeArg and NMDA+ODQ groups did not differ significantly from each other.

Sustained driven activity

The direct perfusion of 100 µM NMDA into the IC also increased the sustained activity (see section 4.4.2). However, when the NMDA was co-perfused with either L-MeArg or ODQ, there was no increase-sustained activity. A two way ANOVA showed a significant interaction term ($F(4,12) = 4.727$, $p = 0.016$) (Figure 4-14F). One way between groups ANOVAs showed that the three groups did not differ significantly during the aCSF baseline or washout condition but in the NMDA (alone +L-MeArg/ODQ) condition the groups differed significantly ($F(2,6) = 6.779$, $p = 0.029$). Post hoc tests revealed that the NMDA (alone) group had a greater sustained response than either the NMDA + L-MeArg group (2.55 ± 0.484) or the NMDA + ODQ group (2.535 ± 0.484). The NMDA+L-MeArg and NMDA+ODQ groups did not differ significantly from each other.

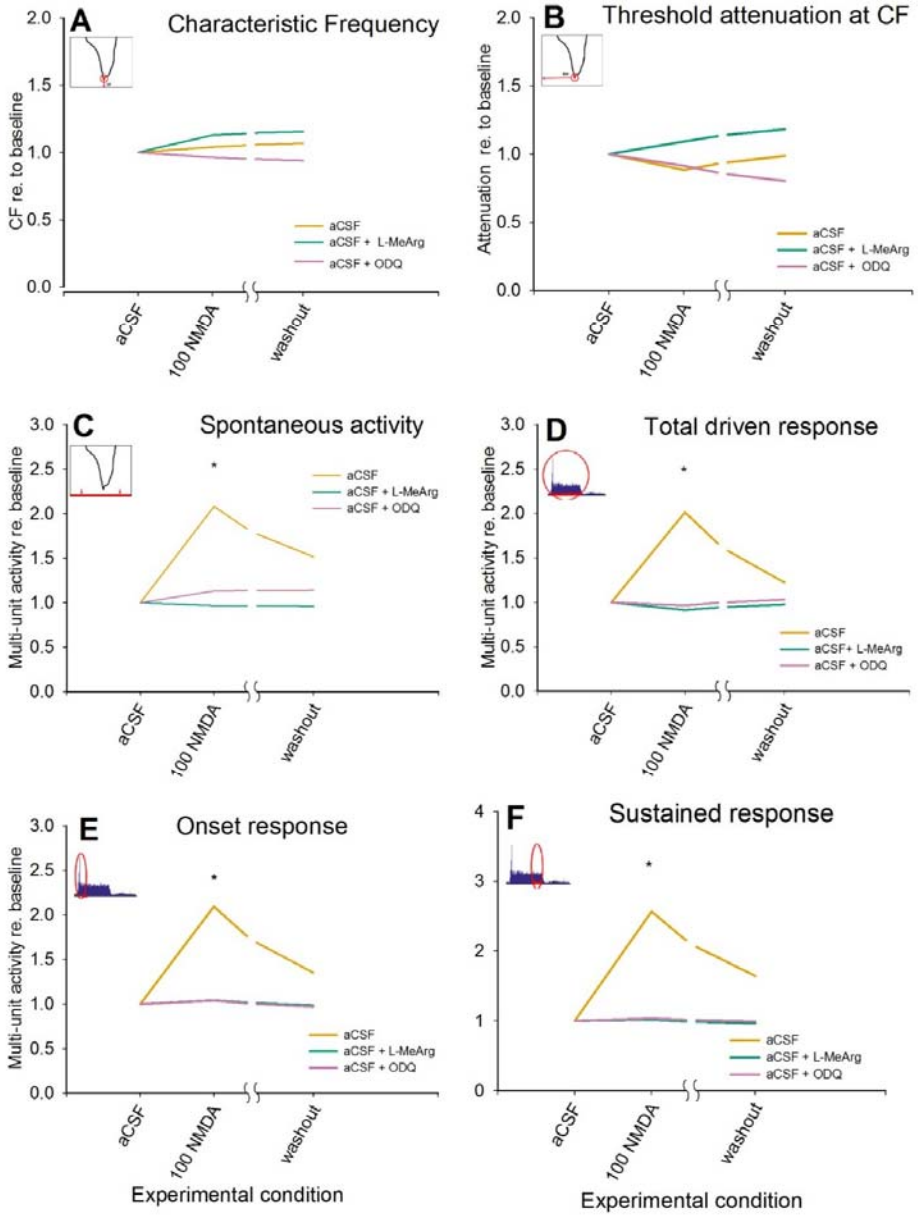

Figure 4-14 Interaction effects between NMDA and the NO modulators L-MeArg and ODQ on neuronal firing in the IC, activity recorded on electrode recording multi-unit clusters responding best to stimulation of 1024 Hz. Note that the lines represent groups means, aCSF n=3, L-MeArg n=3 and ODQ n=3. A. CF B. Threshold attenuation at CF C. Spontaneous activity D. PSTH total activity E. PSTH total sound driven activity F. PSTH Onset activity. Note the break in the x-axis to indicate the difference between washout conditions between the experiments (Figure 4-1). Significant post hoc contrasts between groups are indicated by *.

In addition to the between groups analysis, the data from the L-MeArg and ODQ experiments was subject to a one way within groups ANOVA such that the effect of the initial perfusion of NMDA alone could be compared with the effect of the perfusion of NMDA plus L-MeArg/ODQ.

Entering all the drug conditions from the L-MeArg experimental protocol (Figure 4-1B) and running a series of one-way within subjects ANOVA's for the spontaneous, total driven, onset and sustained response shows how neuronal activity changed over time under the different local perfusion conditions (Figure 4-15).

L-MeArg: spontaneous activity

A one-way within group ANOVA showed that spontaneous activity varied significantly between the different drug conditions ($F(5,10)=12.02$, $p < 0.001$) (Figure 4-15A). Post hoc tests showed that the local perfusion of NMDA (20 minutes) increased the spontaneous activity (2.78 ± 0.39 (3)). Spontaneous activity during the NMDA + L-MeArg (20 minutes) condition was not significantly increased compared to the aCSF washout and the L-MeArg block preceding it. Spontaneous activity did not significantly decrease during the aCSF washout condition (45 minutes).

L-MeArg: driven activity

Driven activity increased during NMDA and reduced again during washout. However there was no increase when NMDA was perfused with L-MeArg. A one-way within group ANOVA showed that total driven activity changed significantly between the different drug conditions ($F(5,10)=13.038$, $p < 0.001$) (Figure 4-15B). Post hoc tests showed that the local perfusion of NMDA (20 minutes) increased the total driven activity (1.66 ± 0.20 (3)). Total driven activity was significantly decreased during the aCSF washout condition (45 minutes) (-1.80 ± 0.21 (3)). The total driven activity during NMDA + L-MeArg (20 minutes) did not show a significant increase compared to that during the aCSF washout and the L-MeArg block preceding it.

L-MeArg: onset activity

A one-way within group ANOVA showed that the onset activity changed significantly between the different drug conditions ($F(5,10)= 9.185, p < 0.002$) (Figure 4-15C). Post hoc tests showed that the local perfusion of NMDA (20 minutes) increased the onset activity (1.92 ± 0.22 (3)) and this was significantly decreased during the aCSF washout condition (45 minutes) (-1.91 ± 0.39 (3)). However, there was no significant increase in onset activity during perfusion of NMDA + L-MeArg (20 minutes) compared to that during the aCSF washout and the L-MeArg block preceding it.

L-MeArg: sustained activity

A one-way within group ANOVA showed that the sustained activity changed significantly between the different drug conditions ($F(5,10)= 3.955, p < 0.031$)(Figure 4-15D). Post hoc tests showed that the local perfusion of NMDA (20 minutes) increased the sustained activity (1.90 ± 0.14), this was not significantly decreased during the aCSF washout condition (45 minutes). There was no significant increase in onset activity during perfusion of NMDA + L-MeArg (20 minutes) compared to that during the aCSF washout and the L-MeArg block preceding it.

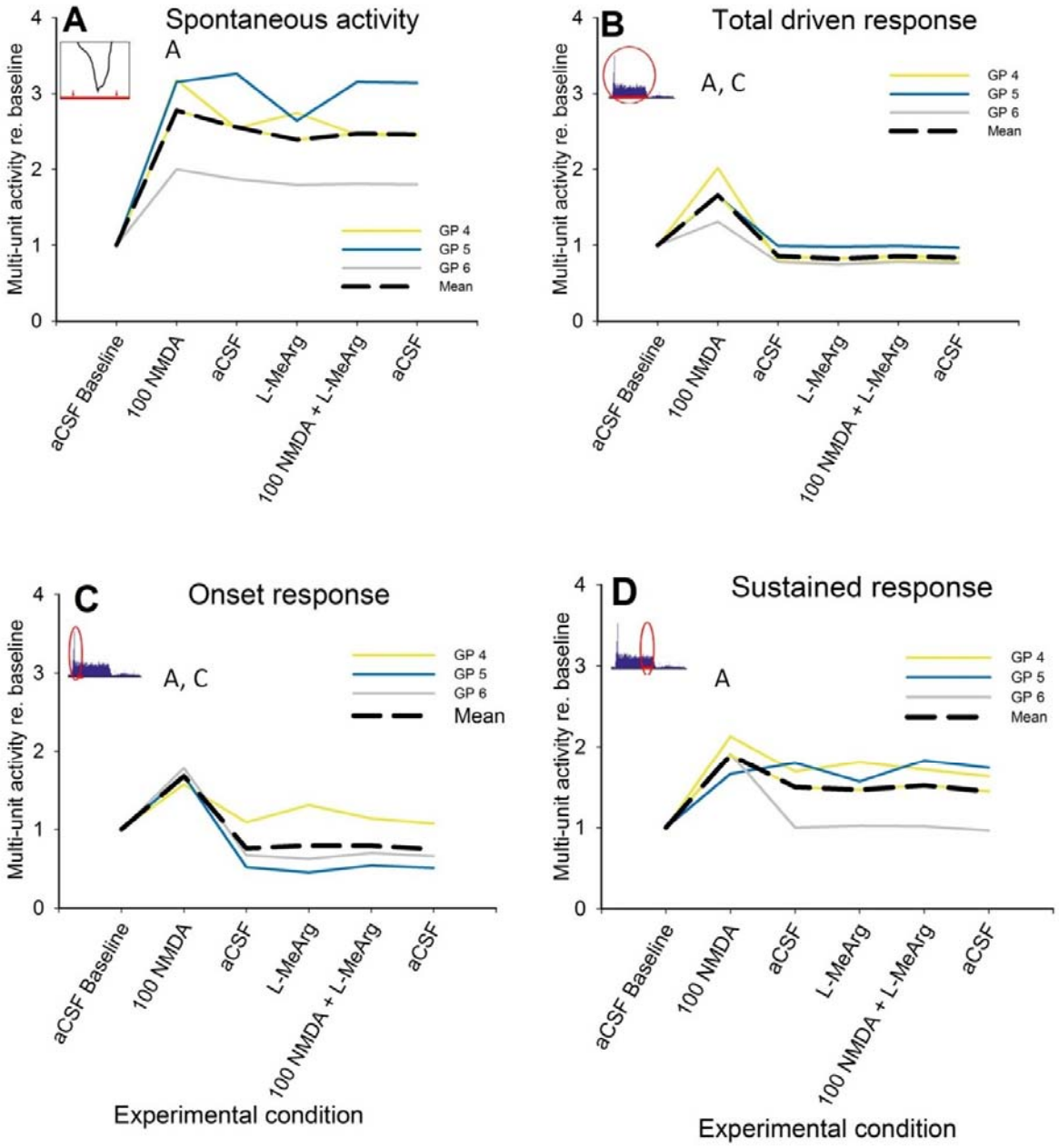

Figure 4-15 neuronal responses in the IC under different local drug perfusion conditions. Each experiment starts off with aCSF, followed by 100 µM NMDA, a washout, L-MeArg, NMDA+L-MeArg and another aCSF washout. The individual data points are given per animal plus the mean across animals in the dashed black line. A. Spontaneous activity. B. PSTH total sound driven activity C. PSTH onset activity. D. PSTH sustained driven response. Significant post hoc contrasts p<0.05 are indicated by A) vs original baseline, B) vs preceding aCSF block, C) vs following aCSF block.

Entering all the drug conditions from the ODQ experimental protocol (Figure 4-1C) and running a series of one-way within subjects ANOVA's on the spontaneous, total driven, onset and sustained response shows how neuronal activity changed over time under the different perfusion conditions (Figure 4-16).

ODQ: spontaneous activity

Spontaneous activity differed significantly between the different drug conditions ($F(5,10)=8.041$, $p < 0.003$)(Figure 4-16A). Post hoc tests showed that the local perfusion of NMDA (20 minutes) increased the spontaneous activity (2.56 ± 0.49 (3)). No significant decrease in the spontaneous activity was observed during the aCSF washout condition (45 minutes). However, no significant increase in spontaneous activity was observed during the perfusion of NMDA + ODQ (20 minutes) compared to the aCSF washout block preceding it.

ODQ: driven activity

Total driven activity changed significantly between the different drug conditions ($F(5,10)=4.703$, $p < 0.018$)(Figure 4-16B). Post hoc tests showed that the local perfusion of NMDA (20 minutes) increased the total driven activity (1.91 ± 0.39). The total driven activity significantly decreased during the aCSF washout condition (45 minutes) (-1.75 ± 0.36). There was no increase in total driven activity in response to the perfusion of NMDA + ODQ (20 minutes) compared to the aCSF washout and the ODQ block preceding it.

ODQ: onset activity

The onset activity changed significantly between the different drug conditions ($F(5,10)= 12.146$,$p <0.001$)(Figure 4-16C). Post hoc tests showed that the local perfusion of NMDA (20 minutes) increased the onset activity (1.79 ± 0.21 (3)). The onset activity was significantly decreased (-1.76 ± 0.19 (3)) during the aCSF washout condition (45 minutes). The perfusion of NMDA + ODQ (20 minutes) did not show a significant increase in onset activity compared to the aCSF washout and the ODQ block preceding it.

ODQ: sustained activity

The sustained activity changed significantly between the different drug conditions ($F(5,10)= 5.733$, $p < 0.009$)(Figure 4-16D). Post hoc tests showed that the local perfusion of NMDA (20 minutes) increased the sustained activity (2.03 ± 0.28). No significant decrease in the sustained activity was observed during the aCSF washout condition (45 minutes). However,

no significant increase was observed in the sustained activity during the perfusion of NMDA + ODQ (20 minutes) compared to the aCSF washout and the ODQ block preceding it.

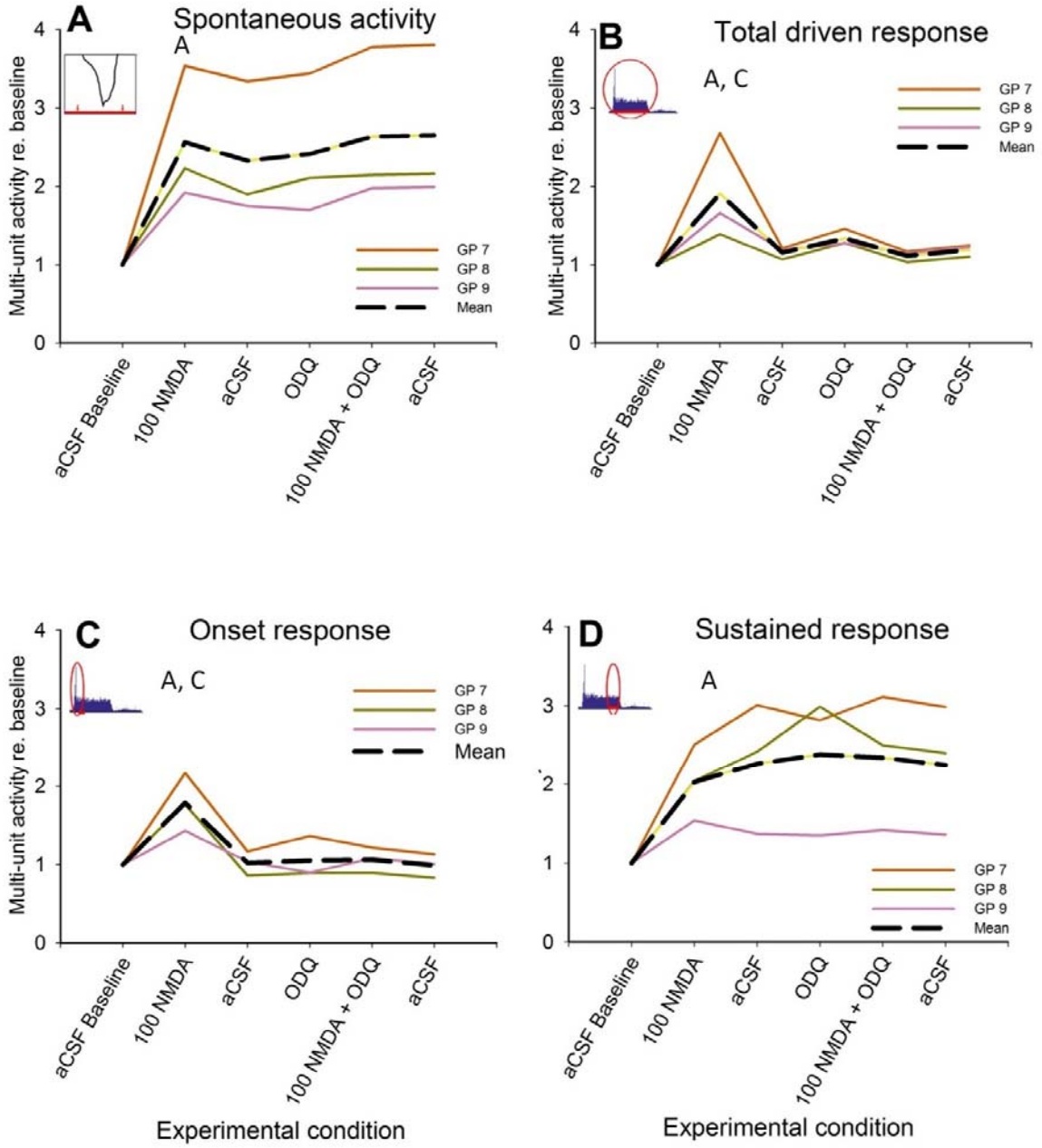

Figure 4-16 neuronal responses in the IC under different local drug perfusion conditions. Each experiment starts off with aCSF, followed by 100 µM NMDA, a washout, L-ODQ, NMDA+ODQ and another aCSF washout. The individual data points are given per animal plus the mean across animals in the dashed black line. A. Spontaneous activity. B. PSTH total sound driven activity C. PSTH onset activity. D. PSTH sustained driven response. Significant post hoc contrasts p<0.05 are indicated by A) vs original baseline, B) vs preceding aCSF block, C) vs following aCSF block.

4.5 Discussion

The immunohistochemistry observations described in chapter 3 showed that nNOS is present in the central nucleus and associates with PSD95 and glutamatergic terminals suggesting that the functions of glutamate, NMDA receptor and NO are mechanistically linked in the central nucleus. The experiments presented here sought to i) determine the role of NMDA receptor mediated transmission in the central nucleus of the IC, ii) determine whether there is tonic NO transmission participating in auditory processing and iii) whether the effects of NMDA receptor activation are mediated wholly or in part by NO and, if so, via what intracellular mechanism.

The data presented in the current chapter revealed new knowledge about the role of NMDA receptor mediated activity and NO signalling in auditory processing. NMDA mimics the effect of endogenous glutamate on the NMDA receptor but has no influence on the other glutamate receptors (e.g. AMPA receptors). Therefore the local perfusion of NMDA in the IC via a microdialysis probe provides a unique window on the role the NMDA receptor plays in the processing of auditory stimuli in the IC. It was found that NMDA increases both spontaneous activity and acoustically evoked activity in the IC, and does so in a concentration dependent manner. Remarkably though, the CF and the threshold sensitivity at CF of the multi-unit activity are unaffected by the local perfusion of NMDA in the IC. The local perfusion of the NOS blocking agent L-MeArg did not alter spontaneous or acoustically evoked multi-unit activity recorded in the IC, suggesting that there is no tonic NO transmission. Further substantiating this conclusion is the finding that blocking sGC with ODQ did not alter the spontaneous or acoustically evoked multi-unit activity. More importantly though, is the finding that the robust NMDA mediated increase in both spontaneous and acoustically evoked multi-unit activity is abolished by blocking the production of NO by the co-perfusion of L-MeArg, indicating that the effect of NMDA is mediated via NO. The observation that blocking the sGC pathway by co-perfusing ODQ with the NMDA also resulted in the loss of the NMDA response is consistent with the notion that NMDA-stimulated NO transmission is acting through sGC.

The local perfusion of NMDA in the IC proved to produce a robust, reliable and consistent increase in neuronal activity, which could both be observed in the FRA and the PSTH measurements. The FRA gives insights on effects occurring over a range of frequencies and attenuation levels, whereas the PSTH shows which part of the response (spontaneous, onset or sustained) is affected, all of which have potentially different underlying mechanisms.

In the current concentration response experiment, higher concentrations of NMDA evoked increasing responses. The exact amount of NMDA delivered to the tissue via the dialysis probe is unknown, but diffusion of molecules through the membrane is inversely related to the flow rate. As an estimate based on literature with comparable flow rates to that used here, approximately 10-20% of the original concentration will reach the immediate area surrounding of the probe (Chefer *et al.*, 2009). The higher the concentration in the probe, the steeper the concentration gradient will be, higher concentrations will diffuse more quickly. Also concentration in the tissue decreases as a cubic function of distance from the probe (Foeller *et al.*, 2001), making the region influenced uncertain. The lowest NMDA concentration, 30 µM of NMDA, did not result in significant increases, but this was mainly due to variability between the animals. This lowest concentration might be more susceptible to variations in the placement of the dialysis probe relative to the recording electrode. The higher concentrations of NMDA, 100 µM and 300 µM, resulted in increasing magnitudes and a prolonged duration of the observed NMDA effect. The 100 µM NMDA concentration increased both the spontaneous activity and the neuronal response to sound stimulation in the central nucleus, both reached a stable new plateau within 10-15 minutes of switching on the perfusion. Prolonged exposure (45 minutes) did not increase the observed effects, suggesting that the concentration of NMDA had plateaued around the recording electrode.

Stopping the NMDA perfusion and switching it for aCSF did reverse the onset and total driven activity in all animals, but for the spontaneous and sustained activity the washouts were more variable between animals and this is perhaps suggesting that these responses stem from a different underlying mechanism. Increased NMDA receptor activity has been reported to lead to excitotoxicity, due to the receptor's high permeability to calcium (Sattler and Tymianski, 2001) however, both the reversibility of some measures and the observation that increasing concentrations evoked increasing effects without an apparent ceiling suggests that the NMDA concentrations used did not result in excitotoxicity.

Studies employing selective AMPA and NMDA receptor antagonists have revealed that acoustic stimulation evokes neuronal activity in the IC via the glutamatergic stimulation of both AMPA and NMDA receptors (Faingold *et al.*, 1989; Kelly and Zhang, 2002; Ma *et al.*, 2002). AMPA receptors appear to mediate the early (20 ms) but not the sustained (20 – 120 ms) response to acoustic stimuli in most neurons in the IC (Zhang & Kelly, 2001; Ma *et al.*, 2002). However, there is some disagreement about whether NMDA receptors contribute to the onset response or are solely mediators of the sustained response. Thus, two studies reported that blocking NMDA receptors in the central nucleus reduced the sustained response substantially in most cells but had little effect on the onset component

of the response (Zhang & Kelly, 2001; Ma *et al.*, 2002). However, a more recent study found that blocking NMDA receptors consistently decreased the later components of the response but also decreased the onset component in many units (Sanchez *et al.*, 2007).

Patch clamp studies in IC slices have shown that responses to NMDA are voltage dependent (Ma *et al.,* 2001) suggesting that AMPA receptor activation (via acoustic stimulation) might be essential for NMDA receptors to be activated. However, in line with the present data, Faingold showed that NMDA increases both acoustically evoked and spontaneous firing of the majority of neurons in the central nucleus (Faingold *et al.*, 1989). These increases in spontaneous activity observed suggest that either there is tonic activation of IC neurons via AMPA receptors such that they are in a depolarized state where NMDA receptors can be activated, or that there are NMDA receptors present which do not display a voltage dependent Mg^{2+} blockade. In line with the first Faingold, reported that NMDA antagonists decreased spontaneous activity.

Previous research suggests that acoustic stimulation of neurons in the IC activates both AMPA and NMDA receptors for all stimuli above attenuation threshold (Zhang and Kelly, 2001). Blocking AMPA receptors reduced both the early (20 ms) and sustained (20 – 120 ms) response to acoustic stimuli in most neurons in the IC, although, in a subset of neurons, responses were completely blocked (Zhang & Kelly, 2001; Ma *et al.*, 2002). Blocking NMDA receptors in the central nucleus reduced the sustained response substantially (>50% reduction) in at least 75 % of the cells recorded, but showed little effect on the onset component of the response (Zhang and Kelly, 2001; Ma *et al.*, 2002). However, in closer agreement with the current findings is a more recent study applying NMDA antagonists using iontophoresis but sampling a larger number of cells, this study found that blocking NMDA receptors has a variable effect on the onset component but always decreases the later components of the response (Sanchez *et al.*, 2007).

In the current study instead of blocking the NMDA receptors, they were artificially stimulated by the local perfusion of NMDA in the central nucleus. Effects were observed both on spontaneous and acoustically driven activity. Within the acoustically driven activity, increases were observed both on the early and sustained components of the response. Although currently little is known about the NMDA subunit expression in the different regions of the IC, in situ hybridization studies have shown that mRNAs for all known subunits are expressed in the central nucleus (Goebel and Poosch, 1999). The effects of NMDA on the early component of the response observed in the current experiments may be governed by NMDA receptors containing the GluN2D subunit that has a lower affinity

for magnesium under resting state conditions, compared to the other subunits, (Kirson and Yaari, 1996) and has been shown to trigger action potentials without the need for depolarization caused by AMPA receptors (Wenzel *et al.*, 1996; Sivaramakrishnan and Oliver, 2006). By using the microdialysis probe a large amount of NMDA was present throughout the central nucleus of the IC affecting not just one single cell but the entire population, including both glutamatergic and GABAergic cells. This could have shifted the normal excitatory/inhibitory balance, which may account for the finding that the biggest change occurred on the onset peak. Also, the NMDA perfusion lasted much longer than the iontophoretic studies, the changes observed here could be due to the enduring presence of NMDA triggering synaptic changes. The later experiments blocking the production of NO and blocking the sGC signalling pathway do suggest that the NO-sGC signalling pathway is underlying the increase in activity. The NO signalling pathway has been shown to be involved with altering the available receptors.

It was of note that the spontaneous activity and sustained part of the acoustically evoked responses did not return to baseline after being enhanced by NMDA, whereas both the onset and total driven response do. Firstly, this suggests that the total driven activity is dominated by the onset response. Moreover, it suggests that the sustained response, which is lower compared to the onset response may be more susceptible to changes in spontaneous firing. The observation that higher doses of NMDA show more robust significantly statistical washout effects support this interpretation. Both types of activity increased to the same extent in relative terms. But in real numbers, the acoustic driven response saw a much larger increase. Spontaneous rates in a given time window increased from 10-15 spikes to 30-45 spikes, while acoustically evoked spikes in the same time window increased from 200 to 600 spikes on average. The sustained response has fewer spikes compared to the onset response, and the number of spontaneous spikes occurring in this time window will affect this part of the response more than the onset part. Higher concentrations of NMDA increased the onset response dramatically and can, therefore, be more easily washed out and detected with N =3.

The fact that (onset) acoustically driven activity returned to baseline whereas the spontaneous did not, suggests that a different mechanism is operating. One possibility is that the persistent increase in spontaneous activity observed may be related to changed synaptic strength which propagates higher spontaneous activity.

The fact that all PSTH measures reported here increased in response to NMDA is a finding that requires further investigation. The question that needs addressing is whether the

spontaneous activity is raised to such an extent that the driven activity rides on top of it. As mentioned above, GluN2D subunits have been shown to be less prone to the voltage dependent magnesium blockade and may impact on the increase in spontaneous activity and early response components. A way of investigating whether this is the case is to use a selective antagonist for this specific subunit together with local NMDA perfusion. Another possible experiment to investigate the Mg2+ dependence of the NMDA receptors in the central nucleus is perfusing NMDA in a Mg2+ free aCSF.

As noted above, local perfusion of NMDA evoked a robust increase in both spontaneous and acoustically evoked neuronal activity. Co-perfusion of L-MeArg with the NMDA completely abolished the NMDA evoked increase. This was evident in a within group as well as a between group analysis. L-MeArg is a non-selective NOS blocker, it functions by competing with L-arginine for binding sites on the NOS protein. L-MeArg cannot be converted to L-citrulline and hence stops the production of NO during the time it is bound to the NOS protein.

Although the concentration of L-MeArg in the brain tissue in the present experiments is unknown, we can assume the concentration outside the probe is around 10% of that in the probe (i.e. 100 µM). Thus, it is likely that this will result in complete inhibition of L-arginine binding to nNOS and hence complete inhibition of NO production. Although the concentration response relationship was not explored here, it seems likely that even lower concentrations would completely block nNOS. Importantly, a slice study investigating direct effects of L-MeArg on neuronal tissue concluded that perfusion of 100 µM L-MeArg significantly reduces the amount of NO produced in the brain in response to NMDA receptor mediated activity (Kendrick *et al.*, 1996). These data also suggest that NMDA receptor mediated glutamate transmission in the central nucleus of the IC is NO dependent.

In the current experiments co-perfusion with ODQ also prevented the NMDA evoked increase in neuronal activity. This finding not only strengthens but extends the L-MeArg findings. ODQ is a small bioactive molecule that competitively binds to the haem domain of sGC - the main downstream target of NO. ODQ prevents the binding of NO and thus stops sGC from undergoing a conformational change that switches on cGMP production. Here ODQ was perfused at a concentration of 500 µM. Schrammel and colleagues showed substantive blockade of sGC by ODQ in the micromolar range suggesting the concentration used here would cause complete inhibition of sGC. Even though NO has the capacity to regulate a whole host of other processes, this finding clearly demonstrates that the NO

dependency of the NMDA receptor mediated glutamate activity is mediated via NO acting on sGC.

Although the effects of NMDA perfusion on both spontaneous and sound driven activity were blocked by L-MeArg and by ODQ, in the current study blocking the production of NO or sGC in the absence of NMDA had no discernible effect on neuronal activity in the IC. This suggests that under normal circumstances, tonic NO levels are not involved in driving the spontaneous or acoustically evoked activity in the central nucleus. Although it is possible that changes in neuronal activity were present but were too subtle to observe with three animals.

NMDA receptor activation has been shown to regulate the surface AMPA receptors and can reduce the number of AMPA receptors during acute noise trauma which has been linked to an increased and faster recovery (Chen et al., 2007). The mechanism via which NMDA receptor activity alters the number of AMPA receptors and the future response is likely to be NO signalling acting on sGC. Evidence has been reported demonstrating that under normal condition low levels of NO bind to the haem of sGC which keeps the protein in a low activity state (Hopper & Garthwaite, 2006; Salerno, 2008; Salerno & Ghosh, 2009), presumably maintaining a homeostasis in synaptic strength. Increases in NO concentrations have been shown to bind to a second site on sGC amplifying its production of cGMP a hundredfold (Cary et al., 2006), presumably leading to adaptations of synaptic strength by altering available receptors. A mechanism allowing quick alteration of the synaptic strength would be beneficial in the auditory system that constantly has to scale its responses to an ever changing acoustic environment. Thus glutamate signals transduced by NMDA receptors lead to an increase in NO that is sensed by sGC which in turn produces cGMP which can lead to an increase or decreased future response due to its involvement in trafficking of AMPA and NMDA receptors.

Apart from the concentration response experiments, all experiments started with a 100 µM NMDA perfusion. Doing this allowed me to check for proper dialysis probe and electrode placement within the IC and gave N=9 for the 100 µM NMDA condition, resulting in a greater statistical power. However, manipulating the neuronal activity in the IC with NMDA prior to the perfusion of L-MeArg and ODQ, may have altered the state of the system and no ‘pure’ L-MeArg or ODQ measurements were obtained, limiting the observations made on the spontaneous activity. However, this is unlikely to have affected the acoustically evoked response because the effects there washed out during prolonged aCSF perfusion. The current protocol was chosen because it allowed every animal to serve as its own control

and reduce variance in measurements. Improper dialysis probe placement or a faulty probe would have been detected by the lack of a NMDA effect.

Very few studies have investigated NO signalling in a functional context. But the studies that have, consistently show, as did the current study, that there is a relationship between the NMDA receptor activity, NO production, and sGC. Although no studies directly investigating the function of NO in auditory processing have been performed, scientists investigating flight reactions in rats perfused exogenous NO in the central nucleus which resulted in an increase in flight behaviours in the animals (De Araújo Moreira *et al.*, 2003) thus showing that exogenous NO can influence activity in the central nucleus.

The FRAs in the current study showed that NMDA-induced increases in neuronal activity were not limited to the CF of the multi-unit activity but were part of an increase in activity across a wide range of attenuation levels and frequencies. The FRA analysis revealed no changes of CF or threshold sensitivity at CF nor any other morphological changes in the FRA. The lack of systematic findings in the FRA analysis in the dose response experiment could be due to the number of animals included. However, the subsequent analysis of 100 µM NMDA, which included nine animals, also failed to find any systematic effects. With N=3 effects can be missed but with N=9 this scenario seems less likely, especially in experiments with experimental animals that are closely genetically related and live under similar circumstances. However, the FRA analysis only allowed areas of changed activity containing at least five pixels in the analysis, this, however, could have led to the exclusion of quite a few changed single pixels. Another measure that could have been valuable but was not performed here would be calculating the total number of changed pixels, and possibly relating this to the side of the CF on which they occur. However, the CF does not usually fall in the middle of the frequency range and observations here would need to be corrected for the number of available pixels on either side of the CF.

Sound duration appears to be encoded in the IC by clusters of spikes around the onset and offset of a neuron's response to auditory stimuli instead of being coded by the entire spike activity (Yin *et al.*, 2008). This phenomenon is mainly observed in neurons that show duration sensitivity and appears to be driven by GABA dampening the AMPA driven response (Yin *et al.*, 2008). In the current experiments occasionally changes in offset activity were observed in response to L-MeArg and or ODQ perfusion in the IC. These findings were, however, rare and may depend on finding the duration sensitive neurons which appear to be rare and weaker in their response in non-echo locating animals. Studies in echo-locating animals have reported 30-60% of the cells in the central nucleus of the IC

to be duration sensitive while in guinea pigs this number is below 20% (Wang *et al.*, 2006; Yin *et al.*, 2008). However collecting more examples of these neurons and studying the effects of NO modulators could provide us with new interesting insights. The influence of both NO modulators on off-set responses again suggests the involvement of NO in altering the synaptic strength.

The current findings do support a role for NO signalling in the local circuitry of the IC. The finding that blocking NO production with L-MeArg or blocking its binding to sGC prevents the otherwise robust increase in neuronal activity in response to the perfusion of NMDA, clearly illustrates that NMDA receptor mediated glutamate activity in the IC is dependent on NO acting via sGC. The subsequent influence of cGMP on the trafficking of AMPA and NMDA receptors would explain the observed phenomena. Although, this aspect of the mechanism remains to be investigated. These findings strengthen the conclusion from the immunohistochemistry chapter that the nNOS observed in the central nucleus is indeed nNOSα and depending on the NMDA receptor activity. The current study is the first to show functional evidence of NO signalling in auditory processing in the IC in an in vivo setting.

Chapter 5. Salicylate Mediated Activity in the IC

5.1 Introduction

Chapter 3 focussed on the localisation of NOS in the IC, explored the neurotransmitter phenotype of cells that express NOS and examined the co-localisation of neurons expressing nNOS with other proteins. Evidence was presented that nNOS is present in the central nucleus. The nNOS puncta in the central nucleus are likely a part of the nNOS-PSD95-NMDA receptor complex, hence in Chapter 4, I focussed on the functional role NMDA receptors and nNOS have in auditory processing in the IC. NMDA receptor activation was shown to increase spontaneous and sound-driven activity and to do so via a mechanism involving NO and sGC.

Salicylate used therapeutically at high doses has long been known to induce the side effect of tinnitus in humans. Evidence from behavioural studies indicates that salicylate reliably and consistently induces tinnitus in rodents (Evans *et al.*, 1981; Jastreboff and Sasaki, 1986; Jastreboff *et al.*, 1988) and, although its mode of action probably differs from that of noise trauma in some respects, in other respects they would be expected to share a common mechanism. Both noise induced and salicylate induced tinnitus are associated with increased NMDA receptor mediated activity in the auditory pathway (Peng *et al.*, 2003; Ruel *et al.*, 2008; Bing *et al.*, 2015).

Studies have shown that systemic application of salicylate may impact directly on both peripheral and central auditory structures. Systemic salicylate administration causes an increase of the spontaneous activity (neuronal discharge in the absence of any auditory stimulation), throughout the auditory pathway (Guitton *et al.*, 2003; Ma *et al.*, 2006; Hwang *et al.*, 2011), including in the IC (Jastreboff and Sasaki, 1986). Given the myriad ascending and descending connections of the IC, this hyperactivity could be generated in one or more of several locations in the auditory pathway and be transmitted to the IC. However, it has been reported that direct application of salicylate to the IC in vitro increases the firing activity of the majority of neurones in the central nucleus of the IC (Basta and Ernst, 2004; Patel and Zhang, 2014) Patel and Zhang also showed direct effects of salicylate in the IC in vivo although they recorded only in the dorsal cortex of the IC.

Salicylate has a wide range of effects on many physiological processes (Jastreboff and Sasaki, 1986; Jastreboff *et al.*, 1988; Vane and Botting, 2003. The issue with systemically applied salicylate in experiments reported thus far is that the salicylate potentially affects the entire physiology including the auditory brainstem pathway of the animal and

determining the origin of its effect has been problematic. Also, findings reported thus far are based on recordings from a selection of individual cells before salicylate and a new group of individual cells after systemic salicylate treatment. Usually there is a gap between the administration and the second set of recordings of at least two or three hours because behavioural animal models have shown that this is the time it takes for salicylate to induce tinnitus(Jastreboff, 1994). The advantage of the multiunit approach used in these experiments is that the same cluster of units is recorded throughout the whole experiment. No recordings of changes in neuronal activity in the IC during this period are currently available, the fact that an increase in spontaneous activity is the end result three hours after systemic salicylate treatment means we cannot see how these effects develop. Changes are likely to occur over time and the onset and time course of these effects could be telling in determining how it affects the auditory pathway. Salicylate uptake rates differ between tissues and the uptake into the brain is especially slow due to salicylate having a low lipid solubility at physiological pH levels which hinders its crossing of the blood brain barrier (Bannwarth *et al.*, 1986). The strong binding of salicylate to the protein albumin is another rate limiting factor for salicylate reaching the brain (Reed and Palmisano, 1975; Jastreboff *et al.*, 1986). Together these factors result in a half-life permeation from plasma levels to cerebrospinal fluid of about two hours in rats (Brodie *et al.*, 1960). During this time, however, salicylate is already affecting the lowest levels of the auditory pathway. Evidence has been found for the stiffening of the outer hair cells, mechano-sensory changes in the cochlea (Cazals, 2000), a loss of absolute sensitivity of the auditory nerve and immediate effects on the NMDA receptors of the cochlea (Guitton *et al.*, 2003).

Studies suggest that both noise-induced and salicylate-induced tinnitus are associated with increased NMDA receptor mediated activity in the auditory pathway (Peng *et al.*, 2003; Ruel *et al.*, 2008) (Bing *et al.*, 2015). Thus, Ruel showed that salicylate-induced increases in spontaneous firing and sound driven responses in auditory nerve fibres were abolished by co-perfusion of the non-competitive NMDA receptor antagonist, MK-801 (Ruel *et al.*, 2008). Abnormalities have been observed in NMDA receptor mediated signalling in animal models of tinnitus at several sites along the auditory pathway (Guitton *et al.*, 2003; Ruel *et al.*, 2008; Hwang *et al.*, 2011). As demonstrated in the previous chapter and by others, NMDA receptors are important mediators of certain aspects of auditory processing in the IC. Thus salicylate induced changes in NMDA receptor mediated signalling in the IC could impact on neuronal activity and might underlie the percept of tinnitus. The connection between the NMDA receptor activity and nNOSα makes NO signalling a viable candidate to be involved in the generation of tinnitus.

The questions to be addressed here are, does salicylate affect spontaneous and/or sound driven neuronal activity in the central nucleus of the IC in vivo, and if so, is the effect mediated locally or indirectly, and does the mechanism involve the NMDA/NO pathway?

Thus in order to extend previous reports that systemic administered salicylate induces increases in spontaneous activity in the IC and study the time course of these effects during the build-up of salicylate concentrations, the first experiment partly replicates previous experiments in which single cell electrophysiological recordings were obtained before and after the administration of a high dose (200 mg/kg) of salicylate via a single systemic injection.

Direct application of salicylate in the IC has been limited to iontophoretic studies, which allow direct application of salicylate on a single cell. In Chapter 4 a microdialysis probe was successfully used to deliver NMDA to the IC, this method allows us to study the effects of drugs on larger neuronal populations over the course of many hours. Thus a second experiment was designed, in which a microdialysis probe was used to deliver salicylate directly into the central nucleus of the IC. The observations made in these recordings will be directly compared with those in which salicylate was administered systemically. In both sets of experiments the electrode remained in place throughout the experiment and the multi-unit activity from the same location was followed before and after the salicylate administration.

5.2 Methods

5.2.1 Experimental Procedure

Two different experimental modes of salicylate delivery were employed to study the effects of salicylate on auditory processing in the IC. In the first set of experiments salicylate was given in a single IP injection. In the second set of experiments salicylate was perfused locally into the central nucleus of the IC using a microdialysis probe. All animals were subjected to the same anaesthetic and surgical procedures, including the insertion of the microdialysis probe as described in Chapter 2. During pilot experiments it became apparent that some guinea pigs are sensitive to a large dose of salicylate and stop breathing in response to it. To avoid complications and premature death, the animals were artificially respired with 100% medical oxygen. For all experiments, electrophysiological recordings were obtained at baseline level in the absence of drug with aCSF flowing through the dialysis probe at the standard speed of 2μL/min. As in previous experiments the recordings were collected for the PSTH and FRA stimulus sets, as described in Chapter 2. To ensure

stable and consistent recordings baseline recordings were collected for at least an hour after insertion of the electrode in the IC. Data was collected continually throughout the day, but for the analysis blocks spaced an hour apart were extracted.

Systemic administration of salicylate

In the systemic salicylate experiment seven pigmented guinea pigs (two male) were used. To allow comparisons with previous and future microdialysis experiments, dialysis probes were implanted and aCSF was perfused during the experiment. A graphic representation of the experimental protocol is shown in Figure 5-1. After the baseline hour, the animals received a single IP injection of sodium salicylate (200 mg/kg at 4ml/kg in 0.1 M PBS). Electrophysiological recordings were continually collected from this time for up to seven hours (n=4), after which the experiment was terminated. In four out of the seven experiments aCSF was perfused throughout the entire experiment, while in the other three, L-MeArg (1000 µM) in aCSF was perfused from the end of hour 3 until the end of the experiment at hour 6.

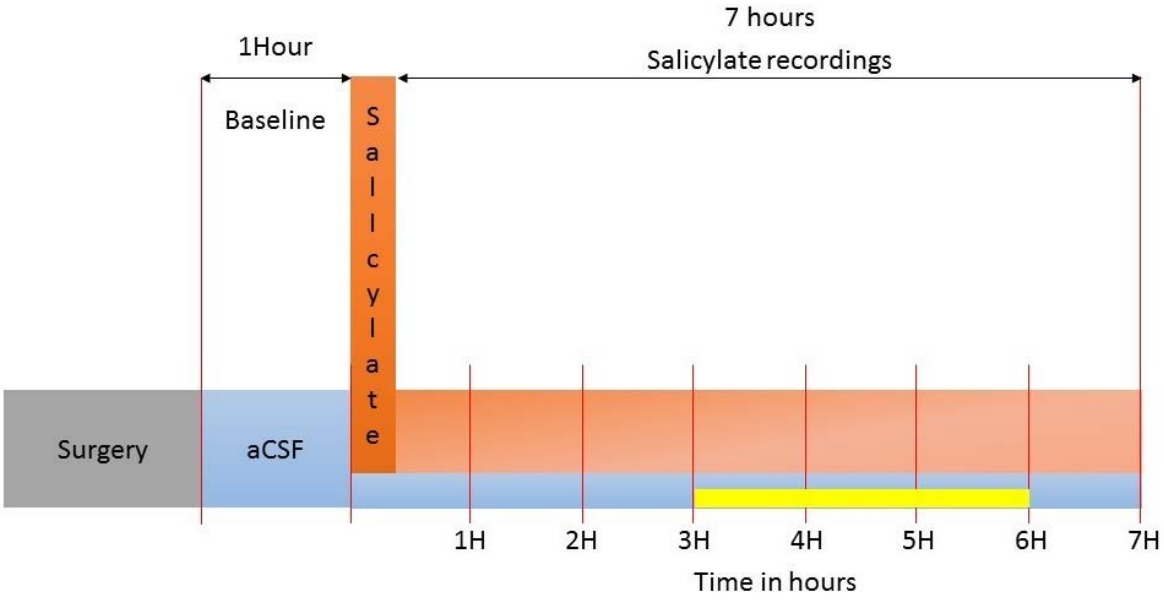

Figure 5-1 Experimental protocol for the salicylate IP experiments. The red lines mark key time points in the experiment. The initial baseline block in blue is followed by the salicylate injection, from that point onwards the short red lines mark the hours post salicylate and are the points included in the data analysis. The blue line indicates the constant flow of aCSF through the dialysis probe (n=4). The other three animals were additionally perfused with L-MeArg (1000 µM) via the probe between hour 3 and 6 as indicated by the yellow bar (n=3).

Local administration of salicylate via microdialysis probe

In the protocol for the local administration of salicylate three pigmented guinea pigs (all female) were used. In Figure 5-2 the experimental protocol is depicted. After baseline recordings, the perfusion was switched from aCSF to 0.1 mM sodium salicylate in aCSF for

two hours. The salicylate concentration was then increased to 1 mM for two hours followed by a further increase to 10 mM for another hour. After five hours of salicylate dialysis at these concentrations, the perfusion was switched to 10mM salicylate plus 1mM L-MeArg. PSTH and FRA recordings were obtained continually throughout the experiment.

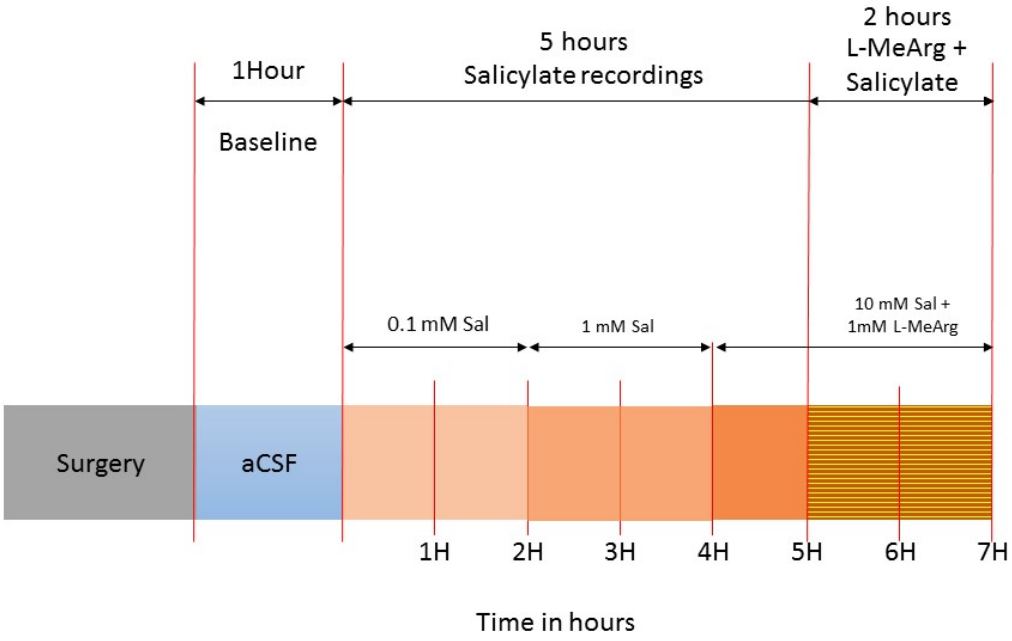

Figure 5-2 Experimental protocol for the local administration of salicylate (Sal) via a microdialysis probe. The red lines mark key time points in the experiment, included in the data analysis. In the baseline condition aCSF was perfused via the probe. After the initial baseline recordings, increasing concentrations of salicylate were perfused through the probe, as shown by the orange gradient. After five hours salicylate (10 mM) and L-MeArg (1 mM) was perfused as indicated by the orange yellow stripes

5.2.2 Data Analysis

Data was extracted for five electrodes along the tonotopic axis each representing the best response at the following frequencies, 256, 512, 1024, 2048 and 4096 Hz. The measures listed in Table 5-1 were calculated from data recorded simultaneously on all five electrodes.

Table 5-1 Measures used in salicylate experiments. The measures are grouped according to their analysis source, either PSTH or FRA.

FRA	PSTH
Characteristic Frequency (CF)	Total driven activity at BF- low attenuation (30dB)
Threshold attenuation at CF	Total driven activity at BF- high attenuation (50 dB)
Area of increased activity	Onset activity at BF- low attenuation (30 dB)
Magnitude of increased activity	Onset activity at BF- high attenuation (50dB)
Area of decreased activity	Spontaneous activity at 120 dB attenuation
Magnitude of decreased activity	

All measures were obtained at regular intervals over the course of the experiment, therefore all data were analysed using a one way repeated measures ANOVA (RM ANOVA) with time (pre and post salicylate) and electrode location (best frequency of the recording site) as within-subjects factors.

The total group of animals in the systemic salicylate experiments consisted of seven animals. All of them received the same dose of salicylate after the baseline recordings, the same recordings were made in all seven animals for the next three hours post salicylate administration. At that point, three animals received L-MeArg perfusion via the dialysis probe while the others remained on an aCSF perfusion. Thus, for the systemic salicylate experiments two separate ANOVAs were performed. One over the first three hours using the full data set from seven guinea pigs and one over the seven hour post salicylate dataset including only four animals. In the local salicylate experiment all three animals followed the same protocol with incremental concentrations of salicylate being perfused via the dialysis probe. Thus, for the local salicylate experiments one ANOVA was performed over all available time periods.

Because the focus in these experiments was on the overall effect of salicylate on neuronal responses in the IC, and the difference between the individual hours was of little interest, the decision was made to restrict the ANOVA results to test for specific patterns existing within the data. The test of within subjects contrast is part of the RM ANOVA output and tests for the presence of a linear, quadratic, cubic or higher order polynomial relationship that describes the neural response as a function of time over the course of the experiment. Of main interest in this instance were the potential linear and quadratic relationships. The linear relationship tests whether a linear non-zero relationship is present, indicating that there is either an increasing or decreasing change in firing over time. A quadratic relationship suggests a more complex change occurs over time, for example, an increase in activity in the first hours followed by a decline, a significant quadratic relationship would describe this inflexion.

When a significant linear relationship was obtained for a factor, the partial *eta* squared measure (η^2) was used as an estimate of the percentage variance explained by this relationship. Partial η^2 values of 0.02 were considered small, 0.13 moderate and anything larger than 0.26 was considered large (Cohen, 1977). Significant linear main effects were followed by a regression analysis to determine the slope of the linear relationship which

allowed comparisons of slopes between conditions. The regressions were forced through the origin to remove the constant from the regression equation leaving the coefficient determining the slope of the relationship.

Because quadratic and cubic relationships are difficult to conceptualise and even harder to express in numbers, when such a relationship was detected, the graphs were used to describe and illustrate the relationship. Higher order polynomials indicate complex patterns and require a priori hypothesis to be considered and were therefore ignored.

5.3 Results

5.3.1 Systemic Administration of Salicylate

A typical response to the systemic administration of salicylate, observed on virtually all electrodes is shown in Figure 5-3. A reduction in the initial response followed by an increase in sound driven activity and spontaneous activity in the later hours of the experiment are clearly visible in the binary FRAs where the original baseline is subtracted. Areas with increased activity appear in red and areas of decreased activity in blue. Typically, the decrease in activity is mainly observed on low frequency side of CF whereas the increase in activity is usually observed around the CF and in the higher frequencies. Some random points of increased activity can also be observed throughout the FRA which suggests an increase in spontaneous activity over time, this is particularly evident at 6 and 7 hours.

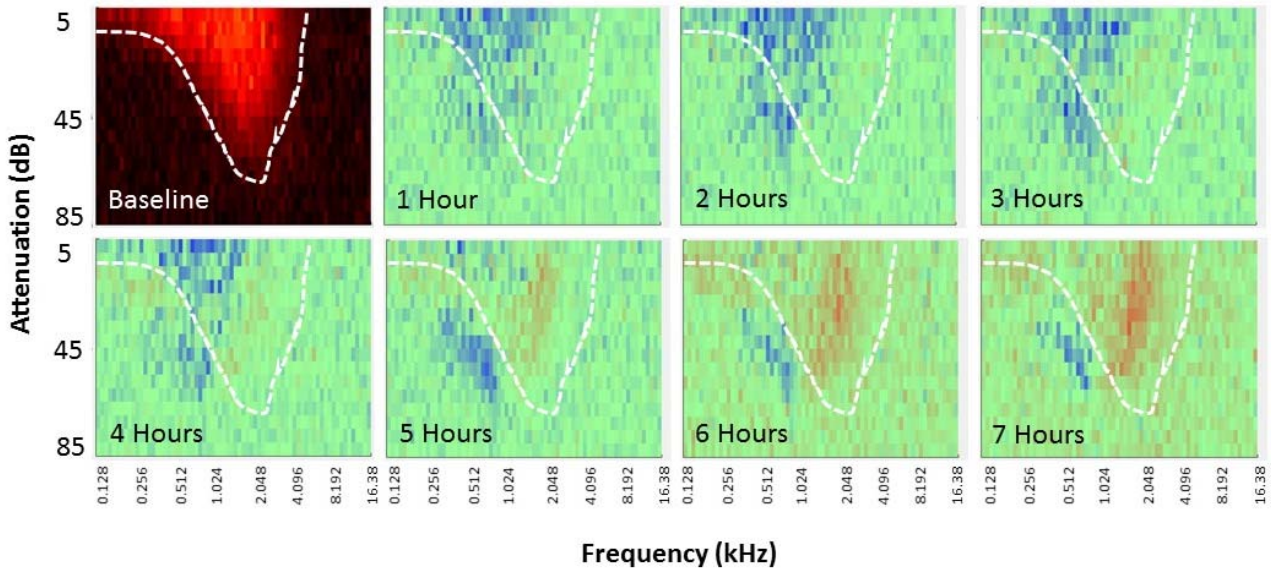

Figure 5-3 in the top left the original baseline FRA is shown, all subsequent FRAs are with baseline subtracted FRAs for each hour after systemic salicylate administration. Blue pixels represent decreases whereas red pixels represent increases in activity. The white outline traces the original FRA outline.

Characteristic frequency increased in response to salicylate

Systemic administration of salicylate (200 mg/kg) caused an upward shift in the CF which was evident at all frequencies (all electrodes) and increased over time. The shift of the CF in response to systemically administered salicylate is clearly visible in all animals (Figure 5-4) and all electrode locations (Figure 5-5). A significant change in the CF was observed after systemic salicylate administration, as shown by the significant non zero linear relationship that was detected for the CF in the first three hours after salicylate treatment (n=7) ($F(1,6) = 7.14$, $p = 0.037$ with $\eta^2 = 0.543$). The regression analysis showed a positive linear relationship over time, demonstrating an upward shift of the CF. No main effect for electrode location or interaction effect was detected over this time. The increase in CF was also observed over the longer time course of seven hours (n=4) ($F(1,3) = 50.51$, $p = 0.006$ with $\eta^2 = .944$). The regression analysis showed a strong positive relationship indicating that salicylate caused a constant upward shift of the CF over seven hours post salicylate administration. No significant main effect for electrode location or interaction effect was observed.

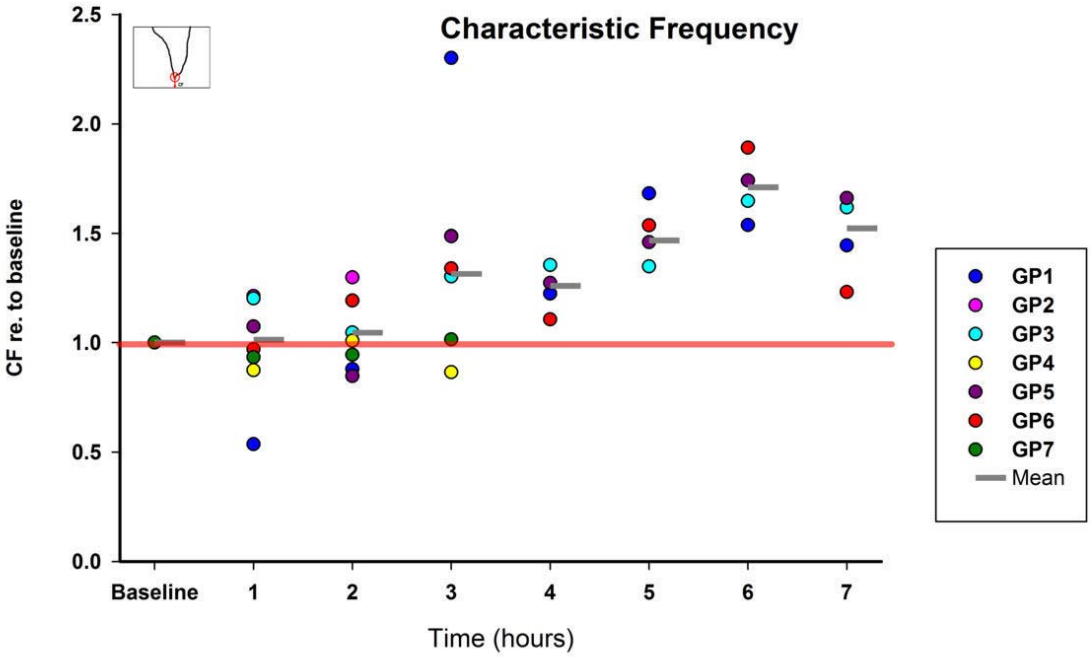

Figure 5-4 compound CF shift averaged across electrodes at each time point, expressed as a ratio to the baseline (red line). The grey bars displays the mean shift across animals, the coloured symbols represent data from individual animals for each time point.

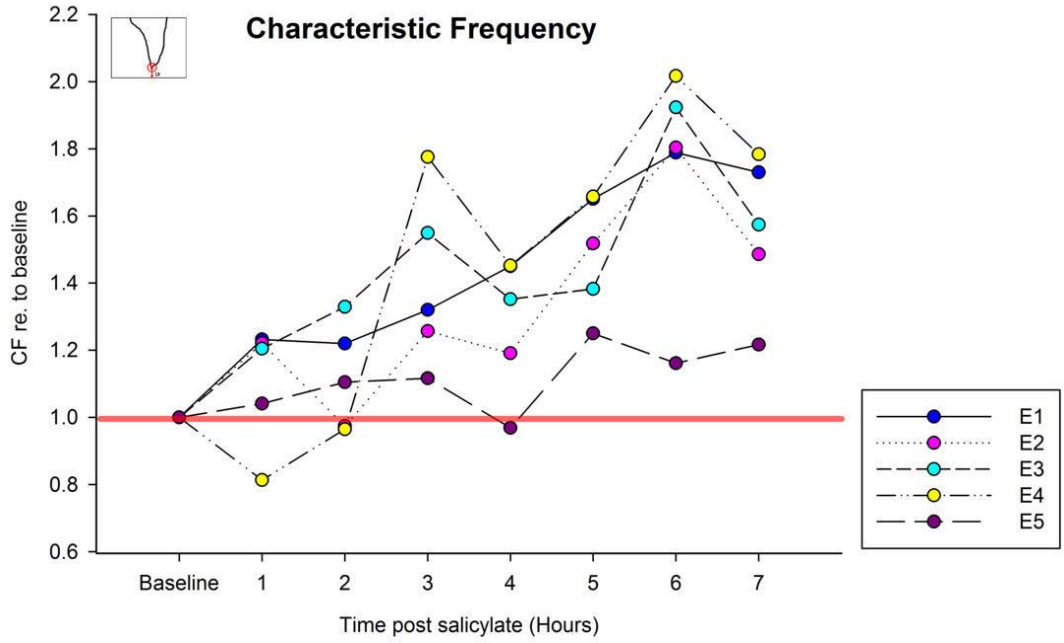

Figure 5-5 CF shift averaged across animals plotted for each electrode location CF is expressed as a ratio to the baseline.

Threshold attenuation at CF was not affected by salicylate

The threshold attenuation of the response did not change over time in response to systemic salicylate. Figure 5-6 and Figure 5-7 shows the attenuation levels at each time point, for each guinea pig (Figure 5-6) and each electrode (Figure 5-7) note that there is no systematic divergence from the baseline attenuation. ANOVA showed no significant linear or quadratic relationships for time post salicylate administration, electrode or the interaction between the two over either the three or the seven hour time period.

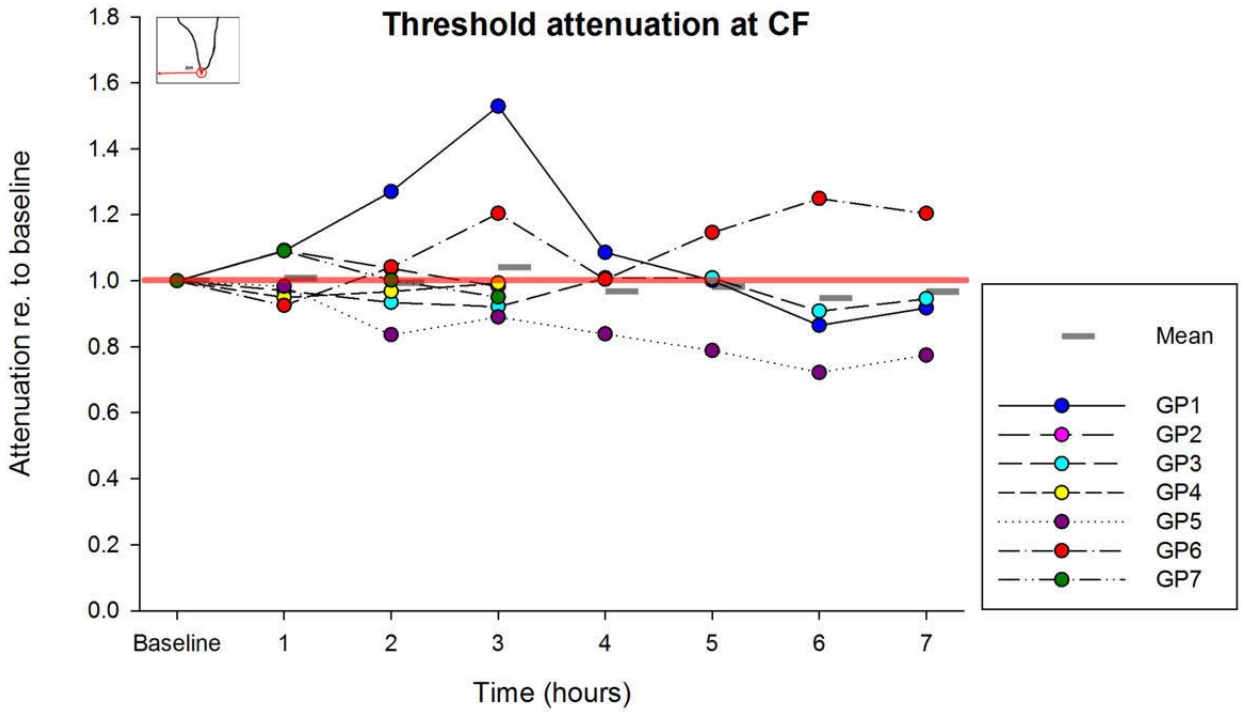

Figure 5-6 the threshold attenuation at CF averaged across frequencies. The grey bars indicate average across animals.

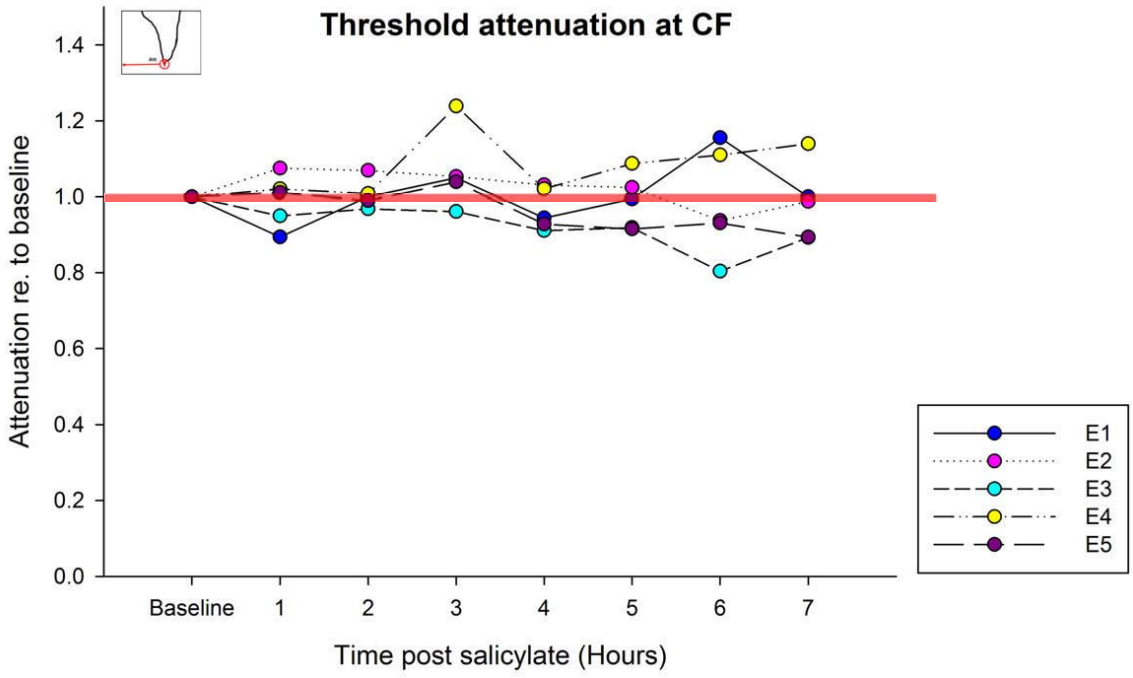

Figure 5-7 Threshold attenuation at CF plotted per electrode location averaged across animals.

Salicylate-induced areas of increased activity

Salicylate administration resulted in the gradual appearance of regions of increased activity in the FRAs measured on all electrodes. Figure 5-8 shows the subtracted and thresholded (binary) FRA, only showing increased activity in this instance, from a single animal for one electrode (E2, CF 512), this analysis shows which pixels, representing a combination of the stimulus frequency and level, have increased their firing rate compared to baseline. The region of increased activity which in this case starts 1 h after systemic salicylate administration increases in size (number of pixels) over the following 6 hours. The latency and rate at which these regions appear varied between animals as is clear by inspecting the three hour point in Figure 5-9, but all animals developed large clusters of increased activity at later times which were firmly established at seven hours post salicylate.

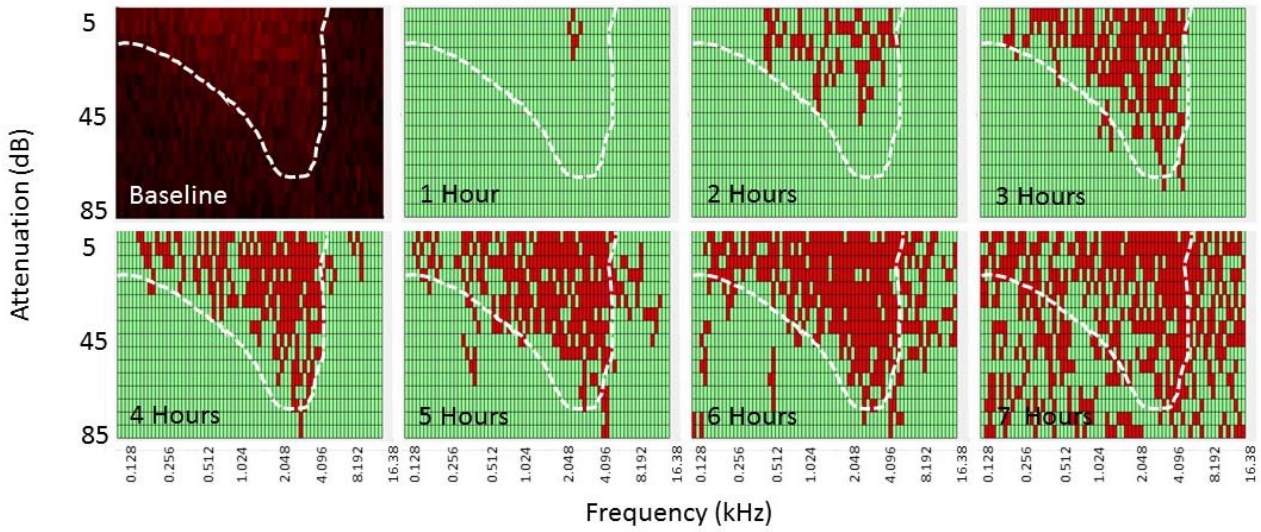

Figure 5-8 in the top left the original baseline FRA is shown, all subsequent FRAs are with baseline subtracted FRA and binarised to only show the regions of increase for each hour after systemic salicylate administration. This time series shows the gradual growth of the region of increased activity. The white line traces the outline of the original FRA.

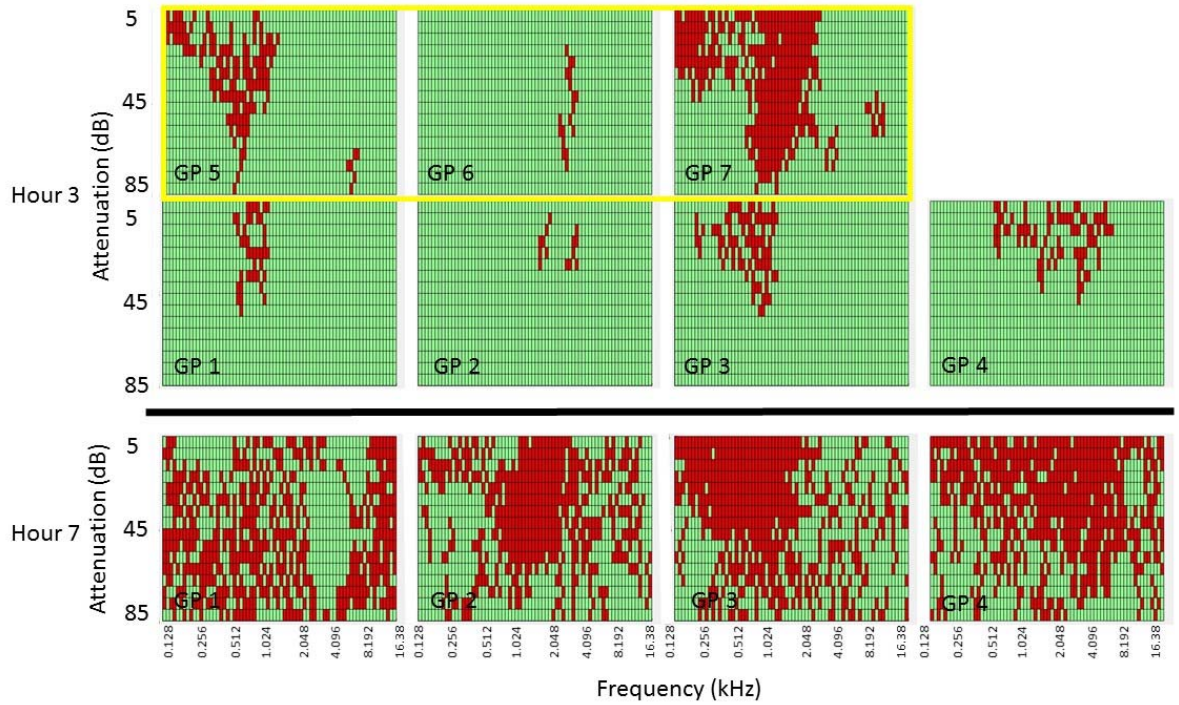

Figure 5-9 Binary baseline-subtracted FRAs depicting the cluster of increased activity from all 7 experiments at hour 3, the time point at which the two experimental protocols diverged and hour 7 for the four salicylate--only experiments. Animals receiving L-MeArg perfusion from hour 3 onwards are displayed in the top row and are highlighted by the yellow frame. The experiment numbers are given in the numbers on the graph.

I examined how the *size* of the cluster of increased activity (defined by the thresholding and connectivity parameters described in Chapter 2 (section 2.4 above) varied over time after salicylate injection. An ANOVA including seven animals and only data at baseline and the first three hours post-salicylate showed that the regions of increased activity grew significantly over the first three hours. Thus there was a significant non-zero linear relationship for time ($F(1,6) = 8.81$, $p = 0.025$. $\eta^2 = 0.60$). Regression analysis showed a β coefficient of 34.59 for this three hour time series. No further polynomial relationships were detected over time implying that there was no plateau or inflexion in the data, thus indicating a positive linear increase over time. No significant relationships were detected for electrode location or the interaction between electrode location and time.

A further ANOVA including data from four animals at baseline and all seven hours post salicylate administration showed that the area of the clusters of increased activity grew as indicated by a significant non-zero linear relationship for time post salicylate administration ($F(1,3) = 15.64$, $p = 0.029$, $\eta^2 = 0.839$). The regression analysis revealed a β coefficient of 51.22 which is a strong positive coefficient indicating a linear relationship. The coefficient over the seven hours is higher compared to the coefficient over the three hours indicating that the increase observed is stronger in later hours, an observation that is evident in Figure

5-10 and Figure 5-11. Figure 5-10 highlights the individual differences in the effect between animals and one animal does not follow the overall observed pattern. No significant main effect was detected for the frequency or the interaction between condition and frequency. These data show that salicylate causes an increase in activity over an increased number of frequencies and attenuations measured in the FRA, irrespective of the electrode location (Figure 5-11).

Having established that salicylate causes an increase in the response of IC neurons to sound stimuli over a progressively widening range of frequency and levels, it is next necessary to quantify this increase.

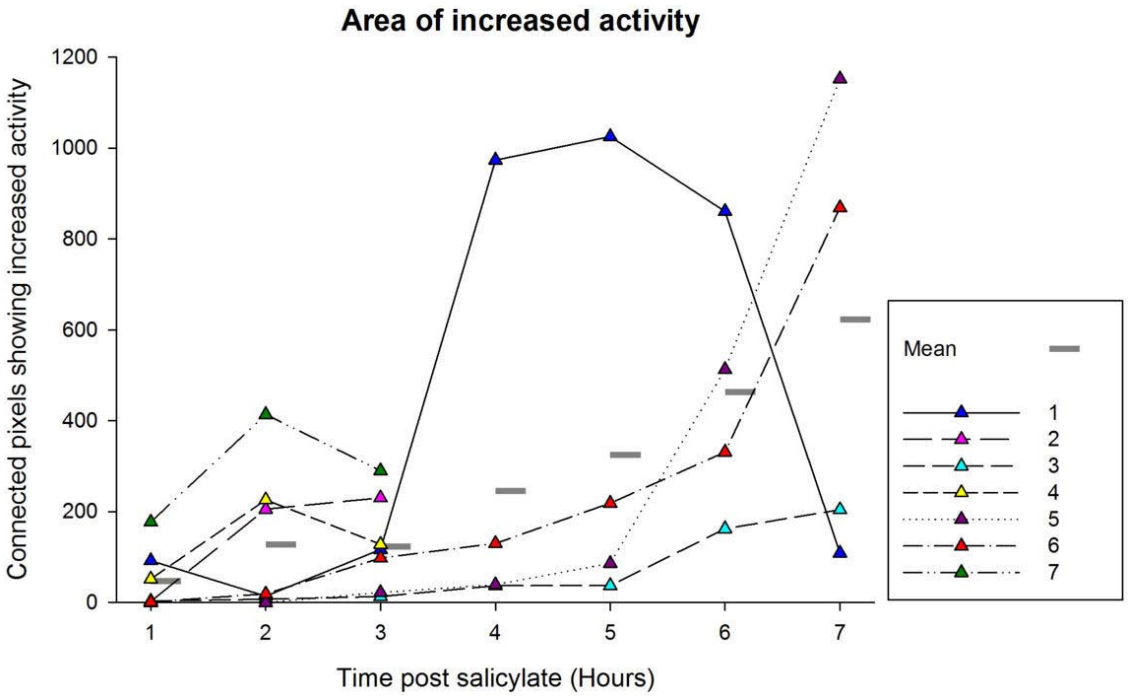

Figure 5-10 The coloured triangles represent the number of pixels in the area of increased activity (in the binary baseline subtracted FRA) averaged across electrodes for each individual animal at the different time points post salicylate injection. The mean of all animals per time point is indicated by the grey lines.

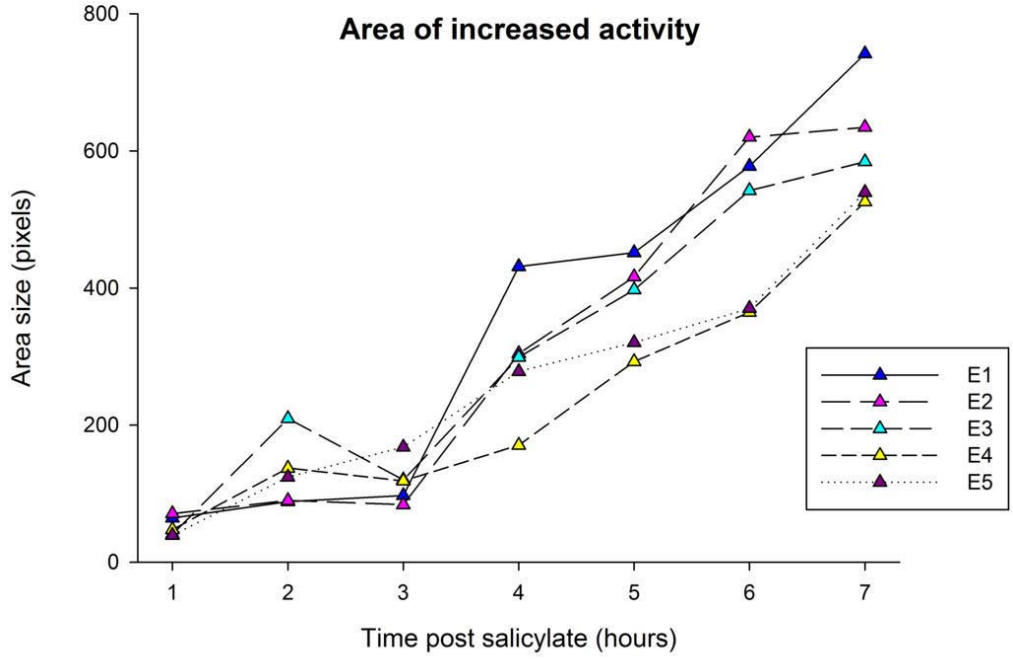

Figure 5-11 The number of pixels making up the areas of expanded activity in the binary subtracted FRA plotted over time, averaged across the seven animals, plotted for the different electrode locations.

Magnitude of increased activity

In addition to the size of the area, I also examined the relative increase in activity compared to the original baseline within the defined area relative to baseline. The magnitude changed significantly over the first three hours post salicylate ($F(1,6) = 154.18$, $p < 0.001$, $\eta^2 = 0.963$). The β coefficient from the regression analysis indicated a positive linear relationship over time, consistent with an increase in magnitude over time. No main effect for electrode location or interaction effect was observed. The picture was more complex when all seven hours post salicylate were taken into account (Figure 5-13). This analysis showed that the relative magnitude varied over time ($F(1,3) = 19.20$, $p = 0.022$, $\eta^2 = 0.865$) and the positive β coefficient from the regression analysis showed that there was an increase in magnitude over time. However a significant cubic relationship for the electrode location within the IC was obtained ($F(1,6) = 8.70$, $p = 0.026$ with $\eta^2 = 0.592$), indicating that increases in magnitude differed between the different electrodes. Inspection of Figure 5-13 suggests that although all electrodes increased their activity the magnitude of increase was greater on the electrodes recording activity with CFs near 256 (E1), 512(E2) and 1024 Hz(E3). No condition x electrode interaction effect was observed.

These data indicate that salicylate causes an increase in driven activity over time that appears to peak around five hours post salicylate. All electrodes irrespective of their

location show an increase in the relative magnitude of activity over time, although he change may differ for different frequency regions of the IC.

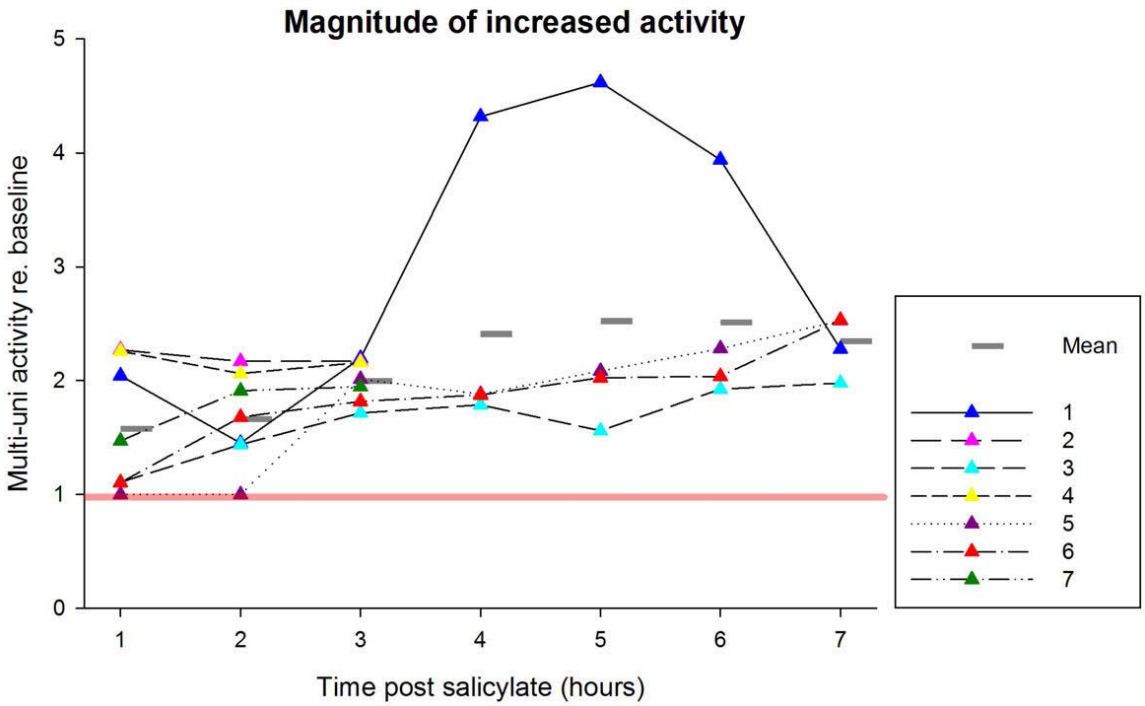

Figure 5-12 The coloured triangles represent the ratio of the activity at each time point compared to baseline (indicated by the red line) for each animal averaged across all electrodes. The mean of all animals per time point is indicated by the grey lines.

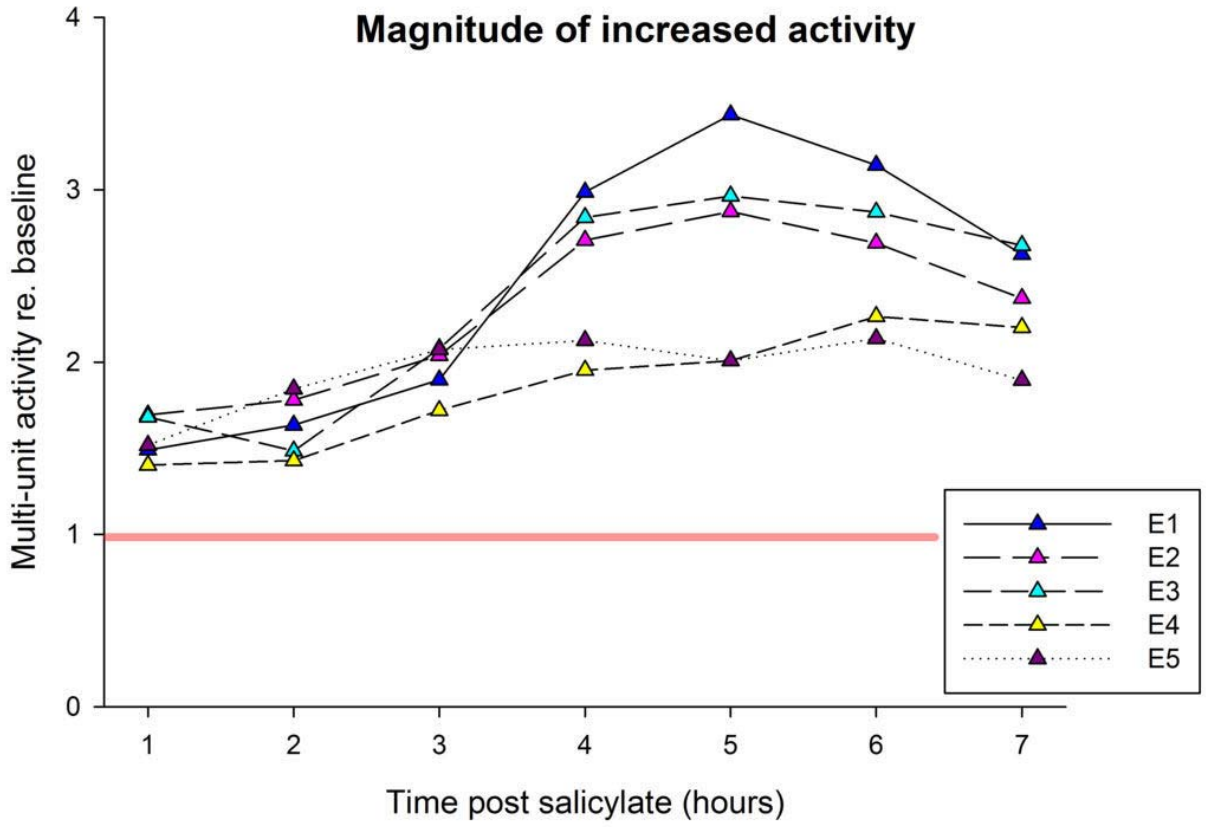

Figure 5-13 The coloured triangles represent the ratio of the activity at each time point compared to baseline (indicated by the red line) averaged across animals, the red line indicates the baseline value.

Salicylate-induced transient areas of decreased activity

Following systemic administration of salicylate, areas of decreased activity were observed on several but not all electrodes. An example of this effect is shown in Figure 5-14 which shows the binary baseline subtracted FRA where the blue pixels represent values in which the firing rate was reduced relative to baseline. In this figure all time points throughout the experiment are shown for this one electrode from an individual animal. Figure 5-15 illustrates the individual variation in latency and duration of the formation of these areas of decreased activity, it also highlights that these regions appear early in the experiment but shrink in the later hours of the experiment.

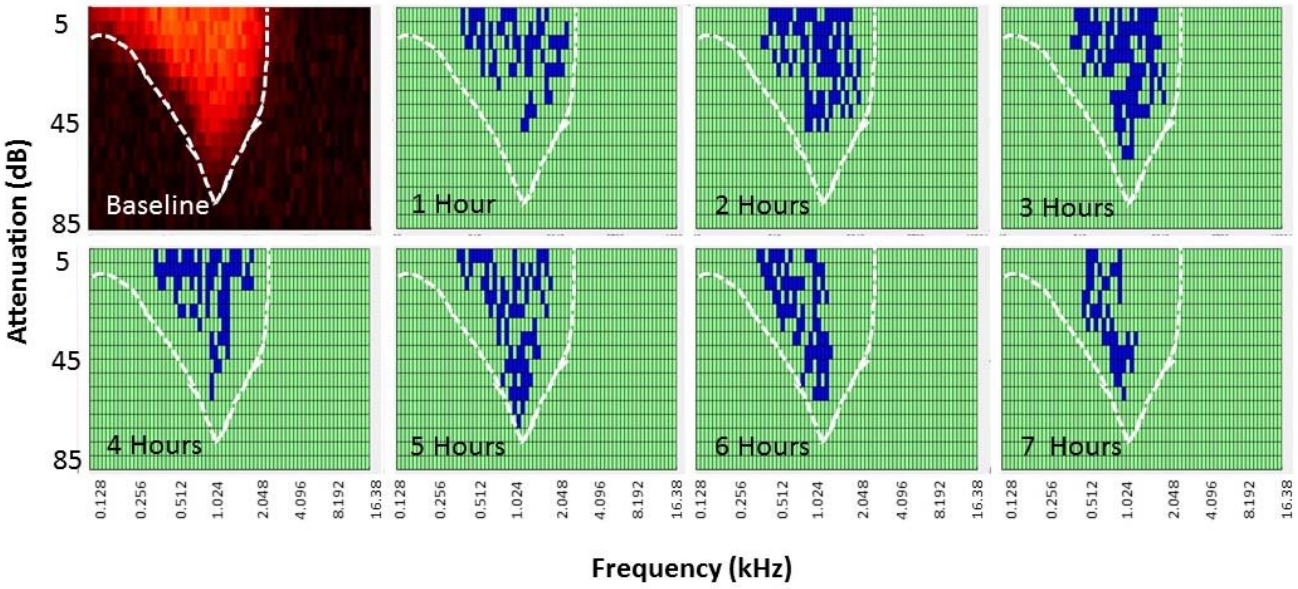

Figure 5-14 in the top left the original baseline FRA is shown, all subsequent FRAs are with baseline subtracted FRA and binarised to only show the regions of decreased activity for each hour after systemic salicylate administration. The white line traces the original FRA outline. The plots show the gradual growth and decline of these areas over the course of the experiment.

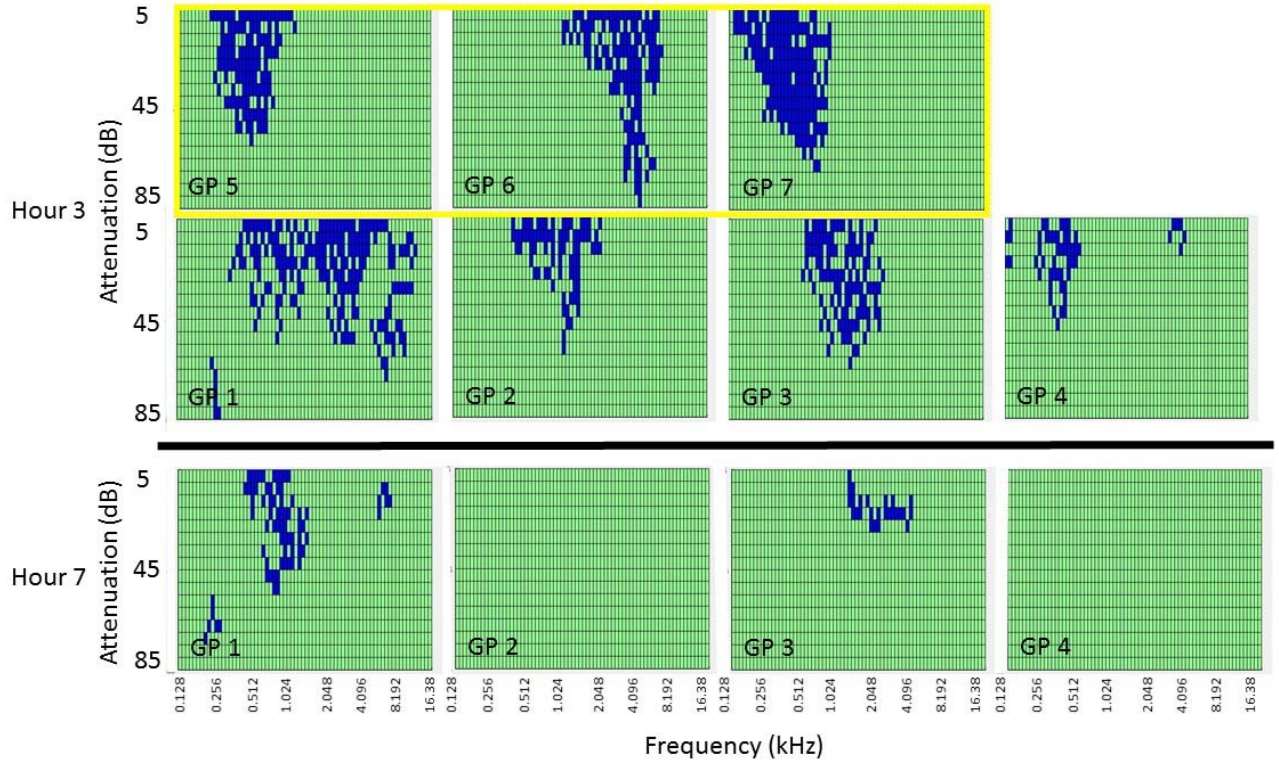

Figure 5-15 with baseline subtracted binarised FRAs showing the areas of decreased activity from all experiments at hour 3, the time point at which the two experimental protocols split and hour 7 for the four full salicylate experiments. Animals receiving L-MeArg perfusion from hour 3 onwards are displayed in the top row and are highlighted by the yellow frame

Statistical analysis revealed that the formation of clusters of reduced activity exhibited a complex pattern over the first three hours. There was a significant linear relationship to time with $F(1,6) = 8.96$, $p = 0.024$, $\eta^2 = 0.60$) with a positive β indicating the cluster grew over time (Figure 5-16 and Figure 5-17). The effect also varied with electrode location. Thus, there was a significant cubic relationship between area of decreased activity and electrode (number/frequency/location) ($F(1,6,) = 7.34$, $p = 0.035$, $\eta^2 = 0.55$). Finally, the time x electrode interaction term also showed a significant cubic relationship ($F(1,6) = 10.01$, $p = 0.019$, $\eta^2 = 0.63$). Figure 5-17 suggests that although areas of reduced activity were seen in the FRAs from all electrodes, FRAs from electrodes with a CF < 1024 Hz (E1, E2 and E3) developed larger clusters in which activity was decreased.

The ANOVA over the full seven hour time points (N=4) gave no indication for any linear, quadratic or cubic relationships over this time period suggesting that no change was detected over this time period. Figure 5-16 and Figure 5-17 show that an initial decrease in activity rapidly goes back to the baseline to the extent that the areas showing decreased activity have mostly disappeared by hour six, although variation between the animals was observed.

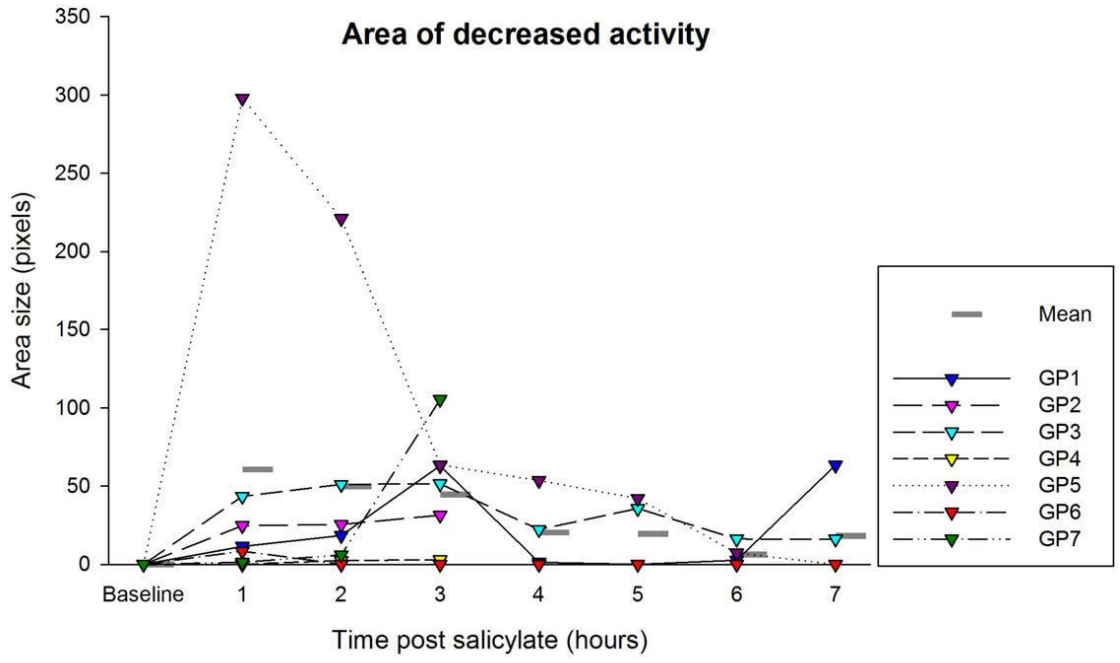

Figure 5-16 The coloured triangles represent the total pixels comprising the area of decreased activity for each individual animal at the different time points post salicylate injection, averaged across electrodes. The mean of all animals per time point is indicated by the grey lines

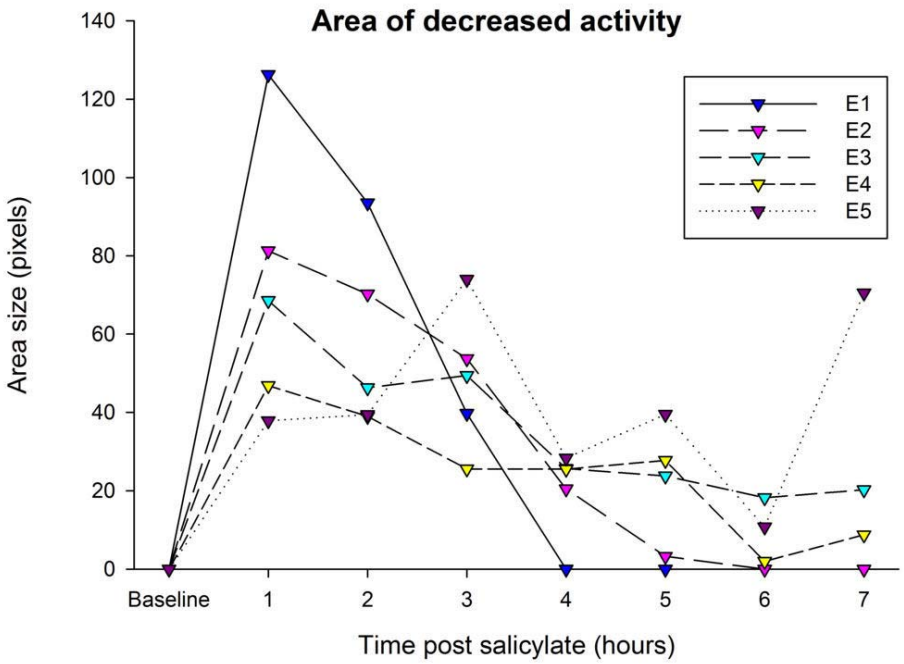

Figure 5-17 the number of pixels comprising the area of decreased activity in the subtracted FRA plotted over time. Data values are averaged across all animals and plotted for the different electrodes.

Having established that regions of decreased activity are observed in the subtracted FRA in all animals for the first few hours, the magnitude of the decrease was then investigated.

Magnitude of decreased activity reaches steady state

The greatest reductions in activity compared to baseline were seen in the first hour after the salicylate administration, but then appeared to stabilise. The RM ANOVA showed that the reduction in firing had both significant linear ($F(1,6) = 9.30$, $p = 0.023$, $\eta^2 = 0.60$) and quadratic ($F(1,6) = 9.24$, $p = 0.023$, $\eta^2 = .61$) relationships to the time post salicylate administration. The regression analysis resulted in a negative β coefficient indicating that the rate of reduction declined over time.

The RM ANOVA over all seven hours revealed a significant cubic relationship for time post salicylate ($F(1,3)=23.493$, $p < 0.017$, $\eta^2 = 0.887$). These results can be best interpreted by inspecting Figure 5-18 and Figure 5-19. In the figures we can see that the mean reduction in firing rate is greatest over the first hour post salicylate and then flattens out and remains stable in spite of the area shrinking, although the individual animals show great variability in actual numbers all show the same direction of the effect.

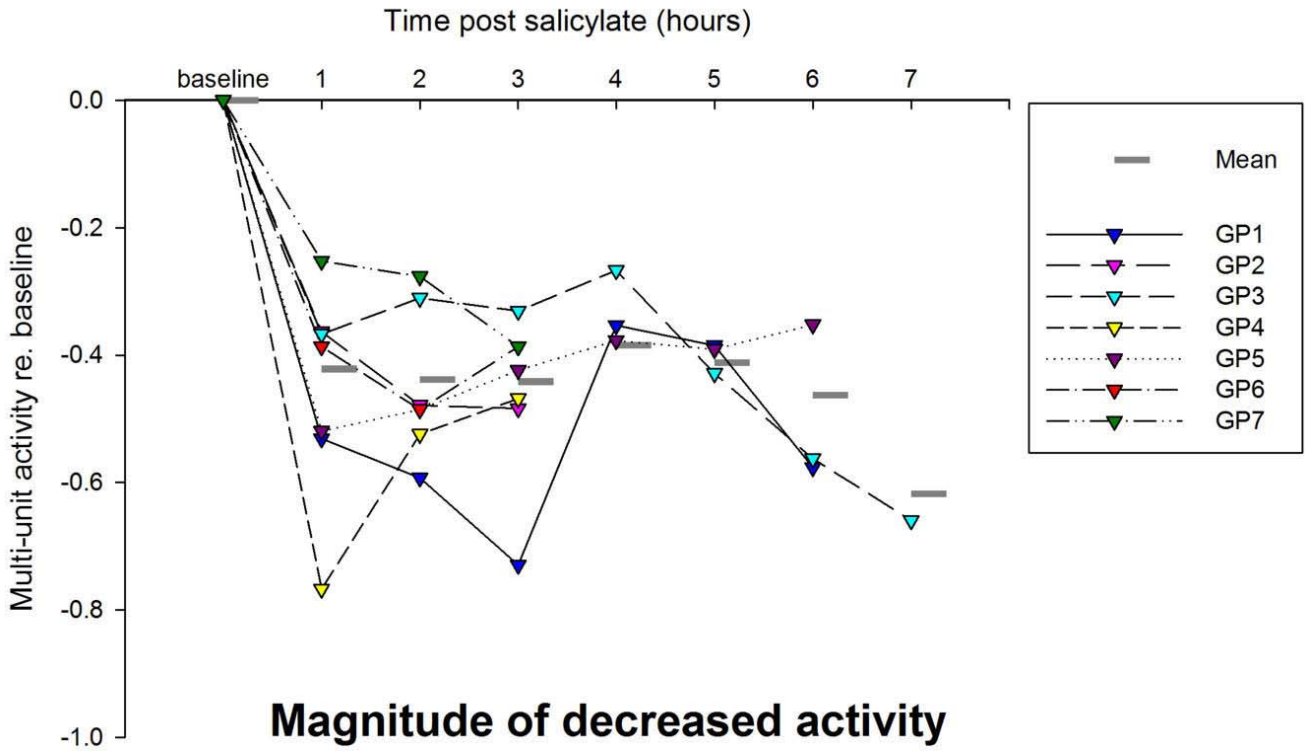

Figure 5-18 The coloured triangles represent the reduction in firing rate averaged across electrodes for each animal. The grey bars indicate the mean across the animals. The baseline was set to be 0.

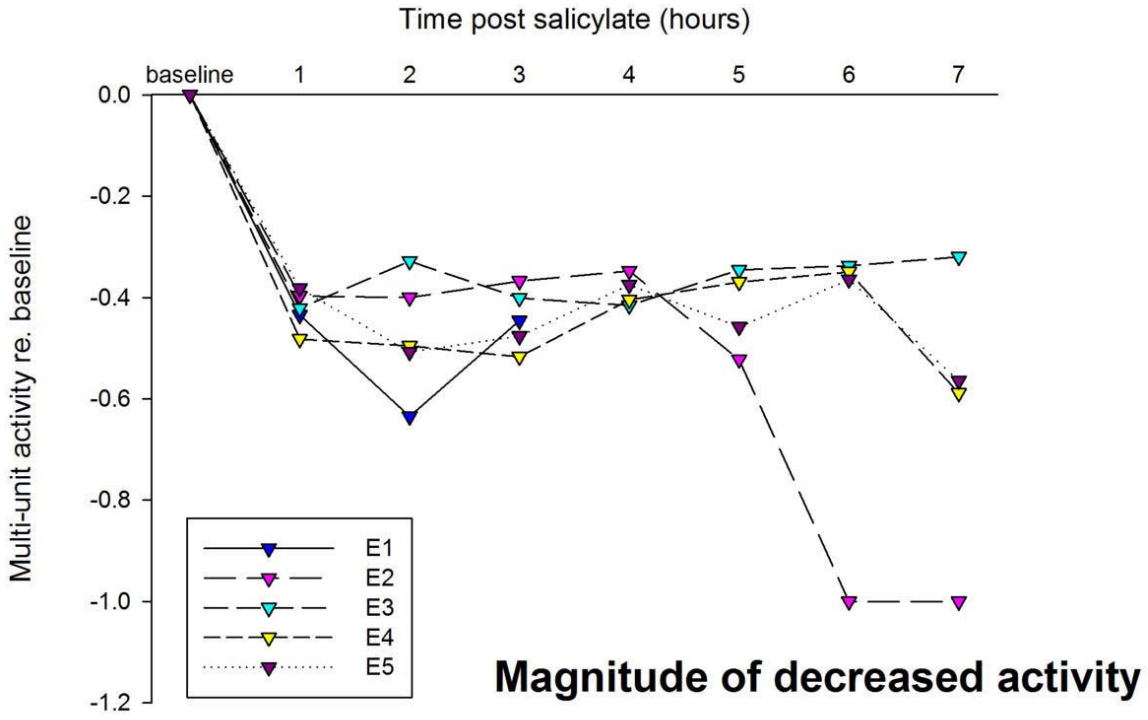

Figure 5-19 The coloured triangles represent the decrease in activity on each electrode averaged across animals at each time point. Baseline was set at 0.

Salicylate increases spontaneous activity

Systemic salicylate-induced an increase in spontaneous activity over the later hours of the experiment. The spontaneous activity was calculated from the highest attenuation level present in the FRA (i.e. the lowest level) effectively silence. In the first three hours no significant relationships were detected indicating that the spontaneous activity remained unchanged in this time period, although there is individual variation between animals, illustrated in Figure 5-20.

The seven hour time line showed an increase in spontaneous activity ($F(1,3) = 12.63$, $p = 0.038$, $\eta^2 = .81$) with a positive β coefficient indicating a positive relationship. No significant main effect of electrode or electrode x time interaction was observed suggesting that the systemic administration of salicylate caused the spontaneous activity to increase over time irrespective of electrode location. There was no sign of an increase in the first three hours, but Figure 5-21 suggests that the onset starts around four hours after salicylate treatment.

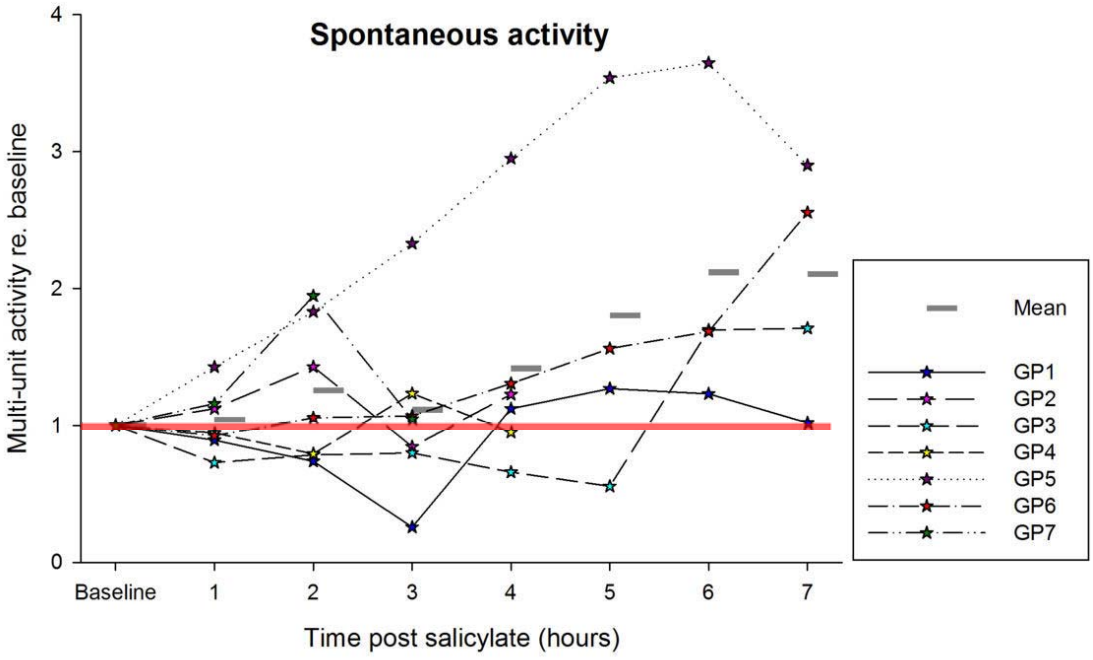

Figure 5-20 Spontaneous activity for the different animals averaged across all electrodes at each time point, expressed as a ratio to the baseline (red line). The grey bars represent the average across animals.

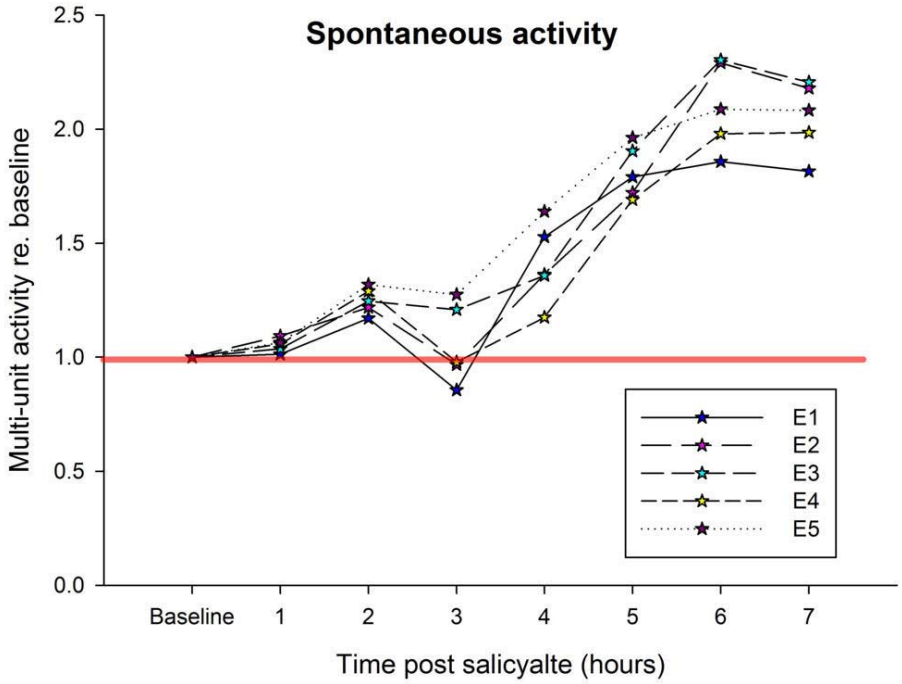

Figure 5-21 Spontaneous activity displayed for the different electrodes averaged across animals, expressed as a ratio to the baseline (red line).

Having established that units show increased and decreased responses to a wide range of frequencies in response to salicylate an important question is what effect it has on the activity elicited by frequencies close to the CF of the multiunit activity.

Total driven activity at low attenuation is not affected by salicylate

Salicylate did not cause any change in the sound driven part of the PSTH in the low attenuation (30dB) condition. Thus the RM ANOVAs in both the three and the seven hour time series showed no significant polynomial trends for time, frequency or the interaction between the two. The figures, Figure 5-22 and Figure 5-23 show almost flat lines.

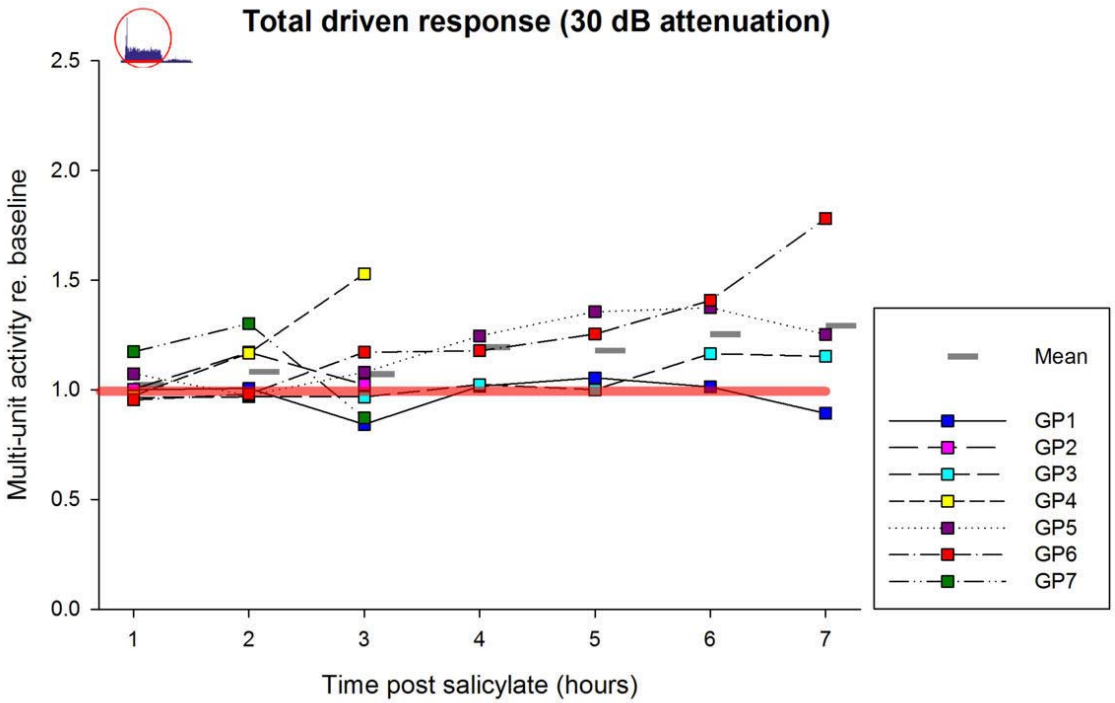

Figure 5-22 Sound evoked activity in the PSTH averaged over all electrodes for each animal, as a function of time post salicylate at each time point. The activity at each time point is expressed as a ratio to the baseline (red line). The grey bares represent the mean across all animals.

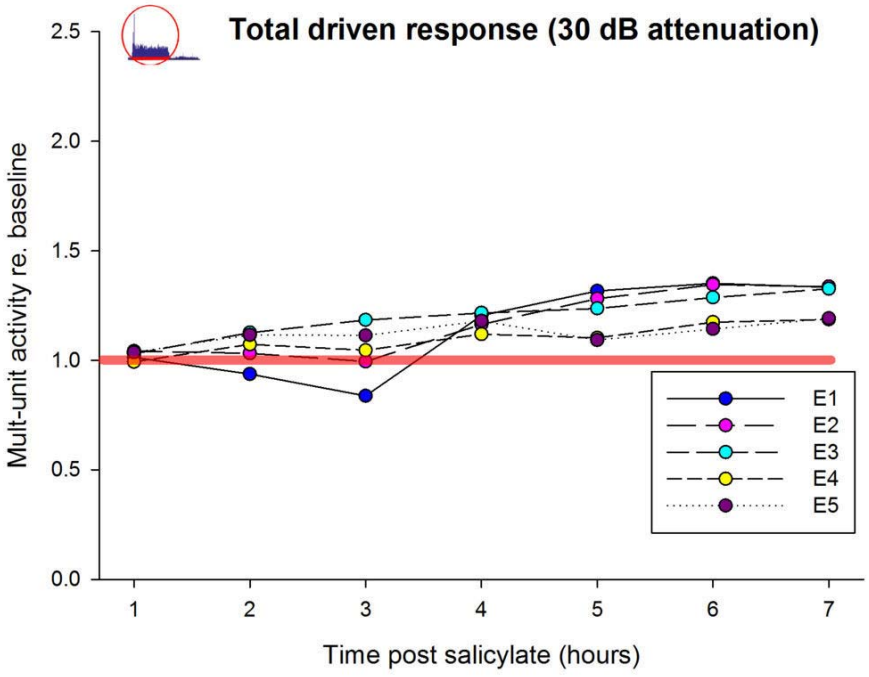

Figure 5-23 the sound driven activity captured in the PSTH, plotted for the different electrodes averaged across the animals. Activity is expressed as a ratio to baseline (red line).

Onset activity at low attenuation is unaffected by salicylate

Salicylate failed to affect the PSTH onset peak in either the three or seven hour time window. Figure 5-24 and Figure 5-25 both illustrate this point. No change in driven activity or onset peak activity was detected in the low attenuation condition.

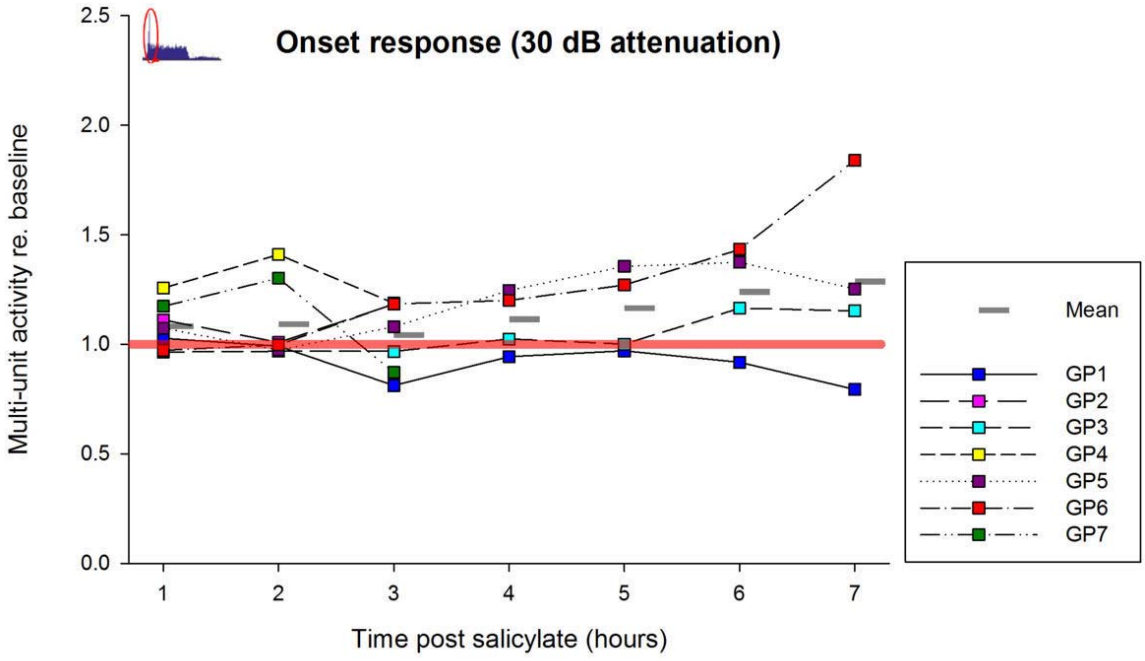

Figure 5-24 the onset peak expressed as a ratio to the baseline (red line) plotted for the individual animals averaged across the electrodes. The grey bars indicate the average across all animals.

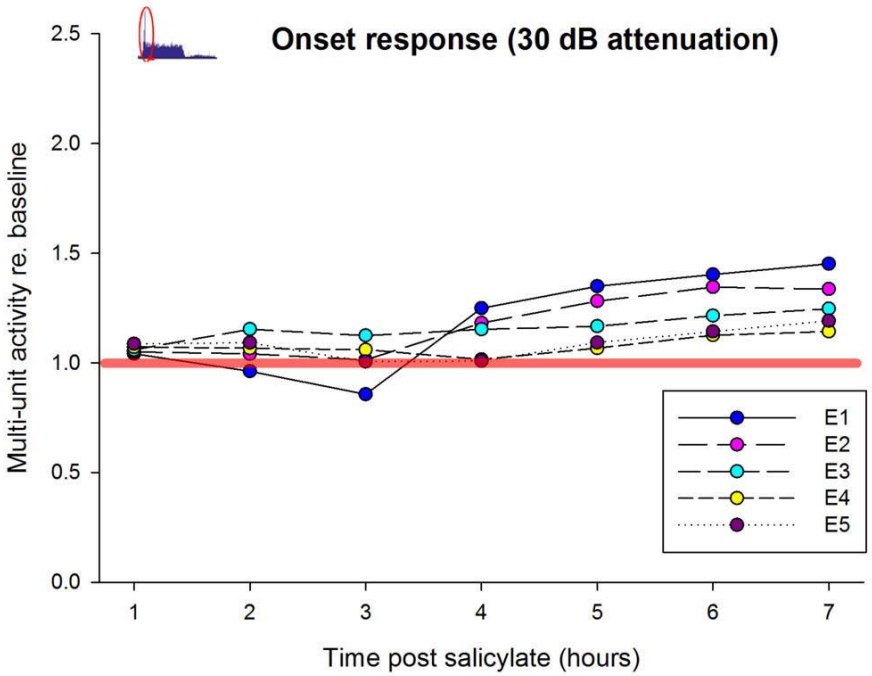

Figure 5-25 the onset peak expressed as a ratio to the baseline (red line) plotted for the different electrodes averaged across the animals.

Total driven activity at high attenuation is unaffected by salicylate

Following salicylate injection, there was no change in the sound driven activity in the high attenuation condition over the three or the seven hour time courses. No linear, quadratic or cubic relationship for time, electrode or the interaction between the two was observed. Due to the variability between the animals, illustrated in Figure 5-26, the total driven activity was not shown to be significantly affected by salicylate.

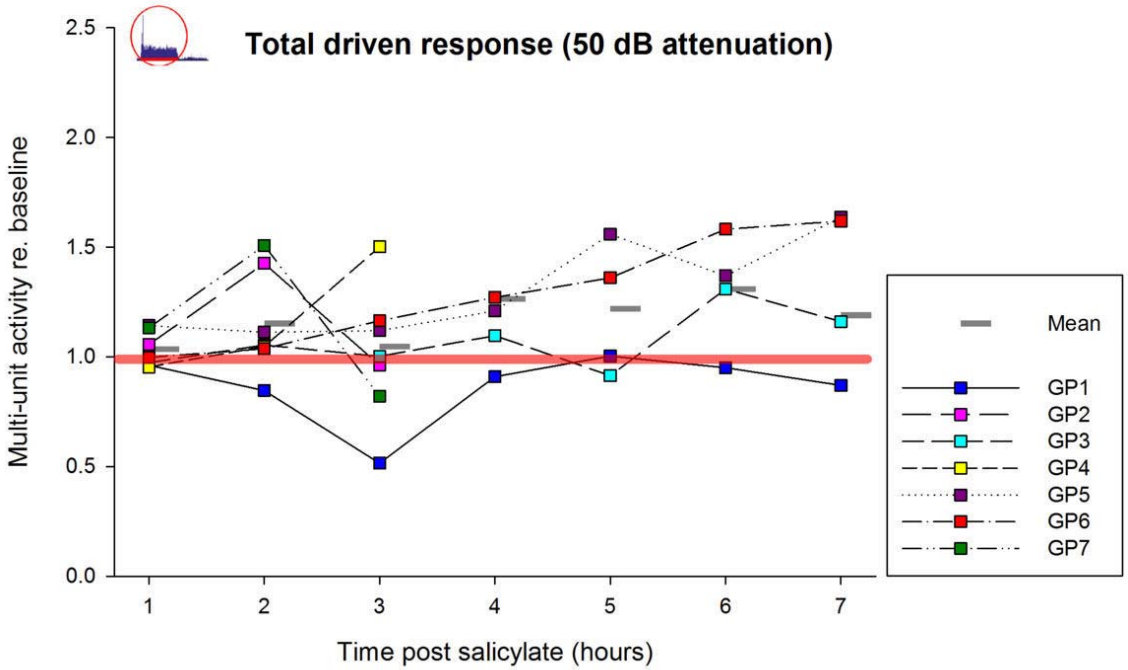

Figure 5-26 the sound driven part of the PSTH per animal averaged over all electrodes at each time point. The activity at each time point is expressed as a ratio to the baseline. The grey bars represent the mean across all animals.

Onset activity at high attenuation is unaffected by salicylate

The onset peak of the driven activity showed no signs of significant systematic change for either the three or the seven hour time window. Figure 5-27 shows the variability between animals, interestingly the variability between animals increases over time. Systemic administration of salicylate does not appear to affect the sound driven response of the neurons at the attenuation levels presented here.

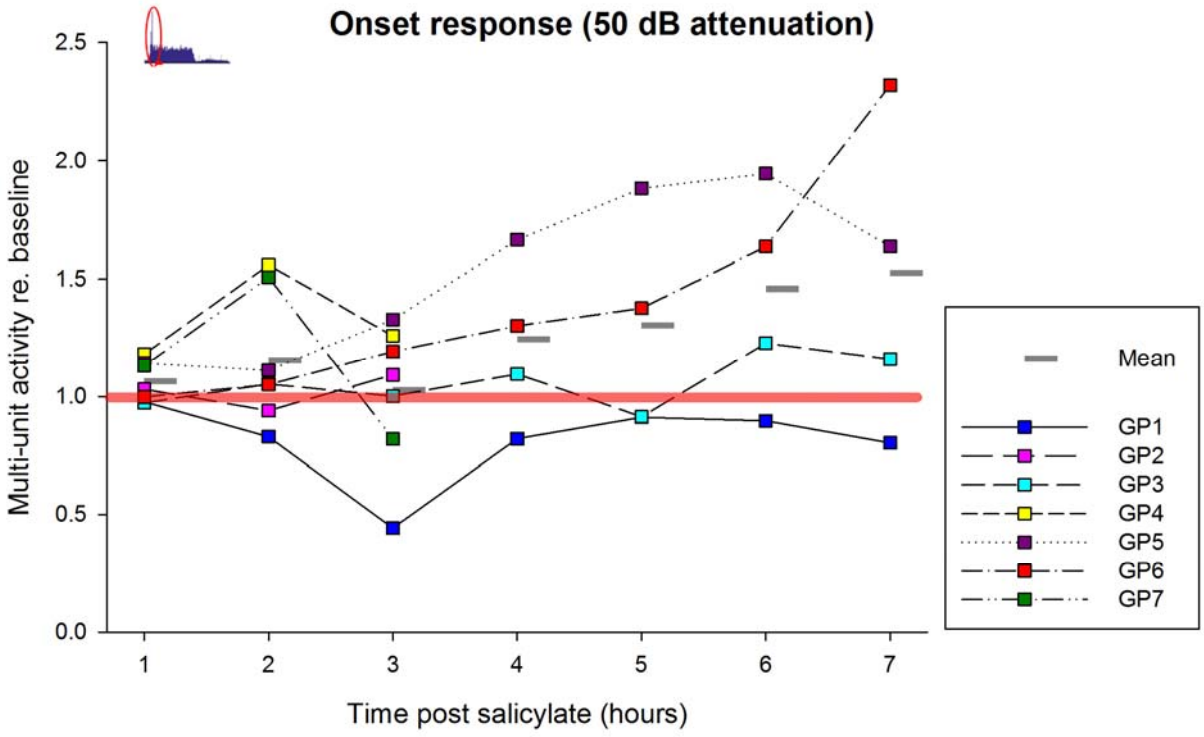

Figure 5-27 the onset peak expressed as a ratio to the baseline plotted for the individual animals averaged across the electrodes. The grey bars indicate the average across all animals.

5.3.2 Local Administration of Salicylate

The local administration of salicylate in the IC will give more insight into how salicylate acts on auditory processing in the IC. Because the local administration of salicylate had a much quicker onset than the systemic administration of salicylate, 4 blocks spaced 12 minutes apart extracted from the first hour post the onset of administration were added to the analysis. Note that the concentration of salicylate perfused through the dialysis probe was increased over time; this is indicated in all plots. Because only time was included in the analysis, and we don't know the exact concentration of salicylate in the tissue, it is not possible in the current analysis to distinguish between duration of perfusion and the concentration of salicylate present. In Figure 5-28 an overview of an experiment with local administration of salicylate is shown. Immediately noticeable is that the FRA increases in area size 3 hours after administration begins, but in contrast to the response to systemic administration of salicylate, there is a reduction in area between 3 and 7 hours. Also apparent is the absence of areas of decreased activity and little increased spontaneous firing due to the absence of random scatter outside of the FRA.

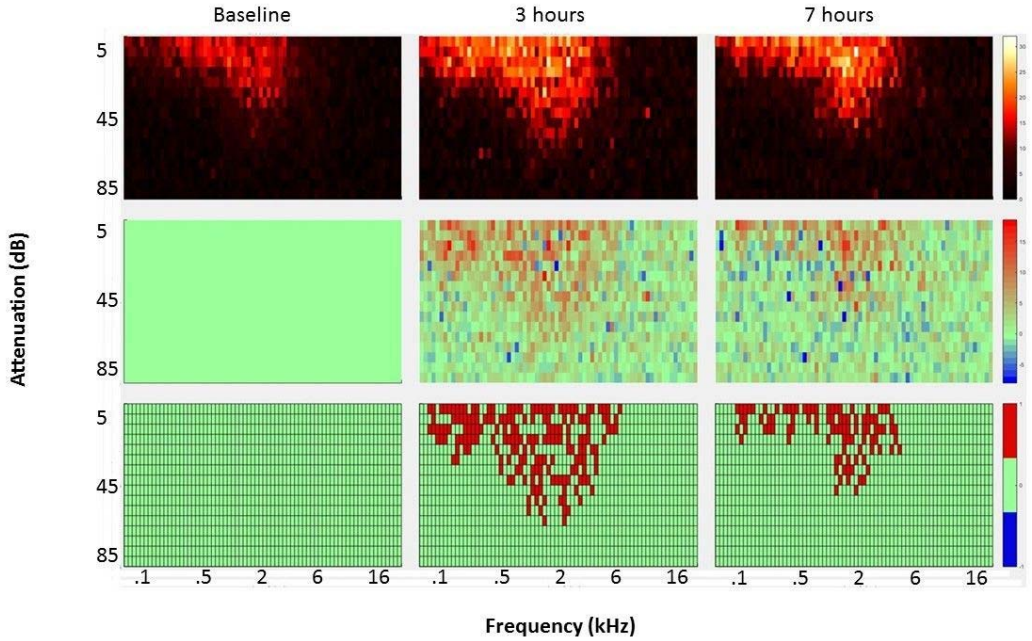

Figure 5-28 Overview of experiment 9050. In the top row the original FRA's are shown for the baseline, 3 hours and 7 hours after salicylate perfusion has started. The second row shows the FRA for that time point following subtraction of the baseline. In the third row the binary FRA's of which the baseline was subtracted are shown. Red pixels represents an increase in activity.

Local salicylate did not affect the CF

Perfusion of increasing concentrations of salicylate failed to alter the CF. Thus the RM ANOVA did not show any relationship for time, electrode location or the interaction between the two. Figure 5-29 and Figure 5-30 shows the CF stays close to the baseline value.

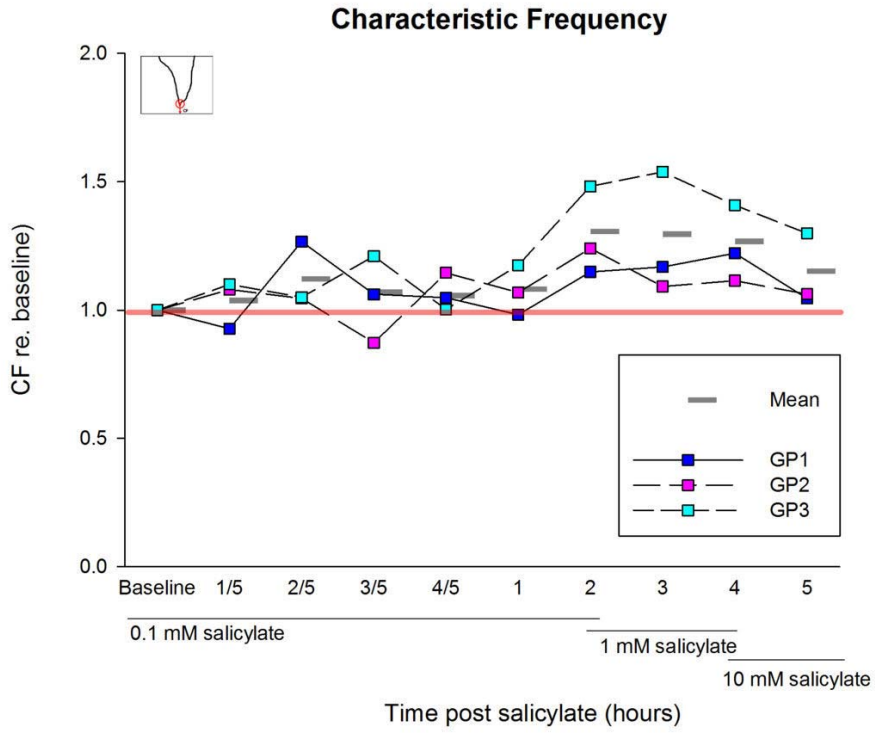

Figure 5-29 the coloured squares represent the CF for every animal averaged across all electrodes at each time point. The CF is expressed as a ratio to the baseline. The grey bars express the mean across animals. The red line indicates the baseline level.

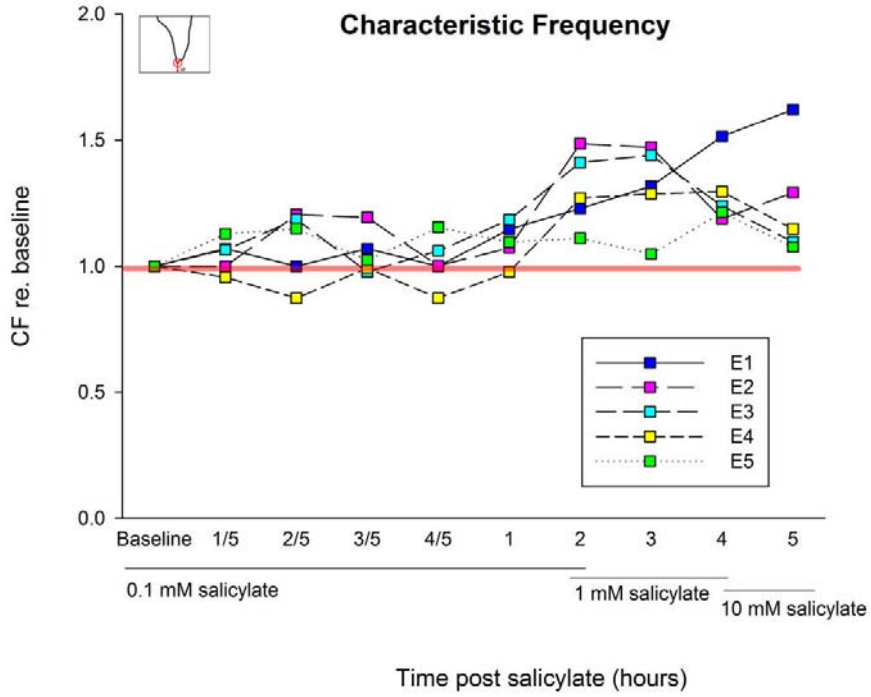

Figure 5-30 the coloured squares represent the CF for each electrode location averages across animals. The CF is expressed as a ratio to the baseline. The red line indicates the baseline level.

Local salicylate did not affect threshold attenuation at CF

No change in threshold attenuation was detected for time post salicylate, electrode or the interaction between the two. In the figures Figure 5-31 and Figure 5-32 the attenuation levels are plotted against the baseline, just as the statistical test indicated no discernible effect is observed. These results suggest that the local administration of salicylate does not cause a shift in CF or threshold of the units.

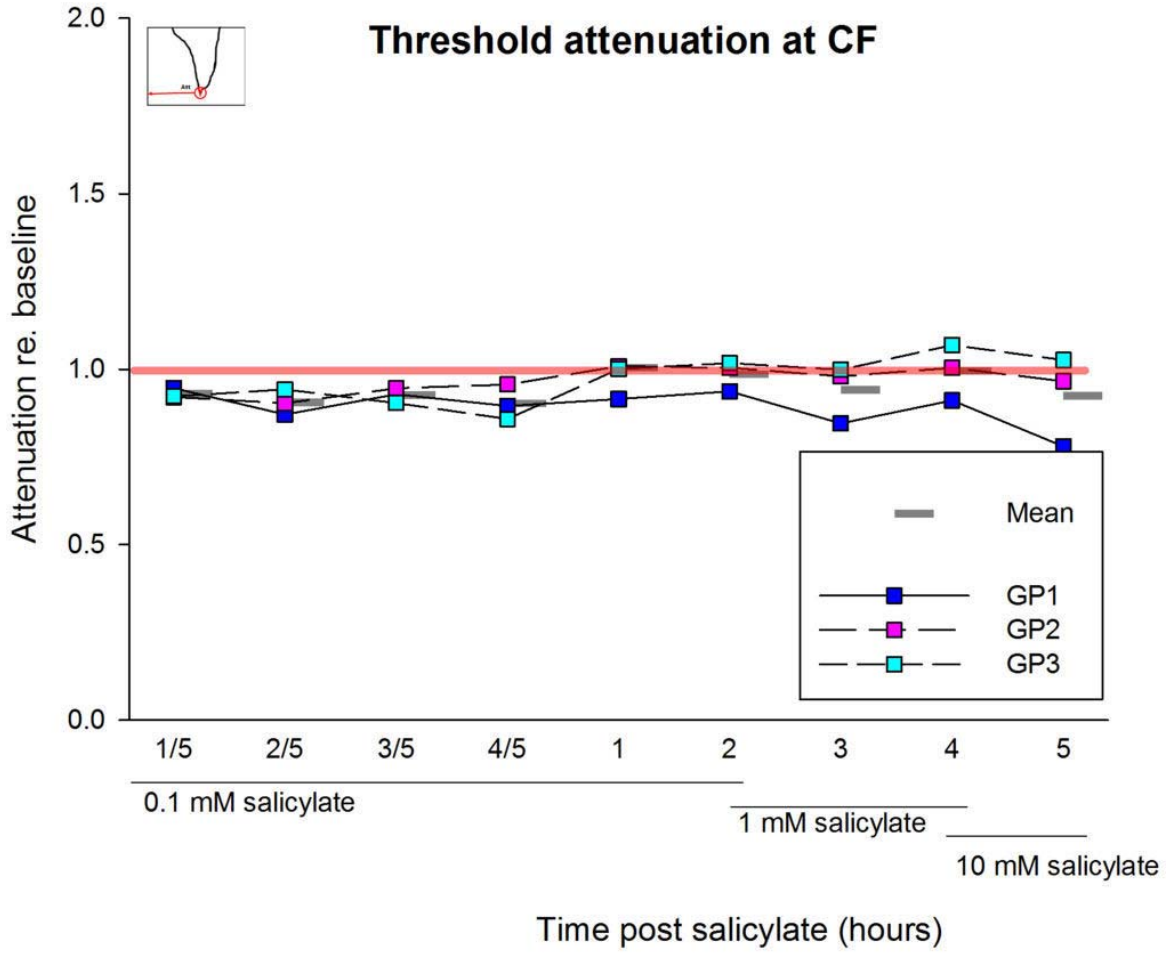

Figure 5-31 the coloured squares represent the attenuation level for each animal averaged across all electrodes on which the CF was obtained. The attenuation level is expressed as a ratio to baseline, indicated by the red line. The grey bars represent the mean across all animals.

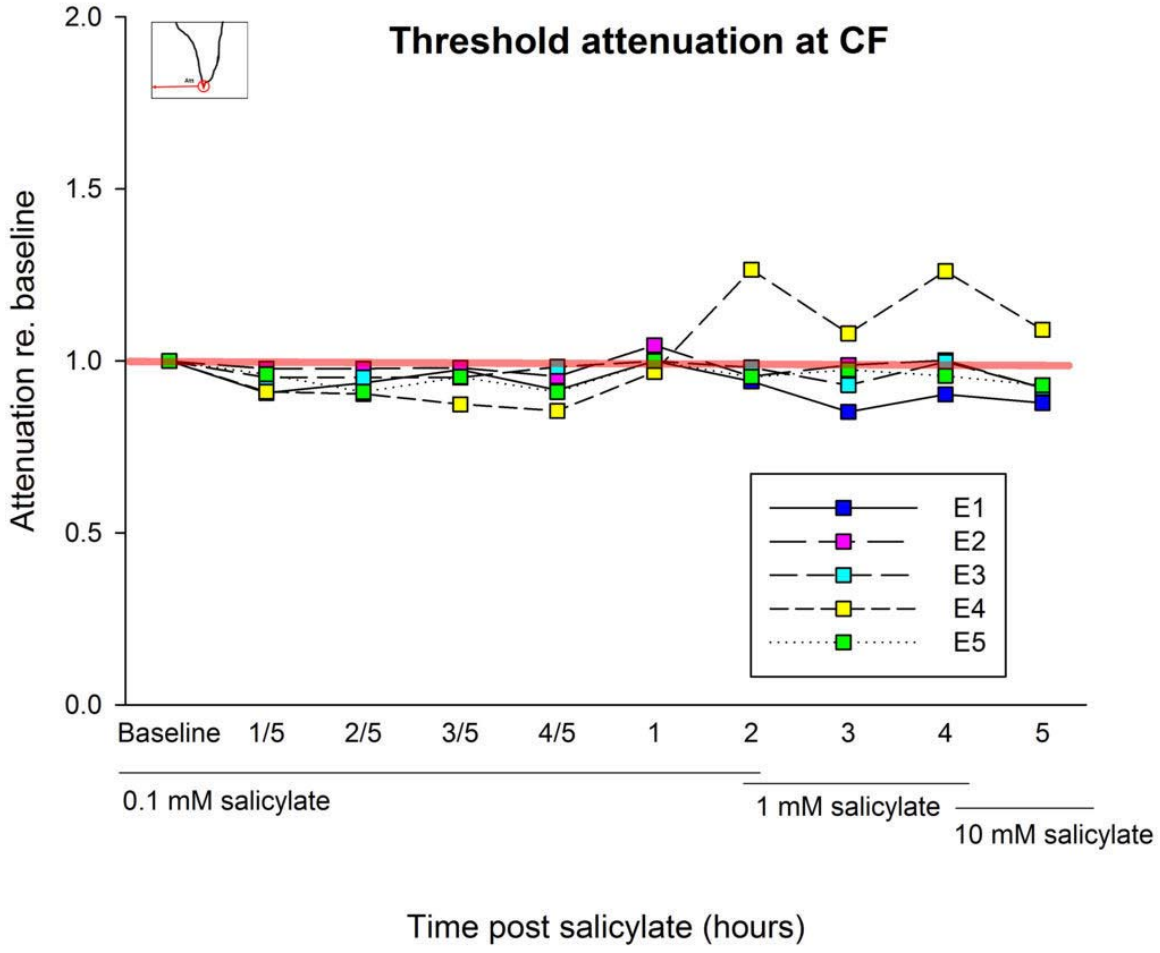

Figure 5-32 the coloured squares represent the attenuation level for each electrode location averaged across all animals, on which the CF was obtained. The attenuation level is expressed as a ratio to baseline, indicated by the red line.

Local salicylate induces areas of increased activity in FRA

Local perfusion of salicylate induced marked changes in the FRA as shown in the example (Figure 5-28). Areas of increased activity were observed within the FRA in response to salicylate. The ANOVA revealed a significant linear relationship ($F(1,2) = 18.53 = 0.049$, $\eta^2 = 0.86$) with the regression analysis showing a positive β coefficient indicating a positive linear relationship. Note that the x-axis is not linear, the first hour is broken down into 12 minute blocks to highlight any early effects. No further polynomial relationship for the number of pixels in which activity increased was observed for either the electrode or the time x electrode interaction term. The increasing linear relationship is clearly visible in Figure 5-33 and Figure 5-34, these figures also illustrate the almost immediate onset of the effect. Effects are apparent twelve minutes after the onset of the salicylate perfusion. Having established that salicylate perfusion induced regions of increased activity in the FRA, the magnitude of this increase was then examined.

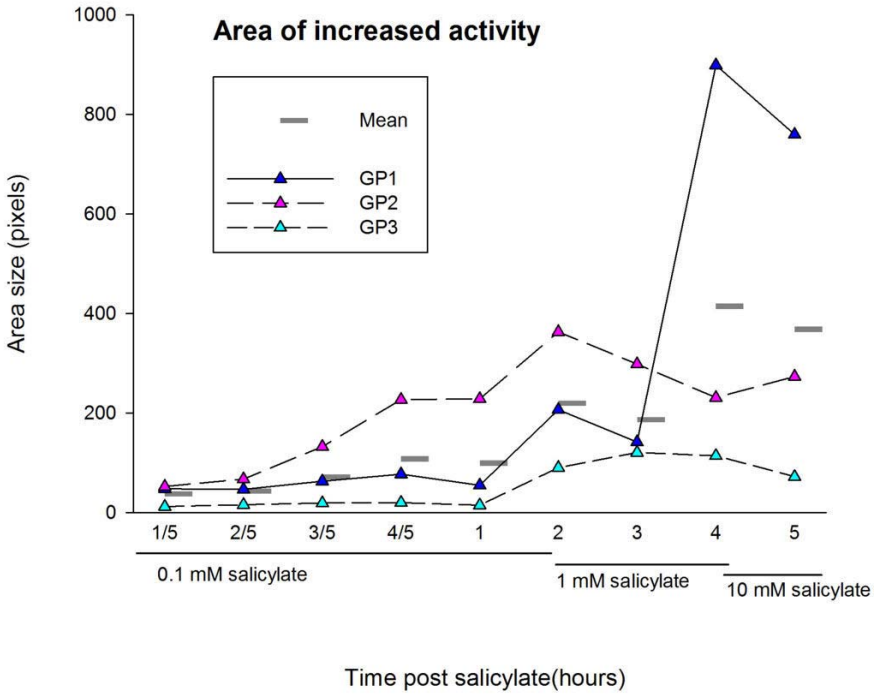

Figure 5-33 the coloured triangles represent the areas of increased activity in pixels averaged across all electrodes for the individual animals at the different time points. The grey bars indicate the mean across animals at each time point. Note the non-linear x-axis depicted the first hour in 12 minute blocks to allow for visualisation of rapid onset effects

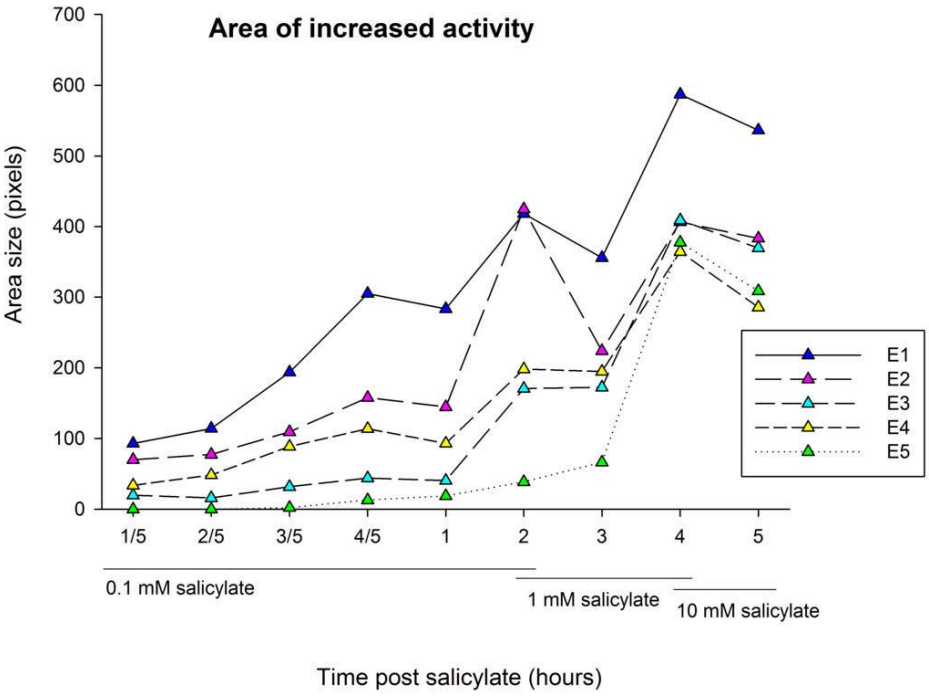

Figure 5-34 the coloured triangles represent the size of the area of increased activity averaged across the animals but plotted for the different electrode locations. Note the non-linear x-axis depicted the first hour in 12 minute blocks to allow for visualisation of rapid onset effects

Magnitude of increased activity grew over time

Salicylate caused the magnitude of the activity increase to grow rapidly within twelve minutes but kept increasing steadily afterwards indicated by a linear relationship ($F(1,2) = 22.50$, $p = 0.042$, $\eta^2 = 0.92$) with a positive β coefficient indicating a constant increase. Note that the x-axis is not linear. No further significant polynomial effects for either electrode location or the interaction effect were observed. Figure 5-35 and Figure 5-36 show that most of this rise in magnitude takes place within the first twelve minutes of 0.1 mM salicylate administration. Note that increasing the dose a hundred fold did not result in any further increase in magnitude.

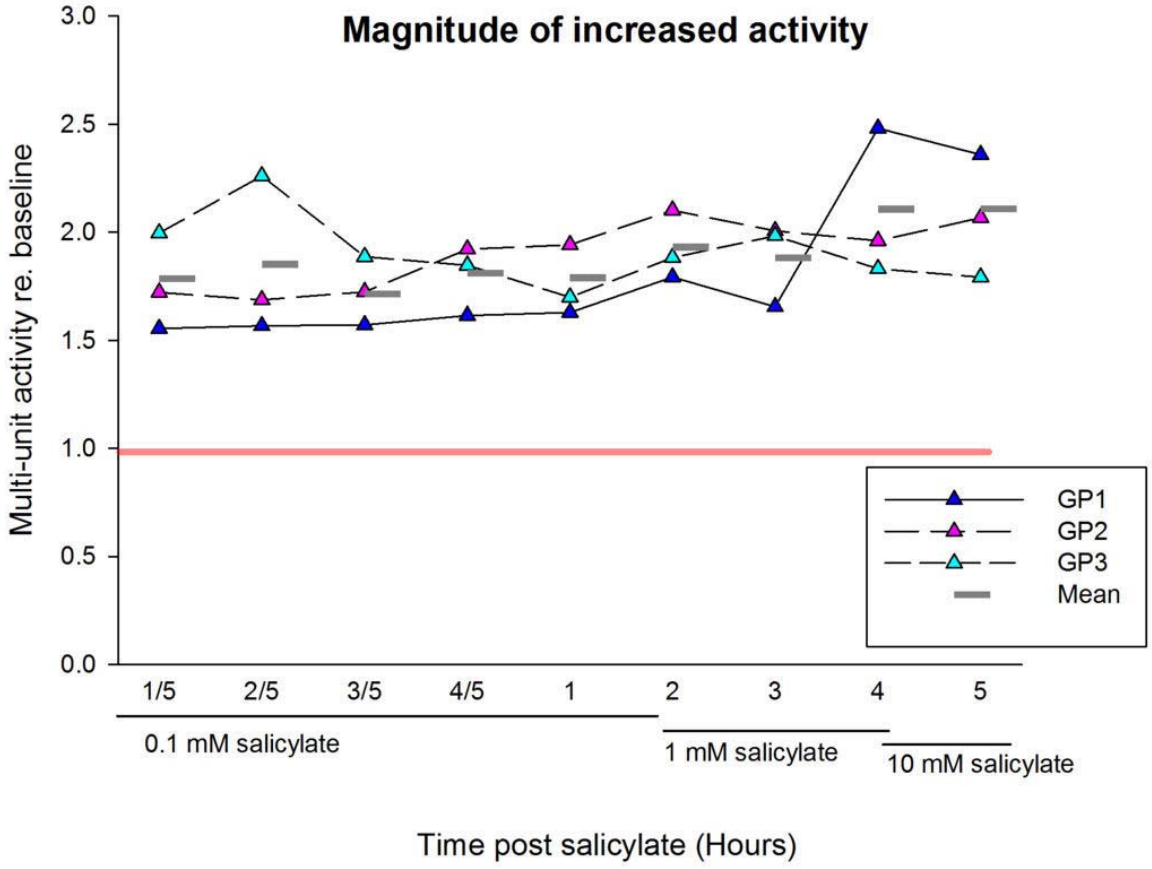

Figure 5-35 the coloured triangles indicate the magnitude of the increased activity for the individual animals, averaged across all electrodes, compared to baseline, indicated by the red line. The grey bars show the mean across all animals for each time point. Note the non-linear x-axis depicted the first hour in 12 minute blocks to allow for visualisation of rapid onset effects

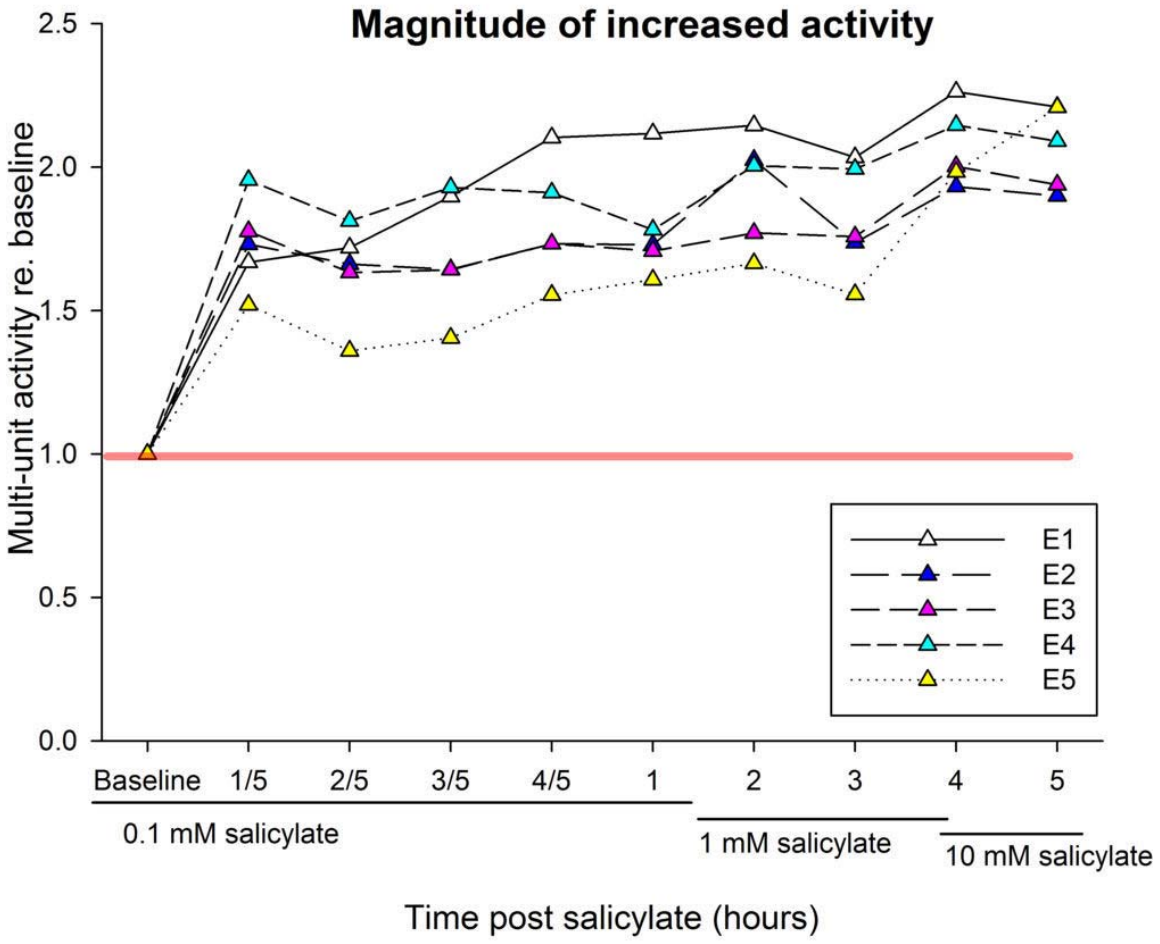

Figure 5-36 the coloured triangles indicate the magnitude of the increased activity for the different electrode locations, averaged across all animals, compared to baseline, indicated by the red line. Note the non-linear x-axis depicted the first hour in 12 minute blocks to allow for visualisation of rapid onset effects

Local salicylate does not trigger the development of areas of decreased activity

Local perfusion of salicylate did not trigger systematic areas of decreased activity in the FRA. In Figure 5-37 it is quite clear that areas of decreased activity only appear in one animal. Visual inspection of the other two animals do reveal a few unconnected pixels where there was a reduction in activity but these did not pass the connectivity protocol, which required 5 or more connected pixels to pass the threshold of being decreased substantially from baseline. Except for this one animal, no systematic areas of decreased activity were observed when salicylate was perfused via the dialysis probe, therefore no statistical testing was done on this data.

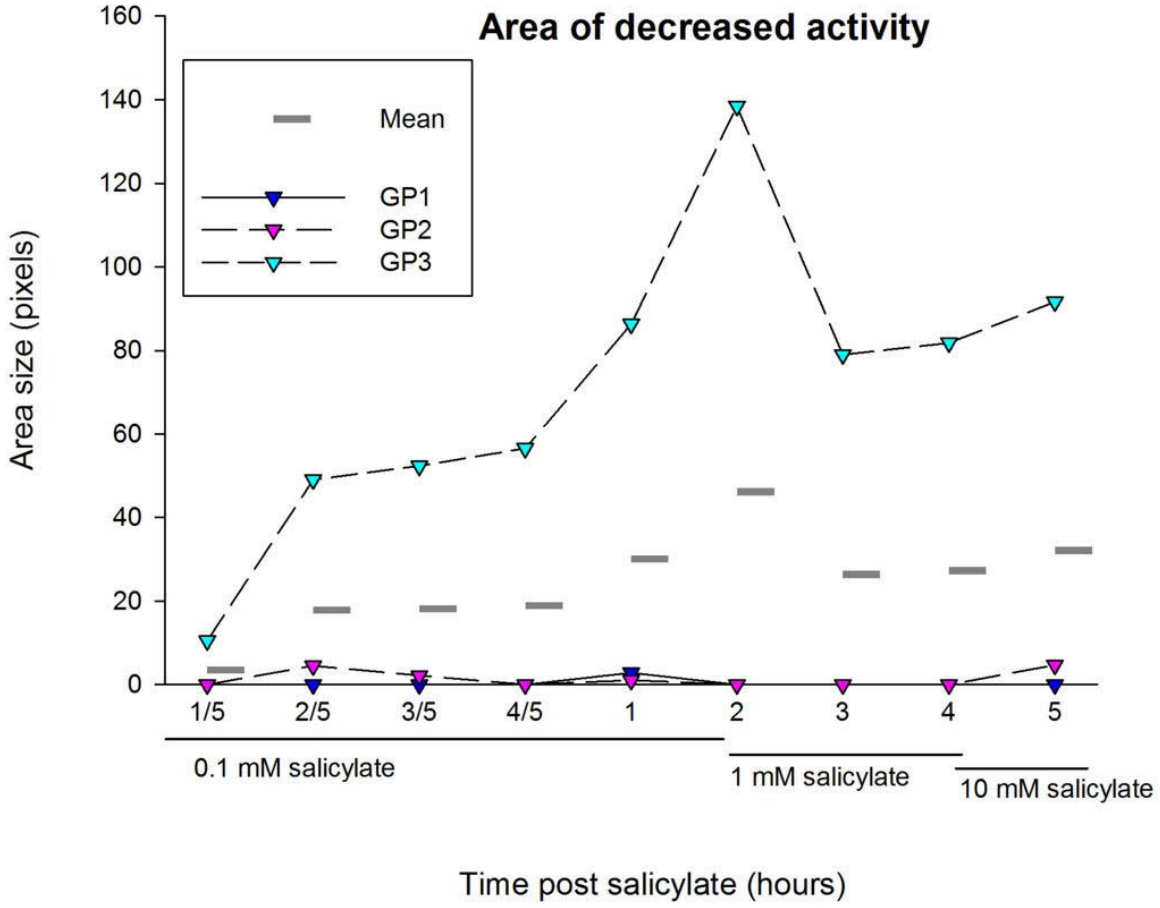

Figure 5-37 the triangles represent the number of connected pixels that show reduced activity for each individual animal averaged across all electrodes. The grey bars represent the mean across all animals. Note the non-linear x-axis depicted the first hour in 12 minute blocks to allow for visualisation of rapid onset effects

Local salicylate decreases the spontaneous activity

Spontaneous activity showed a complex change in response to local administered salicylate. Both a linear and a cubic trend were detected for time post salicylate perfusion. The linear relationship ($F(1,2) = 28.88$, $P = 0.033$, $\eta^2 = 0.94$) with a negative β coefficient indicating a decline and the cubic trend ($F(1,2) = 45.55$, $p = 0.021$, $\eta = 0.96$) suggesting an inflexion in the data. No further polynomial trends for electrode location or interaction were found. In Figure 5-38 and Figure 5-39 the complex response is visible. An initial short lived increase in spontaneous activity was followed by a long lasting decrease in spontaneous activity that remained unchanged when the concentration of salicylate is increased a hundred fold.

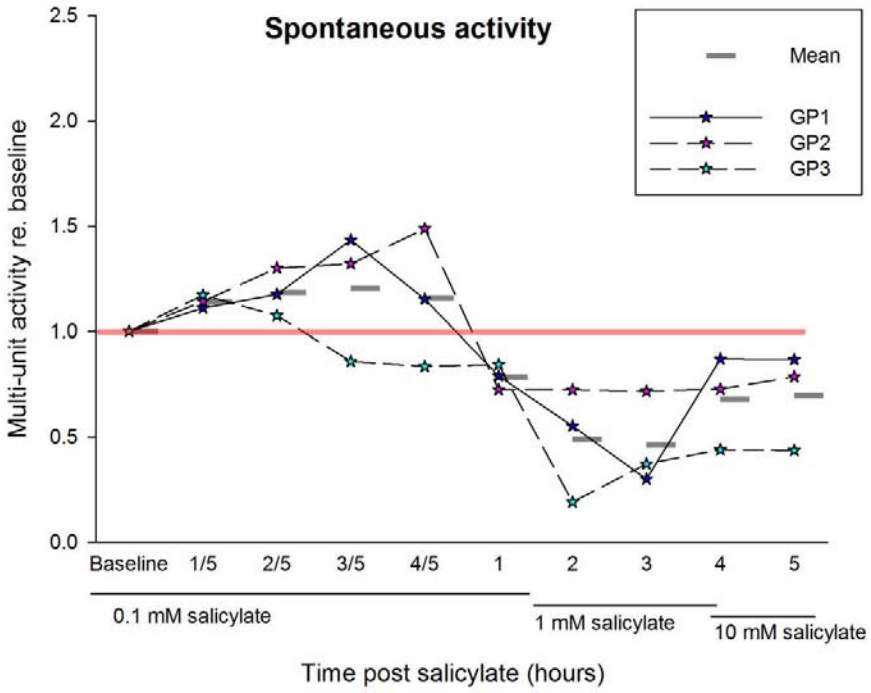

Figure 5-38 the stars represent the spontaneous activity averaged across all electrodes per animal as a ratio to baseline, indicated by the red line. The grey bars represent the mean across all animals. Note the non-linear x-axis depicted the first hour in 12 minute blocks to allow for visualisation of rapid onset effects

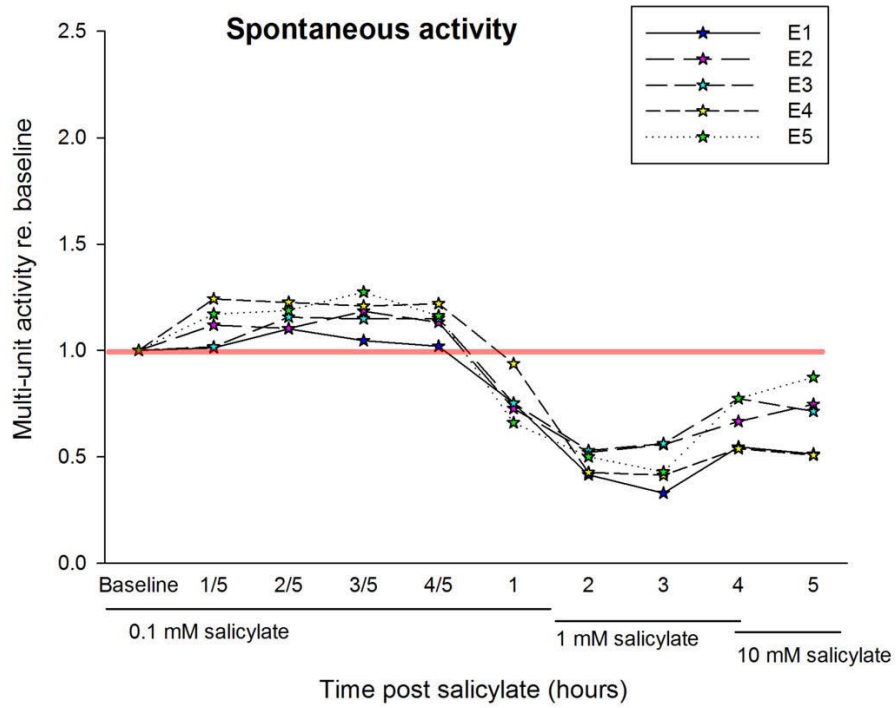

Figure 5-39 the stars represent the spontaneous activity for on the different electrode locations averaged across all animal as a ratio to baseline, indicated by the red line. Note the non-linear x-axis depicted the first hour in 12 minute blocks to allow for visualisation of rapid onset effects

PSTH measures

Local salicylate reduces driven activity at high sound levels

The total driven activity at 30 dB attenuation was reduced over time in response to the local perfusion of salicylate. A significant linear relationship ($F(1,2) = 135.90$, $p = 0.007$, $\eta^2 = 0.99$) was detected, the regression analysis showed a negative β coefficient indicating a decrease in overall sound driven activity over time. No further polynomial relationships for electrode location or the interaction effect were observed. The activity elicited in response to the CF stimuli are plotted as a ratio to baseline in the Figure -5-40 and Figure 5-41.

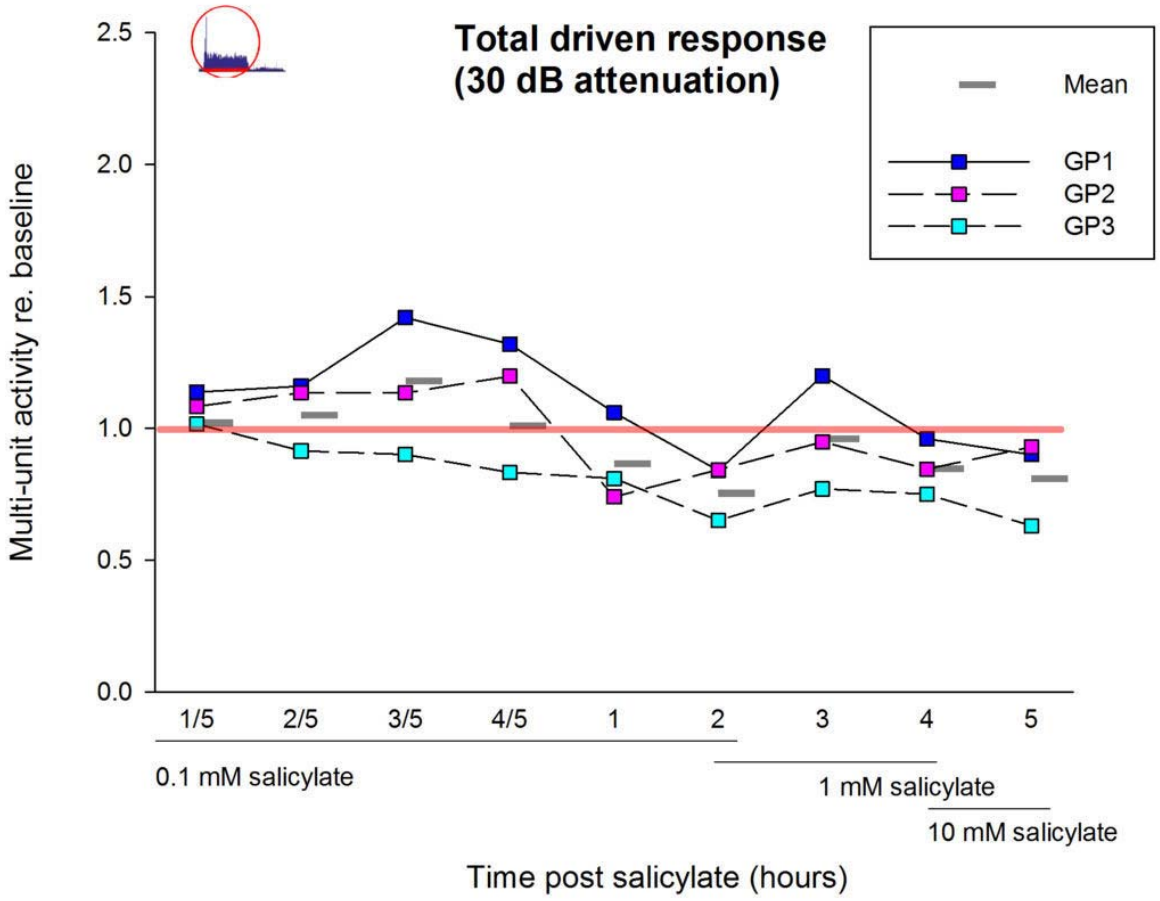

Figure -5-40 The individual squares represent the sound driven activity compared to baseline for the individual animals averaged across electrodes. The baseline is indicated by the red line. The grey bars show the mean across all animals. Note the non-linear x-axis depicted the first hour in 12 minute blocks to allow for visualisation of rapid onset effects

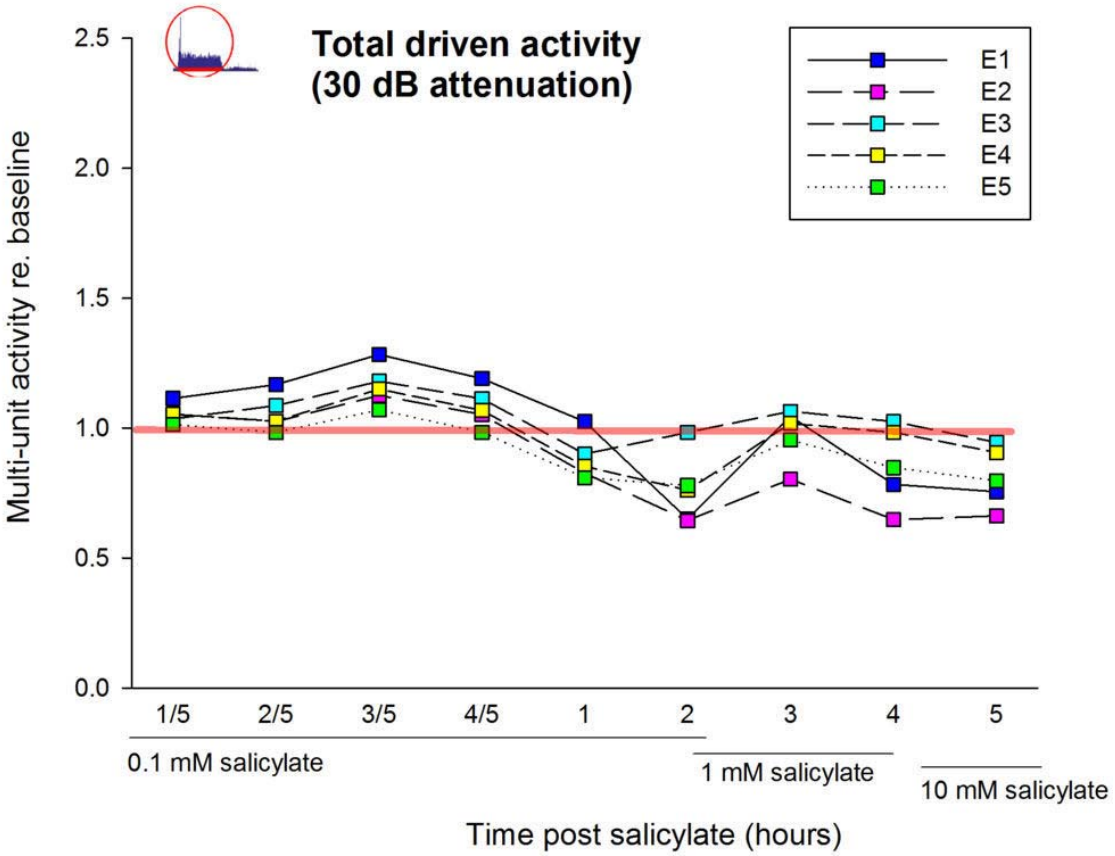

Figure 5-41 the individual squares represent the sound driven activity for the different electrode locations averaged across the animals. The baseline is indicated by the red line. Note the non-linear x-axis depicted the first hour in 12 minute blocks to allow for visualisation of rapid onset effects

Local salicylate has no effect on onset activity at high sound levels

Although local salicylate decreased total driven activity, there was no effect on the onset activity No linear, quadratic or cubic relationship was detected in response to local salicylate. There was no main effect for time, electrode or interaction effect. Figure 5-42 shows the onset response displayed as a ratio to baseline for each time point for each animal averaged

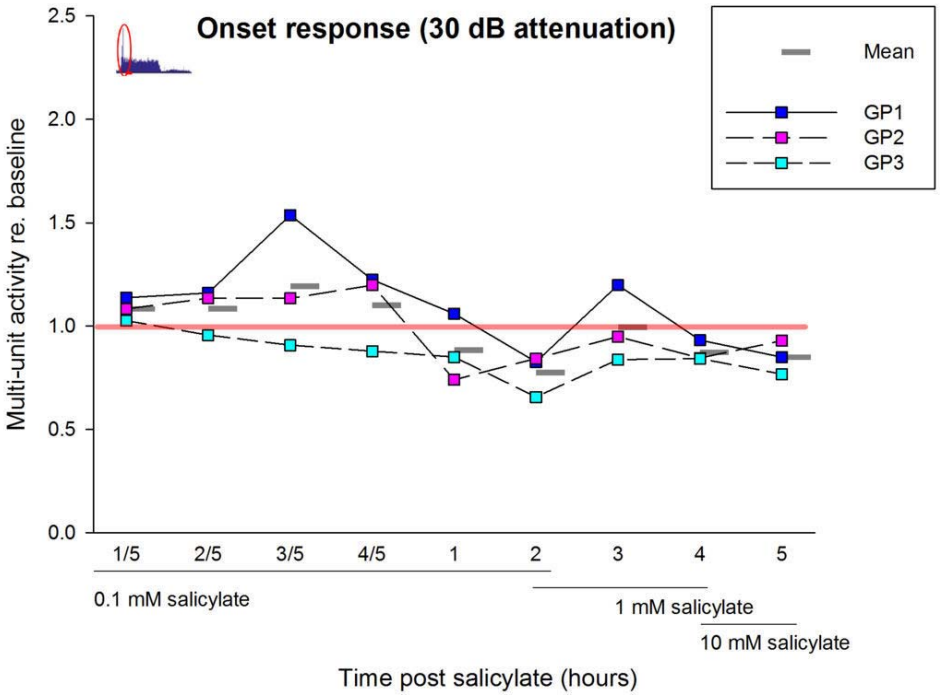

Figure 5-42 PSTH onset as a ratio to baseline, displayed for the individual animals averaged across electrode location. The red line indicated the baseline. The grey bar shows the mean value across animals. Note the non-linear x-axis depicted the first hour in 12 minute blocks to allow for visualisation of rapid onset effects

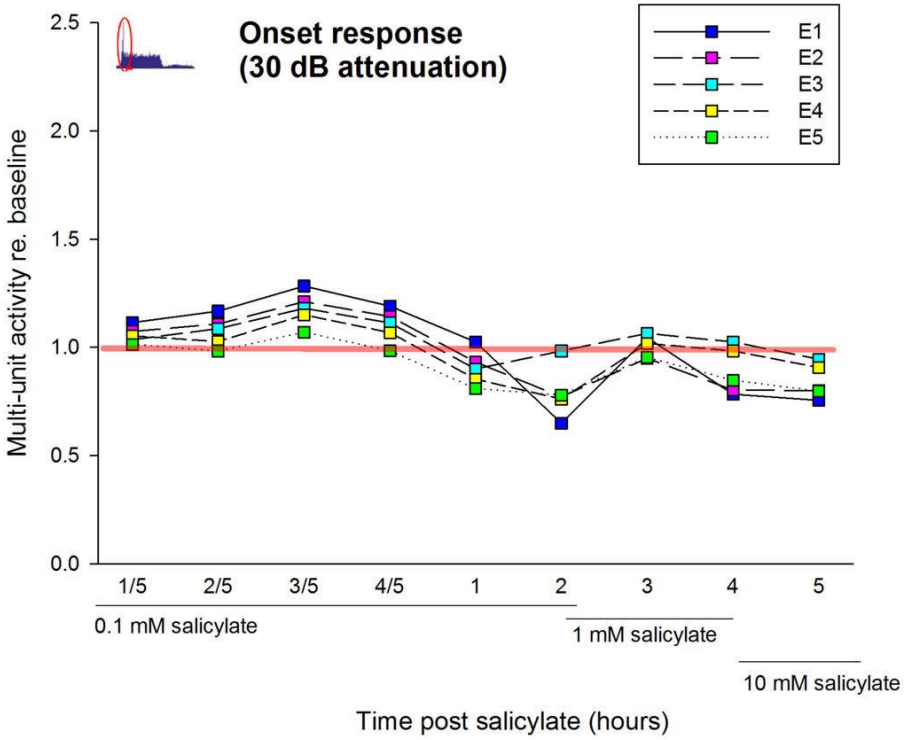

Figure 5-43 PSTH onset as a ratio to baseline, displayed for the different electrodes averaged across animals. The red line indicated the baseline. Note the non-linear x-axis depicted the first hour in 12 minute blocks to allow for visualisation of rapid onset effects

Local salicylate decreased total driven activity in low sound levels

In the high attenuation condition a decrease in the total driven activity was observed in response to local perfused salicylate. A statistical linear relationship for time was detected ($F(1,2) = 98.82$, $p = 0.010$, $\eta^2 = 0.98$) the regression shows a negative β coefficient, indicating a decrease in sound driven activity due to salicylate being perfused in the IC. No further polynomial relationships were observed for electrode location or interaction. In Figure 5-44 and Figure 5-45 the sound driven activity is plotted as a function of time after starting the perfusion of salicylate. No statistically significant differences were observed for the different doses of salicylate perfused.

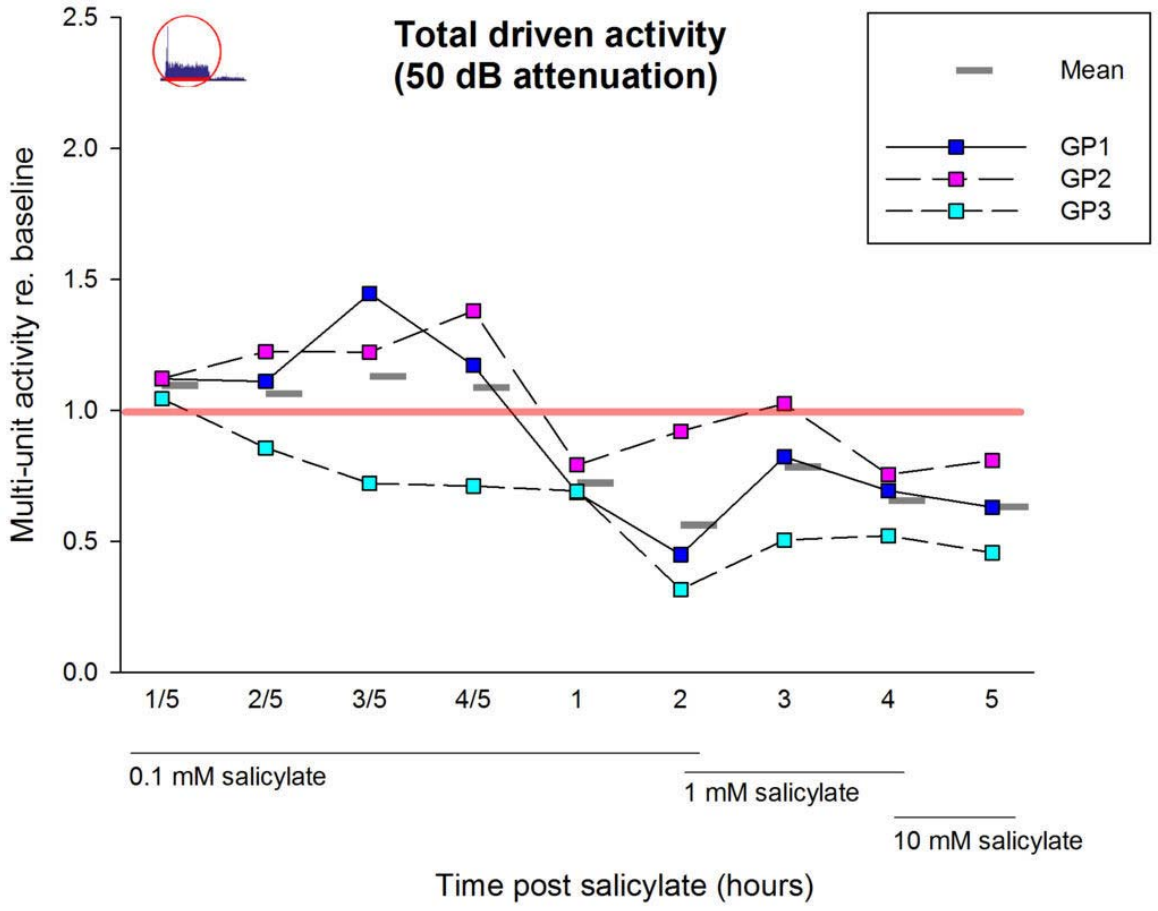

Figure 5-44 the sound driven activity is plotted for each animal averaged across all electrodes as ratio to baseline, the red line marks the original baseline activity. The grey bars indicated the mean change across animals. Note the non-linear x-axis depicted the first hour in 12 minute blocks to allow for visualisation of rapid onset effects

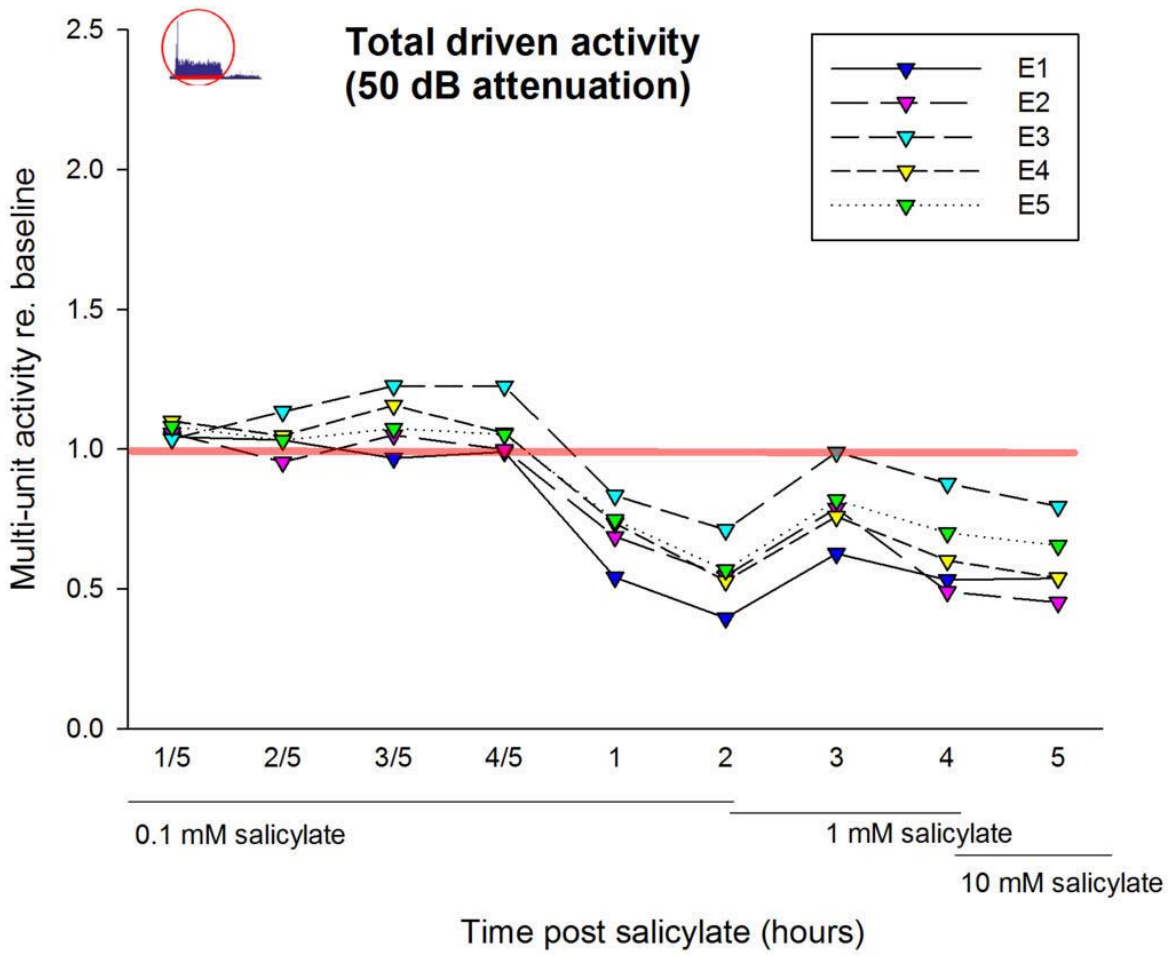

Figure 5-45 the sound driven response on each electrode averaged across the animals as a ratio to baseline, marked by the red line. Note the non-linear x-axis depicted the first hour in 12 minute blocks to allow for visualisation of rapid onset effects

Local salicylate decreases the onset activity

A decrease in the onset activity in response to local perfusion of salicylate was detected. A significant non-zero linear relationship ($F(1,2) = 19.67$, $p = 0.047$, $\eta = 0.91$) with a negative β coefficient from the regression analysis was obtained for the onset activity. No further polynomial relationships were obtained suggesting only time of salicylate perfusion influenced the onset peak. In Figure 5-46 and Figure 5-47 activity during the onset peak is plotted as a function of time averaged across electrodes and animals. The decrease lasts for several hours and does not change when the salicylate dose is increased a hundredfold.

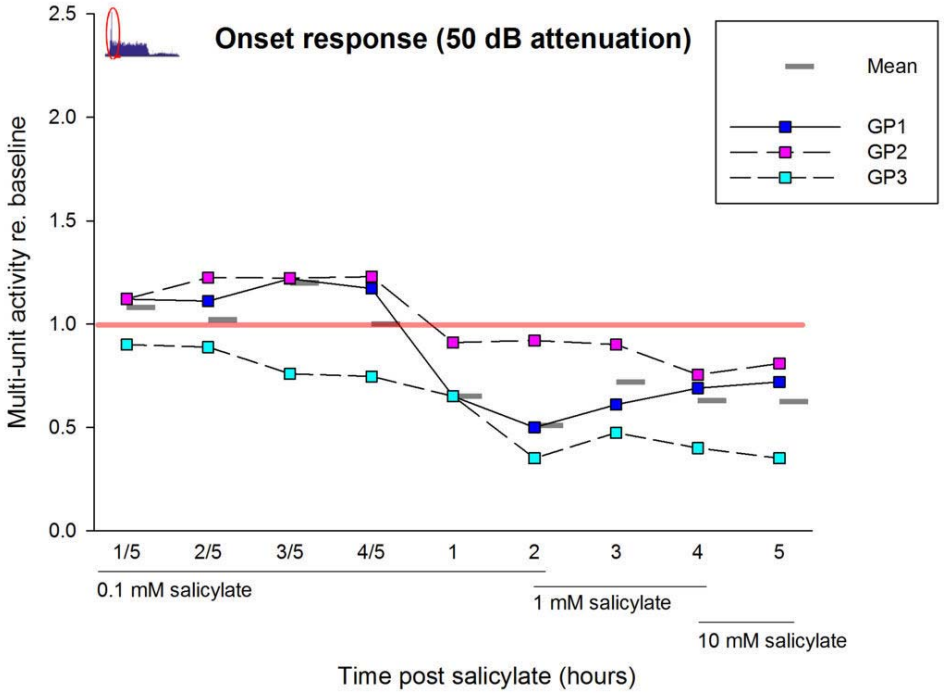

Figure 5-46 PSTH onset activity plotted as a ratio to baseline across electrodes, the baseline is indicated in red. The grey bars indicate the average across all animals. Note the non-linear x-axis depicted the first hour in 12 minute blocks to allow for visualisation of rapid onset effects

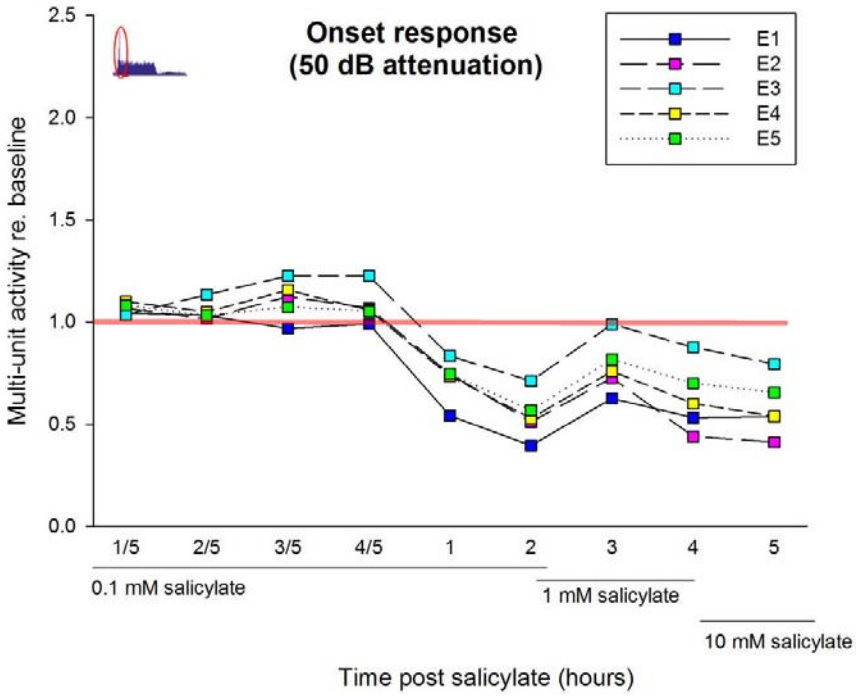

Figure 5-47 PSTH onset activity plotted as a ratio to baseline across animals, the baseline is indicated in red. Note the non-linear x-axis depicted the first hour in 12 minute blocks to allow for visualisation of rapid onset effects

5.3.3 Local Salicylate and Nitric Oxide

In three of the animals that received local salicylate perfusion, the NOS blocker L-MeArg was co-perfused direct into the IC, three hours after the L-MeArg perfusion was started. These data were analysed with two-way mixed design ANOVA where the presence of L-MeArg was entered as a between subjects factor. No interaction effects between the presence of L-MeArg and time post salicylate were detected for the characteristic frequency change, the development of areas of increased or decreased activity, nor for the magnitude of change in either direction or for the increase in spontaneous activity. L-MeArg did not modulate any of the effects of local salicylate.

5.4 Discussion

In this Chapter, I present evidence from two different experiments to further our understanding of the changes that occur in the IC during the course of salicylate-induced tinnitus. Firstly, the data obtained from the systemic administered and locally perfused salicylate aimed to disentangle the direct and indirect effects salicylate has on neuronal processes in the inferior colliculus. Secondly, I tried to establish a possible link of salicylate acting on the NMDA receptor and possible NO signalling cascade.

5.4.1 Summary

Systemically administered salicylate had three effects, an increase in spontaneous activity, an increase in acoustically evoked activity and an upward shift of the CF. Both, the increase in sound-driven activity and the upward shift of the CF were also seen when salicylate was locally perfused, suggesting that that these effects are at least partly mediated within the IC. In contrast, local perfusion of salicylate in the IC resulted in a decrease in spontaneous activity suggesting that the increase in spontaneous activity observed in the systemic experiments does not originate from the IC. The systemic salicylate experiments reported here extend the previous experiments about salicylate effects on auditory processing in the IC. In contrast to these earlier studies where single units were collected before and after salicylate treatment in the experiments reported here the same multi-unit activity was recorded before and up to seven hours after the systemic salicylate administration. This makes it possible to map the development of salicylate-induced effects over time, providing a unique window into the changes in neuronal activity observed in the IC.

5.4.2 Limitations

Some methodological limitations concerning the studies here need to be addressed. For the salicylate experiments the initial systemic dose chose was based on the literature reporting doses between 150 mg/kg up to 450 mg/kg (Jastreboff and Sasaki, 1986; Jastreboff *et al.*, 1988; Yang *et al.*, 2007; Sun *et al.*, 2009; Stolzberg *et al.*, 2012). In the pilot experiments leading up to the current study, I found that higher levels >350 mg/kg of Salicylate led to the premature death of the animal. For practical and ethical reasons the dose of salicylate used was kept below this, in our animals, and set at 200 mg/kg. This dose has been used by several other studies and reliably showed behavioural effects of tinnitus (Kenmochi and Eggermont, 1997; Eggermont and Roberts, 2004; Roberts *et al.*, 2010; Eggermont and Roberts, 2015) as well as increases in spontaneous activity in auditory structures (Kenmochi and Eggermont, 1997; Eggermont and Kenmochi, 1998; Yang *et al.*, 2007; Roberts *et al.*, 2010; Stolzberg *et al.*, 2012; Eggermont and Roberts, 2015). To prevent respiratory arrest the animals were artificially respired with 100% medical oxygen.

The concentration of salicylate that gets into the brain and the IC in these systemic salicylate experiments is not known. Salicylate uptake rates differ between tissues and the uptake into the brain is especially slow due to salicylate having a low lipid solubility at physiological pH levels, thereby hindering the crossing of the blood brain barrier (Bannwarth *et al.*, 1986). The strong binding of salicylate to the protein albumin is another rate limiting factor for salicylate in reaching the brain (Reed and Palmisano, 1975; Jastreboff *et al.*, 1986). The half-life permeation from plasma levels to the cerebrospinal fluid is about two hours (Brodie *et al.*, 1960). There is a marked difference between species where it concerns the binding of salicylate to serum proteins. Guinea pigs display high salicylate binding to the serum albumin, while rats, mice and dogs display a much lower plasma binding (Sturman and Smith, 1967). Meaning that permeation of salicylate into the brain will be slower for guinea pigs compared to rats. Manabe et al. (1997) observed salicylate levels in guinea pigs rising and declining over the course of 10 hours back to baseline levels. They established a direct link between the spontaneous firing rate and the serum concentrations of salicylate in that they rise and fall at similar rates.

Because the concentration of salicylate in the IC is unknown for the systemic experiments it is impossible to directly compare whether the concentrations of salicylate directly perfused into the IC are comparable. However, the local perfusion experiments started out with low concentrations which were increased over time, thereby gathering responses to a range of

concentrations. Regardless of whether the concentrations were comparable, the studies show similar effects in several measures, suggesting that these can be attributed to direct effects of salicylate on neuronal processing in the IC. Whereas the effects that differed between the local and systemic applied salicylate, most notably the spontaneous activity, suggest that these effects arise elsewhere in the auditory pathway.

The question arises to what extent the local salicylate perfusion remains 'local' Extensive perfusion over the course of several hours with incremental concentrations could potentially lead to salicylate leaking out of the IC and affecting other brain regions or organs. No measurements of salicylate blood plasma levels were conducted in either the systemic or local salicylate experiments, so direct comparisons cannot be made, however, the total amount of salicylate administered in the local application is low. The four syringes containing 0.1 mM, 1 mM, 10 mM salicylate and 10 mM + 1 mM L-MeArg together contain in total 8.44 mg of salicylate. Even if we assume that all that salicylate dialysed into the IC and into the animal's circulation, the dose would still be a 25 times lower than the systemic administration and well below the 50 mg/kg dose which has been shown to have no tinnitus inducing effects (Stolzberg *et al.*, 2012).

The sound driven activity which was found to increase in the FRA analysis failed to show consistent changes in the PSTH analysis which seems contradictory. However, this can be accounted for by the way the data was collected and analysed. The electrode was placed in the IC to record across the tonotopic laminae, thereby recording units with similar, but not exactly the same, range of CFs in every animal. To compare between animals the electrodes giving the highest number of spikes in the baseline condition to the set frequencies 256, 512, 1024, 2048 and 4096 were selected. This resulted in the selection of electrodes recording units with CFs close to these frequencies, but not necessarily the same CF. The fact that areas of decreased activity where usually observed on the lower frequency side of the CF whilst the areas of increased activity had the largest magnitude on the high frequency side of the CF leads to problems in this analysis. If the electrode selected for a set frequency had a CF higher than the set frequency the PSTH results were likely to be collected from an area of decreased activity whilst if the unit had a CF lower than the set frequency the reverse was true. This phenomenon is illustrated in Figure 5-48. Owing to this, the data showed great variability between animals and electrodes within animals because the different electrodes within one animal could belong to either group, therefor for the PSTH data in salicylate experiments more electrodes would need to be extracted and calculated and matched up based on a units CF and not the set frequencies.

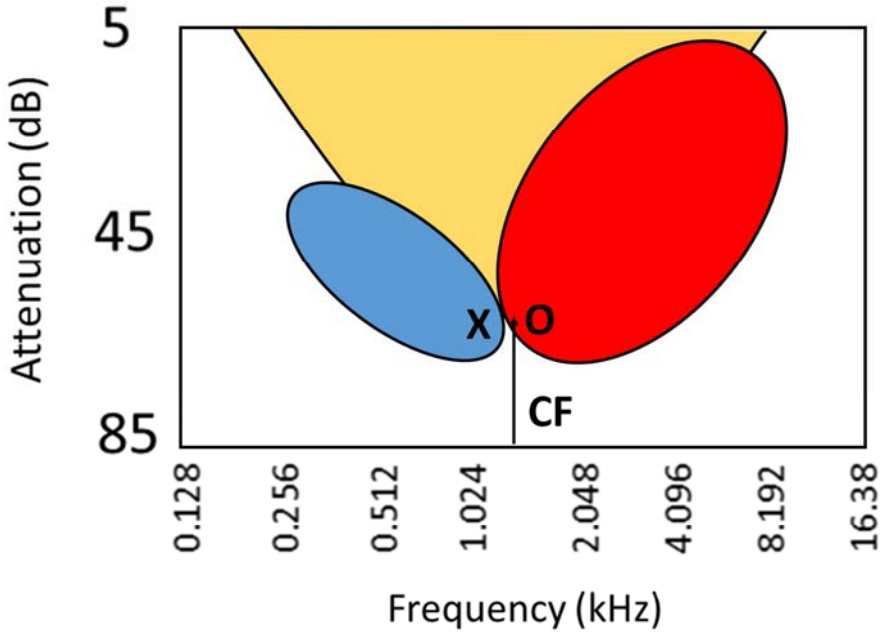

Figure 5-48 cartoon illustrating how units with slightly different CFs could give variable results in the PSTH analysis. Yellow indicates the normal FRA area. Blue is the hypothesized area of decrease and red is the area of increased activity due to salicylate, both are often observed in these regions relative to the CF. Because PSTH were sampled at set frequencies and not the CF of the units they could be sampled from below or above the CF of a unit. X indicates a unit with a CF higher than the set frequency and results in a decrease of activity. O indicates a unit that has lower CF than the set frequency and results in an increase in activity.

Finally the fact that the blocking of NO production by co-perfusing L-MeArg with salicylate did not result in a modulation of the obtained local salicylate effects could be due to methodological issues. The L-MeArg was not perfused into the IC until 5 hours of salicylate in increasing concentrations were perfused in the IC. Salicylate might be potent at triggering processes that cannot be halted once activated, or the L-MeArg concentration was not high enough to overcome the effects of salicylate. Although, the L-MeArg concentration used had been shown to be effective in the NMDA experiments.

Not being able to find any results for the NO modulating drugs in attempting to manipulate the local salicylate-induced effects might reflect the problem that the statistical power of the current studies was low due to the number of animals used per experimental group, especially in the local salicylate experiments. Also, the number of channels extracted was limited because the tools for processing the complete dataset were not fully developed at the time.

Even though the study had some limitations which will affect the scope of the findings none threaten the validity of the results. Some interesting observations were made in the systemic and the local administration of salicylate. Contrasting the two methods led to new insights on where, in the auditory pathway, salicylate can exert its effects.

5.4.3 Systemic Salicylate Shifts the CF upwards but does Not Alter the Threshold Sensitivity

Systemic administration of salicylate increased the CF of the recorded multi-unit activity over time but the threshold sensitivity at CF remained unchanged. Local perfusion of salicylate in the IC did not result in an upward shift of the CF, it also did not affect the threshold sensitivity at CF. The segregation of these findings suggests that the mechanism causing this upward shift in CF does not reside in the IC. It seems unlikely that the CF change is an artefact of the experimental method because in none of the previously described NMDA experiments or in the current local perfusion experiments were changes in CF observed, suggesting that this finding is directly linked to salicylate acting in the auditory pathway but not directly on the IC tissue. This upward shift in CF of neurons has not been described before by previous studies, and likely has not been observed before because these studies could not track the activity from the same units over time. The upward shift in CF makes the neurons more sensitive to higher frequencies a finding that could very well underlie tinnitus, which is often characterised as a high frequency phenomenon.

5.4.4 Direct and Indirect Salicylate have Different Effects over a Range of Frequencies

The question as to what drives this shift in CF was addressed by analysing regions of decreased and increased activity in the FRAs. The regions of increased and the regions of decreased activity observed in the FRA represent changes over a wide range of frequencies and intensity levels. Interestingly, the increased and decreased regions do not occur uniformly across the entire FRA, but tend to have a relationship with the CF. Because they are different phenomena they will be discussed separately, although together they may underlie the shift of the CF.

Direct and indirect salicylate induce areas of increased activity

Both systemic and local administered salicylate result in regions of increased activity. In the systemic administration the regions of increased activity required three to four hours to form whereas the latency was much quicker in the local salicylate experiments. Thus strongly suggesting that this increase in activity is at least partially driven by the direct effects of salicylate on the IC. A finding that corresponds with previous research showing increased metabolic activity in the temporal cortex and the inferior colliculi as a result of salicylate

induced tinnitus using PET and MRI in rats (Paul *et al.*, 2009). In the systemic salicylate conditions the increase in activity is seen in both sound driven and spontaneous areas of the FRA, whereas in the local salicylate condition the increases were largely confined to the sound driven region of the FRA (contrast the examples from Figure 5-9 and Figure 5-28). Another difference between the local and systemic salicylate conditions is the fact that the magnitude of the response continued to increase over several hours in the systemic salicylate condition, whereas in the local perfusion the magnitude of the increase reached a plateau with the lowest dose of salicylate. Further increases of the concentration of salicylate perfused did not alter the magnitude of the increase. The observed difference between the two conditions could be due to salicylate acting on one or more structures (including the cochlea) in the auditory pathway prior to the IC, in the systemic condition. Alternatively, the concentration of salicylate getting into the IC may have been higher in the systemic condition.

Systemic salicylate induces areas of decreased activity

Areas of decreased activity appear rapidly, within the first hour after the systemic administration of salicylate, but are virtually absent in the local perfusion of salicylate. The fact that the onset is so quick and that the maximum size of these regions of decreased activity is reached within the first hour of systemic salicylate administration suggests that this effect is mediated outside of the IC because, due to the relatively slow uptake of salicylate and time it takes for salicylate to cross the blood brain barrier (Brodie *et al.*, 1960) it is likely that there is no salicylate present in the neuronal tissue of the IC during this first hour. Even more compelling evidence for the cause of decreased activity to lie outside of the IC is the segregation of findings between the local and systemic administration of salicylate.

The areas of decreased activity are largest during the first hour after salicylate administration and start shrinking fast. Although the number of frequencies (expressed as an area in the FRA) declines within the second hour leaving only a few small regions in place, the magnitude of the decrease within the remaining regions remains constant.

5.4.5 Spontaneous Activity

In agreement with previous studies, a systemic high dose of salicylate causes an increase the spontaneous discharge of neurons in the central nucleus of the IC (Jastreboff and Sasaki, 1986; Jastreboff *et al.*, 1988; Ma *et al.*, 2006; Berger *et al.*, 2013). In those previous

experiments it was not possible to record activity from the same neurons over the prolonged periods of time required. Activity was recorded from a set of neurons and there was then a delay for a couple of hours to let the salicylate take effect before the responses were measured from another group of cells. From behavioural experiments, we know that behavioural correlates of tinnitus can be perceived two hours after the salicylate treatment in guinea pig and rats (Kizawa *et al.*, 2010; Berger *et al.*, 2013). The current protocol allowed me to track the multi-unit activity at multiple sites as a function of time after salicylate was given. The current experiments replicated the previously reported findings of increased spontaneous activity in the central nucleus of the IC following systemic administration of salicylate. The figures show a gradual increase of spontaneous activity over time post salicylate treatment. Interestingly the other measures obtained in the current experiments showed different time scales, suggesting different points of origin in the auditory pathway.

From the previous studies we know that this increase in spontaneous activity appears to be restricted to activity in the auditory pathway and not to be a general effect that salicylate has on all neurons in the brain. Recordings in the cerebellum showed no increase in the spontaneous activity under the same conditions (Jastreboff *et al.*, 1988). The observation of increased spontaneous activity in the auditory brain stem structures and the IC has often been replicated but no real progress has been made in disentangling whether the observed increase is due to direct effects of salicylate on neurons in the IC or reflect the effects of salicylate at other levels of the auditory system including the cochlea. Previous slice electrophysiology studies have suggested a sensitivity of the IC to direct effects of salicylate. These studies show that 70% of the neurons in the CNIC increase their spontaneous firing rate, while 17% decreased their firing rate (Basta and Ernst, 2004) when the slice is superfused with salicylate.

In contrast to the systemically administered salicylate, the local perfusion of salicylate in the IC in the current experiments reduced the spontaneous activity in the IC. This finding appears to contradict a previous iontophoresis study which reported that local iontophoresis in the dorsal cortex of the IC leads to increased spontaneous activity (Patel and Zhang, 2014). Iontophoresis, is limited to only delivering to the tissue immediately surrounding the probe and can therefore not be used to study population effects. Also, the neurons in the dorsal cortex have different functions and networks from those in the central nucleus. However, close inspection of my graphs shows that immediately after switching on the salicylate perfusion a short lived increase in spontaneous activity can be observed, which declines within the first hour. This increase appears to be small and in order to substantiate

these findings more electrodes from the early time points will need to be extracted to obtain higher statistical power. The observed decrease of spontaneous activity in response to the direct perfusion of a low dose of salicylate starts to return to baseline when the concentration is increased a hundred fold to 10 mM. This suggests that salicylate in low doses may actually be beneficial because the decrease of spontaneous activity and the increase in sound driven activity effectively increases the signal to noise ratio in the brain

5.4.6 Driven/Onset activity at 50 and 70 dB SPL

Systemic administration of salicylate showed different effects on the sound driven response recorded in the PSTH data depending on the intensity level of the sound. PSTH analysis allows a temporal analysis of the response pre, during and after the stimuli. At high intensity levels the total number of spikes elicited by a stimulus near the CF was unchanged, but at low intensity levels, increases in activity were observed, which were comparable to the increases observed in spontaneous activity. The low intensity condition may have been close to threshold in some of the units recorded, and therefore been more susceptible to influences from spontaneous activity.

In the local perfusion conditions, decreases were observed for both the high and low sound intensity levels. Which again argues for the findings of increased activity observed in the systemic condition to have arisen elsewhere in the auditory pathway.

5.4.7 Blocking of NO Production does not alter Local Salicylate Effect

In the local perfusion of salicylate attempts were made to investigate to what extent blocking the NO pathway would have an effect on the salicylate effects. Unfortunately in the current set of experiments no evidence was observed for NO signalling meditating the direct actions of salicylate in the IC. However this absence of evidence may be due to a number of practical reasons that have been addressed above in the study limitations. Salicylate could have a wide range of direct effects on the NO signalling pathway. Salicylate has been shown to directly act on NMDA receptors in auditory centres (Guitton *et al.*, 2003; Ruel *et al.*, 2008; Hwang *et al.*, 2011) as well as directly alter the GABA receptors in the IC (Bauer *et al.*, 2000; Butt *et al.*, 2016), therefore absence of an effect in this study may be due to methodological issues.

5.4.8 Future Research

To make local and systemic experiments more comparable the measurements of serum concentrations of salicylate in the systemic salicylate protocols could be used. Knowing the serum concentration of salicylate in the hours post systemic administration will not directly tell us how much salicylate gets into the brain, but measurements obtained from the dialysate coming out of the probe can be used to estimate how much salicylate reaches the IC. Calculations between the plasma bound salicylate and salicylate in the IC at various time points could be correlated with changes in spontaneous activity, areas of increased or decreased activity or any of the other obtained measures.

To estimate how much salicylate is reaching the brain in the local perfusion protocols the concentration of salicylate in the dialysate coming out of the probe could be compared to the concentration going in, although the extent of perfusion would still be unknown, an attempt to ensure comparable concentrations in the systemic and local perfusion experiments would extend the current findings.

In the systemic salicylate experiments, the spontaneous activity observed appeared to decline near the end of the experiments, but no return of the CF to lower frequencies was observed. Extending the current experiments over longer time courses to confirm the decline of spontaneous activity and study whether the upward shift of the CF is maintained could help shed light on how these measures are related to tinnitus. Behavioural evidence of tinnitus in rats disappears between 24 - 72 hours (Ralli *et al.*, 2010; Stolzberg *et al.*, 2012) (Berger and Coomber, 2015), while the increase in spontaneous activity appears to decline much faster. Extending the duration of the experiments could disentangle these effects.

A more extended dose response curve for the perfusion of local salicylate in the central nucleus of the IC would help moving observations forward. The suggestions in the current experiments that low levels of salicylate might actually be beneficial in hearing could be studied in more detail. Also increasing the number of animals in these groups would help increase the statistical power to detect the more subtle effects of salicylate that may have been missed in the current studies. Establishing the effects of direct perfusion of lower concentrations of salicylate could then be used to study to what extent the NO signalling pathway is involved. The suggestion that low concentrations of salicylate may be beneficial in hearing by increasing the signal to noise ratio in local perfusion is interesting but would carry more weight if it could be replicated in systemic administration experiments.

Obviously, the doses administered would need to be reduced and possibly be administered chronically to take effect but if there is a true effect it has the potential to be beneficial.

Specific studies investigating where in the auditory pathway the effects not mediated by direct salicylate perfusion in the IC originate could be performed by leaving the recording probe in the central nucleus but having microdialysis probes perfusing salicylate in other auditory structures.

5.4.9 Conclusion

This chapter set out to obtain a better understanding of the effects of salicylate and determining which of these are direct effects on the IC and which arise from other sources.

The reported results confirm previous findings of increased spontaneous rate and sound-driven activity in response to systemic salicylate. Since salicylate applied locally in the IC decreased rather than increased spontaneous activity, I conclude that the elevation of spontaneous firing by salicylate is mediated outside the IC. Similarly, the initial effect of systemic salicylate in reducing sound-driven activity in a frequency-selective manner was not mirrored by locally applied salicylate and hence likely originates elsewhere. However, the finding that both locally applied and systemic salicylate raised the CF and increased sound driven activity, suggests that these effects are, at least in part, mediated directly within the IC.

Chapter 6. General Discussion

6.1 Summary

This thesis is concerned with the role NO signalling plays in auditory processing in the IC. Important structural and functional findings were presented that demonstrate new levels of complexity. The current findings will require us to reconsider the contribution of NO in auditory processing in the IC.

In Chapter 3 evidence from immunohistochemistry demonstrated for the first time the presence of nNOS in the central nucleus, a subdivision of the IC previously believed to exhibit little or no nNOS expression. Data in Chapter 4 demonstrated that the nNOS observed in the central nucleus is associated with, and directly influenced by the activity of the glutamate NMDA receptor. The potential role of nNOS in the central nucleus of the IC in tinnitus was the main topic of investigation in Chapter 5. This chapter provided new information about the direct and indirect effects of the tinnitus inducing drug, salicylate, on the IC. Although I was not able to demonstrate a direct link between salicylate-induced activity, presumed to be linked to tinnitus, and nNOS in the central nucleus, limitations in the study may account for this.

6.1.1 Anatomical Findings

Previous studies have demonstrated the abundance of nNOS, the main NO producing enzyme in the brain, in the IC in several species (Herbert *et al.*, 1991; Druga and Syka, 1993; Coote and Rees, 2008). These prior studies reported extensive nNOS or NADPH positive labelling in the lateral and dorsal cortex with relatively little or no expression in the central nucleus of the IC. The new evidence brought forward in Chapter 3 of this thesis demonstrates that with the development of more advanced immunohistochemistry protocols, newer immunofluorescent imaging techniques, and more widely available computing power, the presence of nNOS can be demonstrated in the central nucleus albeit its expression is markedly different compared to the cortices. In the cortices, nNOS is distributed throughout the cell's cytoplasm and labelling is seen in somata and dendrites. However careful inspection suggested that nNOS labelled puncta associated with the cell membrane were also present in these regions. In the central nucleus nNOS expression is virtually confined to puncta. These puncta in the central nucleus were shown to be associated with PSD95, a postsynaptic scaffolding protein that stabilises the NMDA receptor in the active zone of the postsynaptic membrane. Although the microscopy

techniques used did not allow me to determine whether nNOS and PSD95 are physically linked, the association of the nNOS puncta in the central nucleus and PSD95 strongly suggest that this nNOS is located postsynaptically and is likely part of the nNOS-PSD95-NMDA receptor complex.

Further studies in this chapter investigated the neurotransmitter phenotype of the cells expressing nNOS. A minority of the cells expressing either distributed and/or punctate nNOS were shown to have a GABAergic phenotype. Given that few cells in this region are neither GABAergic nor glutamatergic, the data suggest that the majority of nNOS expressing cells in the IC must be glutamatergic. Given the calcium dependence of nNOS, the co-expression of some calcium binding proteins in cells expressing nNOS was explored. Calbindin showed near complete co-localization with nNOS whilst calretinin was rarely found in nNOS positive cells. For parvalbumin the picture was more complex, some parvalbumin positive cells did show distributed nNOS expression in the ventral IC or punctate nNOS expression throughout the central nucleus but many parvalbumin positive cells showed no nNOS labelling. Based on these findings, nNOS cells can express calbindin or parvalbumin but not calretinin.

6.1.2 NMDA Receptor is Functionally Coupled to NO Acting on sGC

The finding that nNOS puncta are present in the central nucleus and are associated with PSD95 (and thus presumably the NMDA receptor) led to the functional studies in Chapter 4. First I sought to determine whether NMDA receptor activity is involved in auditory processing in the IC. The selective activation of this receptor by direct perfusion of NMDA via a microdialysis probe caused an increase in both spontaneous and acoustically-evoked activity in the central nucleus of the IC. Both effects were abolished when NMDA was co-perfused with the nNOS inhibitor, L-MeArg. Evidence substantiating the role of NO and giving further insight into the mechanism by which it operates came from the experiment in which NMDA was co-perfused with ODQ, a sGC blocker. Again the increase in neuronal activity caused by direct perfusion of NMDA was abolished by preventing the binding of NO to sGC. These two findings show that NMDA receptor stimulation can lead to an increase in both spontaneous and acoustically-evoked activity and that this is dependent on both the production of NO and its binding to sGC, thus implicating the involvement of the cGMP pathway. The virtually complete abolition of the NMDA effect suggests that NO acting on sGC is the sole mechanism underlying this effect. The local perfusion of L-MeArg and ODQ

in the absence of NMDA evoked no changes, suggesting that tonic NO transmission is low in the central nucleus of the IC at least in the anaesthetised guinea pig preparation.

6.1.3 Salicylate Exerts Direct and Indirect Effects on Processes in the IC.

Previous studies have demonstrated that increases in spontaneous activity are observed in the VCN, in animal models of tinnitus. In these animal models, the nNOS expression is also upregulated in the same auditory brainstem nuclei (Zheng *et al.*, 2006; Coomber *et al.*, 2015). In view of these findings and given the fact that the IC contains more nNOS expressing neurons than all auditory brainstem centres combined, even without considering the nNOS puncta observed in the central nucleus, it was hypothesised that tinnitus might be associated with upregulation of nNOS signalling in the IC. Mechanisms underlying the generation of the tinnitus percept are currently unknown and besides investigating a possible link between tinnitus and NO signalling, the studies described in Chapter 5 were aimed at furthering our understanding of the mechanisms underlying tinnitus. Here the high dose salicylate model of tinnitus was employed as a practical means to induce tinnitus acutely. High doses of salicylate have been shown to reliably induce transitory tinnitus in both humans and animals (Sée, 1877; Jastreboff *et al.*, 1988; Eggermont and Roberts, 2004; Yang *et al.*, 2007; Roberts *et al.*, 2010; Eggermont and Roberts, 2015). In order to determine which of the effects of salicylate occur directly in the IC, and which were likely to occur in lower (or higher) auditory centres, the effects of systemic administration and local perfusion of salicylate in the IC were compared. Systemically administered salicylate had three effects, an increase in spontaneous activity, and increase in acoustically evoked activity for higher frequencies and an upward shift of the CF. Both, the increase in sound-driven activity and the upward shift of the CF were also seen when salicylate was locally perfused, indicating that these effects are mediated directly within the IC.

6.2 Methodological Considerations and Future Research

6.2.1 Local Drug Delivery

For the questions addressed in this thesis, it was important that drugs were administered directly into the IC. In vivo delivery of drugs in a local fashion can be accomplished using iontophoresis, pressure injections as well as reverse microdialysis. The methodology employed in this thesis was reverse microdialysis because it has a number of advantages over the other two techniques.

1. Microdialysis allows for the examination of drug effects over extended periods of time. Iontophoresis is limited to the concentration of drugs that is preloaded in the barrels and concentrations of drug in the tissue are unknown. In pressure injections, the initial concentration might be known, but a constant declining concentration gradient over time is present. In microdialysis, not unlike iontophoresis, the exact amount of drug perfused through the tissue may be unknown, studies have suggested that approximately 10% of the concentration in the probe is accessing the surrounding tissue. Initially, a gradient with high concentration closest to the probe and lower concentrations further from it is expected, over time it is likely that the entire central nucleus and possibly the entire IC is affected by extended perfusions. Because the microdialysis approach is based on diffusion, the method can be used for extensive periods of time without causing any volume effects. Using a microdialysis probe allowed me to see how effects build up over extended periods of perfusion and also allowed me to make multiple FRA and PSTH measures within each drug condition.

2. Microdialysis allows for the examination of drug effects over a population of neurons. Iontophoresis delivers drugs too locally for this to be possible and likely only affects receptors on the soma or close to the recording probe. Drug delivery by iontophoresis is not able to target distal dendrites of one cell let alone a population of neurons as large as the central nucleus of the IC. Pressure injection, on the other hand, does allow for population studies but is likely to cause displacement of the tissue making recordings from the same units virtually impossible, also larger volumes are likely to disrupt the tissue. Microdialysis does not suffer from these issues because it is based on perfusion down a concentration gradient. A disadvantage, however, is that all cells in the population can be affected resulting in secondary and unpredictable effects. An unexpected shift in the normal excitatory/inhibitory balance could occur, although the fact that the NMDA effects did wash out over time suggests that the system was not permanently disturbed by it.

3. Microdialysis is flexible and adaptable, it can be used to study the effects of several concentrations of a drug (e.g. concentration response curve for NMDA) and combinations of drugs (e.g. NMDA and L-MeArg/ODQ). Repeated pressure injections without disturbing the tissue are virtually impossible making long term recordings from the same units nearly impossible. Microdialysis does not suffer from these drawbacks but online monitoring of drug effects on neuronal activity would be advantageous and give more experimental control.

Some further suggestions for further research to further power the microdialysis aspect of the studies would be to look into diffusion rates of the drugs used. An in vivo investigation to what extent they are metabolised or displaced would help in gaining more experimental control. Although the IC is a relatively isolated structure, diffusion of drugs out of the IC is a possibility and diffusion experiments can help determining to what extent this happens.

Because the recording system used, did not allow for detailed online monitoring of the neuronal responses recorded it was sometimes difficult to gauge whether a drug effect had completely washed out. This resulted in having partial washouts in the experiments reported here, this issue can, however, be dealt with in future experiments by creating custom Matlab scripts that will allow for online comparisons between current responses and the baseline, allowing for more experimental control.

6.2.2 Multi-Electrode Recordings

Multi-unit recording has obvious advantages over single unit recordings in that it allows data to be gathered over the course of many hours and under different drug conditions. It also allows simultaneous recordings across the frequency laminae in the central nucleus. In the current experiments, electrodes with 32 recording contacts spaced 100 μm apart were used, this resulted in a large number of good quality recordings from each animal. Spike sorting allows these recordings to be separated into a several simultaneously single unit recordings with the advantages that they can inform us how different cells respond to the same set of stimuli or drug treatment. Many types of recording probes are available with different arrangements of recording electrodes can be bought or custom made to fit the specific requirements of the experiment. Multi-unit recording is more stable compared to single unit electrophysiology since with the latter it is as a rule impossible to hold single units for long periods as was necessary for the current experiments. Since a large number of recordings were made per animal this allowed post-hoc selection of the electrode that responded best to specific frequencies of interest, thus allowing for greater flexibility.

Although multi-unit recording amasses enormous amounts of data that require new ways of analysis and dealing with, the further advances in computing power and storage being cheap, data can be stored and further analysed in the future. Multiple measures (e.g. single unit responses, PSTH, FRAs and LFPs) can be derived from the same dataset allowing further flexibility and in depth analysis.

Because recordings appeared stable, no control experiments recording activity over many hours with only aCSF perfusion were performed, several of the drug manipulations had no direct effect (e.g. L-MeArg and ODQ) and drugs which did have a direct effect (e.g. NMDA), were shown to reverse (at least partially). Anecdotally (though not formally analysed), online observations of the PSTHs and FRAs were similar over the hours before drug administration started. I am therefore confident that the recordings were stable. The power of the methodology was particularly apparent in the salicylate experiments. The fact that multi-unit recordings were made from the same location, before and after systemic salicylate administration allowed me to track how salicylate-induced effects develop over time in a way not described before. Using this methodology an interesting and unexpected effect of salicylate on the CF was revealed which would not have been possible to observe with single electrode recordings.

Similarly I can be confident that the observed shifts in CF were not the result of inserting a microdialysis probe and a multi-electrode recording probe in close proximity in the IC and recording over many hours because the CF shifts were only observed in response to salicylate (directly and systemically applied) but not in the NMDA, the L-MeArg or the ODQ experiments. Also the fact that the spontaneous activity increased but also decreased in the NMDA concentration response experiments indicates that the constant rise in spontaneous activity in the systemic salicylate experiment can also be attributed to the salicylate.

6.2.3 Drug Doses/Concentrations

By using a microdialysis probe the drug concentration surrounding the probe is unknown, previous studies have suggested that approximately 10% of the original drug concentration within the probe reaches the tissue (Chefer *et al.*, 2009), however, the concentration in the tissue decreases as a cubic function of distance from the probe (Foeller *et al.*, 2001) making statements about the actual drug concentrations difficult. Because the concentration in the tissue cannot be known, I always piloted new drugs by starting with low concentrations and switched to progressively higher concentrations, usually with aCSF washouts in between,

not unlike the NMDA concentration response protocol. Using this methodology I found a concentration response relationship for NMDA in which the effects were qualitatively similar, but quantitatively greater at higher concentrations. Initial L-MeArg and ODQ concentrations were based loosely on those found in in-vitro studies using these drugs, but were piloted and further refined at the end of NMDA dose response experiments.

For the salicylate experiments the initial systemic dose chosen was based on literature reporting doses between 150 mg/kg up to 450 mg/kg (Jastreboff and Sasaki, 1986; Jastreboff *et al.*, 1988; Yang *et al.*, 2007; Sun *et al.*, 2009; Stolzberg *et al.*, 2012). In initial experiments, I started out using 350 mg/kg which reliably induces tinnitus and I anticipated fewer adverse effects compared to higher concentrations. However, the first three guinea pigs all died within 3 hours after the salicylate administration. This was thought to be due to respiratory depression and to prevent this from happening the animals were artificially respired with 100% medical oxygen and the dose of salicylate was titrated down to 200 mg/kg, still well within the tinnitus inducing range. No more deaths occurred after this intervention.

For the local salicylate perfusion, a similar concentration response curve as for NMDA was made, part of which is reported here. The fact that the current salicylate studies failed to show any effects of blocking of nNOS does not necessarily mean that NO signalling is not related to tinnitus. In the current experiments, the salicylate concentration may have been too high or the L-MeArg concentration too low, although the L-MeArg concentration did, of course, prove to be effective in the NMDA experiments. The inability to monitor detailed changes online discussed earlier was partly the cause for the difficulty in finding the appropriate dose for salicylate. Unlike NMDA, salicylate effects took time to build up and they were more subtle. The NMDA related changes were clearly visible during the recordings which enabled me quickly to find the appropriate dose, however with the more subtle salicylate effects I tried perfusing higher concentrations with a result that the optimum was not easily found. Also, it is possible that by starting the perfusion of salicylate into the IC before blocking the production of NO, mechanisms were triggered that could not be stopped. Further dose response studies for L-MeArg, ODQ and salicylate will need to address these issues. Also, the null finding for L-MeArg and ODQ could be due to the duration of the perfusion, the concentration used, the stimuli presented or the low number of animals in the sample.

6.2.4 Influence of Anaesthesia

All animals were anaesthetised with an IP injection of urethane and were further supplemented with either Hypnorm or, in later experiments due to the unavailability of Hypnorm, with Fentanyl and Midazolam. The depth of anaesthesia was checked at regular intervals during the experiment by testing the paw reflex. It was noted that animals receiving Fentanyl and Midazolam needed less supplementary anaesthesia throughout the experiment. It is possible that the Fentanyl and Midazolam have interacted with the salicylate resulting in premature deaths of the animals.

All experiments were performed under anaesthesia and although the brainstem is believed to be less affected by anaesthesia compared to the cortex, the IC does receive a significant degree of cortical input that under anaesthesia, could be influenced. The effects observed on the FRA or the spontaneous activity may all relate to the fact there is no top-down inhibition. Even though the current studies may be influenced by changes in cortical input, they do however reveal that NMDA receptor activity, nNOS activity, and sGC activity can be functionally linked in the central nucleus of the IC. The current experiments also demonstrate that salicylate exerts direct effects on neural responses in the IC, even though these effects might be different in awake and freely behaving animals.

6.3 Implications of Experimental Results

6.3.1 Different Expression Patterns of nNOS Suggest Different Functionality

The anatomical studies presented here demonstrated that the presence of nNOS in the IC is more extensive than previously described. In the cortices, the nNOS expression is seen distributed throughout the cell whereas in the central nucleus the nNOS expression is solely observed in punctate labelling. It is likely, that the cells showing distributed nNOS labelling also have punctate labelling, but that these are being obscured from view by the bright distributed labelling. Evidence was presented demonstrating that the nNOS puncta are associated with PSD95. Although the wide field microscopy employed here does not allow me to rule out the possibility that some of the nNOS puncta may be located in presynaptic terminals, it seems more likely that the nNOS puncta represent postsynaptic nNOS which is coupled to PSD95 in the postsynaptic density.

The nature of the distributed labelling is more difficult to discern and there is the possibility that, while the punctate labelling represents nNOSα bound to PSD95, the distributed labelling represents unbound nNOSα and not nNOSβ. However, while nNOSα has a PDZ domain allowing it to bind to PSD95, the alternate splice variant nNOSβ lacks the PDZ domain and hence cannot associate with PSD95. Thus the two expression patterns observed (punctate and distributed labelling) may represent the two nNOS splice variants nNOSα and nNOSβ, respectively.

Previous work on nNOS, in general, have tended to treat nNOS as a single protein and the studies in the IC are no exception. There is usually no mention of the different splice variants present, however, in studying the expression of nNOS splice variants we are hampered by the fact that NADPH-diaphorase histochemistry and most commercial antibodies do not distinguish between different splice variants. Although we do know from in situ hybridization studies that the mRNAs coding both splice variants are present in most auditory brainstem structures including the IC (Eliasson *et al.*, 1997). It is of note that the mRNAs coding for nNOSα and nNOSβ are often expressed in the same cells, at least in the hippocampus and cortical areas (Eliasson *et al.*, 1997). While they can demonstrate the presence of mRNA, such in situ hybridization studies cannot, however, make any statement about the resulting protein levels in these cells and regions. Given the previous evidence and the current immunohistochemical observations showing two distinct nNOS expression patterns, it is clear we need to entertain the possibility that NO in the IC might perform different functions in different cells. The different distributions suggest different splice variants, and even if they turn out to be the same, the different distributions suggest different functions.

In the literature, the idea has been proposed that NO could operate by volume transmission, as well as being a trans-synaptic signalling molecule. Garthwaite and colleagues demonstrated in hippocampal slices that nNOS is linked to NMDA receptor activity (Garthwaite *et al.*, 1989; Hopper *et al.*, 2004). The amount of NO that can be produced is limited by the number of NMDA receptors present on a dendritic spine. Calculations and mathematical modelling place the amount of NO produced in the synapse in the picomolar range, suggesting that NO produced in this way is at too low a concentration to act as a volume transmitter (Hall and Garthwaite, 2009; Wood *et al.*, 2011; Garthwaite, 2016). However, this assumes that every nNOS protein is directly coupled to an NMDA receptor, and hence ignores any contribution from cytoplasmic nNOSβ (or cytoplasmic nNOSα) which is possibly too far from an NMDA receptor to be directly influenced by its activity. Given that nNOS is dependent on calcium signalling and calcium is tightly regulated by

cells, these signals usually fade within 1-2 µm (Augustine *et al.*, 2003), making it unlikely that NMDA receptors can directly alter the intracellular calcium levels to the level required to activate nNOS proteins not directly associated with the NMDA receptor itself. Thus it seems highly unlikely that nNOSβ is regulated by NMDA receptor activity.

The immunohistochemical evidence presented in Chapter 3 showed that a substantial number of nNOS expressing cells also express the calcium binding proteins calbindin and parvalbumin. These proteins are well known to regulate intracellular calcium levels and trigger secondary messenger systems (Schwaller *et al.*, 2002; Schwaller, 2009), and these may very well have a role to play in regulating nNOS activity. The current experiments also showed a number of nNOS positive cells not labelling for any of the three calcium binding proteins examined, but since the EF-hand calcium binding family comprises over 240 members this cannot be taken as evidence that they do not contain calcium binding proteins. Identifying which calcium binding proteins are co-expressed in nNOS cells may have implications for function. The calcium binding proteins have been heavily investigated and have proven to be far more complex than previously believed (Schwaller *et al.*, 2002; Schwaller, 2009). Given the finding that calbindin positive cells in the IC always contain nNOS, whereas, in contrast, calretinin expression hardly ever does, suggests that there must be a fundamental difference between the cellular functions these two proteins perform.

From non-neuronal cells (e.g. skeletal muscle cells) that express nNOSβ, we know that this protein is attached to and regulated directly by the Golgi-complex (Percival *et al.,* 2010). If this were the case in the IC, you would expect the nNOS labelling to form rings around the nucleus, which was not observed in the current studies. Even though this regulatory mechanism may not necessarily translate directly to neurons, it shows that nNOS can be regulated by other proteins besides PSD95. From the knock out studies, we know that nNOSβ can rescue the phenotype to a great extent when nNOSα is lost (Langnaese *et al.*, 2007). In these models, there is evidence for some remaining NO production and NADPH diaphorase labelling in the brain and no gross neurological symptoms were observed. However, these studies have not investigated auditory processing or the IC and it is likely that neuroplasticity, learning and possible other auditory phenomena are being affected in these animals.

As stated earlier, the in situ hybridization studies showed the presence of both splice variants but a larger amount of nNOSα mRNA is generally detected. However, due to post

translational processing mRNA levels do not directly indicate protein content. Further studies investigating the IC by subdivision could certainly help bring in answers to some of these questions regarding expression levels of the different splice variants. Even in the absence of commercially available antibodies labelling nNOSα and nNOSβ, an in situ study targeting the different subdivisions of the IC would be helpful. For example, if NOSβ mRNA were shown to be present in the cortices but not in the central nucleus, that would substantiate the hypothesis that the distributed nNOS labelling is nNOSβ. Determining the role of nNOSβ is currently difficult because there are no selective synthesis blockers or selective agonist available. Permanent knock out models of nNOSα can be difficult to interpret because they result in changes in nNOSβ expression. An alternative possibility might, therefore, be to use conditional knockouts or disrupt the binding of nNOSα to PSD95 with specific drugs designed for this purpose.

6.3.2 nNOS, the NMDA Receptor and sGC have a Functional Relationship

No studies have directly addressed the functional role of NO in the IC, although some have addressed this in other brain regions. However, this is usually done in a limited way. All studies thus far have employed iontophoretic methods and as discussed above they do suffer from a major limitation, they apply the drugs locally which prevents them from studying population wide effects. The data presented in this thesis employing a microdialysis probe builds on those previous studies and forms a natural extension of them. From previous studies, we know that the vast majority of neurons in the IC are of a glutamatergic neurotransmitter phenotype ((Oliver, 2005b; Wu *et al.*, 2008)) and that glutamatergic connections are abundant (see Chapter 3). The two main receptors in the IC transducing these glutamate signals are the AMPA and the NMDA receptors ((Parks, 2000)).

In this thesis, evidence was presented that demonstrated, in accordance with previous research that the direct perfusion of NMDA increases the auditory evoked response as well as the spontaneous activity observed in the IC. However quite remarkably it does not affect the CF or the threshold measured at CF indicating that it does not alter the sensitivity of the neurons. The subsequent experiments blocking NO production completely abolished the observed increases in activity in response to NMDA. This argues for a direct coupling of the NMDA receptor and the nNOS protein in the IC. Because only nNOSα has the ability to associate itself with the NMDA receptor via their mutual interaction with PSD95, this finding

further substantiates the idea that nNOSα is being expressed in the puncta seen in the central nucleus.

Blocking the binding of NO to sGC thereby interfering with the cGMP pathway showed the same blockade of the otherwise robust NMDA driven increase in activity. This finding demonstrates that the NMDA mediated increase in activity is not only NO dependent but that it is dependent on NO acting on sGC. Previously, NO has been shown to (negatively) regulate presynaptic glutamate release (Ahern *et al.*, 1999) and also to decrease the number of NMDA and AMPA receptors in the post synaptic domain during times of high activity (Steinert *et al.*, 2010). This is hypothesised to be a protective mechanism to limit the amount of calcium entering the cell. Blocking NMDA receptor activity after noise trauma has been shown to prevent the development of tinnitus (Guitton and Dudai, 2007; Steinert *et al.*, 2010) The studies presented in this thesis show that NMDA receptor activation mediates effects in the IC through nNOS and sGC, demonstrating that NO is playing a crucial role in mediating NMDA receptor effects.

The findings in the current research indicate a functional coupling between the NMDA receptor, nNOS activity and sGC activity. This functional coupling between the three proteins, and the fact that some of their splice variants and subunits contain PDZ domains known to associate with PSD95, strongly suggest that this coupling is governed by all three proteins associating with PSD95 into a multiprotein signalling complex. This proposed multiprotein signalling complex is depicted in Figure 6-1 and comprised of the NMDA receptor, nNOSα and sGC all interacting via their PDZ domains with PSD95.

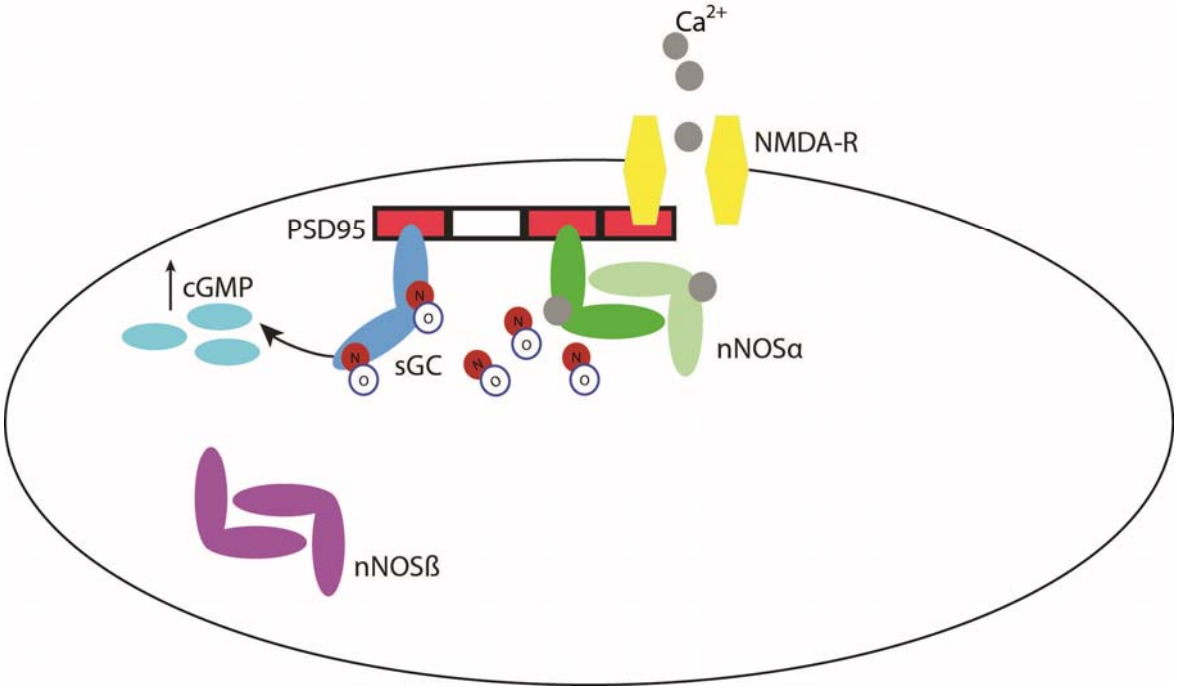

Figure 6-1 proposed multi-protein signalling complex comprised of the NMDA receptor, nNOSα and sGC interacting with the PDZ binding domains of PSD95. The red blocks in PSD95 represent the respective PDZ binding motifs 1, 2 and 3. Calcium is depicted entering the cell via the NMDA receptor and binding to nNOSα. The produced NO travels to the sGC protein which in turn amplifies the cGMP production a hundredfold. nNOSβ is depicted in the cytoplasm but too far from the NMDA receptor to utilise the calcium influx associated with this receptor.

6.3.3 Salicylate Exerts Direct and Indirect Effects on Auditory Processing in the IC

Tinnitus is a widespread auditory phenomenon reported in virtually all populations and across cultures. Due to its subjective nature, it has been difficult to develop an animal model for the disorder. Although these have their flaws, the recently developed behavioural tests measuring whether animals experience tinnitus, have helped to make strides in tinnitus research. Systemic administration of high concentrations of salicylate, chemically similar to the main component of aspirin (acetyl salicylate), results in tinnitus albeit of a transitory nature. Although the underlying cause and duration are different between noise- and salicylate-induced tinnitus, both are believed to share some common mechanism since they both result in the same tinnitus percept.

Virtually all in vivo studies using a systemic administration of salicylate showed an increase in spontaneous activity throughout the auditory pathway, and although good progress in describing the effects of salicylate have been made, we remain uncertain about how the tinnitus percept is being generated. The initial onset of tinnitus has been related to (temporary) deficits of the cochlea, but long term tinnitus has been shown to be independent from the cochlea (House and Brackmann, 1981; Bauer *et al.*, 2008) and is hypothesized to

arise from neuroplastic changes higher in the auditory pathway (Eggermont and Roberts, 2004; Roberts *et al.*, 2010; Guitton, 2012). The IC is uniquely placed in the auditory pathway because virtually all ascending and most descending information is processed here making this a likely structure to be involved in the generation of the tinnitus percept.

To tease apart the mechanisms by which salicylate induces tinnitus, comparisons were made between the systemic administration and direct perfusion of salicylate in the IC. Salicylate has been demonstrated to lead to an increase in the stiffness of outer hair cells, by binding to prestin, which leads to a reduction of input in the auditory brainstem pathway in a similar fashion to noise-induced trauma. Multiple strands of in vivo and in vitro evidence have shown that salicylate influences neuronal activity (Reed and Palmisano, 1975; Stypulkowski, 1990). PET scanning showed widespread effects of salicylate in the auditory brainstem (Wallhäusser-Franke *et al.*, 1996) while recent MRI scanning in mice showed effects of salicylate both on auditory and non-auditory brain structures (Gröschel *et al.*, 2016). These direct effects of salicylate on the brain cannot be discarded as underlying the generation of the tinnitus percept. In fact, if they were to form a part of it, they could potentially help us investigate how noise-induced tinnitus is brought about. The current hypothesis adopted in this thesis is that the tinnitus percept does not originate from the peripheral auditory structures, but is generated in the brain. Pharmacological methods like salicylate and quinine are best suited to study such effects because they allow for selective targeting of regions and cells expressing specific receptors within these regions.

Perfusing NMDA locally in the IC presumably shifts the excitatory/inhibitory balance in favour of excitatory activity because NMDA stimulates the glutamate NMDA receptor (an excitatory receptor), thus resulting in an increase in spontaneous activity. This increase in spontaneous (i.e. non-sound-driven activity) could be considered to be ‘noise’ in the system and is likely to be underlying the tinnitus percept as this increase in ‘noise’ is interpreted in the auditory cortex as an actual sound. A shift in the excitatory/inhibitory balance could also be brought about by changing the inhibitory activity, salicylate has been shown to directly reduce the GABAergic activity in the central nucleus of the IC (Bauer *et al.*, 2000). Because most inhibitory activity that the IC receives is generated in the IC itself, this direct effect of salicylate on GABAergic activity could underlie the increased activity observed here.

Previous in vivo systemic salicylate experiments were not able to track the same units over the course of the entire experiment. They collected a number of single cell recordings before salicylate administration and another set after. By recording the activity from the same

location in the IC, I was able to show that initially salicylate causes a frequency specific decrease in activity in the early hours after administration. Only in the later hours of the experiment is the increase in spontaneous activity as reported in previous studies observed. However, the finding that direct application of salicylate decreases the spontaneous activity rather than increasing it suggests that the observed increase in spontaneous activity in the IC observed in previous studies and here, arises elsewhere in the auditory system. Over the course of the salicylate treatment, the recorded units were seen to shift their CF to higher frequencies without altering their threshold sensitivity. Previous studies obviously were not able to detect this because they sampled different cells at the different time points. The fact that direct perfusion of salicylate in the IC shows the same shift in CF suggests that this effect is at least partially originating from the IC. Salicylate may affect the lower auditory structures in a similar way and these shifting effects along the pathway may prove to be additive. The frequency dependent changes observed in the shape of the FRAs suggest there might be some modulation of inhibition

The current studies failed to demonstrate a link between salicylate-induced effects and the NO signalling pathway. However, the NOS blocking agent L-MeArg was infused after several hours of increasing salicylate concentration perfusion. It is entirely possible that the concentration of L-MeArg was too low, the levels of salicylate were too high or that salicylate-induced effects via NO occur down-stream and hence were not reversible. Clearly, this area of research would deserve further attention especially now that we know that there is nNOS expression present in the central nucleus.

6.4 Future Studies

6.4.1 Future Anatomical Studies

The structural studies reported here brought about new findings about the presence and activity of nNOS in the IC. Findings that may require us to reconsider the role NO plays in the processing of auditory stimuli, but most certainly requires us to further investigate in what types of cells nNOS is expressed. Different protein expressions in cells have been well described in other brain regions and can help to shed light on the processes occurring in the IC.

The close functional link between NMDA receptors and nNOS puncta in the central nucleus will require us to investigate the NMDA receptors in this structure more closely. We know little about NMDA subunit composition in the IC, but from in situ hybridization studies, we

know that mRNAs for all NMDA subunits are expressed in almost equal levels. There is no full description of the NMDA subunit distribution in the different subdivisions of the IC at protein level available yet, but it is possible that certain subunits are more likely to be associated with nNOS expression. In fact nNOSα knockout studies show that the loss of nNOSα is accompanied by the loss of expression of specific NMDA subunits and an upregulation for others throughout the brain (Putzke *et al.*, 2000). Understanding what NMDA receptor subunits are expressed and how they are linked to different nNOS expression patterns can give us clues about their relationship.

The different subcellular distribution patterns of nNOS are suggestive that these may represent nNOSα and nNOSβ however in the absence of commercially available -splice variant specific- antibodies this is a difficult hypothesis to test. Antibodies against both splice variant have successfully been developed in the past (Langnaese *et al.*, 2007) and access to them would mark a major step forward in our ability to visualise the different splice variants, not only to confirm the current hypothesis about the distribution patterns, but will also allow us to study their distributions and co-expression of other proteins (e.g. calcium binding proteins) potentially leading to hypotheses about the roles each splice variant has in the IC. Alternatively, current pan-nNOS antibodies could be used in Western blots using tissue micro dissected from the subregions of the IC. Because nNOSβ is a smaller protein (140 kDa) compared to nNOSα (165 kDa) the expression of the protein would be visible in a distinct band on the Western blot.

The current immunohistochemistry experiments focused on glutamate signalling on nNOS expressing cells, but as suggested above the results observed in the functional studies cannot eliminate the possibility that the changes in spontaneous and sound evoked activity are caused by changes in inhibitory activity. Focussing on, to what extent nNOS expression is associated with GABAergic neurons will need further investigation, as well as relating this to the distribution of both types of nNOS. Because the cells showing distributed nNOS expression are possibly capable of using NO as a volume transmitter, studies should further investigate to what extent targets of NO (e.g. sGC) are present in GABAergic cells.

The findings of the association between nNOS and PSD95 in the central nucleus (Chapter 3) and the functional evidence indicating a close link between nNOS activity acting on the NMDA receptor via sGC (Chapter 4) together with the evidence from literature that sGC can interact with PSD95 suggests the presence of a multiunit protein signalling complex. Future work should investigate whether this proposed signalling complex exists in the

central nucleus and possibly elsewhere in the IC using immunoprecipitation and immunohistochemistry employing confocal methods.

6.4.2 Future Functional Studies

Regardless of whether or not the NMDA receptor, nNOS and sGC are physically linked in a single multi-protein signalling complex, this thesis presented evidence for a functional link between the NMDA receptor, nNOS and sGC. Further functional studies investigating the existence of this complex could be designed aimed at specifically targeting the PDZ domain interactions between the nNOSα protein and PSD95. Drugs doing precisely that, including homotaurine as well as IC87201 and ZL-006 exist and have been used successfully both in vitro and in vivo in disrupting the binding of nNOSα to PSD95 thereby significantly decreasing the amount of NO produced (Dev, 2004; Doucet *et al.*, 2012). Further in vivo studies using this class of drugs should lead to similar results obtained here and would further substantiate the current findings. Although the uncoupled nNOSα could still be active, and not necessarily be completely stopped from functioning.

In both the NMDA and the salicylate studies the range of acoustic stimuli that has been used was limited to only brief pure tones. To study more aspects of auditory processing (e.g. interaural time and level differences) is will be important in future studies to look at a wider a range of sound stimuli.

Some of the studies of this thesis focussed on direct effects of salicylate in the IC. The techniques proved to be a powerful tool and can easily be adapted to examine how activity in ascending and descending system affect the IC. Specific studies on the auditory pathway to investigating the origin of effects not mediated by direct salicylate perfusion in the IC could be performed recording in the central nucleus but perfusing salicylate into other auditory structures and observing these effects in the IC.

Future studies will need to further investigate the salicylate effects observed here, the direct effects of salicylate on the IC provide fascinating windows in the way salicylate effects neuronal tissue. Findings presented here show that shortly after systemic salicylate treatment short lived decreases in activity in spontaneous activity regions of the FRA could suggest that low doses of salicylate help shape the frequency tuning and possibly even improve hearing. Further studies could be aimed at teasing apart to what extent this happens and whether it is a concentration or time dependent effect.

It is unclear what the observed upward shift in the CF evident in the FRA in response to local or systemic salicylate would represent in terms of what the animal perceives: would this shift be noticeable and do these changes represent tinnitus or do they represent something else entirely? Future experiments need to be designed, preferably in awake and possibly trained animals to examine both the electrophysiological and behavioural consequences of these phenomena.

6.5 Final Thoughts

Over the last twenty-five years since it became first apparent that NO can function as a neurotransmitter in the brain, much progress has been made in our understanding of this elusive neurotransmitter. However large gaps in our knowledge still persist, we now know, due to the advances in immunohistochemistry techniques that nNOS is expressed throughout the brain but expression is especially pronounced in the brainstem regions. The original project plan for this thesis had a strong focus on the potential role of NO in tinnitus. However, it quickly became quite apparent that we had a limited understanding of NO signalling in general and knew even less about its role in the processes that take place in the IC. The focus of the project and hence this thesis shifted more towards studying basic properties of nNOS and NO signalling in the IC.

The presence of nNOS in the IC, a predominantly auditory structure indicates that NO plays some role in auditory processing. NO signalling in the IC may be involved in pathological states including tinnitus. It is believed that there is a fundamental difference between onset and the persistence of tinnitus. The onset and transient tinnitus are due to a decrease in input from the auditory sense organs accompanied by increased ‘gain’, however, chronic tinnitus even after the sense organs have healed is probably due to neural plasticity gone awry. The fact that the NO-sGC pathway has been shown to be directly involved in LTP and LTD tells us that NO can alter the synaptic strength and this might be what is underlying persistent tinnitus.

The IC is a hub for the integration of many different strands of information. The IC can be thought of not just in terms of subregions but within these regions specialised organisation exists like for example the tonotopic laminar organisation of the central nucleus and the existence of GABA modules in the lateral cortex.

In order to further our understanding of how NO signalling affects processing in the IC, we will need to ask more specific questions, because the different nNOS distributions in

different subregions suggests the possibility of having different roles within these cells. Evidence presented here strongly suggests that there is not just one NO signalling pathway. Even if most of the produced NO is binding to sGC there would still be multiple possible pathways to be considered, with differences between pre and post synaptic occurring nNOS and sGC. NO has been used by living organisms since the origins of life and can be found in the most ancient and simple of organisms. The NO signalling pathway acting through sGC is observed in simple species without a real nervous system like jellyfish (Moroz and Kohn, 2007). Given its extremely long history in life, it should not come as a surprise that it may perform different functions.

The different subcellular expressions of nNOS may have different regulatory mechanisms and need to be further understood. Treating nNOS as one type of protein occurring in the IC is an oversimplification which holds us back from asking the appropriate questions. The presence of nNOS in the IC is extensive and its abilities affecting other signalling pathways and receptor availability make it all the more important for us to understand how the different expression patterns operate and are regulated.

Throughout the brain, signals are not carried by the signalling molecules themselves but by the receptors detecting these molecules. Just as glutamate binds to both AMPA and NMDA receptors, it is these receptors and their properties that determine the signal transduction and subsequent interpretation of the signal. In calcium signalling it is of no use to ask the question what the role of calcium is in a brain region because calcium is involved in so many different cellular processes even within one cell it performs a multitude of functions. We know that nNOS has a range of potential targets and even when we limit our discussion to its main target sGC we need to consider a variety of subunit compositions with their own unique properties. We need to accept that NO is likely to perform different functions in different cells and quite possibly in different subcellular areas of the same cell.

My thesis has raised important issues about the splice variants, subcellular location, regulation and sub regional distinctions within the IC regarding nNOS. It is evident, that asking the question '*how is NO related to auditory processing in the IC?*' was too naïve a question to ask because the reality of nNOS expression in the IC was more complex than previously thought. However, having uncovered some of these layers of complexity and having proposed some new hypothesis regarding nNOS expression in the IC, I do believe that we are now in a position to take into account these factors and that will help us move toward, and eventually gain a full understanding of NO signalling in the IC.

References

Adams, J.C. (1979) 'Ascending projections to the inferior colliculus', *The Journal of Comparative Neurology*, 183(3), pp. 519-538.

Ahern, G.P., Hsu, S.-F. and Jackson, M.B. (1999) 'Direct actions of nitric oxide on rat neurohypophysial K(+) channels', *The Journal of Physiology*, 520(Pt 1), pp. 165-176.

Ahern, G.P., Klyachko, V.A. and Jackson, M.B. (2002) 'cGMP and S-nitrosylation: two routes for modulation of neuronal excitability by NO', *Trends in Neurosciences*, 25(10), pp. 510-517.

Ahlf, S., Tziridis, K., Korn, S., Strohmeyer, I. and Schulze, H. (2012) 'Predisposition for and Prevention of Subjective Tinnitus Development', *PLoS ONE*, 7(10).

Aitkin, L.M., Dickhaus, H., Schult, W. and Zimmermann, M. (1978) 'External nucleus of inferior colliculus: auditory and spinal somatosensory afferents and their interactions', *Journal of Neurophysiology*, 41(4), pp. 837-847.

Aitkin, L.M., Kenyon, C.E. and Philpott, P. (1981) 'The representation of the auditory and somatosensory systems in the external nucleus of the cat inferior colliculus', *Journal of Comparative Neurology*, 196(1), pp. 25-40.

Alderton, W.K., Cooper, C.E. and Knowles, R.G. (2001) 'Nitric oxide synthases: Structure, function and inhibition', *Biochemical Journal*, 357(3), pp. 593-615.

Altschuler, R.A. and Shore, S.E. (2010) 'Central auditory neurotransmitters', in Palmer, A.R. and Rees, A. (eds.) *The Oxford Handbook of Auditory Science; The Auditory Brain*. Oxford: Oxford University Press, pp. 65-89.

Altschuler, R.A., Tong, L., Holt, A.G. and Oliver, D.L. (2008) 'Immunolocalization of vesicular glutamate transporters 1 and 2 in the rat inferior colliculus', *Neuroscience*, 154(1), pp. 226-232.

Andersen, R.A., Roth, G.L., Aitkin, L.M. and Merzenich, M.M. (1980) 'The efferent projections of the central nucleus and the pericentral nucleus of the inferior collculus in the cat', *Journal of Comparative Neurology*, 194(3), pp. 649-662.

Atkinson, L., Batten, T.F.C., Corbett, E.K.A., Sinfield, J.K. and Deuchars, J. (2003) 'Subcellular localization of neuronal nitric oxide synthase in the rat nucleus of the solitary tract in relation to vagal afferent inputs', *Neuroscience*, 118(1), pp. 115-122.

Augustine, G.J., Santamaria, F. and Tanaka, K. (2003) 'Local calcium signaling in neurons', *Neuron*, 40(2), pp. 331-346.

Baldellon, C., Alattia, J.-R., Strub, M.-P., Pauls, T., Berchtold, M.W., Cavé, A. and Padilla, A. (1998) '15N NMR Relaxation Studies of Calcium-Loaded Parvalbumin Show Tight Dynamics Compared to Those of Other EF-Hand Proteins', *Biochemistry*, 37(28), pp. 9964-9975.

Bannwarth, B., Netter, P. and Gaucher, A. (1986) 'Diffusion of salicylates into cerebrospinal fluid in adults', *Therapie*, 41(6), pp. 409-411.

Basile, C.-É., Fournier, P., Hutchins, S. and Hébert, S. (2013) 'Psychoacoustic Assessment to Improve Tinnitus Diagnosis', *PLOS ONE*, 8(12), p. e82995.

Basta, D. and Ernst, A. (2004) 'Effects of salicylate on spontaneous activity in inferior colliculus brain slices', *Neuroscience Research*, 50(2), pp. 237-243.

Bauer, C.A., Brozoski, T.J., Holder, T.M. and Caspary, D.M. (2000) 'Effects of chronic salicylate on GABAergic activity in rat inferior colliculus', *Hearing Research*, 147(1-2), pp. 175-182.

Bauer, C.A., Turner, J.G., Caspary, D.M., Myers, K.S. and Brozoski, T.J. (2008) 'Tinnitus and inferior colliculus activity in chinchillas related to three distinct patterns of cochlear trauma', *Journal of Neuroscience Research*, 86(11), pp. 2564-2578.

Beattie, E.C., Carroll, R.C., Yu, X., Morishita, W., Yasuda, H., von Zastrow, M. and Malenka, R.C. (2000) 'Regulation of AMPA receptor endocytosis by a signaling mechanism shared with LTD', *Nat Neurosci*, 3(12), pp. 1291-1300.

Belli, H., Belli, S., Oktay, M.F. and Ural, C. (2012) 'Psychopathological dimensions of tinnitus and psychopharmacologic approaches in its treatment', *General Hospital Psychiatry*, 34(3), pp. 282-289.

Bengzon, J., Okabe, S., Lindvall, O. and McKay, R.D.G. (1999) 'Suppression of epileptogenesis by modification of N-methyl-d-aspartate receptor subunit composition', *European Journal of Neuroscience*, 11(3), pp. 916-922.

Berger, J.I. and Coomber, B. (2015) 'Tinnitus-related changes in the inferior colliculus', *Frontiers in Neurology*, 6(MAR).

Berger, J.I., Coomber, B., Shackleton, T.M., Palmer, A.R. and Wallace, M.N. (2013) 'A novel behavioural approach to detecting tinnitus in the guinea pig', *Journal of Neuroscience Methods*, 213(2), pp. 188-195.

Bing, D., Lee, S.C., Campanelli, D., Xiong, H., Matsumoto, M., Panford-Walsh, R., Wolpert, S., Praetorius, M., Zimmermann, U., Chu, H., Knipper, M., Ruttiger, L. and Singer, W. (2015) 'Cochlear NMDA receptors as a therapeutic target of noise-induced tinnitus', *Cell Physiol Biochem*, 35(5), pp. 1905-23.

Boxall, A.R. and Garthwaite, J. (1996) 'Long-term depression in rat cerebellum requires both NO synthase and NO-sensitive guanylyl cyclase', *European Journal of Neuroscience*, 8(10), pp. 2209-2212.

Bredt, D.S., Glatt, C.E., Hwang, P.M., Fotuhi, M., Dawson, T.M. and Snyder, S.H. (1991) 'Nitric oxide synthase protein and mRNA are discretely localized in neuronal populations of the mammalian CNS together with NADPH diaphorase', *Neuron*, 7(4), pp. 615-624.

Brenman, J.E., Chao, D.S., Gee, S.H., McGee, A.W., Craven, S.E., Santillano, D.R., Wu, Z., Huang, F., Xia, H., Peters, M.F., Froehner, S.C. and Bredt, D.S. (1996) 'Interaction of nitric oxide synthase with the postsynaptic density protein PSD95 and α1-syntrophin mediated by PDZ domains', *Cell*, 84(5), pp. 757-767.

Brenman, J.E., Xia, H., Chao, D.S., Black, S.M. and David, S. (1997) 'Regulation of neuronal nitric oxide synthase through alternative transcripts', *Developmental Neuroscience*, 19(3), pp. 224-231.

Brodie, B.B., Kurz, H. and Schanker, L.S. (1960) 'The importance of dissociation constant and lipid-solubility in influencing the passage of drugs into the cerebrospinal fluid', *Journal of Pharmacology and Experimental Therapeutics*, 130(1), pp. 20-25.

Butt, S., Ashraf, F., Porter, L.A. and Zhang, H. (2016) 'Sodium salicylate reduces the level of GABAB receptors in the rat's inferior colliculus', *Neuroscience*, 316, pp. 41-52.

Caicedo, A. and Herbert, H. (1993) 'Topography of descending projections from the inferior colliculus to auditory brainstem nuclei in the rat', *Journal of Comparative Neurology*, 328(3), pp. 377-392.

Cals-Grierson, M.M. and Ormerod, A.D. (2004) 'Nitric oxide function in the skin', *Nitric Oxide - Biology and Chemistry*, 10(4), pp. 179-193.

Cant, N.B. and Benson, C.G. (2003) 'Parallel auditory pathways: projection patterns of the different neuronal populations in the dorsal and ventral cochlear nuclei', *Brain Research Bulletin*, 60(5–6), pp. 457-474.

Cant, N.B. and Hyson, R.L. (1992) 'Projections from the lateral nucleus of the trapezoid body to the medial superior olivary nucleus in the gerbil', *Hearing Research*, 58(1), pp. 26-34.

Cary, S.P.L., Winger, J.A., Derbyshire, E.R. and Marletta, M.A. (2006) 'Nitric oxide signaling: no longer simply on or off', *Trends in Biochemical Sciences*, 31(4), pp. 231-239.

Caspary, D.M., Ling, L., Turner, J.G. and Hughes, L.F. (2008) 'Inhibitory neurotransmission, plasticity and aging in the mammalian central auditory system', *Journal of Experimental Biology*, 211(11), pp. 1781-1791.

Casseday, J.H., Fremouw, T. and Covey, E. (2002) 'The Inferior Colliculus: A Hub for the Central Auditory System', in Oertel, D., Fay, R.R. and Popper, A.N. (eds.) *Integrative Functions in the Mammalian Auditory Pathway*. New York, NY: Springer New York, pp. 238-318.

Cazals, Y. (2000) 'Auditory sensori-neural alterations induced by salicylate', *Progress in Neurobiology*, 62(6), pp. 583-631.

Chefer, V.I., Thompson, A.C., Zapata, A. and Shippenberg, T.S. (2009) 'Overview of Brain Microdialysis', *Current protocols in neuroscience / editorial board, Jacqueline N. Crawley. [et al.]*, Unit7.1-Unit7.1.

Chen, Z., Kujawa, S.G. and Sewell, W.F. (2007) 'Auditory sensitivity regulation via rapid changes in expression of surface AMPA receptors', *Nature Neuroscience*, 10(10), pp. 1238-1240.

Chernock, M.L., Larue, D.T. and Winer, J.A. (2004) 'A periodic network of neurochemical modules in the inferior colliculus', *Hearing Research*, 188(1-2), pp. 12-20.

Cho, K.O., Hunt, C.A. and Kennedy, M.B. (1992) 'The rat brain postsynaptic density fraction contains a homolog of the Drosophila discs-large tumor suppressor protein', *Neuron*, 9(5), pp. 929-942.

Cohen, J. (1977) 'F Tests on Means in the Analysis of Variance and Covariance', in *Statistical Power Analysis for the Behavioral Sciences (Revised Edition)*. Academic Press, pp. 273-406.

Coomber, B., Kowalkowski, V.L., Berger, J.I., Palmer, A.R. and Wallace, M.N. (2015) 'Modulating Central Gain in Tinnitus: Changes in Nitric Oxide Synthase in the Ventral Cochlear Nucleus', *Frontiers in Neurology*, 6(53).

Coote, E.J. and Rees, A. (2008) 'The distribution of nitric oxide synthase in the inferior colliculus of guinea pig', *Neuroscience*, 154(1), pp. 218-225.

Corso-Díaz, X. and Krukoff, T.L. (2010) 'nNOSα and nNOSβ localization to aggresome-like inclusions is dependent on HSP90 activity', *Journal of Neurochemistry*, 114(3), pp. 864-872.

Cowan, R.L., Wilson, C.J., Emson, P.C. and Heizmann, C.W. (1990) 'Parvalbumin-containing gabaergic interneurons in the rat neostriatum', *The Journal of Comparative Neurology*, 302(2), pp. 197-205.

Cull-Candy, S., Brickley, S. and Farrant, M. (2001) 'NMDA receptor subunits: Diversity, development and disease', *Current Opinion in Neurobiology*, 11(3), pp. 327-335.

D'Aldin, C.G., Ruel, J., Assié, R., Pujol, R. and Puel, J.L. (1997) 'Implication of NMDA type glutamate receptors in neural regeneration and neoformation of synapses after excitotoxic injury in the guinea pig cochlea', *International Journal of Developmental Neuroscience*, 15(4-5), pp. 619-629.

Dallos, P. (1992) 'The active cochlea', *The Journal of Neuroscience*, 12(12), p. 4575.

Dawson, T.M., Bredt, D.S., Fotuhi, M., Hwang, P.M. and Snyder, S.H. (1991) 'Nitric oxide synthase and neuronal NADPH diaphorase are identical in brain and peripheral tissues', *Proceedings of the National Academy of Sciences of the United States of America*, 88(17), pp. 7797-7801.

Day, R.O., Graham, G.G., Bieri, D., Brown, M., Cairns, D., Harris, G., Hounsell, J., Platt-Hepworth, S., Reeve, R., Sambrook, P.N. and Smith, J. (1989) 'Concentration-response relationships for salicylate-induced ototoxicity in normal volunteers', *British Journal of Clinical Pharmacology*, 28(6), pp. 695-702.

De Araújo Moreira, F., Molchanov, M.L. and Guimarães, F.S. (2003) 'Flight reactions to nitric oxide in the inferior colliculus of rats depend on NMDA receptor activation', *Pharmacology Biochemistry and Behavior*, 76(1), pp. 35-41.

Dehmel, S., Pradhan, S., Koehler, S., Bledsoe, S. and Shore, S. (2012) 'Noise overexposure alters long-term somatosensory-auditory processing in the dorsal cochlear nucleus-possible basis for tinnitus-related hyperactivity?', *Journal of Neuroscience*, 32(5), pp. 1660-1671.

Demeulemeester, H., Arckens, L., Vandesande, F., Orban, G.A., Heizmann, C.W. and Pochet, R. (1991) 'Calcium binding proteins and neuropeptides as molecular markers of GABAergic interneurons in the cat visual cortex', *Exp Brain Res*, 84(3), pp. 538-44.

Dev, K.K. (2004) 'Making protein interactions druggable: Targeting PDZ domains', *Nature Reviews Drug Discovery*, 3(12), pp. 1047-1056.

Didier, A., Miller, J.M. and Nuttall, A.L. (1993) 'The vascular component of sodium salicylate ototoxicity in the guinea pig', *Hearing Research*, 69(1-2), pp. 199-206.

Dingledine, R., Borges, K., Bowie, D. and Traynelis, S.F. (1999) 'The Glutamate Receptor Ion Channels', *Pharmacological Reviews*, 51(1), pp. 7-62.

Dobie, R.A. (1999) 'A review of randomized clinical trials in tinnitus', *Laryngoscope*, 109(8), pp. 1202-1211.

Dong, S., Mulders, W.H., Rodger, J., Woo, S. and Robertson, D. (2010a) 'Acoustic trauma evokes hyperactivity and changes in gene expression in guinea-pig auditory brainstem', *Eur J Neurosci*, 31(9), pp. 1616-28.

Dong, S., Mulders, W.H.A.M., Rodger, J., Woo, S. and Robertson, D. (2010b) 'Acoustic trauma evokes hyperactivity and changes in gene expression in guinea-pig auditory brainstem', *European Journal of Neuroscience*, 31(9), pp. 1616-1628.

Doucet, J.R. and Ryugo, D.K. (1997) 'Projections from the ventral cochlear nucleus to the dorsal cochlear nucleus in rats', *The Journal of Comparative Neurology*, 385(2), pp. 245-264.

Doucet, M.V., Harkin, A. and Dev, K.K. (2012) 'The PSD95/nNOS complex: New drugs for depression?', *Pharmacology & Therapeutics*, 133(2), pp. 218-229.

Druga, R. and Syka, J. (1993) 'NADPH-diaphorase activity in the central auditory structures of the rat', *NeuroReport*, 4(8), pp. 999-1002.

Duckert, L.G. and Rees, T.S. (1983) 'Treatment of tinnitus with intravenous lidocaine: a double-blind randomized trial', *Otolaryngol Head Neck Surg*, 91(5), pp. 550-5.

Dzubay, J.A. and Jahr, C.E. (1996) 'Kinetics of NMDA channel opening', *Journal of Neuroscience*, 16(13), pp. 4129-4134.

Eggermont, J.J. and Kenmochi, M. (1998) 'Salicylate and quinine selectively increase spontaneous firing rates in secondary auditory cortex', *Hearing Research*, 117(1-2), pp. 149-160.

Eggermont, J.J. and Roberts, L.E. (2004) 'The neuroscience of tinnitus', *Trends in Neurosciences*, 27(11), pp. 676-682.

Eggermont, J.J. and Roberts, L.E. (2015) 'Tinnitus: animal models and findings in humans', *Cell and Tissue Research*, 361(1), pp. 311-336.

Elgoyhen, A.B. and Langguth, B. (2010) 'Pharmacological approaches to the treatment of tinnitus', *Drug Discovery Today*, 15(7-8), pp. 300-305.

Eliasson, M.J.L., Blackshaw, S., Schell, M.J. and Snyder, S.H. (1997) 'Neuronal nitric oxide synthase alternatively spliced forms: Prominent functional localizations in the brain', *Proceedings of the National Academy of Sciences of the United States of America*, 94(7), pp. 3396-3401.

Evans, E.F., Wilson, J.P. and Borewe, T.A. (1981) 'Animal model of tinnitus', *CIBA*. London. pp. 108-129.

Faingold, C.L. (2002) 'Role of GABA abnormalities in the inferior colliculus pathophysiology Audiogenic seizures', *Hearing Research*, 168(1-2), pp. 223-237.

Faingold, C.L., Hoffmann, W.E. and Caspary, D.M. (1989) 'Effects of excitant amino acids on acoustic responses of inferior colliculus neurons', *Hearing Research*, 40(1-2), pp. 127-136.

Faye-Lund, H. and Osen, K.K. (1985) 'Anatomy of the inferior colliculus in rat', *Anat Embryol (Berl)*, 171(1), pp. 1-20.

Feldman, D.E. and Knudsen, E.I. (1998) 'Pharmacological specialization of learned auditory responses in the inferior colliculus of the barn owl', *Journal of Neuroscience*, 18(8), pp. 3073-3087.

Feliciano, M. and Potashner, S.J. (1995) 'Evidence for a glutamatergic pathway from the guinea pig auditory cortex to the inferior colliculus', *Journal of Neurochemistry*, 65(3), pp. 1348-1357.

Fendt, M., Li, L. and Yeomans, J.S. (2001) 'Brain stem circuits mediating prepulse inhibition of the startle reflex', *Psychopharmacology*, 156(2-3), pp. 216-224.

Feng, C. (2012) 'Mechanism of nitric oxide synthase regulation: Electron transfer and interdomain interactions', *Coordination Chemistry Reviews*, 256(3-4), pp. 393-411.

Feng, W. and Zhang, M. (2009) 'Organization and dynamics of PDZ-domain-related supramodules in the postsynaptic density', *Nature Reviews Neuroscience*, 10(2), pp. 87-99.

Fernández-Alvarez, A., Gómez-Sena, L., Fabbiani, M.G., Budelli, R. and Abudara, V. (2011) 'Endogenous presynaptic nitric oxide supports an anterograde signaling in the central nervous system', *Journal of Neurochemistry*, 118(4), pp. 546-557.

Fettiplace, R. and Hackney, C.M. (2006) 'The sensory and motor roles of auditory hair cells', *Nat Rev Neurosci*, 7(1), pp. 19-29.

Foeller, E., Vater, M. and Kössl, M. (2001) 'Laminar analysis of inhibition in the gerbil primary auditory cortex', *JARO - Journal of the Association for Research in Otolaryngology*, 2(3), pp. 279-296.

Fujimoto, H., Konno, K., Watanabe, M. and Jinno, S. (2016) 'Late postnatal shifts of parvalbumin and nitric oxide synthase expression within the GABAergic and glutamatergic phenotypes of inferior colliculus neurons', *Journal of Comparative Neurology*, pp. n/a-n/a.

Garthwaite, J. (1991) 'Glutamate, nitric oxide and cell-cell signalling in the nervous system', *Trends in Neurosciences*, 14(2), pp. 60-67.

Garthwaite, J. (2005) 'Dynamics of cellular NO-cGMP signaling', *Frontiers in Bioscience*, 10(2), pp. 1868-1880.

Garthwaite, J. (2008) 'Concepts of neural nitric oxide-mediated transmission', *European Journal of Neuroscience*, 27(11), pp. 2783-2802.

Garthwaite, J. (2016) 'From synaptically localized to volume transmission by nitric oxide', *Journal of Physiology*, 594(1), pp. 9-18.

Garthwaite, J., Garthwaite, G., Palmer, R.M.J. and Moncada, S. (1989) 'NMDA receptor activation induces nitric oxide synthesis from arginine in rat brain slices', *European Journal of Pharmacology: Molecular Pharmacology*, 172(4-5), pp. 413-416.

Gelfand, S.A. (2016) *Hearing: An introduction to psychological and physiological acoustics*. CRC Press.

Giove, T.J., Deshpande, M.M. and Eldred, W.D. (2009) 'Identification of alternate transcripts of neuronal nitric oxide synthase in the mouse retina', *Journal of Neuroscience Research*, 87(14), pp. 3134-3142.

Goebel, D.J. and Poosch, M.S. (1999) 'NMDA receptor subunit gene expression in the rat brain: A quantitative analysis of endogenous mRNA levels of NR1(Com), NR2A, NR2B, NR2C, NR2D and NR3A', *Molecular Brain Research*, 69(2), pp. 164-170.

Gröschel, M., Götze, R., Müller, S., Ernst, A. and Basta, D. (2016) 'Central Nervous Activity upon Systemic Salicylate Application in Animals with Kanamycin-Induced Hearing Loss - A Manganese-Enhanced MRI (MEMRI) Study', *PLOS ONE*, 11(4), p. e0153386.

Guitton, M.J. (2012) 'Tinnitus: Pathology of synaptic plasticity at the cellular and system levels', *Frontiers in Systems Neuroscience*, (MARCH).

Guitton, M.J., Caston, J., Ruel, J., Johnson, R.M., Pujol, R. and Puel, J.L. (2003) 'Salicylate induces tinnitus through activation of cochlear NMDA receptors', *Journal of Neuroscience*, 23(9), pp. 3944-3952.

Guitton, M.J. and Dudai, Y. (2007) 'Blockade of cochlear NMDA receptors prevents long-term Tinnitus during a brief consolidation window after acoustic trauma', *Neural Plasticity*, 2007.

Guix, F.X., Uribesalgo, I., Coma, M. and Muñoz, F.J. (2005) 'The physiology and pathophysiology of nitric oxide in the brain', *Progress in Neurobiology*, 76(2), pp. 126-152.

Gyurko, R., Leupen, S. and Huang, P.L. (2002) 'Deletion of exon 6 of the neuronal nitric oxide synthase gene in mice results in hypogonadism and infertility', *Endocrinology*, 143(7), pp. 2767-2774.

Hall, C.N. and Garthwaite, J. (2009) 'What is the real physiological NO concentration in vivo?', *Nitric Oxide - Biology and Chemistry*, 21(2), pp. 92-103.

Hardingham, N., Dachtler, J. and Fox, K. (2013) 'The role of nitric oxide in pre-synaptic plasticity and homeostasis', *Frontiers in Cellular Neuroscience*, (OCT).

Hébert, S., Canlon, B. and Hasson, D. (2012a) 'Emotional exhaustion as a predictor of tinnitus', *Psychotherapy and Psychosomatics*, 81(5), pp. 324-326.

Hébert, S., Canlon, B., Hasson, D., Hanson, L.L., Westerlund, H. and Theorell, T. (2012b) 'Tinnitus severity is reduced with reduction of depressive mood - a prospective population study in sweden', *PLoS ONE*, 7(5).

Herbert, H., Aschoff, A. and Ostwald, J. (1991) 'Topography of projections from the auditory cortex to the inferior colliculus in the rat', *Journal of Comparative Neurology*, 304(1), pp. 103-122.

Hering, H. and Sheng, M. (2001) 'Dentritic spines: structure, dynamics and regulation', *Nature Reviews Neuroscience*, 2(12), pp. 880-888.

Hollmann, M. and Heinemann, S. (1994) 'Cloned glutamate receptors', *Annu Rev Neurosci*, 17, pp. 31-108.

Hope, B.T., Michael, G.J., Knigge, K.M. and Vincent, S.R. (1991) 'Neuronal NADPH diaphorase is a nitric oxide synthase', *Proceedings of the National Academy of Sciences of the United States of America*, 88(7), pp. 2811-2814.

Hopper, R., Lancaster, B. and Garthwaite, J. (2004) 'On the regulation of NMDA receptors by nitric oxide', *European Journal of Neuroscience*, 19(7), pp. 1675-1682.

House, J.W. and Brackmann, D.E. (1981) 'Tinnitus: surgical treatment', *Ciba Foundation symposium*, 85, pp. 204-216.

Huang, P.L., Dawson, T.M., Bredt, D.S., Snyder, S.H. and Fishman, M.C. (1993) 'Targeted disruption of the neuronal nitric oxide synthase gene', *Cell*, 75(7), pp. 1273-1286.

Hwang, J.H., Chen, J.C., Yang, S.Y., Wang, M.F., Liu, T.C. and Chan, Y.C. (2011) 'Expression of COX-2 and NMDA receptor genes at the cochlea and midbrain in salicylate-induced tinnitus', *Laryngoscope*, 121(2), pp. 361-364.

Ikura, M. (1996) 'Calcium binding and conformational response in EF-hand proteins', *Trends in Biochemical Sciences*, 21(1), pp. 14-17.

Ito, T., Bishop, D.C. and Oliver, D.L. (2009) 'Two classes of GABAergic neurons in the inferior colliculus', *Journal of Neuroscience*, 29(44), pp. 13860-13869.

Ito, T., Bishop, D.C. and Oliver, D.L. (2011) 'Expression of glutamate and inhibitory amino acid vesicular transporters in the rodent auditory brainstem', *Journal of Comparative Neurology*, 519(2), pp. 316-340.

Ito, T. and Oliver, D.L. (2010) 'Origins of glutamatergic terminals in the inferior colliculus identified by retrograde transport and expression of VGLUT1 and VGLUT2 genes', *Frontiers in Neuroanatomy*, (SEP).

Jacoby, S., Sims, R.E. and Hartell, N.A. (2001) 'Nitric oxide is required for the induction and heterosynaptic spread of long-term potentiation in rat cerebellar slices', *Journal of Physiology*, 535(3), pp. 825-839.

Jang, J.H., Kang, M.J., Ko, G.P., Kim, S.J., Yi, E.C. and Zhang, Y.H. (2015) 'Identification of a novel splice variant of neuronal nitric oxide synthase, nNOSβ, in myofilament fraction of murine cardiomyocytes', *Nitric Oxide*, 50, pp. 20-27.

Jastreboff, P.J., Brennan, J.F. and Sasaki, C.T. (1988) 'An animal model for tinnitus', *Laryngoscope*, 98(3), pp. 280-286.

Jastreboff, P.J., Hansen, R., Sasaki, P.G. and Sasaki, C.T. (1986) 'Differential Uptake of Salicylate in Serum, Cerebrospinal Fluid, and Perilymph', *Archives of Otolaryngology--Head and Neck Surgery*, 112(10), pp. 1050-1053.

Jastreboff, P.J. and Sasaki, C.T. (1986) 'Salicylate-induced changes in spontaneous activity of single units in the inferior colliculus of the guinea pig', *The Journal of the Acoustical Society of America*, 80(5), pp. 1384-1391.

Jenkins, W.M. and Masterton, R.B. (1982) 'Sound localization: Effects of unilateral lesions in central auditory system', *Journal of Neurophysiology*, 47(6), pp. 987-1016.

Jhaveri, S. and Morest, D.K. (1982) 'Sequential alterations of neuronal architecture in nucleus magnocellularis of the developing chicken: A golgi study', *Neuroscience*, 7(4), pp. 837-847,849-853.

Johnson, J.W. and Ascher, P. (1987) 'Glycine potentiates the NMDA response in cultured mouse brain neurons', *Nature*, 325(6104), pp. 529-531.

Kaltenbach, J.A. (2011) 'Tinnitus: Models and mechanisms', *Hearing Research*, 276(1-2), pp. 52-60.

Kelly, J.B. and Caspary, D.M. (2005) 'Pharmacology of the inferior colliculus', in *The Inferior Colliculus*. pp. 248-281.

Kelly, J.B. and Kavanagh, G.L. (1994) 'Sound localization after unilateral lesions of inferior colliculus in the ferret (Mustela putorius)', *Journal of Neurophysiology*, 71(3), pp. 1078-1087.

Kelly, J.B. and Zhang, H. (2002) 'Contribution of AMPA and NMDA receptors to excitatory responses in the inferior colliculus', *Hearing Research*, 168(1-2), pp. 35-42.

Kendrick, K.M., Guevara-Guzman, R., De La Riva, C., Christensen, J., Østergaard, K. and Emson, P.C. (1996) 'NMDA and kainate-evoked release of nitric oxide and classical transmitters in the rat striatum: In vivo evidence that nitric oxide may play a neuroprotective role', *European Journal of Neuroscience*, 8(12), pp. 2619-2634.

Kenmochi, M. and Eggermont, J.J. (1997) 'Salicylate and quinine affect the central nervous system', *Hearing Research*, 113(1-2), pp. 110-116.

Kirson, E.D. and Yaari, Y. (1996) 'Synaptic NMDA receptors in developing mouse hippocampal neurones: Functional properties and sensitivity to ifenprodil', *Journal of Physiology*, 497(2), pp. 437-455.

Kizawa, K., Kitahara, T., Horii, A., Maekawa, C., Kuramasu, T., Kawashima, T., Nishiike, S., Doi, K. and Inohara, H. (2010) 'Behavioral assessment and identification of a molecular marker in a salicylate-induced tinnitus in rats', *Neuroscience*, 165(4), pp. 1323-1332.

Kleckner, N.W. and Dingledine, R. (1988) 'Requirement for glycine in activation of NMDA-receptors expressed in Xenopus oocytes', *Science*, 241(4867), pp. 835-837.

Knipper, M., Köpschall, I., Rohbock, K., Köpke, A.K.E., Bonk, I., Zimmermann, U. and Zenner, H.P. (1997) 'Transient expression of NMDA receptors during rearrangement of AMPA-receptor-expressing fibers in the developing inner ear', *Cell and Tissue Research*, 287(1), pp. 23-41.

Knipper, M., Van Dijk, P., Nunes, I., Rüttiger, L. and Zimmermann, U. (2013) 'Advances in the neurobiology of hearing disorders: Recent developments regarding the basis of tinnitus and hyperacusis', *Progress in Neurobiology*, 111(0), pp. 17-33.

Kolston, J., Osen, K.K., Hackney, C.M., Ottersen, O.P. and Storm-Mathisen, J. (1992) 'An atlas of glycine- and GABA-like immunoreactivity and colocalization in the cochlear nuclear complex of the guinea pig', *Anatomy and Embryology*, 186(5), pp. 443-465.

Kornau, H.C., Schenker, L.T., Kennedy, M.B. and Seeburg, P.H. (1995) 'Domain interaction between NMDA receptor subunits and the postsynaptic density protein PSD95', *Science*, 269(5231), pp. 1737-1740.

Kretsinger, R.H. and Wasserman, R.H. (1980) 'Structure And Evolution Of Calcium-Modulated Protein', *Critical Reviews in Biochemistry*, 8(2), pp. 119-174.

Kurtz, A. and Wagner, C. (1998) 'Role of nitric oxide in the control of renin secretion', *American Journal of Physiology - Renal Physiology*, 275(6 44-6), pp. F849-F862.

Langguth, B. and Elgoyhen, A.B. (2011) 'Emerging pharmacotherapy of tinnitus', *Expert Opinion on Emerging Drugs*, 16(4), pp. 603-606.

Langnaese, K., Richter, K., Smalla, K.H., Krauss, M., Thomas, U., Wolf, G. and Laube, G. (2007) 'Splice-isoform specific immunolocalization of neuronal nitric oxide synthase in mouse and rat brain reveals that the PDZ-complex-building nNOSα β-finger is largely exposed to antibodies', *Developmental Neurobiology*, 67(4), pp. 422-437.

Law, A.J., Weickert, C.S., Webster, M.J., Herman, M.M., Kleinman, J.E. and Harrison, P.J. (2003) 'Expression of NMDA receptor NR1, NR2A and NR2B subunit mRNAs during development of the human hippocampal formation', *European Journal of Neuroscience*, 18(5), pp. 1197-1205.

Le Beau, F.E.N., Rees, A. and Malmierca, M.S. (1996) 'Contribution of GABA- and glycine-mediated inhibition to the monaural temporal response properties of neurons in the inferior colliculus', *Journal of Neurophysiology*, 75(2), pp. 902-919.

Leaver, A.M., Turesky, T.K., Seydell-Greenwald, A., Morgan, S., Kim, H.J. and Rauschecker, J.P. (2016) 'Intrinsic network activity in tinnitus investigated using functional MRI', *Human Brain Mapping*, 37(8), pp. 2717-2735.

LeBeau, F.E.N., Malmierca, M.S. and Rees, A. (2001) 'Iontophoresis in vivo demonstrates a key role for GABAA and glycinergic inhibition in shaping frequency response areas in the inferior colliculus of guinea pig', *Journal of Neuroscience*, 21(18), pp. 7303-7312.

LeDoux, J.E., Sakaguchi, A. and Reis, D.J. (1984) 'Subcortical efferent projections of the medial geniculate nucleus mediate emotional responses conditioned to acoustic stimuli', *Journal of Neuroscience*, 4(3), pp. 683-698.

Lee, S.-J.R., Escobedo-Lozoya, Y., Szatmari, E.M. and Yasuda, R. (2009) 'Activation of CaMKII in single dendritic spines during long-term potentiation', *Nature*, 458(7236), pp. 299-304.

Li, F. and Tsien, J.Z. (2009) 'Memory and the NMDA Receptors', *New England Journal of Medicine*, 361(3), pp. 302-303.

Lockwood, A.H., Salvi, R.J. and Burkard, R.F. (2002) 'Tinnitus', *New England Journal of Medicine*, 347(12), pp. 904-910.

Ma, C.L., Kelly, J.B. and Wu, S.H. (2002) 'AMPA and NMDA receptors mediate synaptic excitation in the rat's inferior colliculus', *Hearing Research*, 168(1-2), pp. 25-34.

Ma, W.L.D., Hidaka, H. and May, B.J. (2006) 'Spontaneous activity in the inferior colliculus of CBA/J mice after manipulations that induce tinnitus', *Hearing Research*, 212(1-2), pp. 9-21.

Malenka, R.C. and Bear, M.F. (2004) 'LTP and LTD: An embarrassment of riches', *Neuron*, 44(1), pp. 5-21.

Malmierca, M.S. (2004) 'The Inferior colliculus: A center for convergence of ascending and descending auditory information', *Neuroembryology and Aging*, 5(3), pp. 215-229.

Malmierca, M.S., Blackstad, T.W., Osen, K.K., Karagülle, T. and Molowny, R.L. (1993) 'The central nucleus of the inferior colliculus in rat: A Golgi and computer reconstruction study of neuronal and laminar structure', *Journal of Comparative Neurology*, 333(1), pp. 1-27.

Malmierca, M.S. and Rees, A. (1996) 'The topographical organization of descending projections from the central nucleus of the inferior colliculus in guinea pig', *Hearing research*, 93(1), pp. 167-180.

Malmierca, M.S., Rees, A., Le Beau, F.E.N. and Bjaalie, J.G. (1995) 'Laminar organization of frequency-defined local axons within and between the inferior colliculi of the guinea pig', *Journal of Comparative Neurology*, 357(1), pp. 124-144.

Malmierca, M.S., Saint Marie, R.L., Merchan, M.A. and Oliver, D.L. (2005) 'Laminar inputs from dorsal cochlear nucleus and ventral cochlear nucleus to the central nucleus of the inferior colliculus: Two patterns of convergence', *Neuroscience*, 136(3), pp. 883-894.

Manabe, Y., Yoshida, S., Saito, H. and Oka, H. (1997) 'Effects of lidocaine on salicylate-induced discharge of neurons in the inferior colliculus of the guinea pig', *Hearing Research*, 103(1-2), pp. 192-198.

Maren, S. and Baudry, M. (1995) 'Properties and Mechanisms of Long-Term Synaptic Plasticity in the Mammalian Brain: Relationships to Learning and Memory', *Neurobiology of Learning and Memory*, 63(1), pp. 1-18.

Marletta, M.A. (1993) 'Nitric oxide synthase structure and mechanism', *Journal of Biological Chemistry*, 268(17), pp. 12231-12234.

Martin, L.J., Blackstone, C.D., Levey, A.I., Huganir, R.L. and Price, D.L. (1993) 'AMPA glutamate receptor subunits are differentially distributed in rat brain', *Neuroscience*, 53(2), pp. 327-58.

Meldrum, B.S. (2000) 'Glutamate as a Neurotransmitter in the Brain: Review of Physiology and Pathology', *The Journal of Nutrition*, 130(4), p. 1007.

Merchán, M., Aguilar, L.A., Lopez-Poveda, E.A. and Malmierca, M.S. (2005) 'The inferior colliculus of the rat: Quantitative immunocytochemical study of GABA and glycine', *Neuroscience*, 136(3), pp. 907-925.

Merzenich, M.M. and Reid, M.D. (1974) 'Representation of the cochlea within the inferior colliculus of the cat', *Brain Research*, 77(3), pp. 397-415.

Morest, D.K. and Oliver, D.L. (1984) 'The neuronal architecture of the inferior colliculus in the cat: Defining the functional anatomy of the auditory midbrain', *Journal of Comparative Neurology*, 222(2), pp. 209-236.

Moroz, L.L. and Kohn, A.B. 1 (2007) 'On the comparative biology of Nitric Oxide (NO) synthetic pathways: Parallel evolution of NO-mediated signaling' Tota, B. and Trimmer, B., pp. 1-44.

Niethammer, M., Kim, E. and Sheng, M. (1996) 'Interaction between the C terminus of NMDA receptor subunits and multiple members of the PSD95 family of membrane-associated guanylate kinases', *Journal of Neuroscience*, 16(7), pp. 2157-2163.

Noel, J., Ralph, G.S., Pickard, L., Williams, J., Molnar, E., Uney, J.B., Collingridge, G.L. and Henley, J.M. (1999) 'Surface expression of AMPA receptors in hippocampal neurons is regulated by an NSF-dependent mechanism', *Neuron*, 23(2), pp. 365-76.

Ochi, K. and Eggermont, J.J. (1996) 'Effects of salicylate on neural activity in cat primary auditory cortex', *Hearing Research*, 95(1-2), pp. 63-76.

Oliver, D.L. (2005a) 'Neural organization in the inferior colliculus', in Winer, J.A. and Schreiner, C.E. (eds.) *The Inferior Colliculus*. New York, NY: Springer New York, pp. 69-114.

Oliver, D.L. (2005b) 'Neuronal organization in the inferior colliculus', in *The Inferior Colliculus*. pp. 69-114.

Oliver, D.L., Ostapoff, E.M. and Beckius, G.E. (1999) 'Direct innervation of identified tectothalamic neurons in the inferior colliculus by axons from the cochlear nucleus', *Neuroscience*, 93(2), pp. 643-658.

Osen, K.K., Lopez, D.E., Slyngstad, T.A., Ottersen, O.P. and Storm-Mathisen, J. (1991) 'GABA-like and glycine-like immunoreactivities of the cochlear root nucleus in rat', *Journal of Neurocytology*, 20(1), pp. 17-25.

Parks, T.N. (2000) 'The AMPA receptors of auditory neurons', *Hearing Research*, 147(1-2), pp. 77-91.

Patel, C.R. and Zhang, H. (2014) 'Local application of sodium salicylate enhances auditory responses in the rat's dorsal cortex of the inferior colliculus', *Frontiers in Neurology*, 5(NOV).

Patneau, D.K. and Mayer, M.L. (1990) 'Structure-activity relationships for amino acid transmitter candidates acting at N-methyl-D-aspartate and quisqualate receptors', *Journal of Neuroscience*, 10(7), pp. 2385-2399.

Paul, A.K., Lobarinas, E., Simmons, R., Wack, D., Luisi, J.C., Spernyak, J., Mazurchuk, R., Abdel-Nabi, H. and Salvi, R. (2009) 'Metabolic imaging of rat brain during pharmacologically-induced tinnitus', *NeuroImage*, 44(2), pp. 312-318.

Paxinos, G., Watson, C.R.R. and Emson, P.C. (1980) 'AChE-stained horizontal sections of the rat brain in stereotaxic coordinates', *Journal of neuroscience methods*, 3(2), pp. 129-149.

Pellegrini-Giampietro, D.E., Gorter, J.A., Bennett, M.V.L. and Zukin, R.S.U. (1997) 'The GluR2 (GluR-B) hypothesis: Ca2+-permeable AMPA receptors in neurological disorders', *Trends in Neurosciences*, 20(10), pp. 464-470.

Peng, B.G., Chen, S. and Lin, X. (2003) 'Aspirin selectively augmented N-methyl-D-aspartate types of glutamate responses in cultured spiral ganglion neurons of mice', *Neuroscience Letters*, 343(1), pp. 21-24.

Peng, Z., Wang, G.P., Zeng, R., Guo, J.Y., Chen, C.F. and Gong, S.S. (2013) 'Temporospatial expression and cellular localization of VGLUT3 in the rat cochlea', *Brain Research*, 1537, pp. 100-110.

Percival, J.M., Anderson, K.N.E., Huang, P., Adams, M.E. and Froehner, S.C. (2010) 'Golgi and sarcolemmal neuronal NOS differentially regulate contraction-induced fatigue and vasoconstriction in exercising mouse skeletal muscle', *The Journal of Clinical Investigation*, 120(3), pp. 816-826.

Platt, S.R. (2007) 'The role of glutamate in central nervous system health and disease – A review', *The Veterinary Journal*, 173(2), pp. 278-286.

Poulos, T.L. (2006) 'Soluble guanylate cyclase', *Current Opinion in Structural Biology*, 16(6), pp. 736-743.

Puel, J.L. (2007) 'Cochlear NMDA receptor blockade prevents salicylate-induced tinnitus', *B-ENT*, 3(SUPPL. 7), pp. 19-22.

Puel, J.L., Ruel, J., Gervais D'Aldin, C. and Pujol, R. (1998) 'Excitotoxicity and repair of cochlear synapses after noise- trauma induced hearing loss', *NeuroReport*, 9(9), pp. 2109-2114.

Putzke, J., Seidel, B., Huang, P.L. and Wolf, G. (2000) 'Differential expression of alternatively spliced isoforms of neuronal nitric oxide synthase (nNOS) and N-methyl-D-aspartate receptors (NMDAR) in knockout mice deficient in nNOSα (nNOSαΔ/Δ mice)', *Molecular Brain Research*, 85(1-2), pp. 13-23.

Qian, A. and Johnson, J.W. (2002) 'Channel gating of NMDA receptors', *Physiology & Behavior*, 77(4–5), pp. 577-582.

Ralli, M., Lobarinas, E., Fetoni, A.R., Stolzberg, D., Paludetti, G. and Salvi, R. (2010) 'Comparison of salicylate and quinine induced tinnitus in rats; development, time course and evaluation of audiological correlates', *Otology & neurotology : official publication of the American Otological Society, American Neurotology Society [and] European Academy of Otology and Neurotology*, 31(5), pp. 823-831.

Reed, J.R. and Palmisano, P.A. (1975) 'Central nervous system salicylate', *Clinical Toxicology*, 8(6), pp. 623-631.

Riquelme, R., Saldaña, E., Osen, K.K., Ottersen, O.P. and Merchán, M.A. (2001) 'Colocalization of GABA and glycine in the ventral nucleus of the lateral lemniscus in rat: An in situ hybridization and semiquantitative immunocytochemical study', *Journal of Comparative Neurology*, 432(4), pp. 409-424.

Roberts, L.E., Eggermont, J.J., Caspary, D.M., Shore, S.E., Melcher, J.R. and Kaltenbach, J.A. (2010) 'Ringing ears: The neuroscience of tinnitus', *Journal of Neuroscience*, 30(45), pp. 14972-14979.

Robertson, D., Bester, C., Vogler, D. and Mulders, W.H.A.M. (2013) 'Spontaneous hyperactivity in the auditory midbrain: Relationship to afferent input', *Hearing Research*, 295(0), pp. 124-129.

Rose, J.E., Gross, N.B., Geisler, C.D. and Hind, J.E. (1966) 'Some neural mechanisms in the inferior colliculus of the cat which may be relevant to localization of a sound source', *Journal of Neurophysiology*, 29(2), p. 288.

Rothe, F., Possel, H. and Wolf, G. (2002) 'Nitric oxide affects the phosphorylation state of microtubule-associated protein 2 (MAP-2) and neurofilament: An immunocytochemical study in the brain of rats and neuronal nitric oxide synthase (nNOS)-knockouts', *Nitric Oxide - Biology and Chemistry*, 6(1), pp. 9-17.

Ruel, J., Chabbert, C., Nouvian, R., Bendris, R., Eybalin, M., Leger, C.L., Bourien, J., Mersel, M. and Puel, J.L. (2008) 'Salicylate enables cochlear arachidonic-acid-sensitive NMDA receptor responses', *Journal of Neuroscience*, 28(29), pp. 7313-7323.

Russwurm, M. and Koesling, D. (2004) 'NO activation of guanylyl cyclase', *EMBO Journal*, 23(22), pp. 4443-4450.

Russwurm, M., Wittau, N. and Koesling, D. (2001) 'Guanylyl Cyclase/PSD95 Interaction: targeting of the nitric oxide-sensitive α2β1 guanylyl cyclase to synaptic membranes', *Journal of Biological Chemistry*, 276(48), pp. 44647-44652.

Ryugo, D.K. and Parks, T.N. (2003) 'Primary innervation of the avian and mammalian cochlear nucleus', *Brain Research Bulletin*, 60(5–6), pp. 435-456.

Sahley, T.L., Hammonds, M.D. and Musiek, F.E. (2013) 'Endogenous dynorphins, glutamate and N-methyl-d-aspartate (NMDA) receptors may participate in a stress-mediated Type-I auditory neural exacerbation of tinnitus', *Brain Research*, 1499, pp. 80-108.

Salerno, J.C. (2008) 'Neuronal nitric oxide synthase: Prototype for pulsed enzymology', *FEBS Letters*, 582(10), pp. 1395-1399.

Salerno, J.C. and Ghosh, D.K. (2009) 'Space, time and nitric oxide - Neuronal nitric oxide synthase generates signal pulses', *FEBS Journal*, 276(22), pp. 6677-6688.

Sanchez, J.T., Gans, D. and Wenstrup, J.J. (2007) 'Contribution of NMDA and AMPA receptors to temporal patterning of auditory responses in the inferior colliculus', *Journal of Neuroscience*, 27(8), pp. 1954-1963.

Sanchez, J.T., Ghelani, S. and Otto-Meyer, S. (2015) 'From development to disease: Diverse functions of NMDA-type glutamate receptors in the lower auditory pathway', *Neuroscience*, 285, pp. 248-259.

Santolini, J. (2011) 'The molecular mechanism of mammalian NO-synthases: A story of electrons and protons', *Journal of Inorganic Biochemistry*, 105(2), pp. 127-141.

Santolini, J., Adak, S., Curran, C.M.L. and Stuehr, D.J. (2001) 'A kinetic simulation model that describes catalysis and regulation in nitric-oxide synthase', *Journal of Biological Chemistry*, 276(2), pp. 1233-1243.

Sattler, R. and Tymianski, M. (2001) 'Molecular mechanisms of glutamate receptor-mediated excitotoxic neuronal cell death', *Molecular Neurobiology*, 24(1), pp. 107-129.

Saur, D., Neuhuber, W.L., Gengenbach, B., Huber, A., Schusdziarra, V. and Allescher, H.D. (2002) 'Site-specific gene expression of nNOS variants in distinct functional regions of rat gastrointestinal tract', *American Journal of Physiology - Gastrointestinal and Liver Physiology*, 282(2 45-2).

Scannevin, R.H. and Huganir, R.L. (2000) 'Postsynaptic organisation and regulation of excitatory synapses', *Nature Reviews Neuroscience*, 1(2), pp. 133-141.

Schaette, R. (2014) 'Tinnitus in men, mice (as well as other rodents), and machines', *Hearing Research*.

Schaette, R., Turtle, C. and Munro, K.J. (2012) 'Reversible induction of phantom auditory sensations through simulated unilateral hearing loss', *PLoS ONE*, 7(6).

Schindelin, J., Arganda-Carreras, I., Frise, E., Kaynig, V., Longair, M., Pietzsch, T., Preibisch, S., Rueden, C., Saalfeld, S., Schmid, B., Tinevez, J.-Y., White, D.J., Hartenstein, V., Eliceiri, K., Tomancak, P. and Cardona, A. (2012) 'Fiji: an open-source platform for biological-image analysis', *Nat Meth*, 9(7), pp. 676-682.

Schindelin, J., Rueden, C.T., Hiner, M.C. and Eliceiri, K.W. (2015) 'The ImageJ ecosystem: An open platform for biomedical image analysis', *Molecular Reproduction and Development*, 82(7-8), pp. 518-529.

Schmid, S., Guthmann, A., Ruppersberg, J.P. and Herbert, H. (2001) 'Expression of AMPA receptor subunit flip/flop splice variants in the rat auditory brainstem and inferior colliculus', *J Comp Neurol*, 430(2), pp. 160-71.

Schmidt, H.H.H.W., Gagne, G.D., Nakane, M., Pollock, J.S., Miller, M.F. and Murad, F. (1992) 'Mapping of neural nitric oxide synthase in the rat suggests frequent co- localization

with NADPH diaphorase but not with soluble guanylyl cyclase, and novel paraneural functions for nitrinergic signal transduction', *Journal of Histochemistry and Cytochemistry*, 40(10), pp. 1439-1456.

Schofield, B.R. (2010) 'Structural organization of the descending auditory pathway', in Palmer, A.R. and Rees, A. (eds.) *The Oxford Handbook of Auditory Science The Auditory Brain*. Oxford: Oxford University Press, pp. 43-64.

Schreiner, C.E. and Langner, G. (1997) 'Laminar fine structure of frequency organization in auditory midbrain', *Nature*, 388(6640), pp. 383-386.

Schwaller, B. (2009) 'The continuing disappearance of "pure" Ca2+ buffers', *Cellular and Molecular Life Sciences*, 66(2), pp. 275-300.

Schwaller, B., Meyer, M. and Schiffmann, S. (2002) ''New' functions for 'old' proteins: The role of the calcium-binding proteins calbindin D-28k, calretinin and parvalbumin, in cerebellar physiology. Studies with knockout mice', *The Cerebellum*, 1(4), pp. 241-258.

Sée, G. (1877) 'Etudes sur l'acide salicylique et les salicylates; traitement due rhumatisme aigu et chronique de la goutte, et de diverses affections du syste' nerveux sensitif par les salicylates', *Bulletin de L'Academie Nationale de Medicine*, 26, pp. 689-706.

Shehata, W.E., Brownell, W.E. and Dieler, R. (1991) 'Effects of salicylate on shape, electromotility and membrane characteristics of isolated outer hair cells from Guinea pig cochlea', *Acta Oto-Laryngologica*, 111(3), pp. 707-718.

Shepherd, G.M. (2003) *The synaptic organization of the brain*. Oxford University Press.

Sivaramakrishnan, S. and Oliver, D.L. (2001) 'Distinct K currents result in physiologically distinct cell types in the inferior colliculus of the rat', *J Neurosci*, 21(8), pp. 2861-77.

Sivaramakrishnan, S. and Oliver, D.L. (2006) 'Neuronal responses to lemniscal stimulation in laminar brain slices of the inferior colliculus', *JARO - Journal of the Association for Research in Otolaryngology*, 7(1), pp. 1-14.

Smits, M., Kovacs, S., de Ridder, D., Peeters, R.R., van Hecke, P. and Sunaert, S. (2007) 'Lateralization of functional magnetic resonance imaging (fMRI) activation in the auditory pathway of patients with lateralized tinnitus', *Neuroradiology*, 49(8), pp. 669-679.

Steinert, J.R., Chernova, T. and Forsythe, I.D. (2010) 'Nitric oxide signaling in brain function, dysfunction, and dementia', *Neuroscientist*, 16(4), pp. 435-452.

Steinert, J.R., Kopp-Scheinpflug, C., Baker, C., Challiss, R.A.J., Mistry, R., Haustein, M.D., Griffin, S.J., Tong, H., Graham, B.P. and Forsythe, I.D. (2008) 'Nitric Oxide Is a Volume Transmitter Regulating Postsynaptic Excitability at a Glutamatergic Synapse', *Neuron*, 60(4), pp. 642-656.

Stolzberg, D., Salvi, R.J. and Allman, B.L. (2012) 'Salicylate toxicity model of tinnitus', *Frontiers in Systems Neuroscience*, (APRIL 2012).

Sturman, J.A. and Smith, M.J.H. (1967) 'The binding of salicylate to plasma proteins in different species', *Journal of Pharmacy and Pharmacology*, 19(9), pp. 621-623.

Stypulkowski, P.H. (1990) 'Mechanisms of salicylate ototoxicity', *Hearing Research*, 46(1-2), pp. 113-145.

Sun, W., Lu, J., Stolzberg, D., Gray, L., Deng, A., Lobarinas, E. and Salvi, R.J. (2009) 'Salicylate increases the gain of the central auditory system', *Neuroscience*, 159(1), pp. 325-334.

Szczepaniak, W.S. and Møller, A.R. (1993) 'Interaction between auditory and somatosensory systems: a study of evoked potentials in the inferior colliculus',

Electroencephalography and Clinical Neurophysiology/ Evoked Potentials, 88(6), pp. 508-515.

Tokunaga, A., Sugita, S. and Otani, K. (1984) 'Auditory and non-auditory subcortical afferents to the inferior colliculus in the rat', *Journal fur Hirnforschung*, 25(4), pp. 461-472.

Trussell, L. 116 (1998) 'Control of time course of glutamatergic synaptic currents' *Progress in Brain Research*. pp. 59-69.

Trussell, L.O. (1997) 'Cellular mechanisms for preservation of timing in central auditory pathways', *Curr Opin Neurobiol*, 7(4), pp. 487-92.

Turner, J.G., Brozoski, T.J., Bauer, C.A., Parrish, J.L., Myers, K., Hughes, L.F. and Caspary, D.M. (2006) 'Gap detection deficits in rats with tinnitus: A potential novel screening tool', *Behavioral Neuroscience*, 120(1), pp. 188-195.

Tzschentke, T.M. (2002) 'Glutamatergic mechanisms in different disease states: overview and therapeutical implications – An introduction', *Amino Acids*, 23(1), pp. 147-152.

Van De Heyning, P., Muehlmeier, G., Cox, T., Lisowska, G., Maier, H., Morawski, K. and Meyer, T. (2014) 'Efficacy and safety of AM-101 in the treatment of acute inner ear tinnitus - A double-blind, randomized, placebo-controlled phase II study', *Otology and Neurotology*, 35(4), pp. 589-597.

Vane, J.R. and Botting, R.M. (2003) 'The mechanism of action of aspirin', *Thrombosis Research*, 110(5-6), pp. 255-258.

Vogler, D.P., Robertson, D. and Mulders, W.H.A.M. (2014) 'Hyperactivity following unilateral hearing loss in characterized cells in the inferior colliculus', *Neuroscience*, 265, pp. 28-36.

Wallace, M., Shackleton, T. and Palmer, A. (2012) 'Morphological and Physiological Characteristics of Laminar Cells in the Central Nucleus of the Inferior Colliculus', *Frontiers in Neural Circuits*, 6(55).

Wallhäusser-Franke, E. (1997) 'Salicylate evokes c-fos expression in the brain stem: Implications for tinnitus', *NeuroReport*, 8(3), pp. 725-728.

Wallhäusser-Franke, E., Braun, S. and Langner, G. (1996) 'Salicylate alters 2-DG uptake in the auditory system: A model for tinnitus?', *NeuroReport*, 7(10), pp. 1585-1588.

Wang, J., van Wijhe, R., Chen, Z. and Yin, S. (2006) 'Is duration tuning a transient process in the inferior colliculus of guinea pigs?', *Brain Research*, 1114(1), pp. 63-74.

Wei, L., Ding, D., Sun, W., Xu-Friedman, M.A. and Salvi, R. (2010) 'Effects of sodium salicylate on spontaneous and evoked spike rate in the dorsal cochlear nucleus', *Hearing Research*, 267(1-2), pp. 54-60.

Wenzel, A., Villa, M., Mohler, H. and Benke, D. (1996) 'Developmental and regional expression of NMDA receptor subtypes containing the NR2D subunit in rat brain', *Journal of Neurochemistry*, 66(3), pp. 1240-1248.

Winer, J.A., Larue, D.T., Diehl, J.J. and Hefti, B.J. (1998) 'Auditory cortical projections to the cat inferior colliculus', *Journal of Comparative Neurology*, 400(2), pp. 147-174.

Winer, J.A., Saint Marie, R.L., Larue, D.T. and Oliver, D.L. (1996) 'GABAergic feedforward projections from the inferior colliculus to the medial geniculate body', *Proceedings of the National Academy of Sciences of the United States of America*, 93(15), pp. 8005-8010.

Winer, J.A. and Schreiner, C.E. (2005a) 'The Central Auditory System: A Functional Analysis', in Winer, J.A. and Schreiner, C.E. (eds.) *The Inferior Colliculus*. New York, NY: Springer New York, pp. 1-68.

Winer, J.A. and Schreiner, C.E. (2005b) *The inferior colliculus*. New York: Springer.

Wood, K.C., Batchelor, A.M., Bartus, K., Harris, K.L., Garthwaite, G., Vernon, J. and Garthwaite, J. (2011) 'Picomolar nitric oxide signals from central neurons recorded using ultrasensitive detector cells', *Journal of Biological Chemistry*, 286(50), pp. 43172-43181.

Wu, M.-d., Kimura, M., Hiromichi, I. and H. Helfert, R. (2008) 'A classification of NOergic neurons in the inferior colliculus of rat according to co-existence with classical amino acid transmitters', *Okajimas Folia Anatomica Japonica*, 85(1), pp. 17-27.

Wynne, B., Harvey, A.R., Robertson, D. and Sirinathsinghji, D.J.S. (1995) 'Neurotransmitter and neuromodulator systems of the rat inferior colliculus and auditory brainstem studied by in situ hybridization', *Journal of Chemical Neuroanatomy*, 9(4), pp. 289-300.

Yang, G., Lobarinas, E., Zhang, L., Turner, J., Stolzberg, D., Salvi, R. and Sun, W. (2007) 'Salicylate-induced tinnitus: Behavioral measures and neural activity in auditory cortex of awake rats', *Hearing Research*, 226(1-2), pp. 244-253.

Yi, B., Hu, S., Zuo, C., Jiao, F., Lv, J., Chen, D., Ma, Y., Chen, J., Mei, L., Wang, X., Huang, Z. and Wu, H. (2016) 'Effects of long-term salicylate administration on synaptic ultrastructure and metabolic activity in the rat CNS', *Scientific Reports*, 6, p. 24428.

Yin, S., Chen, Z., Yu, D., Feng, Y. and Wang, J. (2008) 'Local inhibition shapes duration tuning in the inferior colliculus of guinea pigs', *Hearing Research*, 237(1-2), pp. 32-48.

Zhang, H. and Kelly, J.B. (2001) 'AMPA and NMDA receptors regulate responses of neurons in the rat's inferior colliculus', *Journal of Neurophysiology*, 86(2), pp. 871-880.

Zhang, X., Yang, P., Cao, Y., Qin, L. and Sato, Y. (2011) 'Salicylate-induced neural changes in the primary auditory cortex of awake cats', *Neuroscience*, 172, pp. 232-245.

Zhang, Y. and Wu, S.H. (2000) 'Long-term potentiation in the inferior colliculus studied in rat brain slice', *Hearing Research*, 147(1-2), pp. 92-103.

Zhao, Y., Brandish, P.E., Ballou, D.P. and Marletta, M.A. (1999) 'A molecular basis for nitric oxide sensing by soluble guanylate cyclase', *Proceedings of the National Academy of Sciences of the United States of America*, 96(26), pp. 14753-14758.

Zhao, Y. and Marletta, M.A. (1997) 'Localization of the heme binding region in soluble guanylate cyclase', *Biochemistry*, 36(50), pp. 15959-15964.

Zheng, Y., Seung Lee, H., Smith, P.F. and Darlington, C.L. (2006) 'Neuronal nitric oxide synthase expression in the cochlear nucleus in a salicylate model of tinnitus', *Brain Res*, 1123(1), pp. 201-6.

Zhou, L. and Zhu, D.-Y. (2009) 'Neuronal nitric oxide synthase: Structure, subcellular localization, regulation, and clinical implications', *Nitric Oxide*, 20(4), pp. 223-230.